

**In Situ Health Monitoring of Adhesively Bonded Joints during Fatigue Using
Carbon Nanotube Network**

Roham Mactabi

A Thesis

in

The Department

of

Mechanical and Industrial Engineering

Presented in Partial Fulfillment of the Requirements

For the Degree of Master of Applied Science (Mechanical Engineering) at

Concordia University

Montreal, Quebec, Canada

November 2011

© Roham Mactabi, 2011

CONCORDIA UNIVERSITY

School of Graduate Studies

This is to certify that the thesis prepared

By: Roham Mactabi

Entitled: **In Situ Health Monitoring of Adhesively Bonded Joints during Fatigue Using Carbon Nanotube Network**

and submitted in partial fulfillment of the requirements for the degree of

Master of Applied Science (Mechanical Engineering)

Complies with the regulations of the university and meets the accepted standards with respect to originality and quality.

Signed by the final examining committee:

_____ Chair
Dr. Z.C. Chen

_____ Examiner
Dr. R. Ganesan

_____ Examiner
Dr. M. Elektorowicz

_____ Supervisor
Dr. S.V. Hoa

Approved by

Chair of Department or Graduate Program Director

2011

Dean of Faculty

ABSTRACT

In Situ Health Monitoring of Adhesively Bonded Joints during Fatigue Using Carbon Nanotube Network

R. Mactabi

Adhesive joints have widespread applications in aerospace and automotive industries, but predicting catastrophic failures during dynamic loads is very difficult due to the inaccessibility of the bonded interface. We have developed a new technique based on carbon nanotube (CNT) sensors that can monitor the bond integrity and is capable to predict failure well in advance. The conductive network inside the adhesive is very sensitive to crack initiation, propagation and delamination, therefore in-situ measurement of the bond resistance is capable of recording events that lead to failure. In 90% of the samples the change in bond resistance remains below 10% of the initial value up to approximately 80% of the fatigue life, and then the resistance increases rapidly due to crack propagation and interfacial delamination. As the increase in resistance typically occurs over a few hundreds to thousand cycles it is possible to define a resistance that corresponds to a safety limit before catastrophic failure. Moreover, the addition of 1 wt% MWCNTs inside the adhesive increased the joints shear strength and fatigue life by 10% and 20% respectively. The decrease in electrical resistance due to addition of only 0.5 wt% was more than 7 orders of magnitude.

Acknowledgment of Dedication

This thesis would not have been possible unless with wonderful support and help of my supervisor, Dr. S.V. Hoa, who encouraged me throughout the entire MASc thesis program; I owe my deepest gratitude to him.

I am also grateful to Dr. Rosca for his supports and suggestions which facilitate the understanding of the project to me.

It is a pleasure to thank those who made this thesis possible, Dr. Ming Xie and Mr. Heng Wang.

I also would like to thank Dr. Gerard J. Gouw who supported me when I arrived to Canada and without his help it would have been so difficult to adapt to the environment.

It was an honor to me to work and study alongside the members of CONCOM research group of Dr. Hoa.

And last but not least, I am indebted to my parents and my brother for their lovely supports and inspiration throughout my life which led me to where I am right now. I also would like to thank my friends, Arash Naseri, Mehdi Shahparnia, Alireza Pazooki and many more for their unconditional supports.

Contents

List of Figures	x
List of Tables	xvi
1 Introduction	2
1.1 Motivations and Objectives.....	3
2 Literature Review	6
2.1 Structural Health Monitoring	6
2.1.1 Motivation.....	7
2.1.2 Passive and Active SHM	9
2.1.3 NDE and SHM.....	9
2.1.4 Non-Destructive Evaluation.....	9
2.2 Structural Health Monitoring in Adhesively Bonded Joints	11
2.3 Electrical Resistance Monitoring Using Sensors	18
2.3.1 Carbon Nanotubes.....	19
2.3.1.1 Introduction	19
2.3.1.2 Carbon Nanotube Synthesis.....	21
2.3.1.3 Properties	22
2.3.2 CNT Reinforced Adhesives	22
2.4 Damage Detection and Prognosis Using CNT Networks or Sensors.....	23

2.5	Problem Definition and Objectives	28
3	Experimental.....	31
3.1	Introduction	31
3.2	Materials.....	32
3.2.1	2024 T3 Aluminum.....	32
3.2.2	Epoxy Adhesive	33
3.2.3	Curing Agent.....	33
3.2.4	Multiwall Carbon Nanotubes (MWCNTs)	34
3.3	Sample Fabrication Procedure	35
3.3.1	End Tab Preparation	35
3.3.2	Substrate Preparation	35
3.3.3	Adhesive Preparation	38
3.3.4	Assembly and Curing.....	39
3.4	Tests	42
3.4.1	Electrical Resistance Measurement	42
3.4.2	Apparent Shear Strength Measurement	43
3.4.3	Fatigue Life Measurement	45
3.4.4	In-Situ Health Monitoring of Single Lap Joints during Fatigue Test	46
3.5	Scanning Electron Microscopy (SEM)	47
4	Results and Discussions.....	49

4.1	Introduction	49
4.2	Electrical resistance.....	49
4.2.1	Adhesive Joints with 0.5 wt% MWCNT Loading	50
4.2.2	Adhesive Joints with 1 wt% MWCNT Loading.....	51
4.2.3	Comparison.....	51
4.2.4	Adhesive Joints with 2 wt% MWCNT Loading.....	52
4.2.5	Summary.....	53
4.3	Apparent Shear Strength	55
4.3.1	Apparent Shear Strength for Joints Containing 0 wt% MWCNT.....	55
4.3.2	Apparent Shear Strength for Joints Containing 0.5 wt% MWCNT	56
4.3.3	Apparent Shear Strength for Joints Containing 1 wt% MWCNT.....	57
4.3.4	Apparent Shear Strength for Joints Containing 2 wt% MWCNT.....	58
4.3.5	Comparison.....	59
4.3.6	Summary.....	60
4.3.7	Fracture Mechanism.....	60
4.4	Fatigue.....	61
4.4.1	Fatigue Life for Single Lap Joints Containing No MWCNTs.....	62
4.4.2	Fatigue Life for Single Lap Joints Containing 0.5 wt% MWCNTs	65
4.4.3	Fatigue Life for Single Lap Joints Containing 1 wt% MWCNTs	66
4.4.4	Fatigue Life for Single Lap Joints Containing 2 wt% MWCNTs	67

4.4.5	Comparison and Summary.....	68
4.5	In situ Health Monitoring during Fatigue Test.....	71
4.5.1	Single lap joints containing 0.5 wt% MWCNT	71
4.5.1.1	Summary.....	82
4.5.2	Single lap joints containing 1 wt% MWCNT	83
4.5.2.1	Summary.....	94
4.5.3	Single lap joints containing 2 wt% MWCNT	94
4.5.3.1	Summary.....	102
4.5.4	Comparison.....	102
4.5.5	Summary.....	103
4.5.6	SEM Images of the Fracture Surface of Single Lap Joints after Fatigue..	104
4.5.6.1	Single Lap Joints with No MWCNTs.....	104
4.5.6.2	Single Lap Joints containing 0.5 wt% MWCNTs	108
4.5.6.3	Single Lap Joints containing 1 wt% MWCNTs	113
4.5.6.4	SEM Image of Glass Beads.....	115
4.5.6.5	Comparison.....	117
4.5.6.6	Conclusion.....	118
5	Conclusions and Future Works.....	120
5.1	Conclusion.....	120

5.2	Future Works.....	122
6	References	123
	Appendix I) Electrical resistance signatures of all specimens tested under fatigue	128
	Joints with 0.5 wt% MWCNT.....	128
	Joints with 1 wt% MWCNT.....	143
	Appendix II) Electrical resistance signatures of adhesively bonded graphite composites	158
	1 wt% MWCNT-reinforced-adhesively bonded graphite fiber laminates	158

List of Figures

Figure 2-1 General evolution of man-made objects from simple to complex [9].....	7
Figure 2-2 Benefit of SHM for end users [9]	8
Figure 2-3 Schematic Diagram showing how nanotube is formed from sheet of graphite [35]	20
Figure 2-4 a) arm chair b) zig zag structures of nanotube [35]	20
Figure 2-5 Resistance change with deformation for a 0.5 w% nanotube epoxy composite loaded in tension [48].....	24
Figure 2-6 Load displacement resistance curve for a) 0 specimen b) 0/90 specimen [48]	25
Figure 2-7 Resistance curves for initial loading (undamaged) and reloading (damaged) laminates [48].....	25
Figure 2-8 Mechanical, electrical and acoustic emission responses of specimens a) showing adhesive failure, b) showing adhesive and composite failure [51].....	27
Figure 2-9 Mechanical and electrical response of specimens undergoing incremental cyclic loading showing a) adhesive failure, b) adhesive and composite failure [51].....	28
Figure 3-1 EPON 862 a) chemical b) molecular structures [54]	33
Figure 3-2 Epikure W chemical and molecular structures [54].....	34
Figure 3-3 Schematic of aluminum end tab.....	36
Figure 3-4 Schematic of aluminum substrate	36
Figure 3-5 Calendaring machine	39
Figure 3-6 Vacuum oven.....	39
Figure 3-7 Alignment fixture	40
Figure 3-8 Single lap joint geometry.....	40
Figure 3-9 Assembled single lap joint on the fixture	41
Figure 3-10 Fixture to hold assembled single lap joints inside the oven for curing	41
Figure 3-11 Assembled samples mounted on the fixture and ready to be cured	41
Figure 3-12 Set up schematic of 4-probe technique	43
Figure 3-13 Set up schematic of 2-probe technique	43
Figure 3-14 Single lap joint aligned and mounted on the MTS machine using L shape guides	44

Figure 3-15 Fatigue test set-up	47
Figure 4-1 Joints electrical resistance for samples containing 0.5 wt% MWCNT	50
Figure 4-2 Joints electrical resistance for samples containing 1 wt% MWCNT	51
Figure 4-3 Resistance comparison between 0.5 and 1 wt% CNT loaded specimens	52
Figure 4-4 Joints electrical resistance for samples containing 2 wt% MWCNT	52
Figure 4-5 Average electrical resistance comparison between the joints containing 0, 0.5, 1, and 2 wt% MWCNT	54
Figure 4-6 Joint apparent shear strength for specimens containing no MWCNT	55
Figure 4-7 Joint apparent shear strength for specimens containing 0.5 wt% MWCNT	56
Figure 4-8 Shear strength vs. electrical resistance for single lap joints containing 0.5 wt% MWCNT	57
Figure 4-9 Joint apparent shear strength for specimens containing 1 wt% MWCNT	57
Figure 4-10 Shear strength vs. electrical resistance for single lap joints containing 1 wt% MWCNT	58
Figure 4-11 Joint apparent shear strength for specimens containing 2 wt% MWCNT	58
Figure 4-12 Shear strength vs. electrical resistance for single lap joints containing 2 wt% MWCNT	59
Figure 4-13 Average shear strength comparison between the joints containing 0, 0.5, 1, and 2 wt% MWCNT	59
Figure 4-14 Fracture surface of specimens a) containing 0.5 wt% and b) 1 wt% MWCNT	61
Figure 4-15 Single lap joint fatigue life for specimens containing 0 wt% MWCNT	63
Figure 4-16 Single lap joints fatigue life distributions for specimens with 0 wt% MWCNT	63
Figure 4-17 SEM image of a fracture surface of a sample containing no MWCNTs after the sample was broken due to fatigue loading	64
Figure 4-18 Single lap joint fatigue life for specimens containing 0.5 wt% MWCNT	65
Figure 4-19 Single lap joints fatigue life distributions for specimens with 0.5 wt% MWCNT	65
Figure 4-20 Single lap joint fatigue life for specimens containing 1 wt% MWCNT	66
Figure 4-21 Single lap joints fatigue life distributions for specimens with 1 wt% MWCNT	67
Figure 4-22 Single lap joint fatigue life for specimens containing 1 wt% MWCNT	68
Figure 4-23 Single lap joints fatigue life distributions for specimens with different MWCNT loadings	69
Figure 4-24 Single lap joints average fatigue failure cycles for different CNT loadings	69

Figure 4-25 SEM images of fracture surface of a samples containing 0.5 wt% MWCNT showing CNT bridging in different magnifications a) shows the fracture surface and b, c, and d show magnified images	70
Figure 4-26 SEM images of fracture surface of a samples containing 1 wt% MWCNT showing CNT bridging in different magnifications a) shows the fracture surface and b, c, d and e show magnified images	71
Figure 4-27 Electrical resistance signature vs. fatigue life of sample number 11 containing 0.5 wt% MWCNTs (sample 0.5-11)	72
Figure 4-28 Electrical resistance ratio vs. fatigue life for sample 0.5-11	73
Figure 4-29 Electrical resistance signature vs. fatigue life of sample number 15 containing 0.5 wt% MWCNTs (sample 0.5-15)	73
Figure 4-30 Electrical resistance ratio vs. fatigue life for sample 0.5-15	74
Figure 4-31 Electrical resistance signature vs. fatigue life of sample number 16 containing 0.5 wt% MWCNTs (sample 0.5-16)	74
Figure 4-32 Electrical resistance ratio vs. fatigue life for sample 0.5-16	75
Figure 4-33 Electrical resistance signature vs. fatigue life of sample number 21 containing 0.5 wt% MWCNTs (sample 0.5-21)	75
Figure 4-34 Electrical resistance ratio vs. fatigue life for sample 0.5-21	76
Figure 4-35 Electrical resistance signature vs. fatigue life of sample number 26 containing 0.5 wt% MWCNTs (sample 0.5-26)	76
Figure 4-36 Electrical resistance ratio vs. fatigue life for sample 0.5-26	77
Figure 4-37 Superposition of normalized electrical resistance ratios of the 5 example specimens containing 0.5 wt% MWCNT	77
Figure 4-38 Average electrical resistance signatures of all 30 specimens containing 0.5 wt% MWCNTs	78
Figure 4-39 Slope of the average resistance signature curve from 60% of the life to 90% of the life	79
Figure 4-40 SEM images of the fracture surface of a single lap joint containing 0.5 wt% MWCNTs and evidence of multiple cracks (The image was taken after the sample was broken)	81

Figure 4-41 Long-distance microscopic view of the edge of sample 0.5- 7, a) beginning of the test b) bellow 60% of the fatigue life, c) first sign of delamination around 90% of the life, c) final failure at 30811 cycles.....	82
Figure 4-42 Long-distance microscopic view of the edge of sample 0.5- 10, a) beginning of the test b) bellow 60% of the fatigue life, c) first sign of delamination around 85% of the life, c) final failure at 14350 cycles.....	83
Figure 4-43 Electrical resistance signature vs. fatigue life of sample number 4 containing 1 wt% MWCNTs (sample 1-4).....	84
Figure 4-44 Electrical resistance ratio vs. fatigue life for sample 1-4.....	84
Figure 4-45 Electrical resistance signature vs. fatigue life of sample number 9 containing 1 wt% MWCNTs (sample 1-9).....	85
Figure 4-46 Electrical resistance ratio vs. fatigue life for sample 1-9.....	85
Figure 4-47 Electrical resistance signature vs. fatigue life of sample number 10 containing 1 wt% MWCNTs (sample 1-10).....	86
Figure 4-48 Electrical resistance ratio vs. fatigue life for sample 1-10.....	86
Figure 4-49 Electrical resistance signature vs. fatigue life of sample number 18 containing 1 wt% MWCNTs (sample 1-18).....	87
Figure 4-50 Electrical resistance ratio vs. fatigue life for sample 1-18.....	87
Figure 4-51 Electrical resistance signature vs. fatigue life of sample number 19 containing 1 wt% MWCNTs (sample 1-19).....	88
Figure 4-52 Electrical resistance ratio vs. fatigue life for sample 1-19.....	88
Figure 4-53 Superposition of normalized electrical resistance ratios of the 5 example specimens containing 1 wt% MWCNT.....	89
Figure 4-54 The average electrical resistance signatures of all 30 specimens containing 1 wt% MWCNTs.....	89
Figure 4-55 Slope of the average resistance signature curve from 60% of the life to 90% of the life.....	90
Figure 4-56 SEM images of the fracture surface of a single lap joint containing 1 wt% MWCNTs and evidence of multiple cracks (The image was taken after the sample was broken).....	91

Figure 4-57 Long-distance microscopic view of the edge of sample 1- 6, a) beginning of the test b) bellow 60% of the fatigue life, c) first sign of delamination around 83% of the life, d) final failure at 10580 cycles	93
Figure 4-58 Long-distance microscopic view of the edge of sample 1- 21, a) beginning of the test b) bellow 60% of the fatigue life, c) first sign of delamination around 88% of the life, d) final failure at 7041cycles.	93
Figure 4-59 Electrical resistance signature vs. fatigue life of sample number 1 containing 2 wt% MWCNTs (sample 2-1).	95
Figure 4-60 Electrical resistance ratio vs. fatigue life for sample 2-1	95
Figure 4-61 Electrical resistance signature vs. fatigue life of sample number 2 containing 2 wt% MWCNTs (sample 2-2).	96
Figure 4-62 Electrical resistance ratio vs. fatigue life for sample 2-2	96
Figure 4-63 Electrical resistance signature vs. fatigue life of sample number 3 containing 2 wt% MWCNTs (sample 2-3).	97
Figure 4-64 Electrical resistance ratio vs. fatigue life for sample 2-3	97
Figure 4-65 Electrical resistance signature vs. fatigue life of sample number 4 containing 2 wt% MWCNTs (sample 2-4).	98
Figure 4-66 Electrical resistance ratio vs. fatigue life for sample 2-4	98
Figure 4-67 Electrical resistance signature vs. fatigue life of sample number 5 containing 2 wt% MWCNTs (sample 2-5).	99
Figure 4-68 Electrical resistance ratio vs. fatigue life for sample 2-5	99
Figure 4-69 Superposition of normalized electrical resistance ratios of all 5 specimens containing 2 wt% MWCNT	100
Figure 4-70 The average electrical resistance signatures of all 5 specimens containing 2 wt% MWCNTs	100
Figure 4-71 Slope of the average resistance signature curve from 60% of the life to 90% of the life	101
Figure 4-72 Comparison between the electrical resistance signatures of samples containing 0.5, 1 and 2 wt% MWCNTs.	103
Figure 4-73 Fracture surface of a sample containing 0wt% MWCNTs which was broken after 19898 cycles. (Sample 0-19).	104

Figure 4-74 Magnified image of the square area marked on Figure 4-73, a) 500 μ m, b) 100 μ m.....	105
Figure 4-75 Fracture surface of a sample containing 0wt% MWCNTs which was broken after 18193 cycles. (Sample 0-17).....	106
Figure 4-76 Fracture surface of a sample containing 0wt% MWCNTs which was broken after 12726 cycles. (Sample 0-11).....	107
Figure 4-77 Magnified image of the marked area on Figure 4-73 (b).....	108
Figure 4-78 Fracture surface of a sample containing 0.5 wt% MWCNTs which was broken after 9200 cycles. (Sample 0.5-9).....	109
Figure 4-79 Magnified image of marked section a) and b) on Figure 4-78.....	109
Figure 4-80 Fracture surface of a sample containing 0.5 wt% MWCNTs which was broken after 18193 cycles. (Sample 0.5-4).....	110
Figure 4-81 Magnified image of the marked area (a) on Figure 4-80	111
Figure 4-82 a) Fracture surface of a sample containing 0.5 wt% MWCNTs which was broken after 36000 cycles. (Sample 0.5-14) and b) magnified image of the square marked area (b).....	112
Figure 4-83 Fracture surface of a sample containing 1 wt% MWCNTs which was broken after 5255 cycles. (Sample 1-29).....	113
Figure 4-84 Magnified image from the marked area a) and b) on Figure 4-83	113
Figure 4-85 a) Fracture surface of a sample containing 1 wt% MWCNTs which was broken after 14000 cycles. (Sample 1-28) and b) magnified image of the marked area on a).....	114
Figure 4-86 Fracture surface of a sample containing 1 wt% MWCNTs which was broken after 135750 cycles. (Sample 1-13).....	115
Figure 4-87 SEM image of glass bead on the fracture surface of a joint with 0 wt% MWCNTs.....	116
Figure 4-88 SEM image of glass bead on the fracture surface of a joint with 0.5 wt% MWCNTs.....	116
Figure 4-89 SEM image of glass bead on the fracture surface of a joint with 1 wt% MWCNTs.....	117

List of Tables

TABLE 2-1 Comparison between Non-Destructive and Destructive test methods [11]	11
TABLE 3-1 Components of 2024 T3 aluminum alloy [55]	32
TABLE 3-2 Physical and mechanical properties of 2024 T3 aluminum alloy [55]	32
TABLE 3-3 Physical and mechanical properties of EPON 862 [56]	33
TABLE 3-4 Physical properties of DETDA [56]	34
TABLE 3-5 MWCNT elements [58]	34
TABLE 3-6 MWCNT typical properties [58]	35
TABLE 3-7 Surface pre-treatment detail [5]	37

Chapter 1

Introduction

1 Introduction

Adhesive joints are great alternatives to traditional mechanical joints due to their low cost, low weight, and ease of manufacturing. They also minimize stress concentration by uniformly distributing the stress through the contact surfaces. However, adhesively bonded joints are more vulnerable to fatigue, and creep cracks and dynamic crack propagation under cyclic loading are the primary reason for catastrophic failure in them [1]. Although theoretically structures are designed with safe-life principles to withstand catastrophic failures, damage detection is an important issue in maintenance of structures especially of aircraft and space structures. Damages that are visible can easily be dealt with and actions can be taken to maintain the integrity of the structures. On the other hand, there are undetected and hidden damages which can be caused by low velocity impacts and fatigues. The growths of these damages, which cause catastrophic failures, are of great concern to end-users. Therefore, the design challenge for adhesive joints is not only to increase their strength but to bring confidence in their safety; this confidence can be obtained by in situ health monitoring and damage detection of the joint itself. Little has been done to monitor the state of the adhesively bonded joints during its fatigue life. Most researchers have focused on the effect of different parameters such as joint thickness, overlap length, substrate thickness, existence of fillet in adhesive, and substrate pre-treatment techniques on the fatigue life of the adhesive joints [2-6]. Since traditional structural health monitoring (SHM) techniques require intensive human involvement and are expensive, they are only applied in laboratory experiments rather than full size structures. Moreover, structural polymeric adhesives are insulating material; therefore, most of the traditional SHM techniques cannot be applied on them. However, carbon

nanotube-reinforced adhesives have superior electrical and mechanical properties than neat adhesives; and there is growing interest in using carbon nanotubes (CNT) as in situ sensors in composite structures to monitor the health of the structure itself. Introducing carbon nanotubes inside polymeric adhesives create conductive networks which are sensitive to damage and cracks inside the adhesive. Therefore, it is possible to monitor the electrical resistance change of CNT-reinforced adhesively bonded joints and use the electrical resistance signature as a mean to evaluate the state of the joints during their service lives.

1.1 Motivations and Objectives

Due to their excellent specific properties aluminum has been widely used in aerospace and automobile industries [7]. However, one of the challenges is to bond aluminum parts to each other and to other materials. Since traditional bolted joints add to the weight of the structures and create stress concentration in the joint area, adhesive bonds have been introduced as alternatives to overcome these problems. Adhesive joints are, however, susceptible to fatigue and creep cracks thus experiencing catastrophic failures [8]. Hence, there is a need to increase their strength and provide an on-line monitoring technique to bring in enough confidence for their use in high-tech industries.

In this study electrical resistance measurement technique is employed for in situ health monitoring of adhesively bonded aluminum joints during fatigue loading using carbon nanotube as in situ sensors. Aluminum is chosen as substrates materials since it is a highly conductive metal. Therefore, the effectiveness of carbon nanotube network, formed inside the adhesive, is evaluated for damage detection and the capability of the technique to predict the residual life of the joints during fatigue testing is investigated.

Besides the electrical resistance monitoring technique, the electromechanical properties of CNT-reinforced adhesively bonded joints using different CNT concentrations are investigated and the results are compared to neat adhesive bonded joints to ensure that the addition of carbon nanotubes inside the adhesive improves the electromechanical properties of the joints.

Chapter two provides detailed literature about the structural health monitoring in general and methods that have been developed to monitor adhesively bonded joints. It introduces the electrical resistance method and the use of carbon nanotubes as in situ sensors to detect damages in composite structures. The synthesis, properties and applications of CNTs are also given in this chapter. The previous studies that have been carried out in the area of damage detection and health monitoring of adhesive joints and composite structures are explained briefly. The motivations and objectives of this thesis project are given at the end of this chapter.

Chapter three explains the fabrication procedures to produce single lap joints containing different CNT concentrations. The test set up and procedures are also described in this chapter.

The results for shear and fatigue tests and the in situ monitoring technique are presented and discussed in detail in chapter four.

Chapter five presents the significant outcome of this thesis project and recommendation for future works.

Chapter 2

Literature Review

2 Literature Review

2.1 Structural Health Monitoring

“Structural Health Monitoring (SHM) aims to give, at every moment during the life of a structure, a diagnosis of the “state” of the constituent materials, of the different parts, and of the full assembly of these parts constituting the structures a whole [9].” The diagnosed status of the structure must remain in the design specification sphere, although the state can change due to aging, to environmental conditions, and to incidents. Since the state is monitored at every moment, the full history of the structure is recorded and with the help of Usage Monitoring, prognosis (damage evolution, residual life, etc.) can also be provided. By considering only the first function of SHM, diagnosis, one can say that SHM is an improved way of Non-Destructive Evaluation (NDE). Although this prospective towards SHM is partially true, SHM is much more. SHM can be considered as a way to make artefact materials and structures smart. The concept of intelligent and Smart Materials/Structures (SMS) found its application in civil and aeronautic industries since the end of 1980s. In present day, they act as driving forces for innovation in all industries. The SMS concept is a step in the general evolution of man-made objects from simple to complex (Figure 2-1). Generally three types of SMS exist: SMS controlling their shape, SMS controlling their vibration, SMS controlling their health. SHM integrated structures and materials belong, at least in the short terms, to the less smart type of SMS. Actually, the main achievements in SHM field are to make materials/structures sensitive by embedding sensors. A simple but superficial analogy to SHM structures is the nervous system of living beings. The embedded sensors in the

structures and the central processor are the nerves and the brain in living body, respectively. The damage is detected by sensors then the central processor builds a diagnosis and a prognosis and decides of the actions to undertake [9].

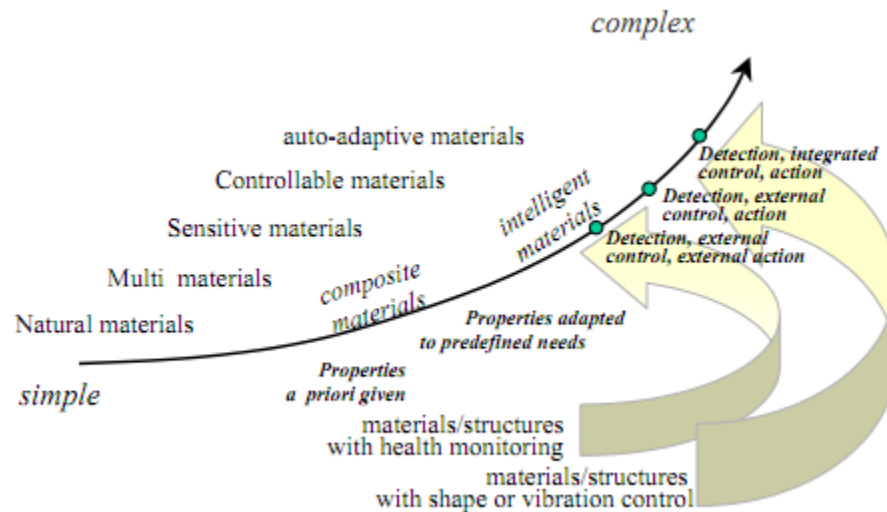


Figure 2-1 General evolution of man-made objects from simple to complex [9]

2.1.1 Motivation

Continuous monitoring of technical structures is provided by the structural health monitoring methodology. The early detection of damage by using SHM techniques leads to prolonging the life of the aging structures. Moreover, understanding the real time integrity of in-service structures is a very eminent purpose for manufacturer, end users, and maintenance. The main benefits of SHM are as followings [9]:

- Optimize use of the structure, minimize downtime, and prevention of catastrophic failures,
- Product improvement,

- Drastic change in maintenance services: i) by replacing the scheduled and periodic maintenance inspections with performance-based maintenance, and by reducing the labour work; ii) by drastic reduction of human involvement, therefore dropping labour, downtime and human errors.

The economical benefits of SHM systems are of prominent interests for end-users. In effect, structures with SHM systems profit the end-users by constant maintenance cost and constant reliability, whereas for classical structures without SHM maintenance cost increases and reliability decreases (Figure 2-2). Moreover in aeronautic domain, due to the permanent presence of sensors in structures, it is possible to reduce the safety margins in some essential parts thus reducing the structure weight, improving the performance, and lowering the fuel consumption [9].

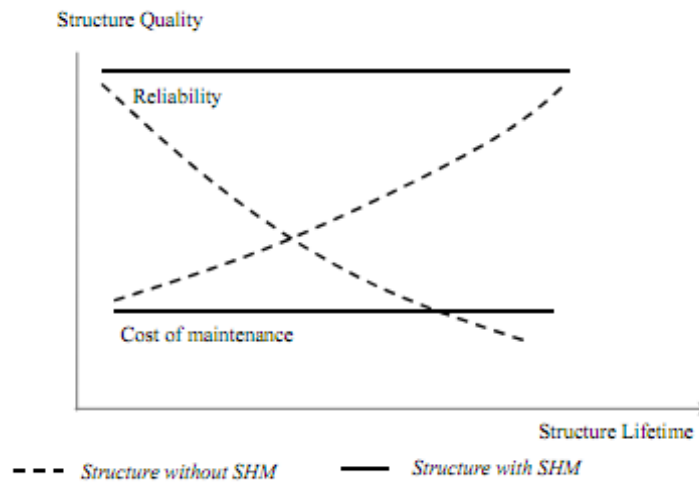


Figure 2-2 Benefit of SHM for end users [9]

2.1.2 Passive and Active SHM

The SHM structures, embedded with sensors, interact with their surrounding environment and their states and physical parameters are evolving. “Passive monitoring” is the case that the examiner is just monitoring the evolution caused in the material without actuating any perturbation in the structure. In “active monitoring” the examiner uses actuators to perturb the structures parameters and then monitors the response of the structure [9].

2.1.3 NDE and SHM

The basis of SHM and NDE are the same. NDE techniques monitor the state of the structures in specified intervals, whereas in SHM the state of the material is being inspected throughout the life cycle of the structure at every moment. Therefore, by integrating sensors and actuators inside the inspected structure and monitoring the structure at every point in its service time, most NDE techniques can be transformed into SHM techniques [9].

2.1.4 Non-Destructive Evaluation

Industrial products may consist of thousand components and parts. Every part within a product has been designed to perform a function. The integrity of the whole product depends upon the functionality of its individual parts. The ability of the part to perform its function within an acceptable time period, which is one of the important user’s expectations, is called its reliability. The part reliability depends upon multiple factors such as design, raw materials, and manufacturing. These factors control the level of defects in final products. There are also different flaws that may occur during the life time of a component subjected to external loadings. The defects should be detected, evaluated and monitored in manufacturing stages and throughout the product life service

to increase its level of quality. High product quality increases the reliability of the product and in turn the safety of the machines, thus bringing economic returns to the clients. Therefore, there is need to have techniques to examine and control the defects in the products without impairing their functionality. These techniques can be categorized into two general classes: destructive and non-destructive. Destructive methods are based on fracture mechanics and the specimen tested will be destroyed [10,11]. It is interesting to compare the non-destructive test method with destructive ones to better understand the important aspects of NDT (TABLE 2-1) [10,11].

NDT methods range from simple to complex. The simplest one is visual inspection. If multiple surface defects are detected by this method, there is often little need to use more complicated methods. More than one technique is usually used to detect the whole structure or sometimes one technique should be used to confirm and validate the results obtained from another one [10,11].

Although "non-destructive testing has no clearly defined boundaries", R. Halmshaw, 1991, the most commonly NDT methods used in industry are as followings: visual inspection, liquid penetrant inspection, magnetic particle inspection, eddy current testing, ultrasonic testing, radiology, acoustic emission, alternating current potential drop, alternating current field measurement, and thermography [10,11]. "Each NDT method is especially suited for a particular task and hence does not compete with, but complement each other [11]".

Non-Destructive	Destructive
<p data-bbox="315 296 461 327">Limitations</p> <ul data-bbox="363 359 846 596" style="list-style-type: none"> <li data-bbox="363 359 846 428">• Need to verify the reliability of the measurements <li data-bbox="363 464 732 495">• Qualitative measurement <li data-bbox="363 527 846 596">• Experienced and expert inspector required to interpret the results <p data-bbox="315 688 461 720">Advantages</p> <ul data-bbox="363 751 846 1226" style="list-style-type: none"> <li data-bbox="363 751 846 821">• Test can be done directly on the components <li data-bbox="363 856 846 968">• Many NDT can be done on one part and all properties can be measured <li data-bbox="363 1003 581 1035">• In situ testing <li data-bbox="363 1066 672 1098">• Test can be repeated <li data-bbox="363 1129 634 1161">• Little preparation <li data-bbox="363 1192 483 1226">• Rapid 	<p data-bbox="873 296 1019 327">Advantages</p> <ul data-bbox="922 359 1404 596" style="list-style-type: none"> <li data-bbox="922 359 1263 390">• Reliable measurements <li data-bbox="922 422 1127 453">• Quantitative <li data-bbox="922 485 1404 596">• Direct correlation between test measurements and material properties <p data-bbox="873 688 1008 720">Limitation</p> <ul data-bbox="922 751 1404 1199" style="list-style-type: none"> <li data-bbox="922 751 1404 821">• Tests are not done on the components directly <li data-bbox="922 856 1404 926">• One or few properties can be measured by one test <li data-bbox="922 961 1404 1031">• In service measurement is not possible <li data-bbox="922 1066 1404 1136">• In service property change cannot be measured <li data-bbox="922 1171 1321 1199">• Time consuming and costly

TABLE 2-1 Comparison between Non-Destructive and Destructive test methods [11]

2.2 Structural Health Monitoring in Adhesively Bonded Joints

In complex structures, due to size limitations and manufacturing processes, presence of joints is inevitable [7,12]. Conventional bolted joints create stress concentration thus reduce the integrity of the structures. Besides the integrity reduction, bolted joints add to the weight of the structures therefore increase the fuel consumption [12]. Adhesively bonded joints, as substitutes to traditional mechanical joints, have been extensively used

in aerospace, electrical, and automotive industries due to the low cost, low weight, and ease of manufacturing [7]. Contrary to traditional joints, in adhesive joint the stress is distributed through the contact surfaces between the two jointed pieces thus minimizing stress concentration [7-12]. Moreover, adhesive bonding enables the possibility of joining dissimilar materials. However, adhesive joints have some drawbacks such as, substrate surface pretreatment requirement to improve the adhesion and the inability of the joint to be disassembled for maintenance and damage inspection [7-12]. Adhesive joints are also more susceptible to creep and fatigue cracks and catastrophic failure is common between them [7-13]. Therefore, it is highly required to monitor the state of the joint throughout its service life. This section provides detail literature about the techniques that were used to monitor adhesively bonded joints and also techniques which were used to monitor bolted joints that could be employed for adhesive joints as well. Jacek M. et al. [14] investigated an ultrasonic method to monitor bonding processes and evaluation of the cold setting adhesive bonded wood laminates. They concluded that the acoustic transmission was sensitive to different bond types and curing phases and it was reasonably correlated with bond strength development. Shuo Yang et al. [15] applied a vibration damping and frequency measurements as a non-destructive method to detect weak joints in adhesively bonded composite sandwich beams. They proposed that the vibration frequencies and mode shapes depend upon joint stiffness and mass; and since structure mass and stiffness change due to damage and defects, the difference in vibration frequencies and mode shapes between the defect free structure and damaged structure can be utilized as a mean to detect degraded bonds. They concluded that the technique is an effective method in detecting damage in bonded joints however; damping measurement

appears to be more reliable. T. Mickens et al. [16] investigated a single-based vibration method to detect, locate and approximately quantify damage in an aircraft wing tip. They bonded four piezoelectric patches on the wing root to send and receive vibration signals alternatively. They stimulated the damage by loosening of the screw joints or rivets. They observed the change in stiffness due to promoted damage affected the local vibration response in high frequencies. R. Jones et al.[17] investigated the application of fiber Bragg grating (FBG) sensors in monitoring the structural health of a composite repair attached to aluminum skins separated by a honeycomb sandwich core. The fiber optic sensors were attached to the composite repair and aluminum skin and the change in their wavelength, which is the key mean to measure strain, were measured precisely. They observed that the strain increased as the crack propagates towards the optic sensors and continued to increase as it passed them. Their study demonstrated the capability of optical sensor arrays to monitor crack growth. C.J. Brotherhood et al. [18] examined three different ultrasonic methods namely as, conventional normal incident longitudinal and shear wave and a high power ultrasonic method to detect kissing bonds in adhesive joints. Kissing bond is a term referred to a failure mechanism in adhesive bonds caused due to poor adhesion between adhesive layer and the substrates. Their study demonstrated that the high power ultrasonic technique was more sensitive at low contact pressures to detect kissing bonds, while conventional longitudinal wave inspection were more effective for higher contact pressures. However, they suggested that combination of two or more ultrasonic techniques could improve the quality assessment of the bonded joints. I. Hersberg et al. [19, 20] assessed optical fiber Bragg grating sensors for structural health monitoring of glass fiber reinforced polymer composite T-joints. They developed a

technique to embed and position optical fibers successfully into the joint interface. “The Bragg grating is designed to reflect only a narrow band of wavelengths propagating in the fiber;” Therefore, as the fiber is strained, the reflected wavelength changes. They also performed a finite element modeling to determine the strain distribution due to artificially disbond the T-joint and compared the analytical data with the experimental results. They concluded that the fiber Bragg grating sensors along with FEM analysis could be promising means for damage assessment. J. Palaniappan et al. [21, 22] embedded chirped fiber Bragg grating within an adherend in adhesively bonded composite joints to monitor the integrity of the structure. They proposed that the changes in reflected spectra of the embedded sensors could be used to monitor disbonding in composite joints. In this study the composite joint was subjected to cyclic loading and monitored using embedded sensors. They observed a shift of the low-wavelength end of the reflected spectrum to lower wavelengths as disbond initiated, whereas, the disbond growth caused a movement of perturbation towards higher wavelengths. Baruch Karp et al. [23] studied the end effect of a cantilever beam by attaching surface strain gages at the immediate vicinity of the joint. They observed that the end effects measured through surface strain gages could identify small changes in the clamping condition. Ze Zhang et al.[24] investigated the capability of stiffness degradation measurement on fatigue life prediction of adhesively bonded composite joints. They concluded that linear stiffness degradation occurred due to fatigue loading. They observed a critical stiffness and elongation at which failure occurred. Renos et al. [25] assessed a vibration based technique using impulse hammer response method for damage detection in bonded composite pultruded sections. They observed that the technique was only sensitive to significant damage. Timothy et al. [26,

27] proposed chaotically amplitude-modulated ultrasonic waves method combined with time series algorithms to locate damage and classify damage conditions in composite skin-to-spar joints. Piezoelectric patches were attached to the composite joints and ultrasonic waves were imparted to the structure and the structural response was recorded. They concluded that the technique was capable of detecting small level of damage even for complicated geometries. Ivan et al. [28] evaluated an analytical method to monitor the bolted joints using electrical conductivity measurement. They concluded that their theoretical study is useful for detecting loosening failure in bolted joints. Frank Balle et al. [29] employed electrical resistance measurement technique for damage assessment of ultrasonically welded aluminum/carbon-fiber joints. Since the fibers were directly welded to the aluminum substrate it made it possible to monitor the change in electrical resistance during fatigue. They realized that this technique was sensitive to micro-structural damages and had better results compare to the results from strain gages attached to the surface of the aluminum. Andrea et al. [30] studied the capability of embedded fiber Brag grating sensors to monitor fatigue crack growth in composite adhesively bonded joints. They embedded array of optic sensors to the side of the single lap tapered joint in thick composite laminate. Their study demonstrated that the optical sensors were capable of detecting and monitoring crack propagation during fatigue test even in the case that crack propagated through the plies of the thick composite laminate. The techniques that were used to monitor the state of the joints in described articles can be categorized into 5 general methods as follow: 1) ultrasonic base, 2) vibration base, 3) mechanical property measurement, 4) fiber optic (strain base), and 5) electrical resistance measurements.

In ultrasonic base techniques ultrasonic and acoustic waves are propagated through the materials using an actuator most preferably piezoelectric ones and the response of the material is recorded using the same actuator or a receiver sensor which is another piezoelectric patch. The response of the material changes due to damage and cracks; hence it can be used as a mean to assess the state of the structure. Ultrasonic techniques are sensitive to small cracks and have good resolution. However, the technique has several drawbacks; it requires sensors to be attached to the structures therefore, the surface of the structure should be available and the technique is capable to locally detecting the damage since sensors cannot be attached to the whole structure. It needs sophisticated instrumentation and expert examiner which makes the technique highly expensive. It poses high downtime since the technique usually cannot be used as on line health monitoring technique [18,26, 27].

Vibration base methods, uses the vibration and damping response of the structures to detect damage and defects inside the materials. The change in the microscopic structures of the materials due to damage, aging, and environmental condition, alter the vibration and damping responses of the structure. This technique is sensitive and has good resolution however it is difficult to distinguish the aging and environmental effects on the structural responses from that of damage effects; hence, the technique needs analytical calculation to distinguish the differences. The technique needs expert examiner and expensive instruments and is often used as offline health monitoring technique [15, 16,25].

Mechanical property measurement technique, measures the change in mechanical properties of the structure throughout its service life. The change in mechanical

properties can be correlated with damages occurred inside the structure. The technique is capable of predicting an allowable property reduction such as stiffness reductions which is correlated to the state of the structure. However, the technique requires sophisticated equipments, complicated set-up and extensive calculations [23-24].

Strain base techniques, uses strain sensors to record the strain changes in the structures due to damage occurrence and crack initiation and propagations. There is a growing interest in using fiber optic sensors as strain sensors to monitor structures especially civil structures. They are attached on the surface of the structures or embedded inside them. They only reflect specific wavelengths and as crack initiates and propagates the strain caused in the optic sensors changes the wavelength and the change in wavelength can be correlated to damage. The technique is sensitive to superficial cracks and damages and is capable of detecting damages in the vicinity of the sensors. The technique, however, can be used as a potentially promising in situ monitoring technique. The main challenge is to embed the fiber optics, due to their micron size, inside the materials without degradation of the structure; and for the attached sensors the main challenge is to protect them from external loading and environmental conditions. The technique is expensive; nonetheless, the growing interest in using them in high tech industries such as civil and aerospace may lead to the technique to become inexpensive and justify their use in online health monitoring of the structures [17,19,22, 30,31].

Electrical resistance monitoring technique, records the change in electrical resistance of the structure due to inside damage. It does not require sophisticated instrumentation and is inexpensive; it is used as on line health monitoring technique. The technique requires the structure to be conductive. Nonetheless, the technique is greatly sensitive in

conductive composite materials since they are inherently sensitive materials. Therefore, electrical resistance monitoring technique is an excellent monitoring technique to be used as in situ techniques for conductive composite materials [9,29].

2.3 Electrical Resistance Monitoring Using Sensors

As discussed in previous section many of the classical NDE and SHM techniques, which are used for periodic maintenance, require extensive human labor and expensive procedures. Moreover, the accidents and failures which occur between successive overhauls will not be detected in periodic inspection. Therefore, there is rising interest in developing sensitive materials or structures with ability to provide real-time information about the material itself. To obtain sensitive materials one natural way is to use the material itself as a sensor. Clearly, Carbon Fiber (CF) and Carbon Nanotubes (CNT) composites are amongst these sensitive materials. Since carbon fibers and carbon nanotubes are conductive materials the measurement of the global electrical resistance of the composite structures containing CF or CNT can be a promising technique for monitoring the composite structural integrity. In carbon fiber composite laminates the fiber breakage, fiber/matrix debonding, matrix microcracks, and delamination contribute to electrical resistance increase. Therefore, monitoring the electrical resistance change can give valuable information about the formation of defects and their severity. In randomly distributed carbon fiber or carbon nanotubes composites the electrical threshold plays an important role. Since polymer adhesives are insulating matrices ($\rho \approx 10^{13}$ to 10^{15} Ωm) the composite electrical conductivity varies dramatically from a critical reinforcement rate or percolation threshold, which corresponds to the formation of continuous conducting path by conducting particles thus making the composite

conductive. This conductive path can form by real contact between the particles or by the inter-particle tunneling effect which in fact the current goes through a thin layer of polymer. The formation of cracks inside conductive composites breaks the conductive path thus increases electrical resistance. This technique needs neither sophisticated equipment nor extensive human involvement. It has promising future in composite materials and structures in on line health monitoring [9]. Moreover, it is important to mention that carbon Nanotubes (CNT) attracts the attention of many researchers due to its multifunctional properties [32-41]. CNT reinforced polymer adhesives have shown superior electromechanical properties compared to neat adhesives. Therefore, electrical resistance measurement technique can be utilized to monitor the structural health of adhesively bonded joints reinforced with carbon nanotubes. The following section provides detail about carbon nanotubes, its synthesis, and its incorporation inside polymer adhesives.

2.3.1 Carbon Nanotubes

2.3.1.1 Introduction

Carbon nanotubes (CNTs) are fullerene structures, geometrical cage-like structures. Fullerenes were first developed by Smalley and co-workers in mid 1980s [32]. This discovery led to the synthesis of carbon nanotubes by Iijima in 1991 [33]. Carbon nanotubes can be considered as rolled graphite sheets into cylinders. Graphite is a 2-D sheet of carbon atoms. Each carbon atom is connected to three other carbon atoms in its neighborhood. Thus the interconnected networks of carbon atoms arrange hexagonal arrays. Rolling graphite sheets form different nanotube structures. These different structures are distinguished by their chirality. Chiral vector can be envisaged as a vector

that connects two points, on different side of a graphite sheet, that coincide on each other after the tube is formed (Figure 2-3).

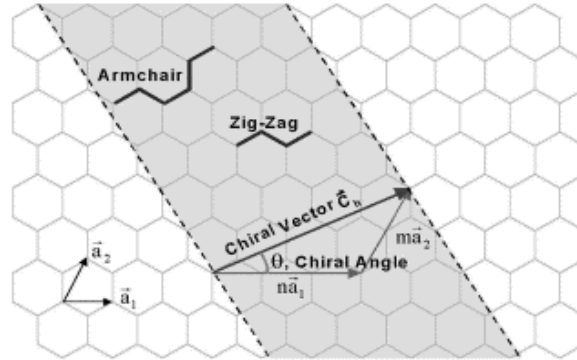


Figure 2-3 Schematic Diagram showing how nanotube is formed from sheet of graphite [35]

There are two special structures based on the special orientation of chiral vector. If the chiral angle is zero the carbon atoms arrangements on the circumference of nanotube form a zig-zag structure. In the case of chiral angle of 30, the arrangement is armchair.

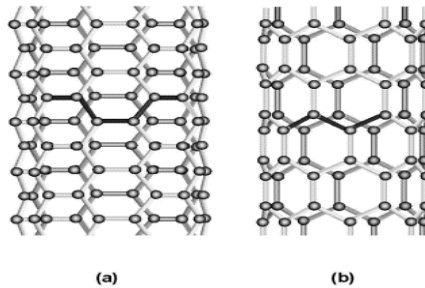


Figure 2-4 a) arm chair b) zigzag structures of nanotube [35]

Chirality affects the properties of nanotubes, for instance, electrical properties of nanotubes can change from graphite semi-metal behavior to super-conductive metal behavior. In addition to tubes chirality, nanotubes can exist in the form of single walled (SW) or multi walled structures (MW). Multi walled nanotubes are the concentric single walled tubes which are held together by a secondary van der Waals forces [34-37].

2.3.1.2 Carbon Nanotube Synthesis

There are different methods for synthesis of single wall and multi wall carbon nanotubes. These methods include arc-discharge, laser ablation, gas catalytic growth from carbon monoxide, and chemical vapor deposition (CVD) from hydrocarbons. Arc-discharge technique, first used by Iijima to synthesis nanotubes, comprises of purely graphite rods as cathode and anode which are brought together to produce a stable arc. Synthesized carbon nanotube then deposits on cathode along with shell of fused material. Other procedures are required to separate the carbon nanotubes from the impurities. Laser ablation was first used to synthesize fullerenes. In this technique a laser beam is used to vaporize the graphite target held in an elevated temperature of 1200°C and controlled environment. The carbon nanotubes are then deposited on a collector. Since the source of graphite, the anode in arc and the target in laser, is limited, the high cost of high scale productions of CNTs is prohibitive. This major drawback led to developing better and cheaper techniques for scaled up productions of CNTs. Gas-phase and chemical vapor deposition solved this problem. In these techniques the source of the carbon is the carbon carrying gas which can be fed continually to the system by flowing gas. CVD is the most common method to synthesize nanotubes in which a hydrocarbon gas (methane, carbon monoxide, and acetylene) is decomposed on a metal substrate (Ni, Fe, or Co) and produces multiwall carbon nanotube. The advantages of the CVD technique are its high purity of the byproduct CNTs and also its ability to produce aligned arrays of carbon nanotubes [34, 37].

2.3.1.3 Properties

Since their discovery by Iijima in 1991 numerous researches have been investigating their physical and mechanical properties. The SWCNT density is about 1.22-1.40 g/cm³, one-half of that of the aluminum [35]. Their elastic modulus is 1 TPa, comparable to diamond, and their tensile strength is over 150 GPa higher than that of high-strength steel [35]. The resilience of SWCNT is distinctively superior to that of metal and conventional carbon fibers. Iijima et al.'s experiments show that nanotubes are remarkably resilient. They can bend reversibly up to 110°[35]. Their fracture strain is between 10 to 30%, where as carbon fibers have the fracture strain range of 0.1% to 2% [34]. CNTs possess extraordinary electrical and thermal properties. While copper wires burn out at about 1x10⁶ (amp/cm²), electrical current carrying capability of CNTs is about 1x10⁹ (amp/cm²), three orders of magnitude higher. The thermal conductivity of SWCNT is 6000 W/mK at room temperature, where that of diamond is 3320 W/mK. They are stable up to 2800 °C in vacuum and 750 °C in air. Metal wires in microchips melt at 600-1000 °C [35]. Great electrical and thermal property along with high specific stiffness and strength, and high aspect ratios of carbon nanotubes make them promising candidates as reinforcement for composites for both structural and functional applications.

2.3.2 CNT Reinforced Adhesives

Concerns such as lead-free environmental legislation, metallic corrosion, and lightweight electronic assemblies have grown interests in applications of lead-free conductive adhesives to tackle these issues. Metal filled adhesives are considered as one of the lead-free adhesives. These adhesives need up to 80 wt% metal filler to reach minimum electrical resistivity. However, the mechanical property of the matrix is degraded due to

the high metal filler loading [38]. Therefore CNT-reinforced adhesives become promising in replacing metal filled ones. The electro-mechanical properties of CNT-reinforced adhesives were reported to be superior to neat adhesive by many researchers. Sangwook et al. [39] studied the through thickness thermal conductivity in aligned carbon nanotubes adhesive bond. Their study revealed significant enhancement of bonding performance as well as improvement in through thickness thermal conductivity. They reported 32 and 45 % increase in shear strength by adding 1 and 5 w% of CNT, respectively. In the study of Suzhu et al. [40] it was observed that the percolation threshold as low as 0.5 w% CNTs was enough to make the insulating adhesive conductive. The study of Suzhu et al. [42] showed that the addition of CNTs to the epoxy significantly enhanced the durability of adhesive joint. It was revealed that at an optimum value of approximately 1 wt% CNTs maximum increase in joint durability could be achieved. However, L. Roy et al. [43] did not achieve great increase in adhesive mechanical strength by incorporating CNTs. H.P. Wu et al. [44] compared 2 different isotropical conductive adhesives (ICA) developed by MWCNT and silver coated CNT (SCCNT) with traditional ICA. They reported better conductivity and shear strength for both SCCNT and MWCNT compared to traditional ICA. Kuang et al. [45] investigated the use of epoxy/MWCNT as adhesive to joint composite substrates and concluded that there was 45.6% increase in the joint shear strength while adding 5 w% MWCNT.

2.4 Damage Detection and Prognosis Using CNT Networks or Sensors

Baughman et al. [46] first reported the intrinsic coupling between the electrical and mechanical properties of CNT which makes them outstanding candidates for in situ sensing. Chunyu Li et al. [47] studied the use of CNT as mechanical sensors in variety of

sensing applications such as mass, strain, humidity, and temperature sensors. Thonstenson et al. [48] demonstrated in their study that carbon nanotubes forms conductive network in an epoxy and this conductive network can be utilized as highly sensitive sensors for detecting the onset, nature, and evaluation of damage in advanced polymer-based composites. They performed tensile tests on nanotube/epoxy specimens and monitored the specimen electrical resistance by highly sensitive voltage-current meter. They observed a highly linear relationship between the specimen deformation and electrical resistance, (Figure 2-5).

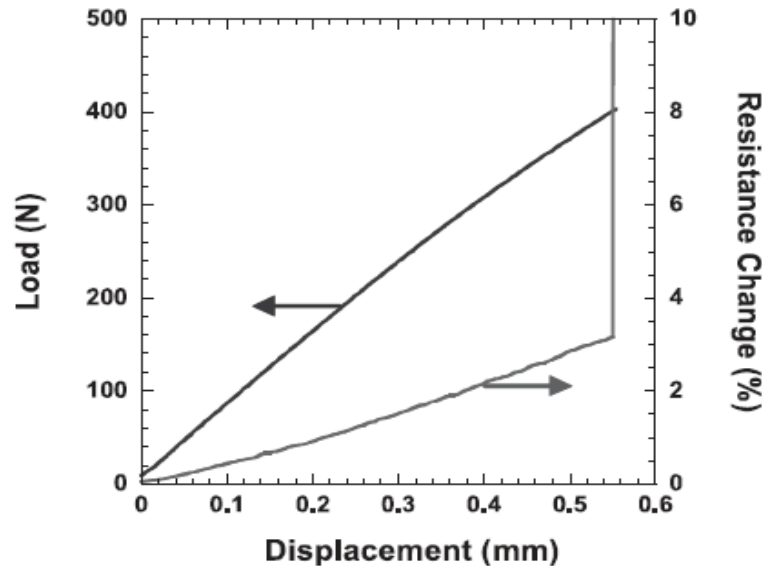


Figure 2-5 Resistance change with deformation for a 0.5 w% nanotube epoxy composite loaded in tension

[48]

They produced 0 unidirectional and 0/90 cross ply laminates consisting of 5 plies with a cut in the middle lamina to promote ply delamination during tensile testing. They observed linear increase in both specimen configuration resistances due to initial deformation followed by a sharp increase in resistance with initiation of delamination Figure 2-6. They also investigated the effect of loading, un-loading, and reloading on

electrical resistance. The experiment was done so that when initial crack was observed, due to increase in resistance, they stopped the test. They reported that after unloading, the resistance decreased nearly to its original value as the cracks were closed by the outer plies pressure; upon reloading specimen showed sharp increase in resistance corresponding that permanent damage was done to the specimen Figure 2-7. Their study depicts the promising application of CNT as in situ sensors in polymeric composites.

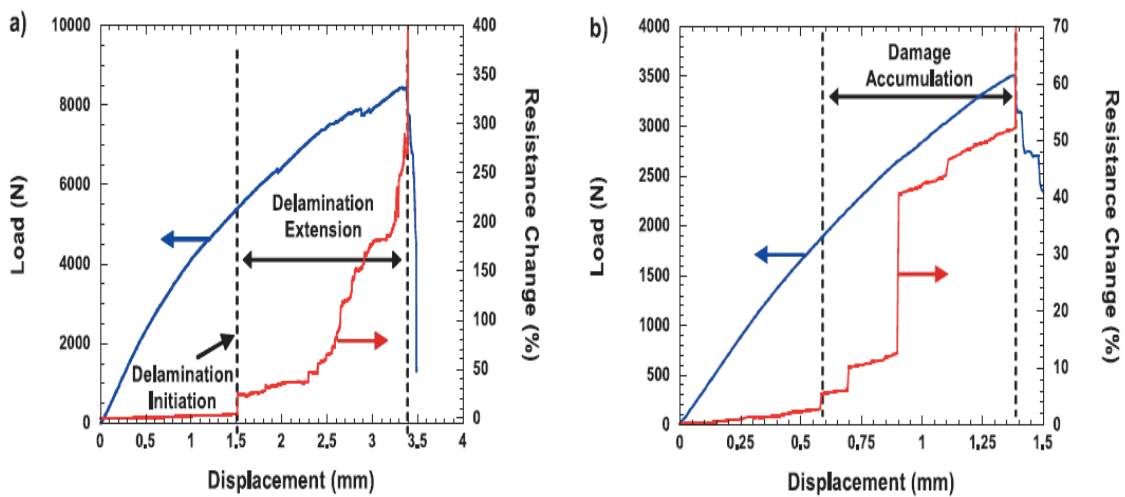


Figure 2-6 Load displacement resistance curve for a) 0 specimen b) 0/90 specimen [48]

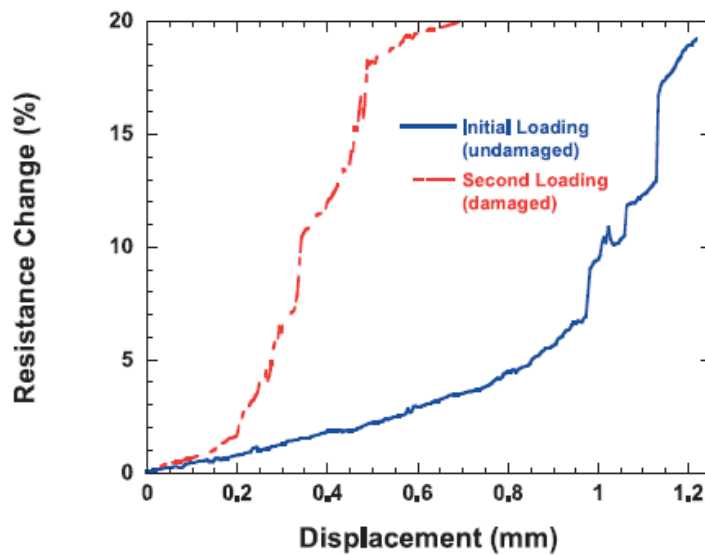


Figure 2-7 Resistance curves for initial loading (undamaged) and reloading (damaged) laminates [48]

M. Nofar et al. [49] reported the sensing capability of CNT network in detecting the failure region in laminated composite subjected to static and dynamic loading. They also studied the difference of sensitivity between strain gauges and CNT network inside the polymer. They concluded that the CNT network is more sensitive in detecting and predicting the cracked regions than strain gauges due to existence of CNT network throughout the structure as whole rather than locally attached strain gauges that are only able to detect cracks in selected areas. Limin Gao et al. [50] studied the integration of carbon nanotube inside glass fiber laminated composite to detect the formation of microscale damage and evaluate the damage evolution and failure mechanisms in cyclic loading. They also reported that electrical resistance measurement of carbon nanotube network is a potential non invasive technique to sense damage in composite structures. W. Zhang et al. [1] investigated the sensitivity potential of volume and through thickness resistance measurement of CNT reinforced graphite fiber composites in monitoring delamination. They observed that CNT network was highly sensitive to the delamination length, showing that CNT additives could be used as real time sensors to size the delamination and monitor its growth rate. The same technique can be used for in service health monitoring of adhesively bonded metal-metal, metal-composite, and composite-composite joints. Thostenson et al. [13] reported “the unique capability of carbon nanotube network as in situ sensors for sensing local composite damage and bolt loosening in mechanically fastened glass/epoxy composite joints.” They examined the single lap and double lap configuration specimens and measured the electrical resistance change due to applied loading. They observed linear increase in electrical resistance till approximately 60% of the ultimate load followed by deviation from linear increase in

both configurations. They believed the resistance signature corresponded to the initial stages of bearing damage in the composite and the subsequent formation of longitudinal cracks. In the recent study of Amanda S. Lim et al. [51] they investigated the ability of CNT networks to sense and distinguish different types of damage in adhesively bonded hybrid composite-metal joints. They fabricated hybrid joints using vinyl ester as an adhesive to bond glass composite to stainless steel substrates. Carbon nanotubes were also added to the composite substrates near the joint interface to make the glass composite substrates conductive in the vicinity of the joint interface. They promoted different failure conditions by changing the surface treatment of the substrates and by intentionally introducing higher void contents inside the composite specimens. They observed different signature resistance response for different failure mechanism during tensile loading. They observed step like manner increase in resistance signature of the joints showing adhesive failure and gradual resistance increase response for the joints showing combined adhesive and composite failure during tensile loading (Figure 2-8).

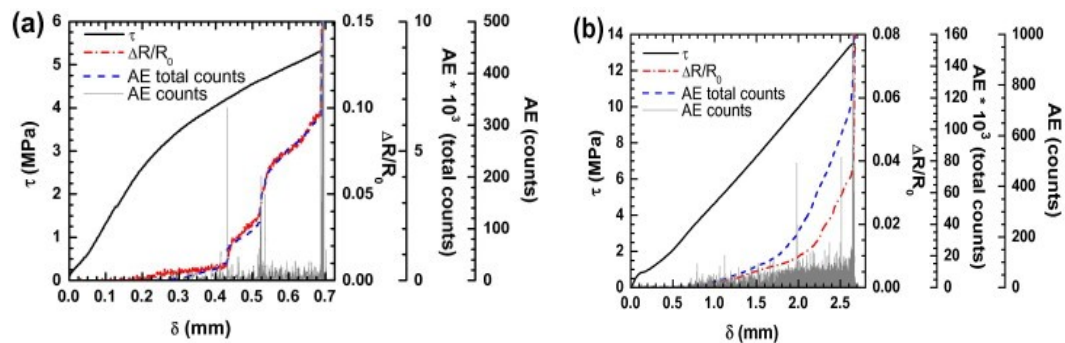


Figure 2-8 Mechanical, electrical and acoustic emission responses of specimens a) showing adhesive failure, b) showing adhesive and composite failure [51]

They also performed incremental cyclic loading to evaluate the resistance signature of the joints due to progressive damage. They observed a good agreement between the incremental cyclic loading response and quasi static loading response of the joints

showing the same type of failure mechanism. They observed the step wise manner increase and gradual increase in resistance base line in specimens showing adhesive failure and showing adhesive-composite failure, respectively (Figure 2-9).

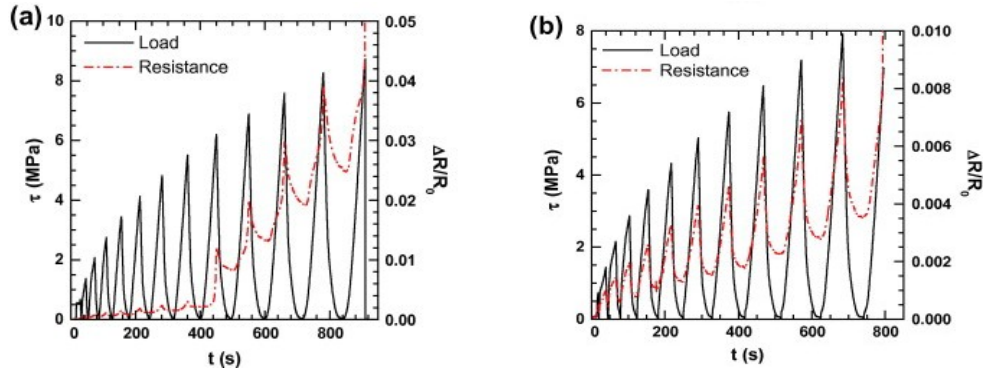


Figure 2-9 Mechanical and electrical response of specimens undergoing incremental cyclic loading showing a) adhesive failure, b) adhesive and composite failure [51]

Their study depicted the capability of identifying different failure mechanism based on resistance measurement signature during quasi static and incremental cyclic loading.

2.5 Problem Definition and Objectives

As it was explained before most of the monitoring techniques for adhesively bonded joints were either off-line methods, expensive or were only evaluating the failure mechanisms of the joints and detecting the occurrence of damage. Damage detection is an important requirement to improve the quality of a structure and increase its service life, however, damage detection by itself will not provide required confidence in wide application of adhesively bonded joints. Therefore, there is a need to provide an in-situ monitoring technique which is capable of evaluating the state of the structure and predicting its residual life. To fill this gap of in-situ health monitoring of adhesive bonds, this study intends to monitor the state of adhesively bonded aluminum joints during fatigue life using carbon nanotube as sensors and provides a technique to predict the state

of the joints at each moment or in other words predict the residual life of the joints. In our study, Epon 862 is used as an adhesive to join aluminum substrates. Carbon nanotubes as sensors are added to the adhesive to make it conductive then the electrical resistance signature of the joints containing different concentration of carbon nanotubes are monitored during fatigue test. The results are evaluated to assess the effectiveness of carbon nanotube network as in situ sensors to monitor the health of the adhesively bonded joints and predict their residual life.

Chapter 3

Experimental

3 Experimental

3.1 Introduction

As it was mentioned in previous chapters, joints are essential parts in complex structures thus they have to be designed to withstand service loadings and environment. Since bolted joints add to the weight of the structures, adhesive joints can be used as promising alternatives. However, adhesive joints cannot be disassembled for periodic maintenance, therefore, it is essential to provide a structural health monitoring technique to evaluate the state of the joints throughout their service life. Nevertheless most of the available structural health monitoring techniques requires the materials to be electrically conductive, while adhesives are naturally insulating materials. Hence, MWCNTs can be introduced to adhesive joints to make them conductive. In this study we developed a technique, using carbon nanotube network, to evaluate the health of single lap joints during fatigue life. Despite of the fact that this study focuses on the structural health monitoring of adhesively bonded joints, it is of prime importance to make sure that the addition of MWCNTs does not degrade the mechanical properties of the joints. Therefore, single lap joints were fabricated and mechanically tested to assess the capability of our technique in monitoring the health of the structure and also to evaluate the mechanical properties of the joints containing MWCNT. This chapter describes in detail, the materials used and their properties, the sample fabrication, and the experimental procedures.

3.2 Materials

Single lap joints were produced using aluminum substrates, epoxy adhesive, MWCNT, and epicure curing agent. Industrial grade MWCNTs with average length and diameter of 3.3 μm and 11.5 nm respectively were purchased from NanoLab Inc. Epon 862 and Epikure W as epoxy resin and curing agent were purchased from Hexion Specialty Chemicals. 2024 T3 aluminum plates were purchased from McMaster Carr.

3.2.1 2024 T3 Aluminum

Since 2024 T3 aluminum alloy is a high strength material with good machinability and fatigue strength, it is the most widely aluminum alloy used in aircraft structures. Its main alloying elements are copper and magnesium. Copper adds to its mechanical strength though reduces its corrosion resistance [56]. TABLE 3-1 and TABLE 3-2 provide the components and properties of 2024 T3 aluminum alloy.

TABLE 3-1 Components of 2024 T3 aluminum alloy [55]

Component	Wt. %	Component	Wt. %
Al	90.7-94.7	Mg	1.2-1.8
Cr	Max 0.1	Mn	0.3-0.9
Cu	3.4-3.8	Si	Max 0.5
Fe	Max 0.5	Ti	Max 0.15
		Zn	Max 0.25

TABLE 3-2 Physical and mechanical properties of 2024 T3 aluminum alloy [55]

Density	2.78 g/cc	Electrical Resistivity	5.82e-06 ohm-cm
Tensile Strength	483 MPa	Yield Strength	385 MPa
Modulus of Elasticity	73.1 GPa	Poisson's Ratio	0.33
Shear Modulus	28 GPa	Shear Strength	283 MPa
Fatigue Strength	138 MPa	CTE, linear 250°C	24.7 $\mu\text{m}/\text{m}\cdot^\circ\text{C}$

3.2.2 Epoxy Adhesive

Epon resin 862 (Diglycidyl Ether of Bisphenol F) is a widely used aerospace adhesive. It is a low viscosity resin made from epichlorohydrin and Bisphenol-F and it contains no diluents or modifiers. It has superior mechanical, adhesive, chemical resistance, and electrical properties when cross-linked with appropriate curing agent [57]. Figure 3-1 shows chemical and molecular structures of Epon 862 resin. Physical and mechanical properties of Epon 862 resin are shown in TABLE 3-3.

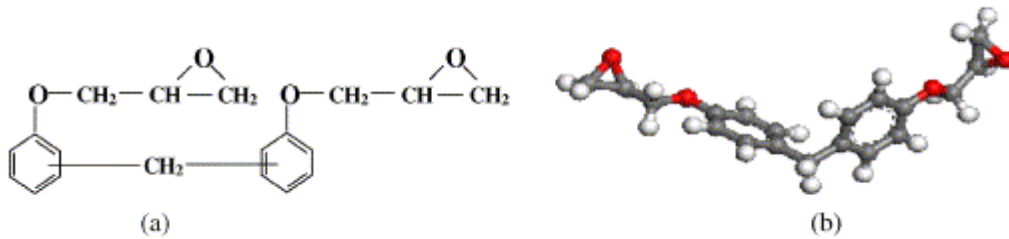


Figure 3-1 EPON 862 a) chemical b) molecular structures [54]

TABLE 3-3 Physical and mechanical properties of EPON 862 [56]

Density	1.17 g/cm ³	Weight per Epoxide	165-173 g/eq
Viscosity at 25°C	25-45 p	Flash Point	>150°C

3.2.3 Curing Agent

Epikure W is an aromatic amine curing agent, which its main ingredient is diethyltoluenediamine (DETDA) [54]. Figure 3-2 illustrates the chemical and molecular structures of DETDA. Physical properties of Epikure W curing agent are shown in TABLE 3-4.

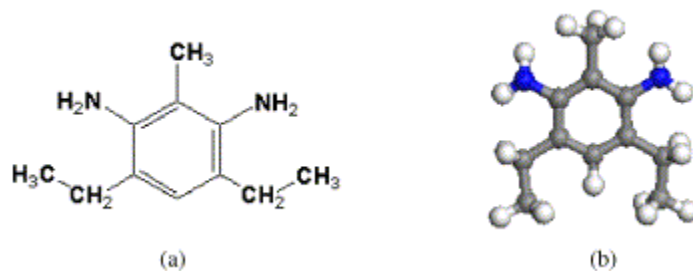


Figure 3-2 Epikure W chemical and molecular structures [54]

TABLE 3-4 Physical properties of DETDA [56]

Equivalent Weight	200 g/eq	Density	1.02 g/cm ³
Viscosity at 25°C	5-20 P	Flash Point	135°C
Solubility in Water	slight	Parts Per Hundred	26.4 phr

3.2.4 Multiwall Carbon Nanotubes (MWCNTs)

Multiwall carbon nanotubes are produced using chemical vapor deposition (CVD) technique by NanoLab Inc. High purity of multiwall carbon nanotube, more than 95%, promotes its multifunctional properties. Its high aspect ratio and large surface area makes it a perfect additive to improve electrical, chemical, and mechanical properties of structural adhesives. TABLE 3-5 demonstrates the ingredients of MWCNT. Typical properties of MWCNT are shown in TABLE 3-6.

TABLE 3-5 MWCNT elements [58]

Elements	Wt. %
Carbon	98.92
Sulfur	0.14
Iron	0.94

TABLE 3-6MWCNT typical properties [58]

Inside Diameter	3-5 nm	Outside Diameter	13-16 nm
Length	10-30 μm	Number of Walls	3-15
Bulk Density	140-160 Kg/mm^3	Electrical Conductivity	$>10^{-2}$ S/cm
Specific Surface Area		233 m^2/g	

3.3 Sample Fabrication Procedure

The procedure to make single lap joints is as follows: end tabs preparation, substrate preparation, adhesive preparation, assembly and curing.

3.3.1 End Tab Preparation

End tabs were produced using the same aluminum to be attached to the end of each substrate to make the geometry of the single lap joints symmetric thus eliminating the bending moment that would have been generated due to small offset in loading during the mechanical testing. End tabs were cut to sheets of 1x1x1/16 inch (25.4 x 25.4 x 1.58 mm) using shear cut (Figure 3-3). They were filed to remove the sharp edges. Finally they were sonicated in acetone bath for 15 minutes to remove dust and grease of their surfaces.

3.3.2 Substrate Preparation

Aluminum sheets were cut into plates with dimensions of 4x1x1/16 inch then they were filed to clean the sharp edges (Figure 3-4). Next the substrates were sonicated for 15 minutes in acetone bath to remove the dust and grease from their surfaces. The cleaned substrates were surface treated in chromic acid solution ($\text{Na}_2\text{Cr}_2\text{O}_7, \text{H}_2\text{SO}_4$) for 40 minutes in 65°C . Surface treatment plays an important role in strengthening the adhesive bond. When aluminum is exposed to air, aluminum passive oxide layer occurs, which is not

suitable for bonding. Pre-treatment is necessary to remove contaminants such as lubricants and oils and also provides the suitable contact between the adhesive and substrate surface which promotes successful adhesion between the two. There are different surface pre-treatment techniques in literature. The most commonly used ones on aluminum substrates are: caustic etch (CE), tucker’s agent (TR), CSA etch, abrasive polishing, and solvent wiping. TABLE 3-7 briefly explains each technique. A.M Pereira et al. in their study concluded that CSA etching technique provides the best fatigue strength on aluminum single lap joints [5, 53]. Therefore, in this study CSA technique was used as substrate surface treatment technique. After immersing the substrates in acid solution, they were rinsed in water and acetone to remove the acid from their surface.

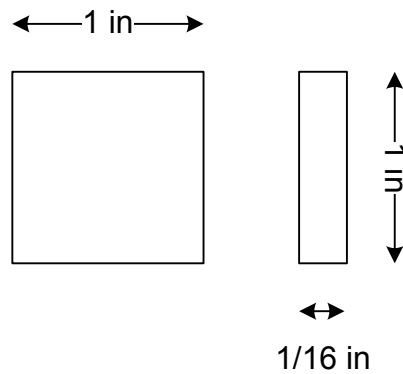


Figure 3-3 Schematic of aluminum end tab

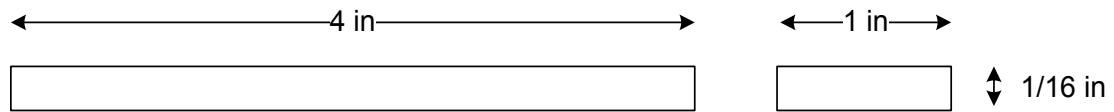


Figure 3-4 Schematic of aluminum substrate

TABLE 3-7 Surface pre-treatment detail [5]

Surface Preparation Technique	Procedure
Caustic Etch (CE)	Dip specimens in NaOH, H ₂ O solution for 5-15 min at 60-70 °C, rinse in water, immerse in HNO ₃ , rinse in water and dry
Tucker's Reagent (TR)	Dip specimens in HCL, HNO ₃ , HF, H ₂ O solution for 10-15 min, rinse in water and dry. This procedure can be repeated till desired effect is obtained
CSA	Immerse specimens in sodium dichromate-sulphuric acid solution (650 g H ₂ O distilled, 75 g Na ₂ Cr ₂ O ₇ , 275 g H ₂ SO ₄) at 60-65 °C. Rinsed in water and dry.
Abrasive Polishing (AP)	The surface is randomly abraded using P220 grade sandpaper and cleaned using dry air
Solvent Wiping (SW)	Wiping by acetone solvent

3.3.3 Adhesive Preparation

Batches of adhesive suspension with different CNT concentrations, namely as 0, 1, 0.5, and 2 wt% were prepared. Each batch contained weight percentage of MWCNT, of EPON 862, and of Epicure W which made a mixture of 15 grams. The amount of each substituent was measured using equations (3-1) to (3-3).

$$CNT_{weight} = CNT_{wt\%} \times 15 \quad (3-1)$$

$$Epoxy_{weight} = \frac{15 - CNT_{weight}}{1.264} \quad (3-2)$$

$$Curing\ Agent_{weight} = Epoxy_{weight} \times 0.264 \quad (3-3)$$

A beaker was weighed on the scale and then the scale was set to zero. MWCNT was added inside the beaker as required amount measured using the equation. Then the epoxy was poured inside the beaker and at the end the curing agent was added to the whole mixture. Since each batch was produced right before being used to make the single lap joints and the reactivity of the curing agent at room temperature was low, we added the curing agent to the mixture before dispersing nanotubes inside the adhesive. Therefore there was no difficulty regarding the shelf time of adhesive suspensions. After adding all the ingredients, the suspension was mixed using a spatula before it was three-roll milled. There are different techniques to disperse nanotubes inside adhesive such as, ultrasonic processing and shear mixing, which includes simple shearing, dissolver disk, planetary mixer, and three roll milling. Three roll milling technique was chosen to disperse the nanotube inside the epoxy adhesive since it is solvent free, scalable, and uniformly applies shear on the entire volume of the suspension [52]. In three-roll milling technique

the gaps between the rollers, the speed of rolling and number of passes play important role in the quality of the dispersion and the electrical conductivity threshold of the mixture. Rosca et al. studied the effect of different gaps and rolling speeds on dispersion and they concluded that medium shear intensity and moderate number of passes brought about sufficient dispersion [52]. Therefore, in this study the following sequence of passes were used for CNT dispersion: 2 passes with gap of 50 μm , 1 pass of 20 μm , and 3 passes of 10 μm , all at the speed of 100 rpm. After dispersion the suspensions were degassed inside vacuum oven for 20 minutes at 80°C. Figure 3-5 and Figure 3-6 show three-roll milling machine (calendaring machine), and the vacuum oven.



Figure 3-5 Calendaring machine



Figure 3-6 Vacuum oven

3.3.4 Assembly and Curing

To assemble the joints an aluminum fixture, Figure 3-7, was designed and manufactured to create single lap joints with geometry and configuration as shown in Figure 3-8.

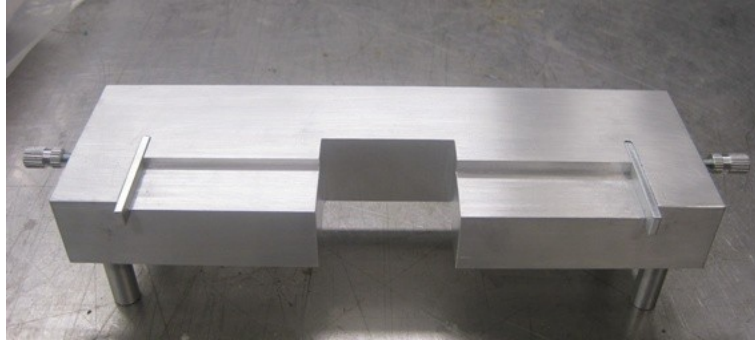


Figure 3-7 Alignment fixture

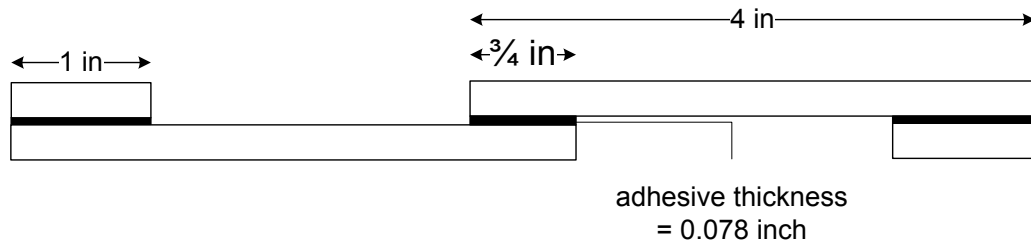


Figure 3-8 Single lap joint geometry

To create each joint, adhesive layer was applied on one aluminum substrate using a spatula. The layer width was considered a little more than the required width to make sure there was no dry spot on aluminum substrates. The substrate was then fixed on the left side of the fixture. Glass beads were poured on the adhesive layer using a spatula to control the final thickness of the adhesive layer as 0.2 mm with acceptable tolerances. Afterward, an adhesive layer was drawn on the other substrate and the substrate was fixed on top of the first one to make the assembly. At the end the two substrates were fixed using C clamps, Figure 3-9. Finally end tabs were attached to each substrate using the same adhesive and paper clips to hold them in place. Another aluminum fixture was designed and created to mount the single lap joints on it and put the fixture inside the oven for curing, Figure 3-10 and Figure 3-11. The samples were cured in the oven for 4

hours at 175°C as advised by the resin manufacturer. By each batch of adhesive suspension, 10 single lap joints were produced for testing.

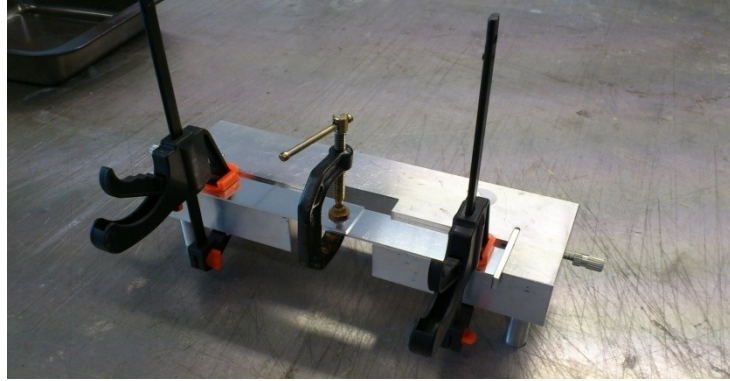


Figure 3-9 Assembled single lap joint on the fixture



Figure 3-10 Fixture to hold assembled single lap joints inside the oven for curing



Figure 3-11 Assembled samples mounted on the fixture and ready to be cured

3.4 Tests

Samples with different CNT concentrations were tested to measure their electrical resistance, shear strength, fatigue life, and they were also health monitored during fatigue test using in situ electrical resistance measurement technique.

3.4.1 Electrical Resistance Measurement

Initially 4-probe technique was used to measure the joints electrical resistance using current source (Keithly 6220 DC) and nanovoltmeter (Keithly 218A). However, due to the fact that 2-probe technique was more convenient to be used for in situ health monitoring, the results between 2-probe and 4-probe techniques were compared and since the measured electrical resistances using 2 different techniques showed less than 1% difference, 2-probe technique was used for the rest of the experiments. Figure 3-12 and Figure 3-13 show the set up schematic for the 2 techniques. Since aluminum is highly conductive the electrodes were directly attached to aluminum substrates. Therefore the measured electrical resistance was consisted of 5 elements namely as, substrate 1, substrate 2, adhesive layer, contact resistance between substrate 1 and adhesive layer, and contact resistance between substrate 2 and adhesive layer, R_1 , R_2 , R_3 , R_4 , R_5 , respectively. Electrical resistances of the samples, R , were measured before they were used for shear or fatigue testing. It is important to mention that R_1 and R_2 did not change during the tests due to the fact that the aluminum substrates were always intact throughout the entire tests. However, the adhesive resistance changed due to crack initiations and propagations and the contact resistances changed due to delamination between the adhesive layer and substrates.

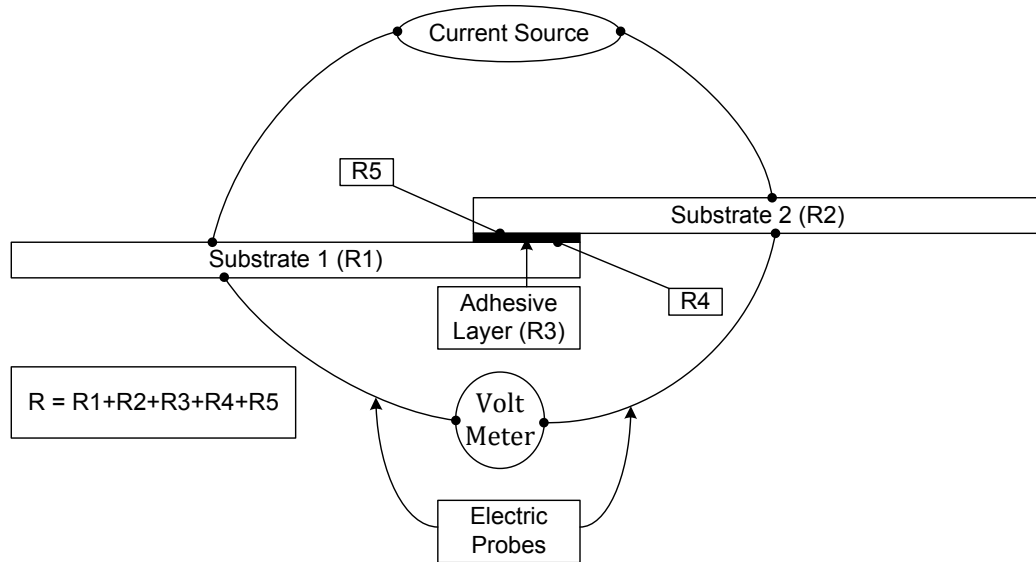


Figure 3-12 Set up schematic of 4-probe technique

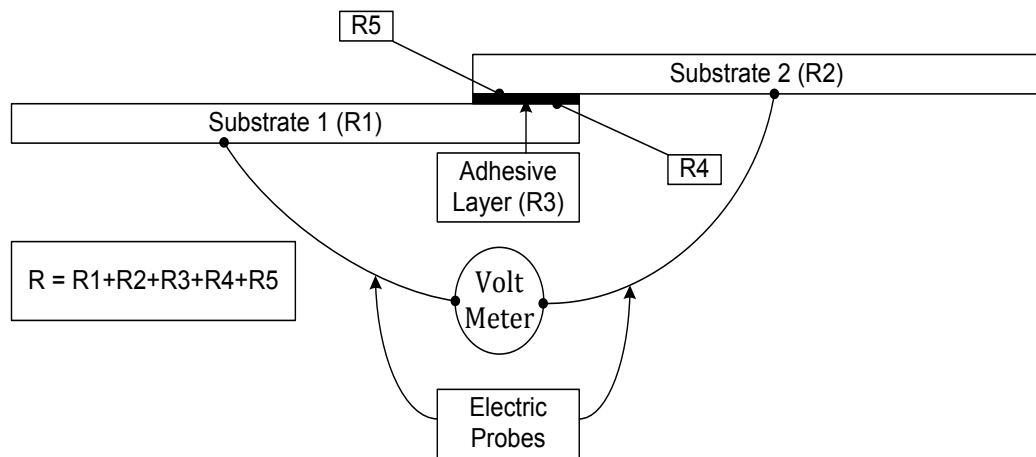


Figure 3-13 Set up schematic of 2-probe technique

3.4.2 Apparent Shear Strength Measurement

Apparent shear strengths of adhesively bonded aluminum joints were measured to compare the mechanical properties of joints with different CNT loadings. Moreover, the average shear strengths of joints with different CNT loadings were used as reference for maximum and minimum loading in fatigue tests of the corresponding joints. Shear test was performed according to ASTM D1002-05 standard. 100 KN MTS tensile machine, at

the crosshead speed of 1.3 mm/min, was used to measure the apparent shear strength. Each sample was mounted on the MTS machine. To make sure the samples were perfectly aligned two L shape guides were attached to the top and bottom jaws of the MTS grips and the side of the samples was rested against the guide as shown in Figure 3-14.

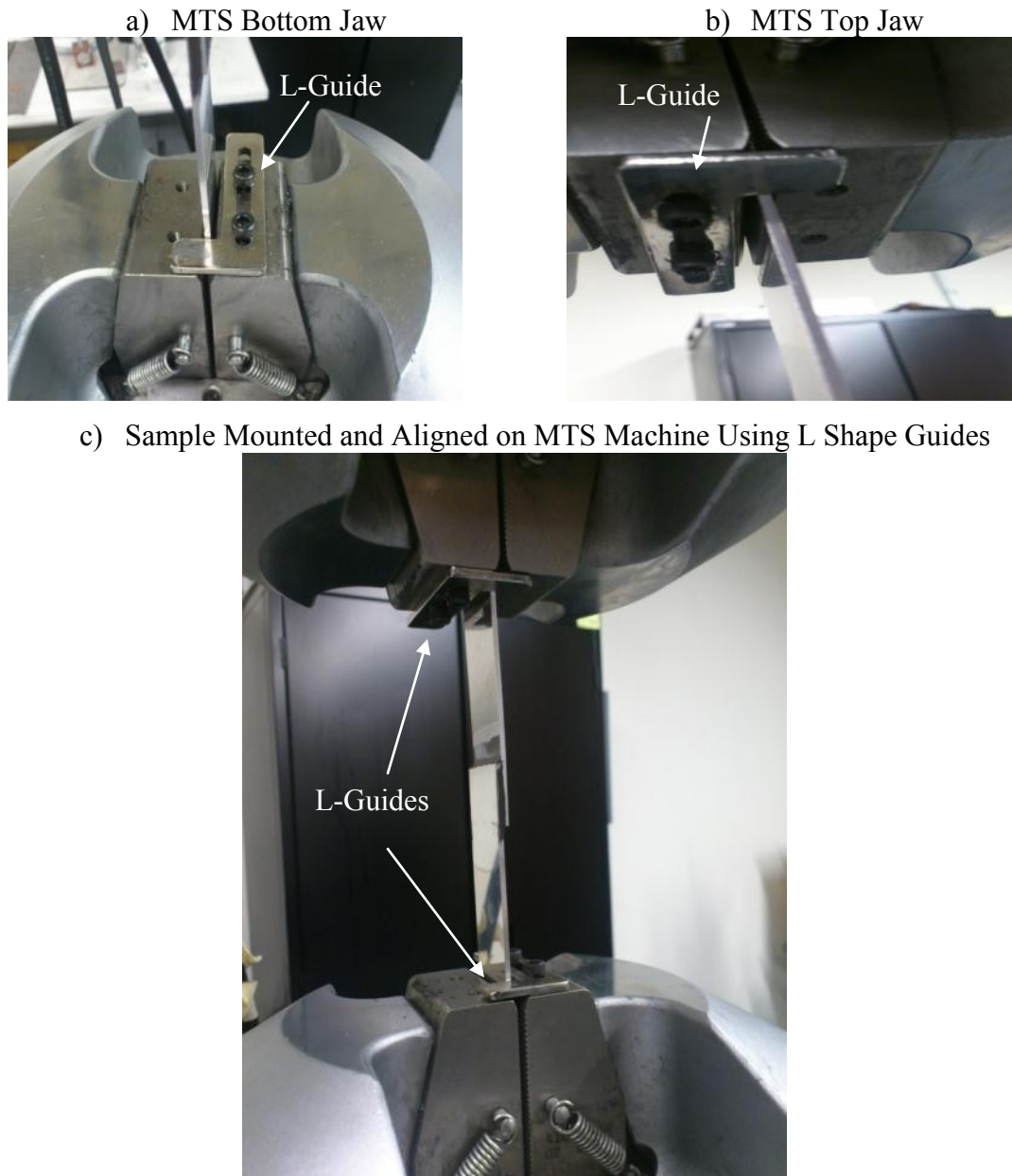


Figure 3-14 Single lap joint aligned and mounted on the MTS machine using L shape guides

The samples were rested on the guides first then the pressure was applied on the bottom jaw to hold one substrate, next the displacement and load on MTS controller were set to zero, and finally the switch for top jaw was activated and the sample was grabbed at both ends. At this moment the program was manually started and continued to run till complete fracture of the joint. Maximum load applied on each sample to break the joint was recorded as apparent shear load. Single lap joints containing 0, 0.5, 1, 2 wt% CNT were tested. 30 samples of each CNT concentration were tested to calculate the average shear strength of each CNT loading except for 2 wt% CNT loaded samples. For 2 wt% CNT loaded specimens, only 5 samples were tested due to the fact that their fatigue results showed dramatic decrease (more than 50%) compared to specimens with no CNT. The average shear strengths were used to compare the mechanical properties of joints with different CNT concentrations. The MTS machine measured the apparent shear load and the apparent shear strength was calculated using equation (3-4).

$$\tau = \frac{F}{A} \quad (3-4)$$

τ , apparent shear strength in MPa

F, apparent shear load in N

A, joint area mm² (A = joint width x joint length)

3.4.3 Fatigue Life Measurement

Fatigue test was performed on 30 samples of each CNT concentration namely as, 0, 0.5, 1 wt% CNT and on 5 samples containing 2 wt% CNT. The experiment was performed

according to ASTM D3166-99 standard. Maximum load σ_{\max} , was set at 60% of the average shear load measured from shear test to expedite the fatigue test since lower maximum fatigue load would result in excessive time required to finish the tests. The ratio of 0.1 was used to measure minimum load σ_{\min} , according to the standard. The 100 KN MTS tensile machine was used to do the fatigue tests. The procedure to mount the samples on the MTS machine was the same as described in previous section. All tests were performed at 10 Hz until final failure occurred. The fatigue cycle in which the joint was broken was recorded as fatigue life of that joint.

3.4.4 In-Situ Health Monitoring of Single Lap Joints during Fatigue Test

The state of the samples was monitored using electrical resistance measurement technique, while they were being fatigue tested. After mounting the sample on the MTS machine, electrical probes connected to the nanovoltmeter, were attached to each substrate. The voltmeter was connected to the data acquisition system to record and to save the joint electrical resistance at every second till its final failure. The results were plotted on an excel sheet as resistance vs. time. The electrical probes were directly attached to the aluminum substrates rather than being inserted inside the adhesive. This is because it was more convenient; it was not degrading the mechanical properties of the joints unlike in the case of inserting wire; and more importantly it was possible to measure the contact electrical resistances between the adhesive layer and each substrate. The contact resistances were of great importance in monitoring the health of the joints especially at the final stages of their fatigue lives. Figure 3-15 shows the in-situ health monitoring set-up.

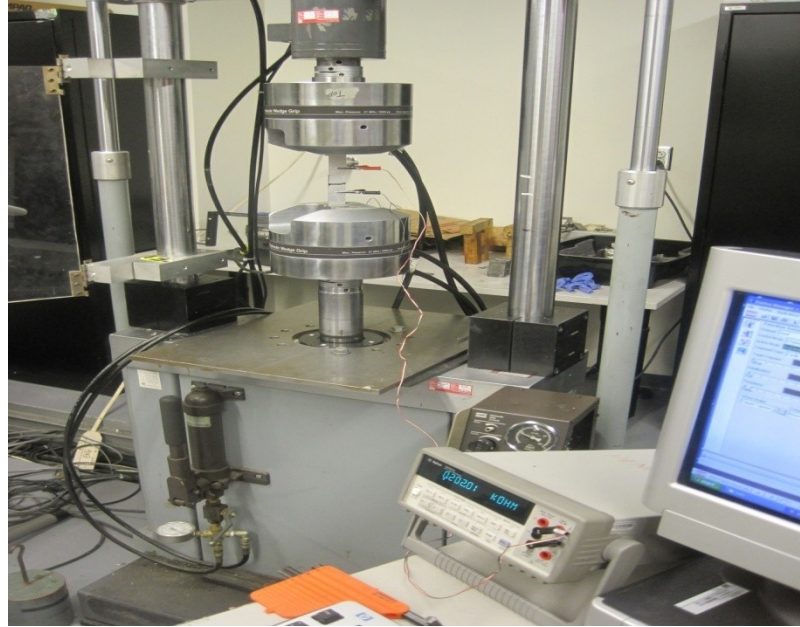


Figure 3-15 Fatigue test set-up

3.5 Scanning Electron Microscopy (SEM)

The fracture surface of samples containing 0, 0.5, and 1wt% MWCNTs which were broken due to fatigue testing were investigated using Hitachi S-4700 FE-SEM at McGill University. The images were compared to evaluate the effect of different MWCNTs loading on the fracture mechanism of single lap joints. The fracture surface of specimens was plasma coated to improve the quality of SEM images.

Chapter 4

Results and

Discussions

4 Results and Discussions

4.1 Introduction

The main focus of this study was in-situ health monitoring of adhesively bonded joints during fatigue life. Therefore, fatigue test is the prime experiment to evaluate our technique. However, preliminary testing is required to perform fatigue test. Shear strength test was performed first to assess the maximum shear load required to break the samples. The average shear load is then used to calculate the loading required for fatigue testing. Moreover, since introduction of MWCNTs would change the electromechanical properties of adhesive joints, it was important to compare the electromechanical properties of the joints containing MWCNTs with different wt. % to each other and to the joints with neat adhesive as the reference. This chapter provides detail results and discussions for each experiment.

4.2 Electrical resistance

The test set-up and technique to measure the electrical resistance were explained in section 3.4.1. All sample electrical resistances except for the joints with neat epoxy adhesive were measured and recorded. The results for 0.5 and 1 wt% CNT reinforced adhesive joints were compared to each other. However, due to fewer numbers of specimens for 2 wt% CNT loading, the result for specimens containing 2 wt% CNT is presented separately.

4.2.1 Adhesive Joints with 0.5 wt% MWCNT Loading

Electrical resistances of 60 specimens were measured and recorded prior to shear and fatigue tests. The results are shown in Figure 4-1. The average electrical resistance for 0.5 wt% MWCNT loaded joints was 6877 Ω . The standard deviation of the data is 3845 Ω . Large standard deviation in electrical resistance is due to fact that the specimens were cured in high temperature. High temperature curing decreases the viscosity of the resin mixture during curing, which allows the nanotube network to reshape. This event can highly affect the electrical resistance of final product. Therefore, it was expected to witness large standard deviation in the samples initial electrical resistance. Even though there is a large standard deviation of resistance from sample to sample, this should not affect the monitoring of the integrity of the joint using the electrical resistance. This is because the monitoring technique utilizes the difference in electrical resistance from the reference resistance and once a sample is under consideration its reference resistance is fixed. Nevertheless, using room temperature curing agent would lower the standard deviation.

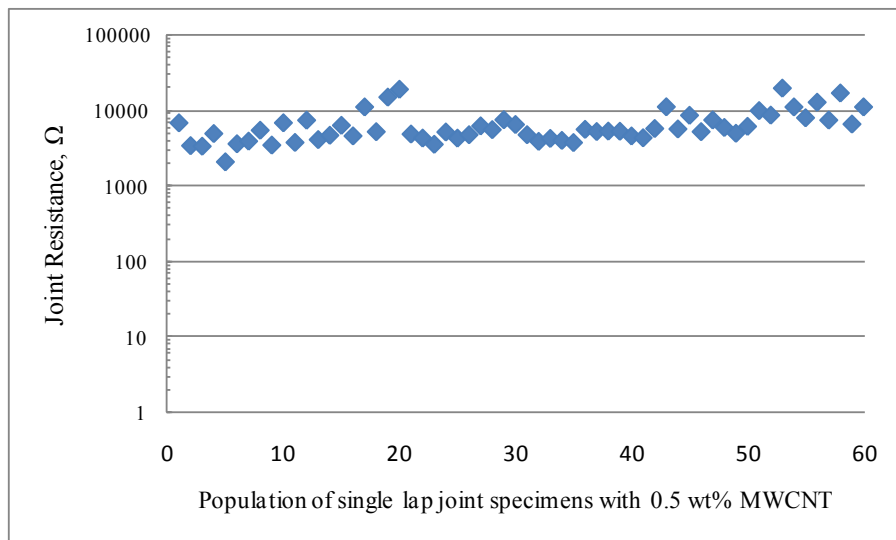


Figure 4-1 Joints electrical resistance for samples containing 0.5 wt% MWCNT

4.2.2 Adhesive Joints with 1 wt% MWCNT Loading

Electrical resistances of 60 specimens were measured and recorded prior to shear and fatigue tests. The results are shown in Figure 4-2. The average electrical resistance for 1wt% MWCNT loaded joints was 550 Ω . The standard deviation for the data is 451 Ω . The same fact as described in section 4.2.1 can explain high standard deviation in the case of 1 wt% MWCNTs loading.

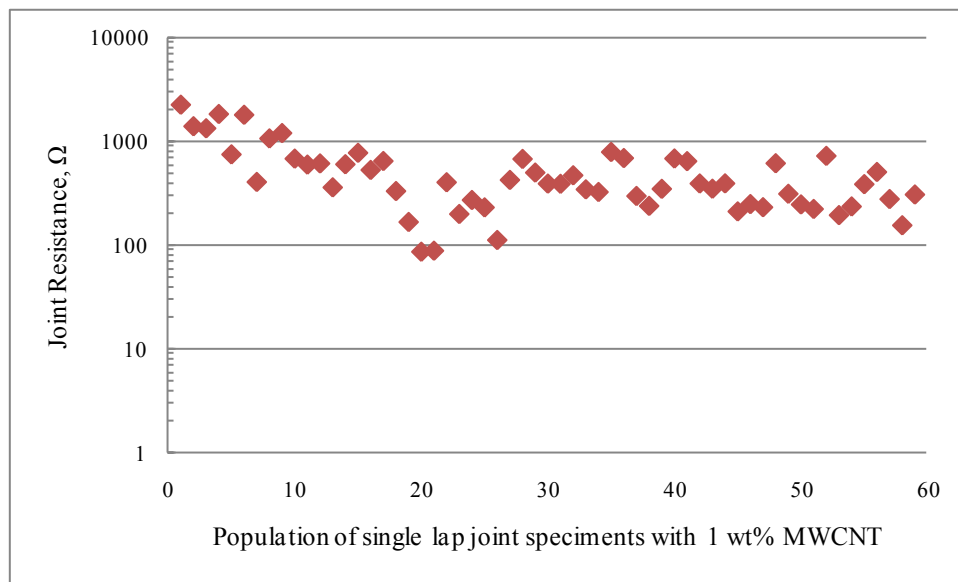


Figure 4-2 Joints electrical resistance for samples containing 1wt% MWCNT

4.2.3 Comparison

Figure 4-3 shows the comparison between the electrical resistance of single lap joints containing 0.5 and 1 wt% MWCNT.

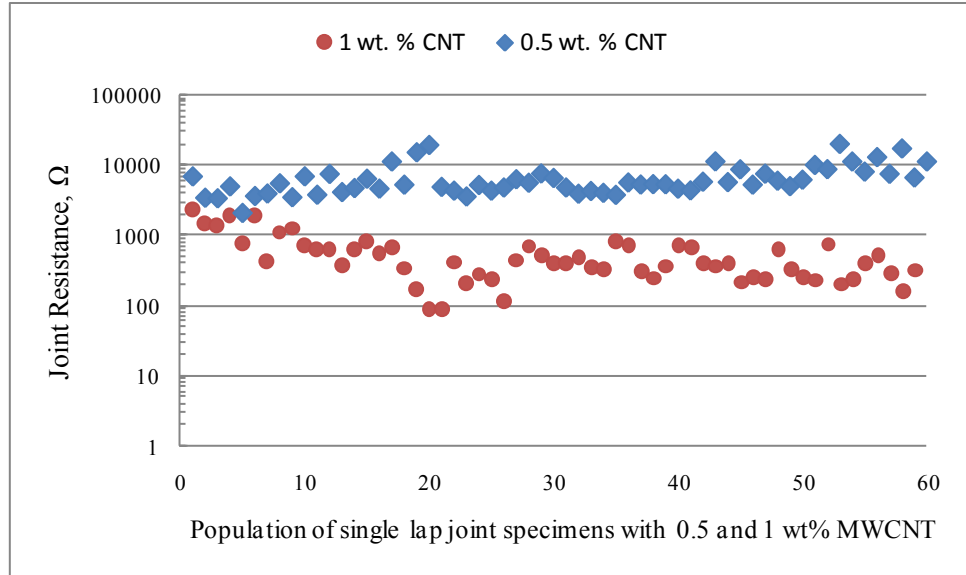


Figure 4-3 Resistance comparison between 0.5 and 1 wt% CNT loaded specimens

4.2.4 Adhesive Joints with 2 wt% MWCNT Loading

Electrical resistances of 10 specimens were measured and recorded prior to shear and fatigue tests. The results are shown in Figure 4-4. The average electrical resistance for 2 wt% MWCNT loaded joints was 63 Ω. The standard deviation of the data is 31 Ω.

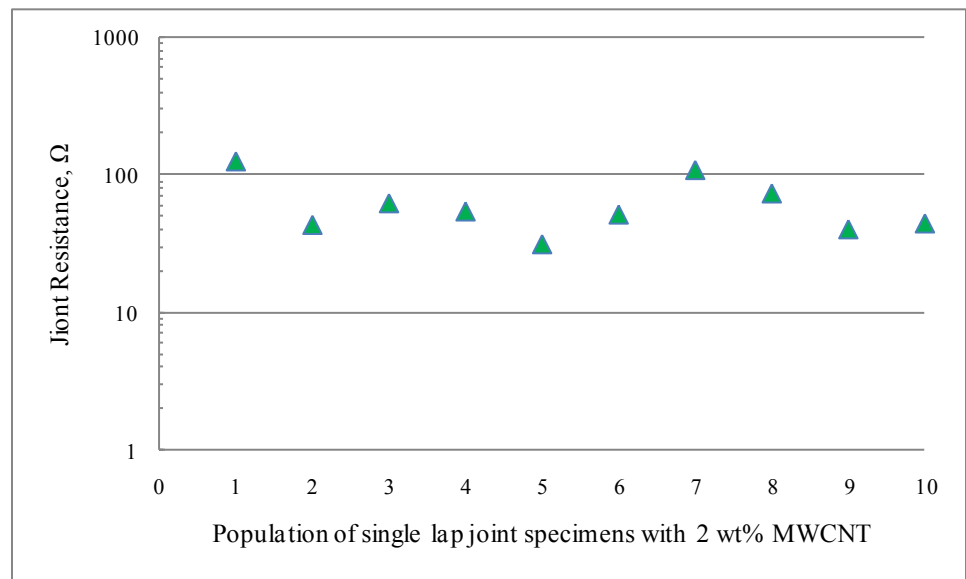


Figure 4-4 Joints electrical resistance for samples containing 2 wt% MWCNT

4.2.5 Summary

Joint with neat adhesive has resistance of $5 \times 10^{11} \Omega$. Adding 0.5 and 1 wt% of MWCNT decreased the resistance 7 and 8 orders of magnitude to 6877Ω and 550Ω respectively. By adding 2 wt% of MWCNT the resistance reduces 10 orders of magnitude to 63Ω . Therefore, the addition of MWCNT inside adhesive improved the electrical properties of the joints. Figure 4-5 shows the comparison between the average electrical resistances of the joints containing different concentrations of MWCNTs.

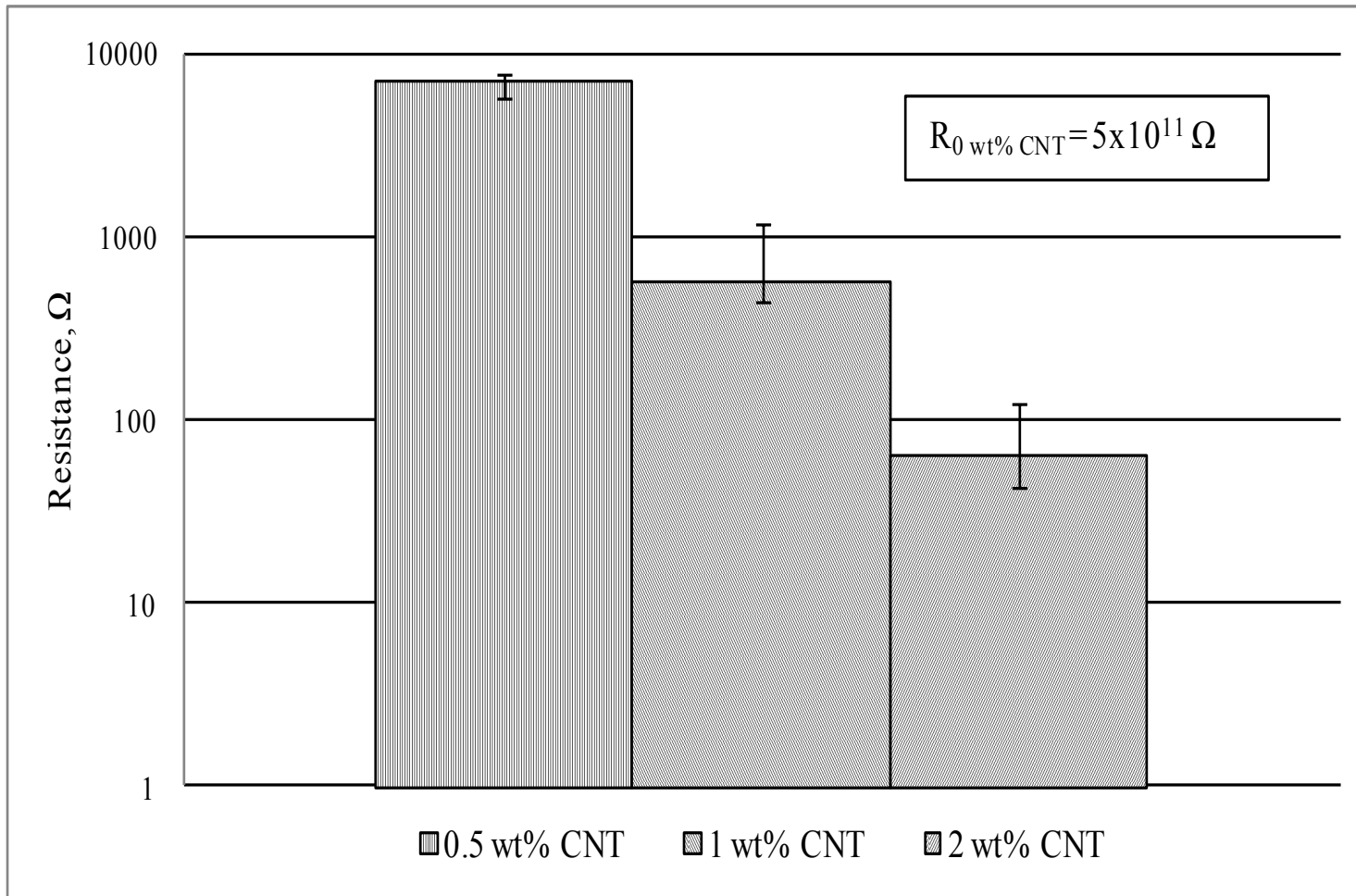


Figure 4-5 Average electrical resistance comparison between the joints containing 0, 0.5, 1, and 2 wt% MWCNT

4.3 Apparent Shear Strength

Apparent shear strength of the single lap joints was measured as explained in section 3.4.2. Joints with different MWCNT concentrations were tested to evaluate the effect of CNT addition on the mechanical properties of adhesive joints. 30 specimens for each CNT concentrations, namely as 0, 0.5, and 1 wt% were tested. In the case of the joints containing 2 wt% CNT, only 5 specimens were produced and shear tested. High concentrations of MWCNT create high content of agglomerates inside the adhesive and thus reduce the mechanical properties especially fatigue life. The fatigue results for joints containing 2 wt% MWCNTs showed dramatic reduction; therefore, the author considered 2 wt% CNT loaded specimens as not satisfactory and ceased testing more samples.

4.3.1 Apparent Shear Strength for Joints Containing 0 wt% MWCNT

Joints with neat adhesive were produced and tested as reference for comparison. The results for shear strengths of all 30 specimens are presented in Figure 4-6. The average apparent shear strength was calculated to be 17.5 MPa. The standard deviation of the data is 2.5 MPa.

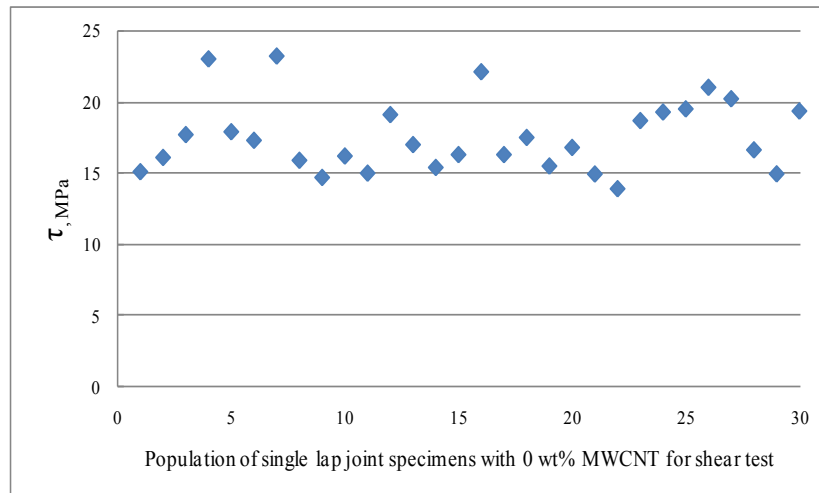


Figure 4-6 Joint apparent shear strength for specimens containing no MWCNT

4.3.2 Apparent Shear Strength for Joints Containing 0.5 wt% MWCNT

The apparent shear strengths of all 30 specimens containing 0.5 wt% MWCNT are presented in Figure 4-7. The average shear strength was calculated to be 19.6 MPa. The standard deviation of the data is 2.3 MPa. Since it was assumed that there would be a correlation between the joints initial resistance and final shear strength, the shear strengths of the joints were plotted versus initial electrical resistances ordered from the lowest resistance to the highest resistance and shown in Figure 4-8. However, on the contrary to the assumption, the results clearly indicate that there is no correlation between the initial resistance and the shear strength of the joints. Therefore, it is not possible to evaluate the quality of the joints only by measuring the initial electrical resistance prior to testing.

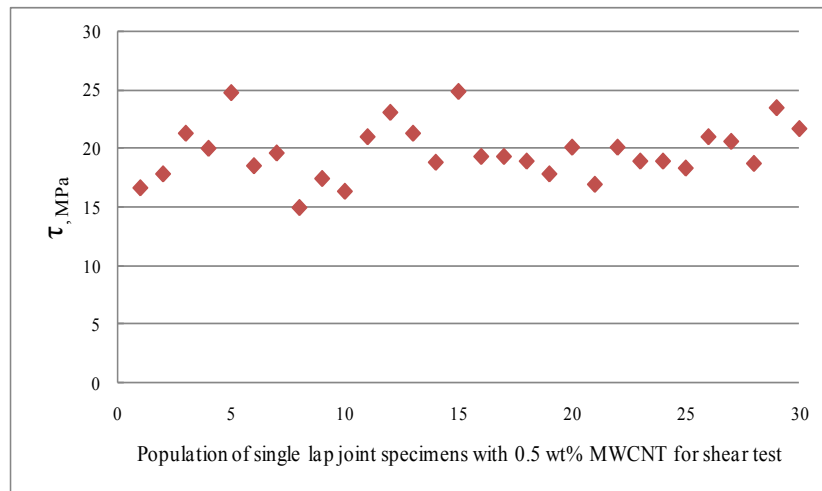


Figure 4-7 Joint apparent shear strength for specimens containing 0.5 wt% MWCNT

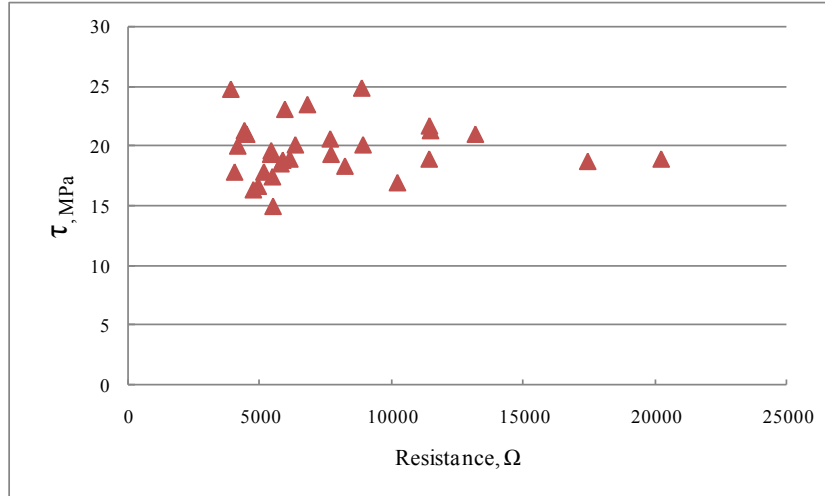


Figure 4-8 Shear strength vs. electrical resistance for single lap joints containing 0.5 wt% MWCNT

4.3.3 Apparent Shear Strength for Joints Containing 1 wt% MWCNT

Figure 4-9 shows the apparent shear strengths of all 30 specimens containing 1 wt% MWCNT. The average shear strength of the joints was 19 MPa. The standard deviation of the data is 2.3 MPa. Figure 4-10 shows the shear strength versus electrical resistance ordered from the lowest resistance to the highest resistance. As it is clear from the figure there is no correlation between the electrical resistance and shear strength of the joints containing 1 wt% MWCNT.

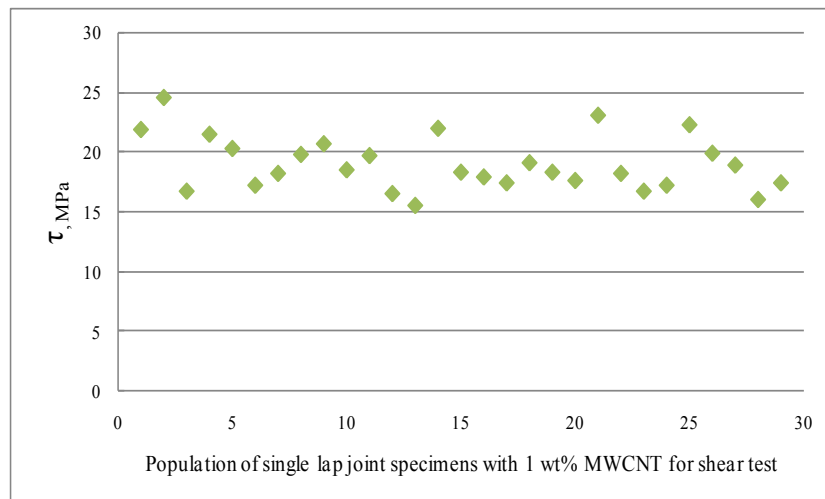


Figure 4-9 Joint apparent shear strength for specimens containing 1 wt% MWCNT

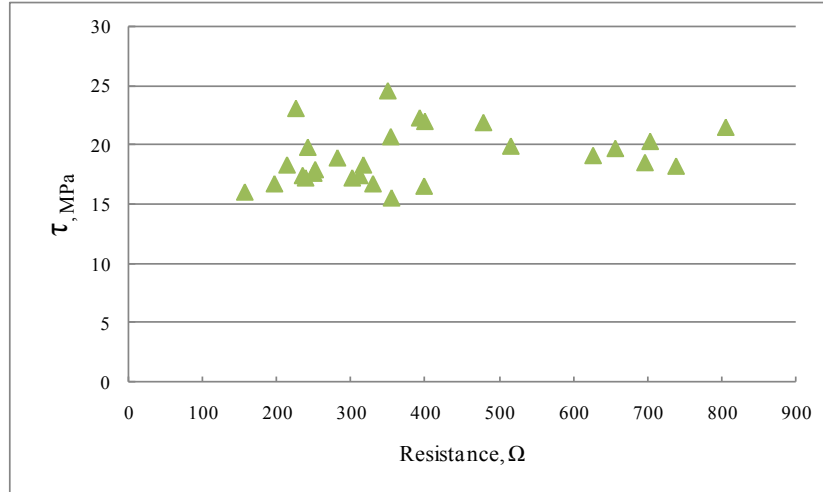


Figure 4-10 Shear strength vs. electrical resistance for single lap joints containing 1 wt% MWCNT

4.3.4 Apparent Shear Strength for Joints Containing 2 wt% MWCNT

Apparent shear strengths of all 5 specimens containing 2 wt% MWCNT are presented in Figure 4-11. The average shear strength was calculated as 19.7 MPa. The SD of the data is 1.9 MPa. Figure 4-12 shows the apparent shear strengths versus joint electrical resistances in ascending order. It indicates there is no correlation between the joints initial resistance and shear strength.

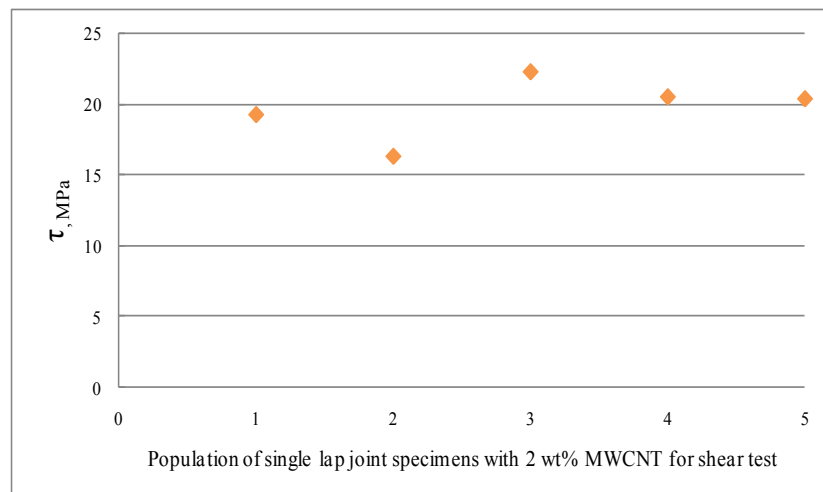


Figure 4-11 Joint apparent shear strength for specimens containing 2 wt% MWCNT

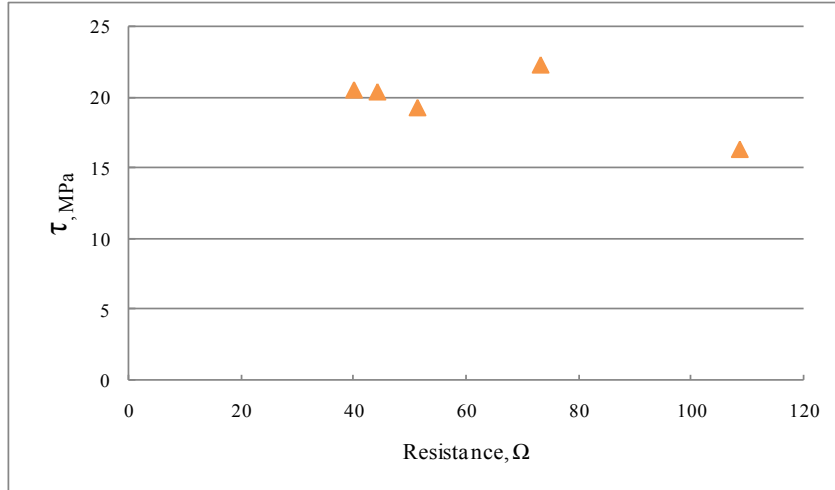


Figure 4-12 Shear strength vs. electrical resistance for single lap joints containing 2wt% MWCNT

4.3.5 Comparison

Figure 4-13 shows the comparison between the average shear strengths of single lap joints containing 0, 0.5, 1, and 2 wt% MWCNT.

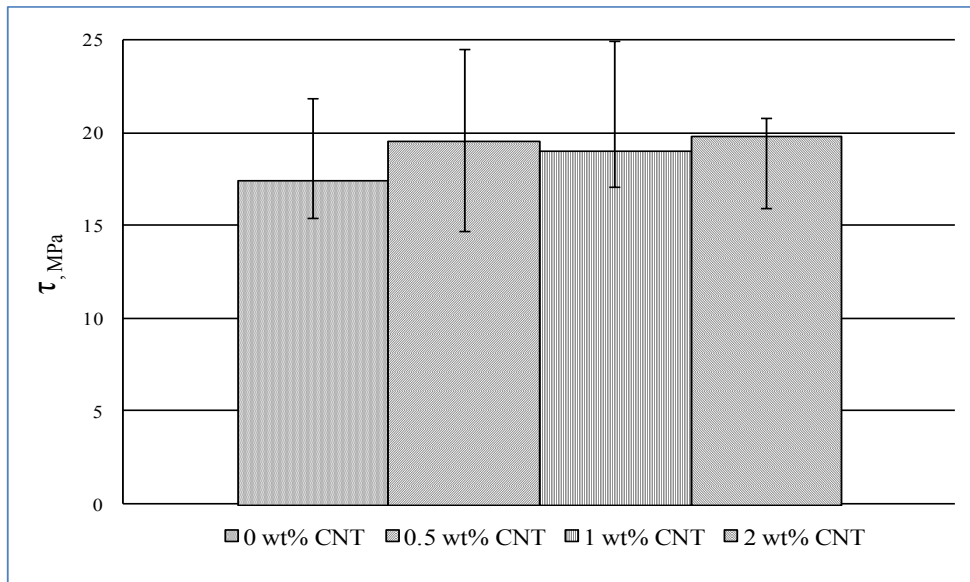


Figure 4-13 Average shear strength comparison between the joints containing 0, 0.5, 1, and 2 wt% MWCNT

4.3.6 Summary

Addition of MWCNT resulted in approximately 10% increase in shear strength of CNT reinforced bonded joints compared to the joints bonded with neat adhesive. However, increasing the amount of CNT from 0.5 to 2 wt% did not introduce significant difference on the shear strengths of the joints. Therefore, it is concluded that the addition of 0.5 wt% MWCNT is sufficient enough to improve the shear strength of adhesively bonded joints.

4.3.7 Fracture Mechanism

Fracture mechanism of adhesive joints can be categorized into 3 types, cohesive, adhesive and substrate failure. In cohesive failure mode, the fracture occurs inside the adhesive layer and the evidence of such a fracture mechanism is the existence of adhesive on both substrates after bond failure. This failure mode occurs due to degradation of the strength and other mechanical properties of the adhesive which can be caused by curing errors in manufacturing stage or by environmental attacks in service [18]. Adhesive failure mode represents the failure in the interfacial layer between the adhesive and the substrates. This failure usually occurs due to insufficient bonding strength between the adhesive layer and the substrates. In this type of failure mode, the adhesive stays on one substrate after fracture. Substrate failure, which the name clearly describes it, occurs while the substrate strength is lower than the bond. Figure 4-14 shows the fracture surface of specimens containing 0.5 wt% and 1 wt% MWCNTs after they were broken. The fracture surfaces clearly indicate that the fracture mechanism of all samples were adhesive failure.

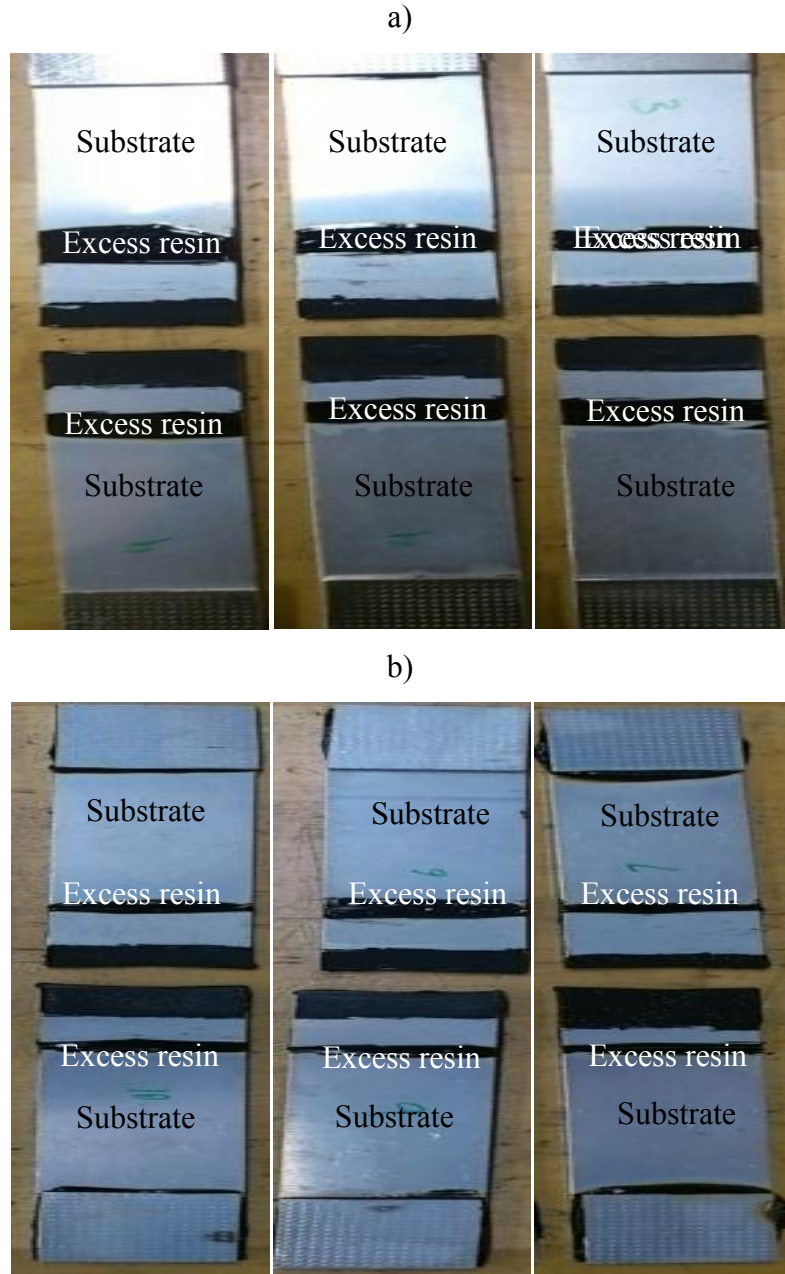


Figure 4-14 Fracture surface of specimens a) containing 0.5 wt% and b) 1 wt% MWCNT

4.4 Fatigue

The test set-up and procedures for fatigue test were explained in section 3.4.3. 30 single lap joints of each MWCNT concentrations except for 2 wt% were fatigue tested. For 2 wt% MWCNT concentration only 5 specimens were tested. Fatigue tests were performed

on the specimens based on two objectives, 1) to compare the fatigue life of single lap joints containing different percentages of CNT 2) to evaluate the state of the joints during their fatigue life by using electrical resistance technique. Since the addition of MWCNTs to the adhesive was a requirement for our in-situ health monitoring technique, it was important to make sure that their addition would not deteriorate the fatigue life of the adhesive joints. Therefore, this section explains the results achieved for the first objective.

4.4.1 Fatigue Life for Single Lap Joints Containing No MWCNTs

Single lap joints with neat epoxy adhesive were fatigue tested. The results were used as reference for comparison. The maximum load was set at 60% of the average shear load. The average shear load for samples with neat epoxy was 8300 N thus the maximum load was set to 5000 N. The ratio between the max loading and min loading was 0.1 hence the min load was set to 500 N. Figure 4-15 shows the fatigue life of all 30 single lap joints with no MWCNTs. Fatigue results usually have large scatter due to the complexity of the test itself, therefore, the fatigue life distribution is shown in Figure 4-16. The average fatigue life of the joints with 0 wt% MWCNT was calculated as the average of the fatigue lives of all 30 specimens tested and it was 20,900 cycles. The failure mechanism was observed to be mainly adhesive. Figure 4-17 shows the fracture surface of a single lap joint with no MWCNTs which was broken due to fatigue loading. Multiple cracks are also visible in the image.

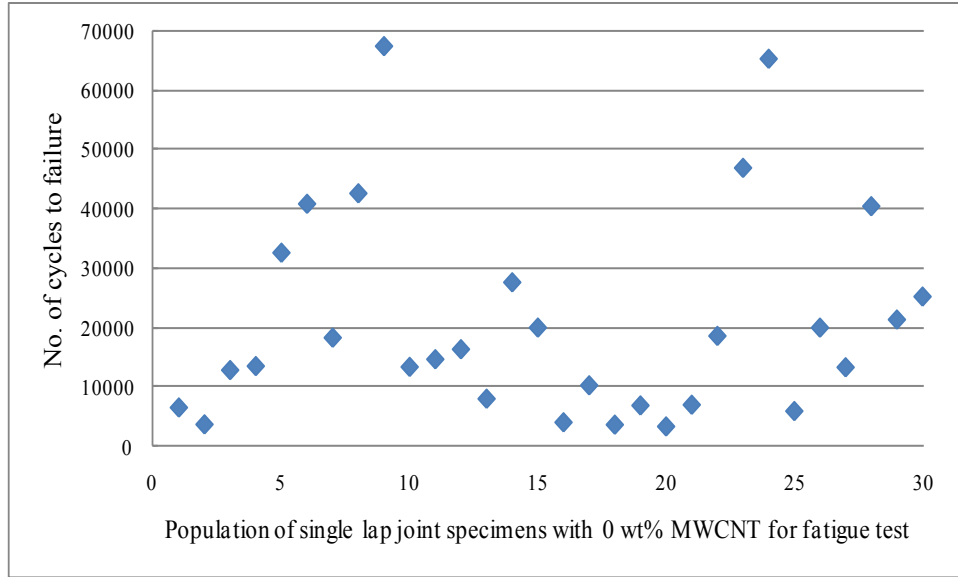


Figure 4-15 Single lap joint fatigue life for specimens containing 0 wt% MWCNT

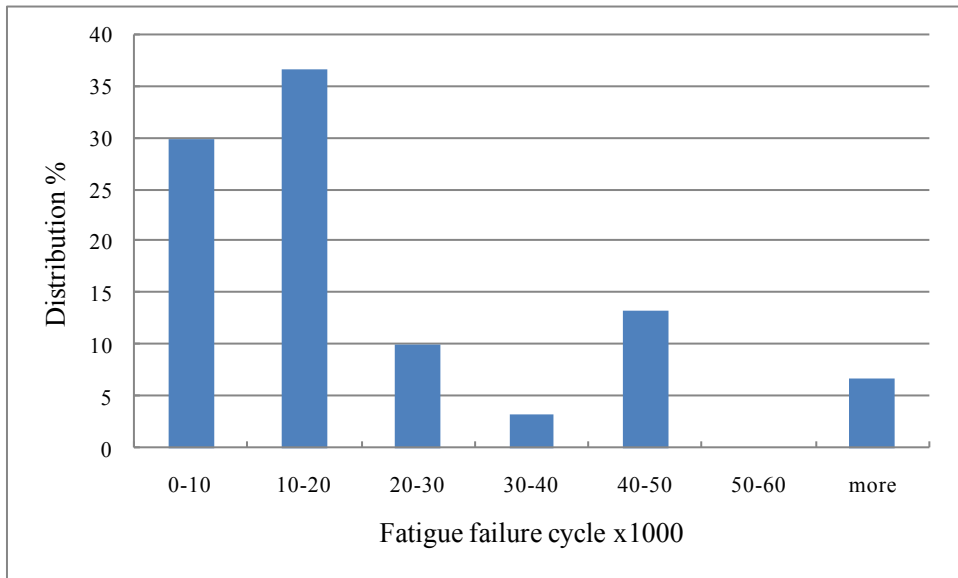


Figure 4-16 Single lap joints fatigue life distributions for specimens with 0 wt% MWCNT

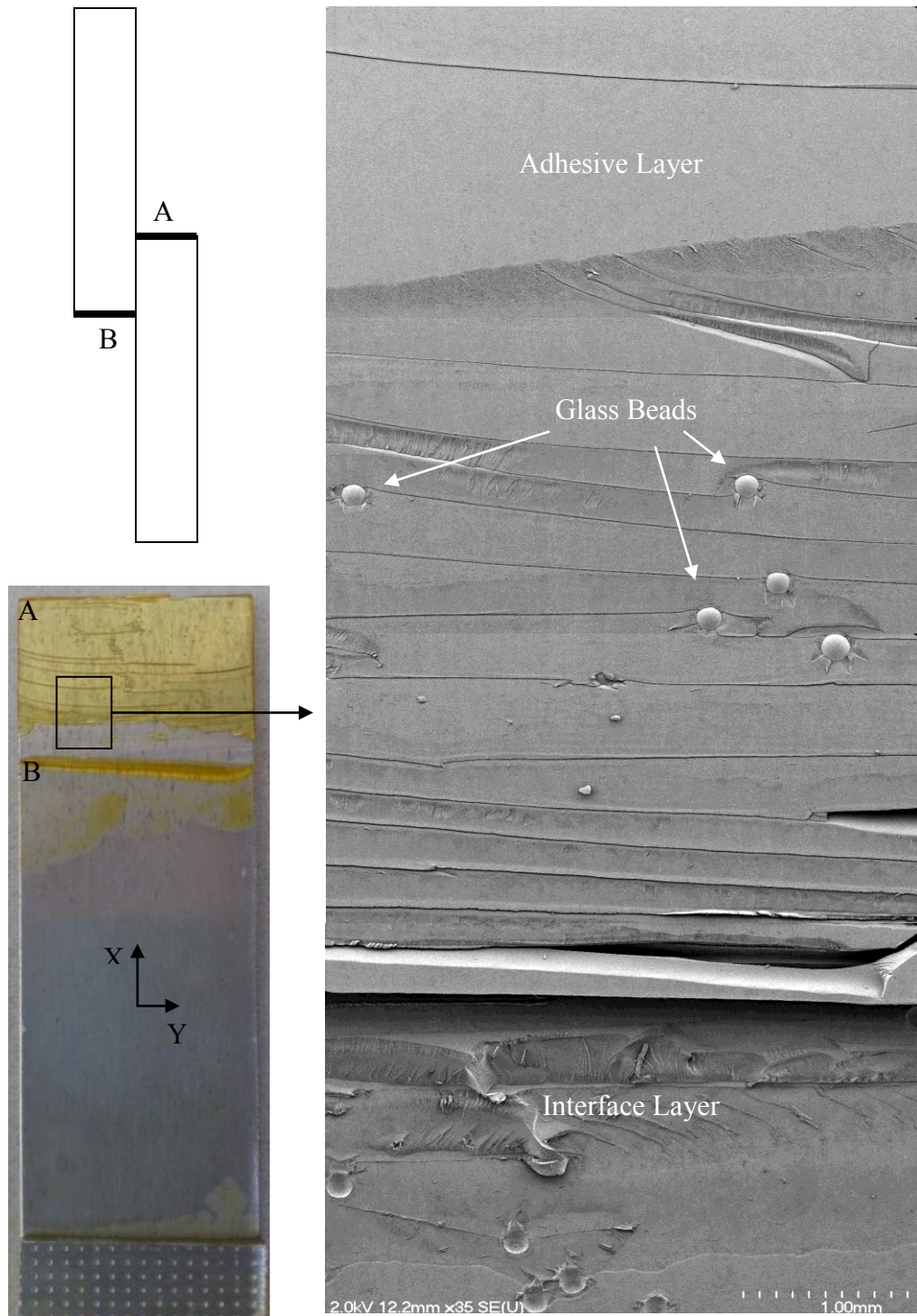


Figure 4-17 SEM image of a fracture surface of a sample containing no MWCNTs after the sample was broken due to fatigue loading

4.4.2 Fatigue Life for Single Lap Joints Containing 0.5 wt% MWCNTs

30 specimens containing 0.5 wt% MWCNT were fatigue tested. The maximum loading for fatigue tests was set as 5700 N corresponding to 60% of the average shear load, 9500 N, calculated in shear tests. The minimum load for fatigue test was set as 570, 10% of the maximum load. Figure 4-18 displays the fatigue life of all 30 samples containing 0.5 wt% MWCNT. The fatigue life distribution is shown in Figure 4-19.

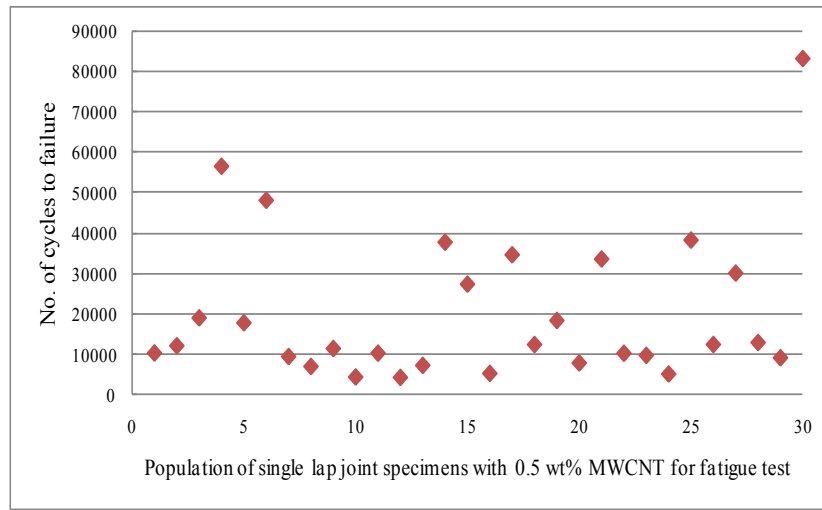


Figure 4-18 Single lap joint fatigue life for specimens containing 0.5wt% MWCNT

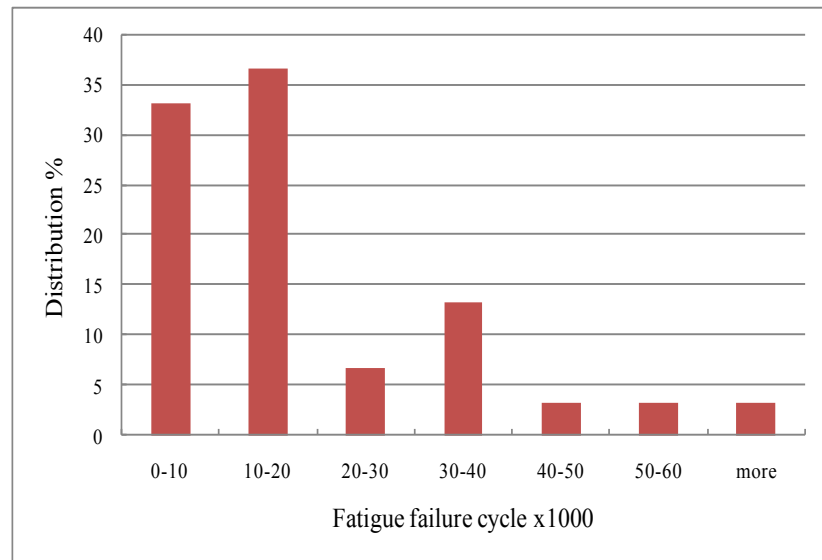


Figure 4-19 Single lap joints fatigue life distributions for specimens with 0.5 wt% MWCNT

The average fatigue life of the joints with 0.5wt% MWCNT was calculated as the average of the fatigue lives of all 30 specimens tested and it was 20,040 cycles. SEM image on fracture surface of single lap joints containing 0.5 wt% MWCNTs are given in section4.5.1.

4.4.3 Fatigue Life for Single Lap Joints Containing 1 wt% MWCNTs

30 specimens containing 1 wt% MWCNT were fatigue tested while the maximum load was set as 5500, 60% of the average shear load which was calculated as 9200. The minimum load was 550, 10% of the maximum load. Figure 4-20 and Figure 4-21 show the fatigue life and the distribution of the fatigue life of all the specimens containing 1 wt% MWCNT. The average fatigue life of the joints with 1wt% MWCNT was calculated as the average of the fatigue lives of all 30 specimens tested and it was 25,300 cycles. SEM image on fracture surface of single lap joints containing 1 wt% MWCNTs are given in section 4.5.2.

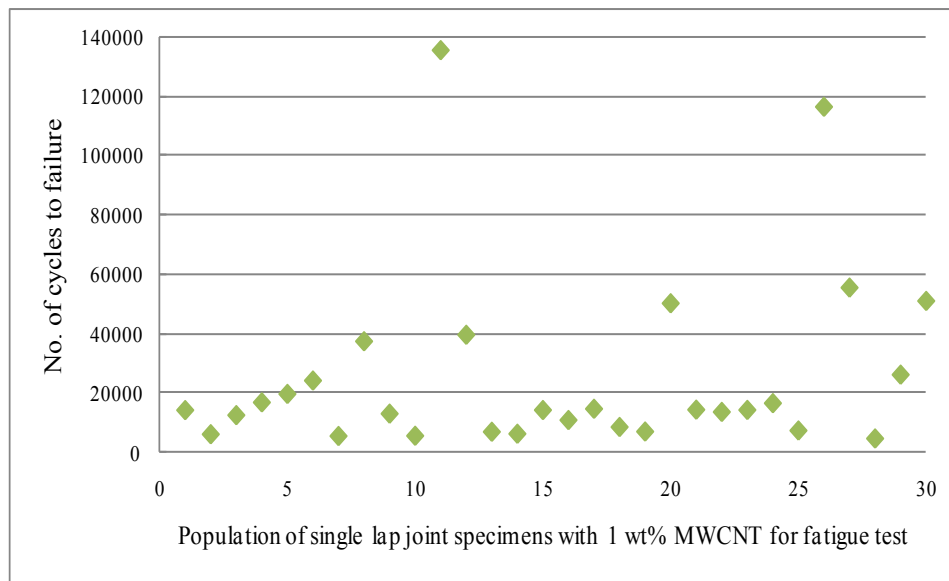


Figure 4-20 Single lap joint fatigue life for specimens containing 1 wt% MWCNT

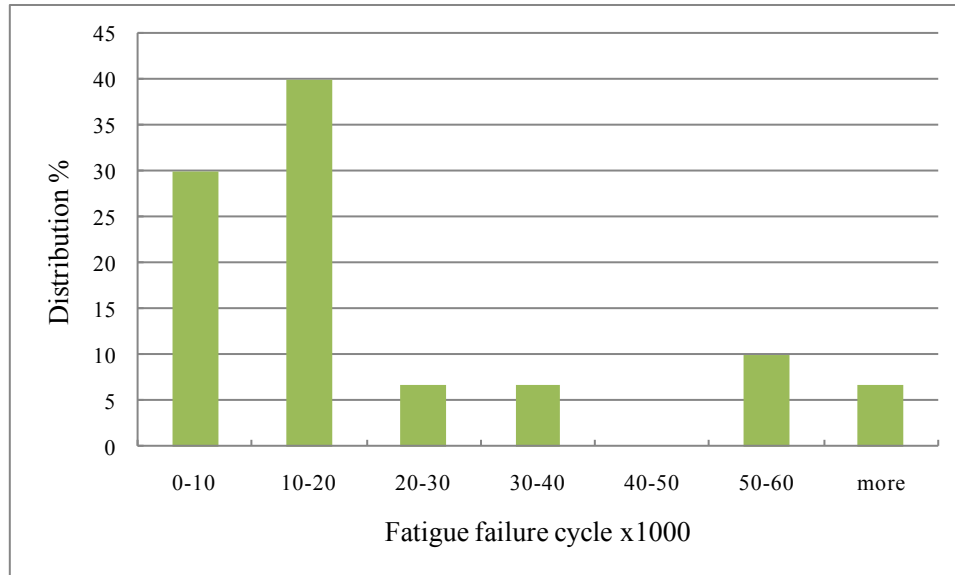


Figure 4-21 Single lap joints fatigue life distributions for specimens with 1 wt% MWCNT

4.4.4 Fatigue Life for Single Lap Joints Containing 2 wt% MWCNTs

Even though the average shear strength of the joint containing 2 wt% MWCNT, as 19.7 MPa, was more than the joints with neat epoxy, the results for fatigue tests were not promising. Consequently, only 5 specimens were tested for fatigue. The fatigue life of the samples is shown in Figure 4-22. As the figure indicates all the samples were broken bellow 20,000 cycles and the average fatigue life was calculated as 8450 cycles. The results show that the addition of 2 wt% MWCNTs results in approximately 40% reduction in their fatigue life compared to the joints with neat epoxy. Hence, it is clear that the addition of 2 wt% or more MWCNTs is not effective to improve the mechanical properties of adhesive joints due to the fact that the large numbers of CNT agglomerates which are more possible to be formed with high amount of CNT loadings, lead to the weakening of the adhesive joint.

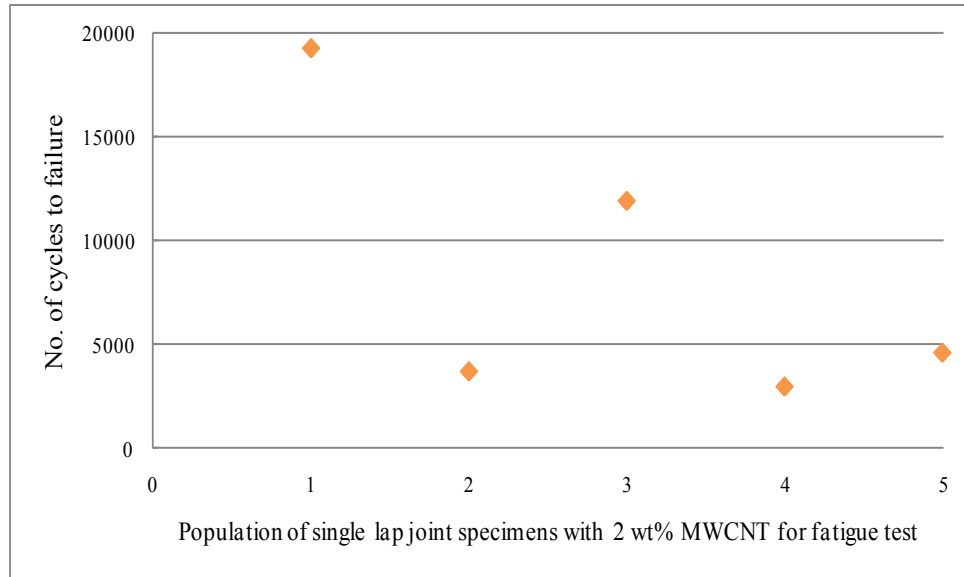


Figure 4-22 Single lap joint fatigue life for specimens containing 1 wt% MWCNT

4.4.5 Comparison and Summary

Figure 4-23 shows the fatigue life distributions of the single lap joints with different CNT loadings. The figure indicates that different MWCNTs loadings (except for 2 wt%) follow the same trend. For all the samples containing 0, 0.5, 1 wt% MWCNTs approximately 70% of them were broken below 20,000 cycles and the rests were broken above 20,000 cycles. However, for the joints containing 2 wt% MWCNTs, all 5 specimens were broken below 20,000 cycles. The average fatigue life of each MWCNTs loading was calculated by dividing the sum of all samples fatigue lives of that CNT loading by the total number of samples. The results are shown in Figure 4-24. The result shows no significant change in fatigue life due to addition of 0.5 wt% CNT. However, introducing 1 wt% CNT improved the average fatigue life by 20%. Nanotube bridging, pullouts and breakage contributed to increase in fatigue life. Figure 4-25 and Figure 4-26 show SEM images of CNT bridging on fracture surface of samples containing 0.5 and 1 wt% which were broken through fatigue test. Increasing CNT concentration up to 2 wt%

dramatically reduced the fatigue life. High CNT concentration resulted in high agglomerates and these reduced the joint fatigue failure cycle. It is also important to mention that adhesive failure was the failure mechanism in all the specimens. SEM images of Single lap joint fracture surface with nanotubes are shown in section 4.5.

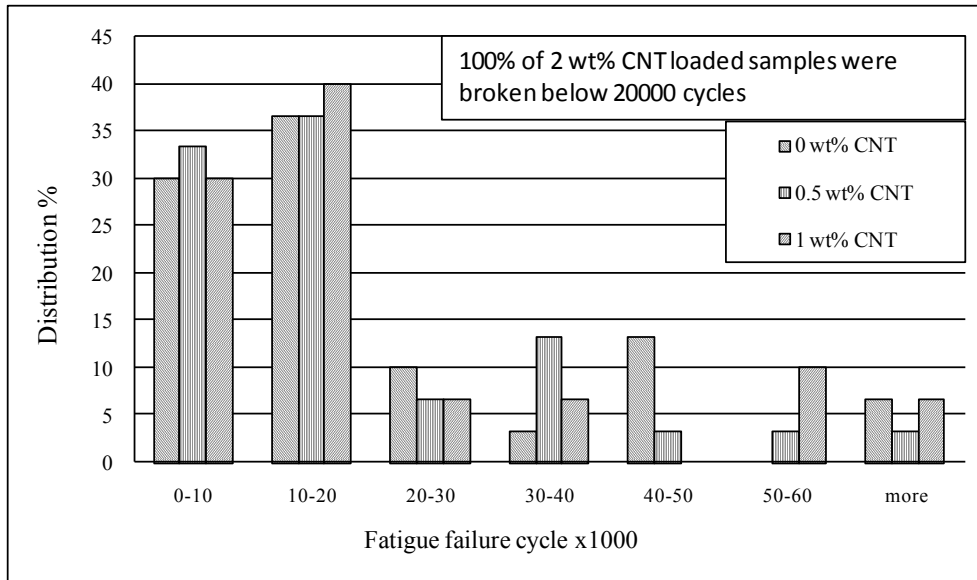


Figure 4-23 Single lap joints fatigue life distributions for specimens with different MWCNT loadings

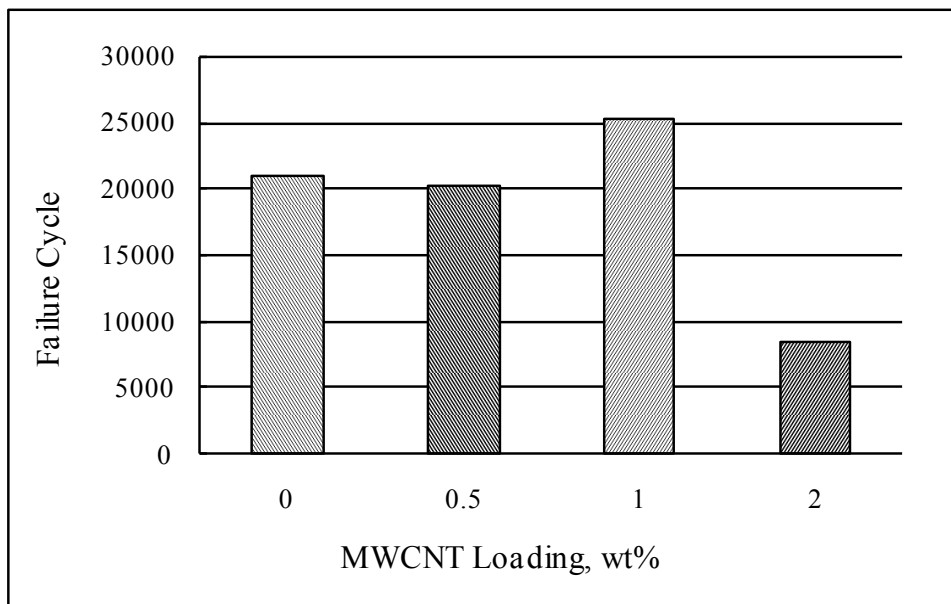


Figure 4-24 Single lap joints average fatigue failure cycles for different CNT loadings

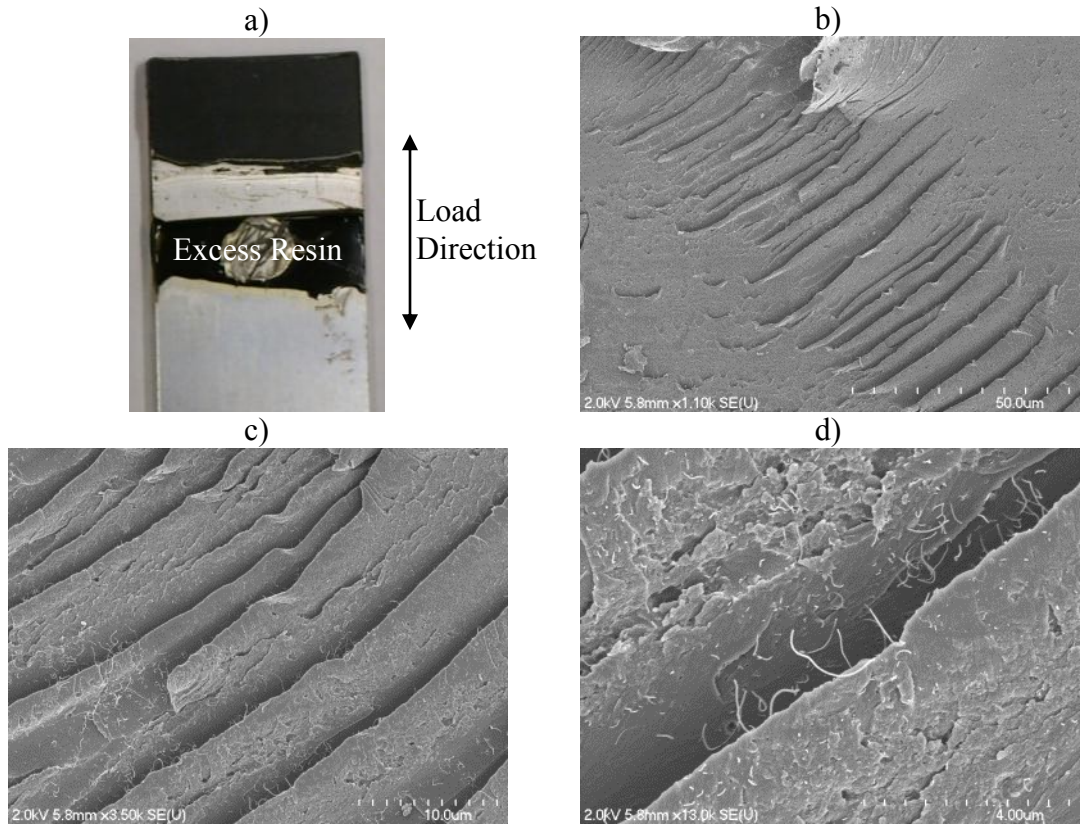


Figure 4-25 SEM images of fracture surface of a samples containing 0.5wt% MWCNT showing CNT bridging in different magnifications a) shows the fracture surface and b, c, and d show magnified images

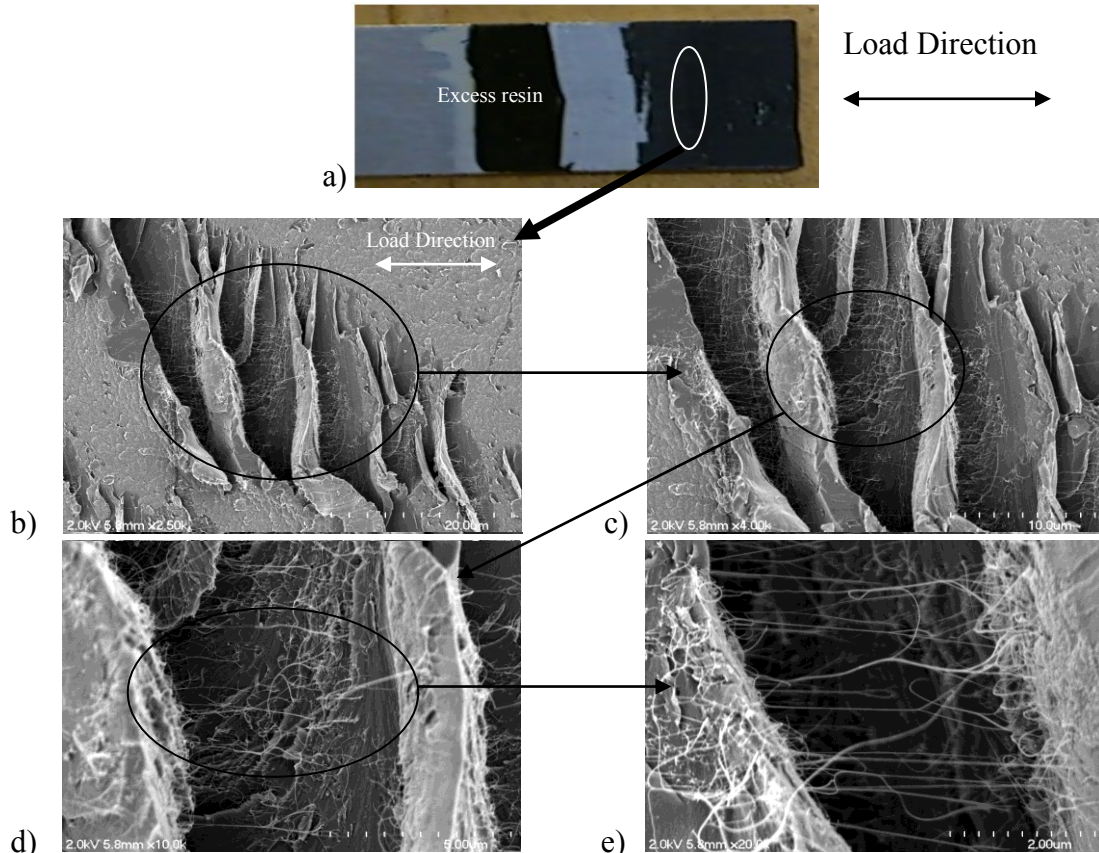


Figure 4-26 SEM images of fracture surface of a samples containing 1 wt% MWCNT showing CNT bridging in different magnifications a) shows the fracture surface and b, c, d and e show magnified images

4.5 In situ Health Monitoring during Fatigue Test

The electrical resistance signatures of all the samples that were fatigue tested were recorded during the tests. The change in resistance from the initial joint resistance was used as a reference to evaluate the state of the joint. It was assumed that the increase in resistance would occur while cracks initiated and propagated and continued to increase dramatically till the final failure of the joint.

4.5.1 Single lap joints containing 0.5 wt% MWCNT

Figure 4-27 to Figure 4-36 show 5 examples of electrical resistance signature and electrical resistance ratio of the joints containing 0.5 wt% MWCNTs. The electrical resistance signatures and ratios for all the specimens are shown in Appendix I. Each

graph provides the initial resistance, final resistance and the failure cycle of the joints. Samples numbering is based on the concentration of the nanotubes, for instance, sample 0.5-11 represents sample number 11 which contains 0.5 wt% MWCNTs. The numbering of the samples from 1 to 30 is completely arbitrary and is only a means to refer to the specimens. Electrical resistance ratio is referred to the change ratio of the electrical resistance of joints at every second from the initial joint electrical resistance. Figure 4-37 shows the superposition of normalized resistance ratios of the 5 example specimens.

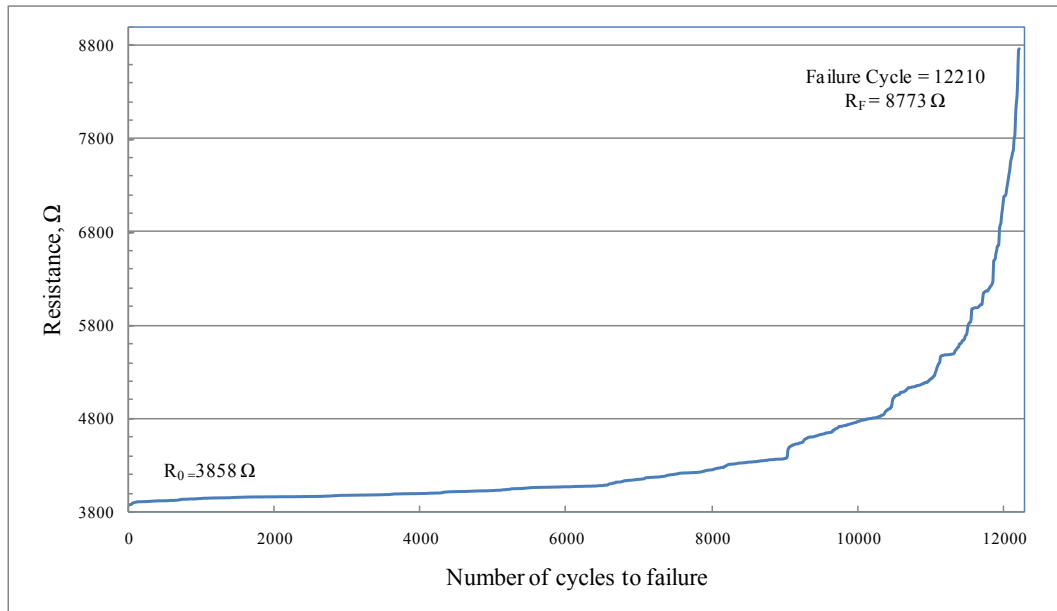


Figure 4-27 Electrical resistance signature vs. fatigue life of sample number 11 containing 0.5 wt% MWCNTs (sample 0.5-11)

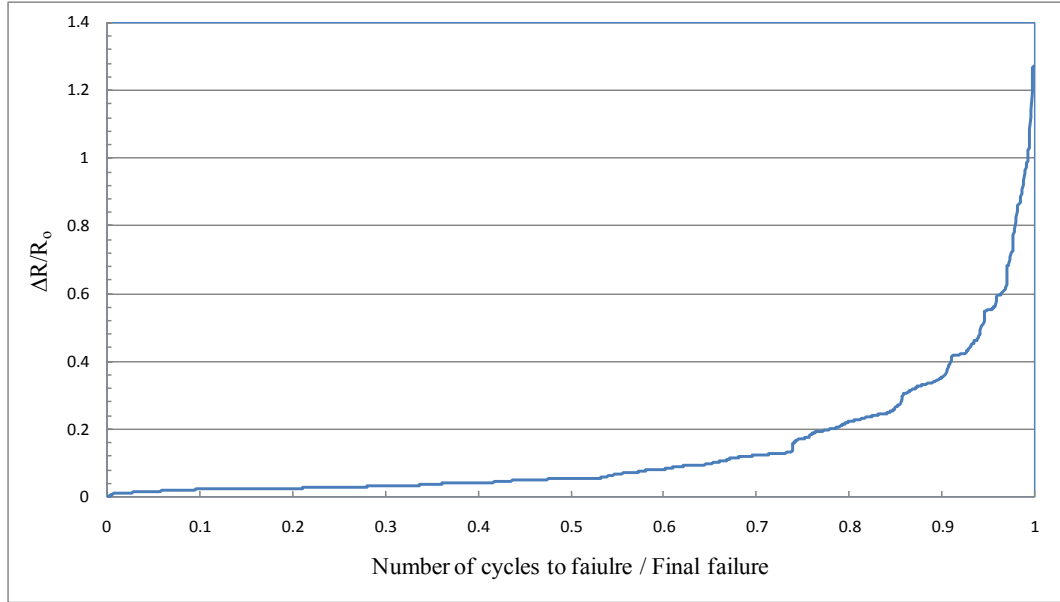


Figure 4-28 Electrical resistance ratio vs. fatigue life for sample 0.5-11

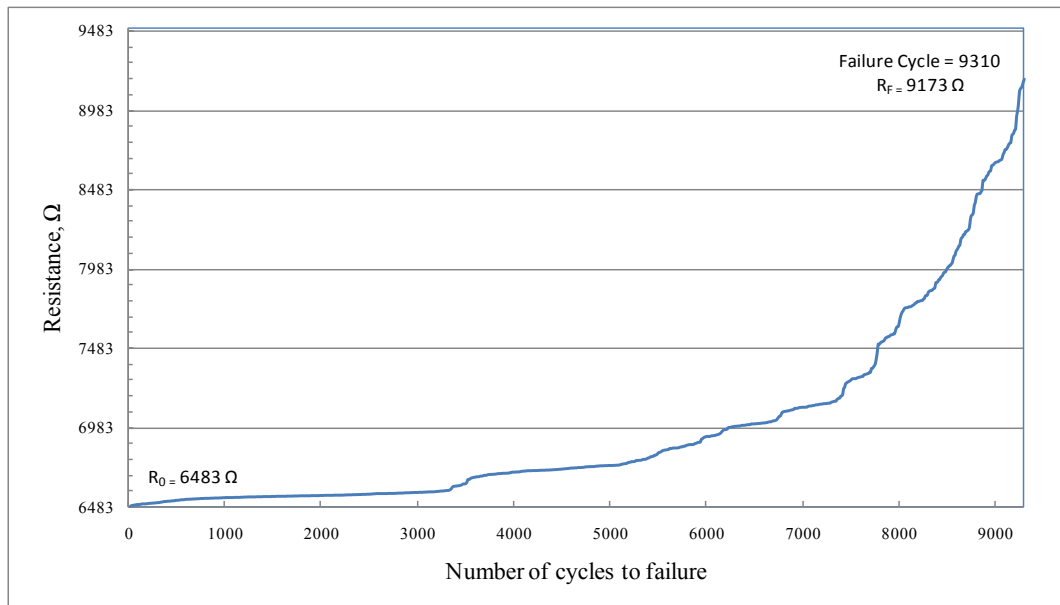


Figure 4-29 Electrical resistance signature vs. fatigue life of sample number 15 containing 0.5 wt% MWCNTs (sample 0.5-15)

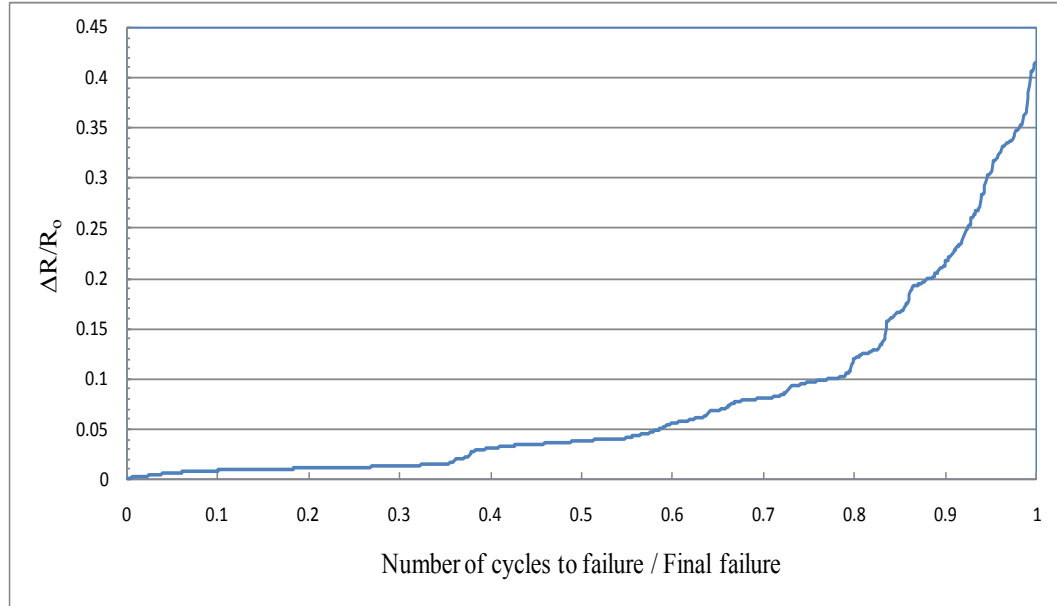


Figure 4-30 Electrical resistance ratio vs. fatigue life for sample 0.5-15

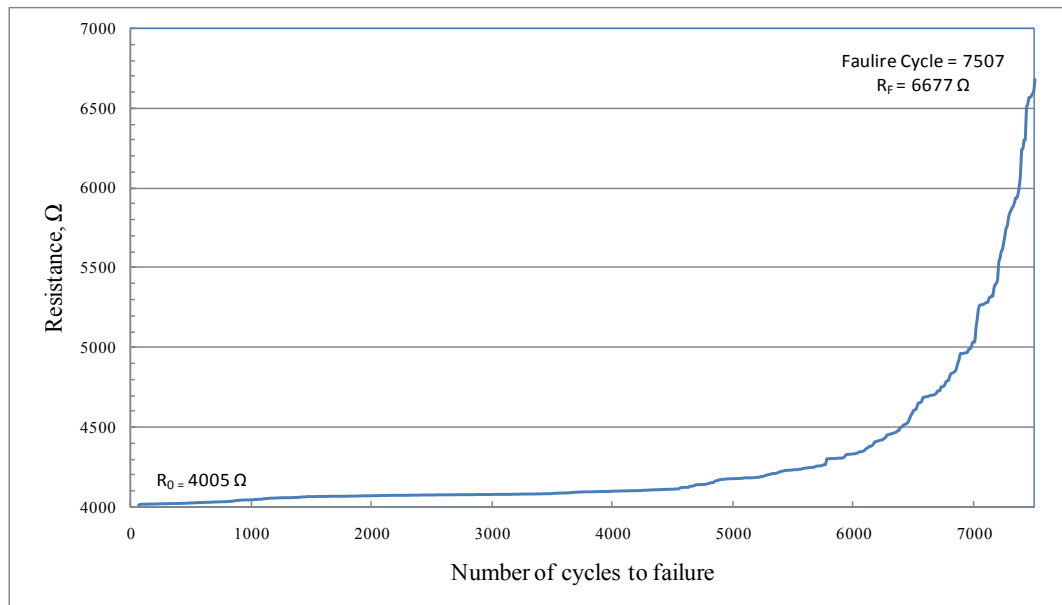


Figure 4-31 Electrical resistance signature vs. fatigue life of sample number 16 containing 0.5 wt% MWCNTs (sample 0.5-16)

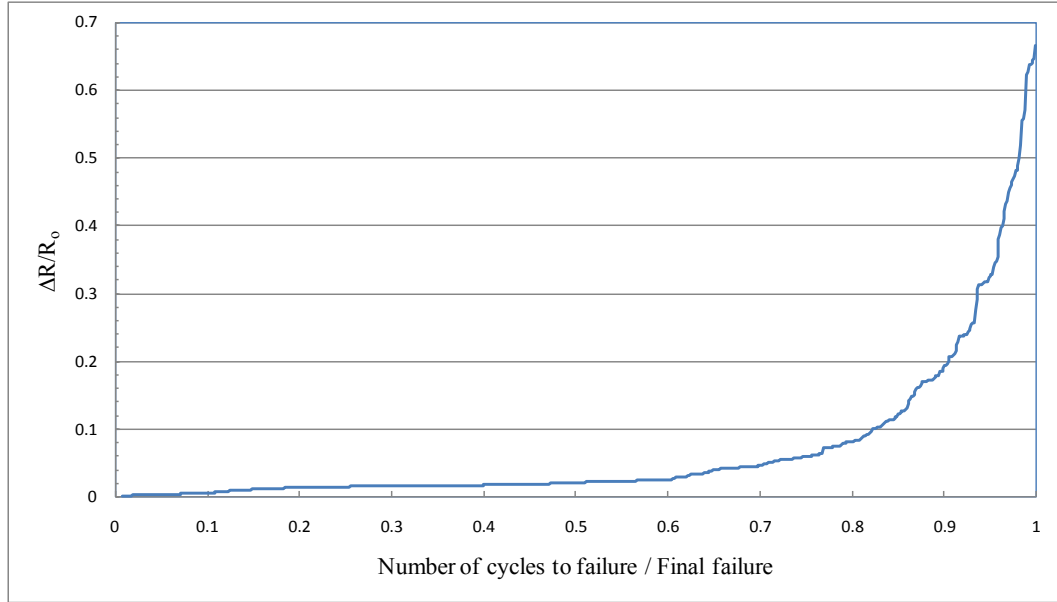


Figure 4-32 Electrical resistance ratio vs. fatigue life for sample 0.5-16

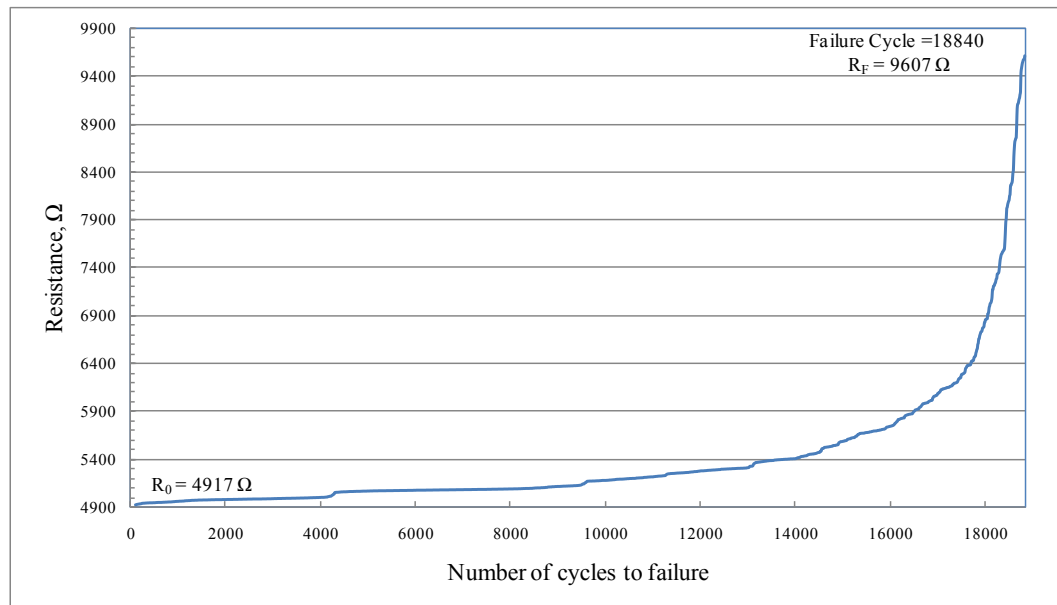


Figure 4-33 Electrical resistance signature vs. fatigue life of sample number 21 containing 0.5 wt% MWCNTs (sample 0.5-21)

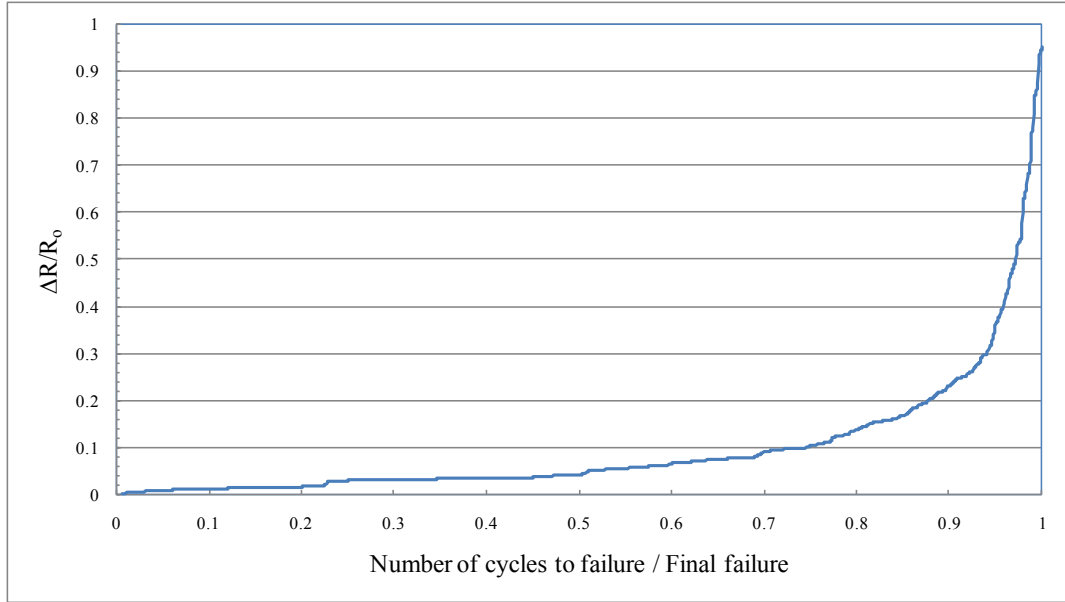


Figure 4-34 Electrical resistance ratio vs. fatigue life for sample 0.5-21

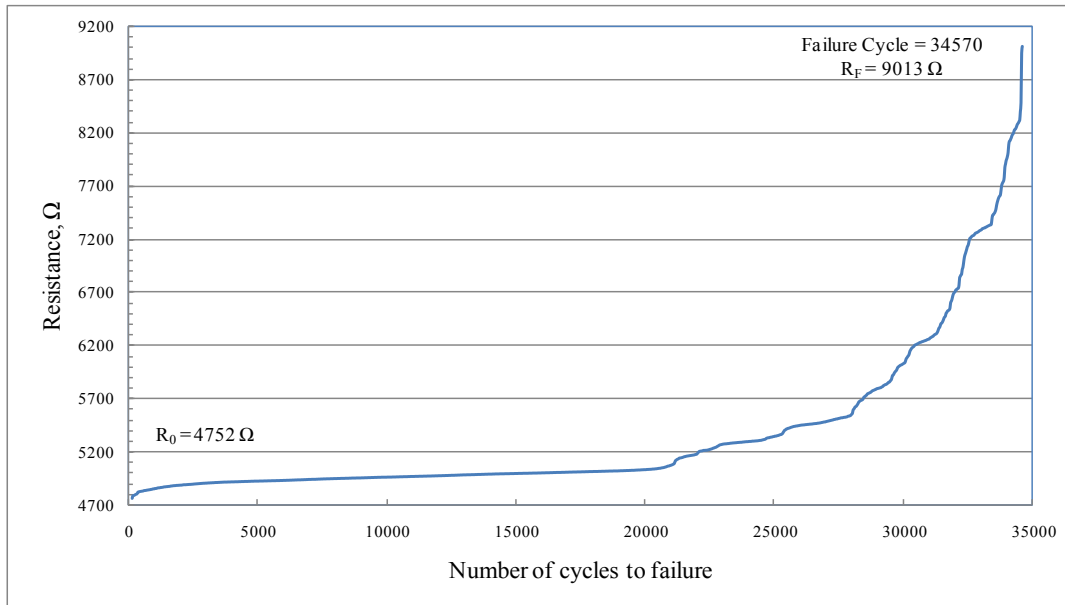


Figure 4-35 Electrical resistance signature vs. fatigue life of sample number 26 containing 0.5 wt% MWCNTs (sample 0.5-26)

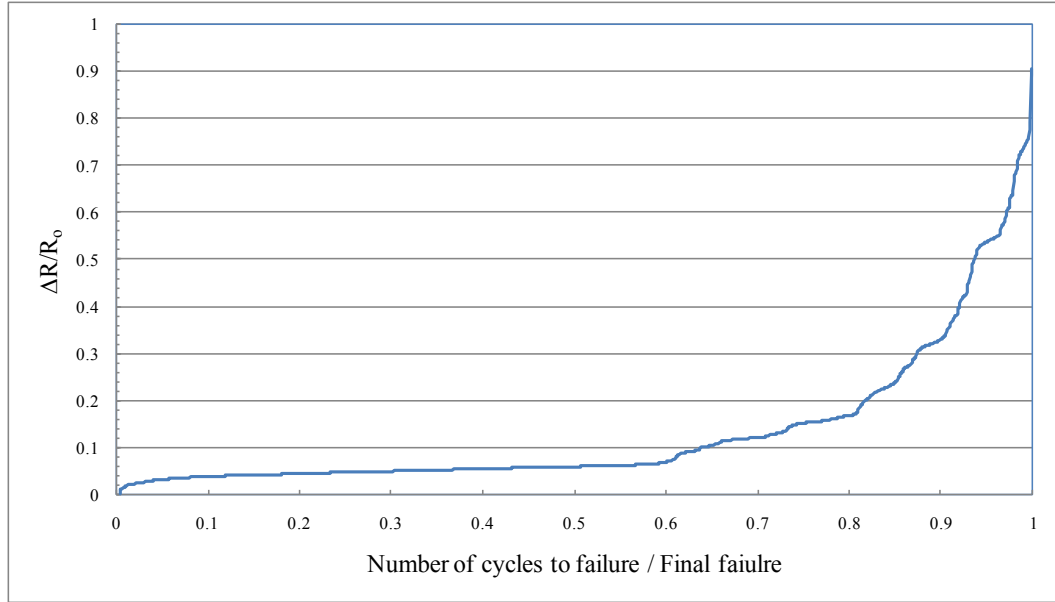


Figure 4-36 Electrical resistance ratio vs. fatigue life for sample 0.5-26

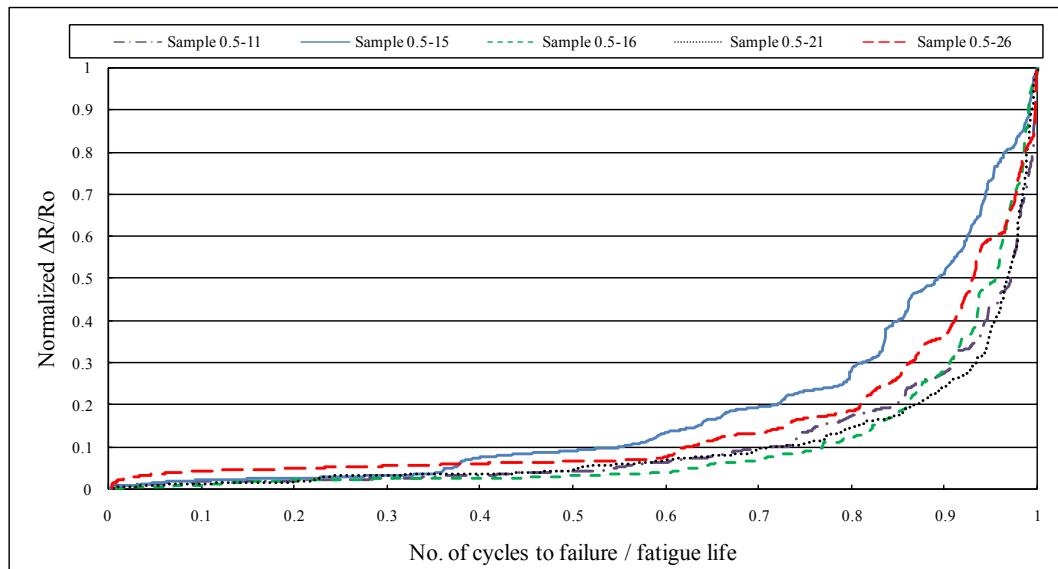


Figure 4-37 Superposition of normalized electrical resistance ratios of the 5 example specimens containing 0.5 wt% MWCNT

Figure 4-38 shows the average electrical resistance signatures of samples containing 0.5 wt% MWCNTs. The average electrical resistance change at each 10% fatigue life interval was calculated and the measured values were plotted. Then the Trendline function was used to draw and calculate the best curve to fit the data. The curve shows that the change

in electrical resistance follows an increasing pattern throughout the fatigue test. At the beginning of the fatigue test the resistance change is negligible or minimal, between 0 to 10% increase of the initial resistance; as the test progresses the resistance perturbation increases rapidly, to more than 10% of the initial value; finally as the specimen approaches its final failure the resistance change becomes more pronounced and follows a drastic increase to more than 50% of the initial resistance.

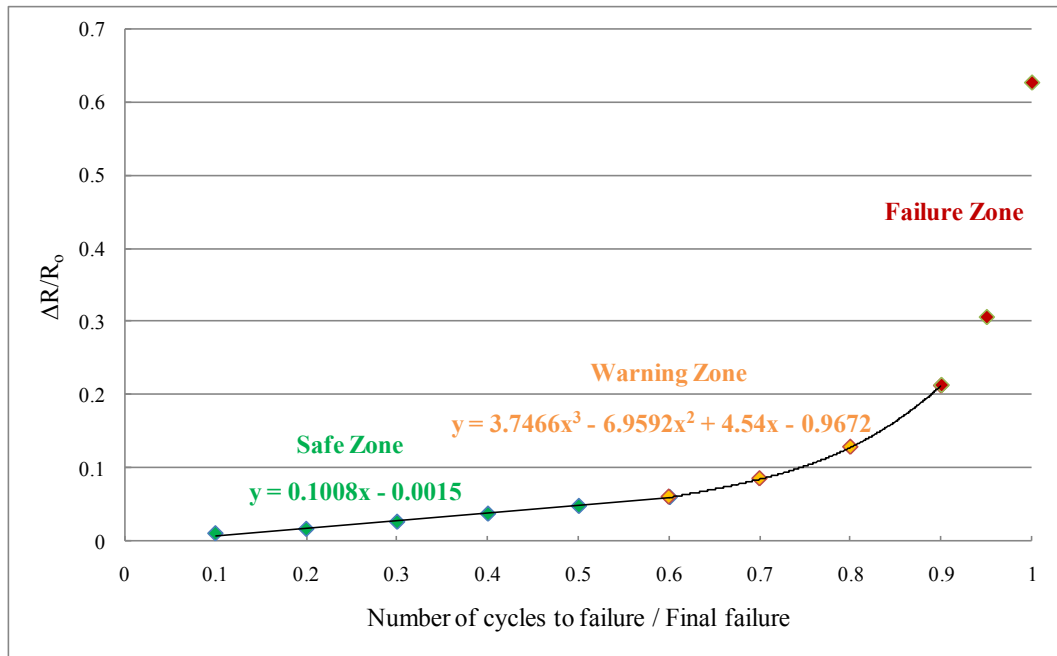


Figure 4-38 Average electrical resistance signatures of all 30 specimens containing 0.5 wt% MWCNTs

The resistance signature therefore, can be divided into three phases or zones and each phase can be recognized by the amount of change in resistance and/or by the slope of the curve. Phase 1, which is the safe zone, contains up to 60% of the joints life. This zone can be recognized either by resistance change of less than 10% of the initial resistance or by the slope of the resistance signature curve of less than 0.1 ($\Omega/100$ Cycle). A Matlab code was generated to calculate the resistance curve slope at each point. The slight change in resistance can be explained by initiation of few cracks inside the adhesive layer which in

turn breaks the carbon nanotube networks. This zone is considered as the safe zone since it covers up to 60% of the life of the samples with no evidence of catastrophic damage which would impair the application of the joint. Therefore, if the resistance signature of a single lap joint indicates that the joint is in this phase the joint is safe for its performance.

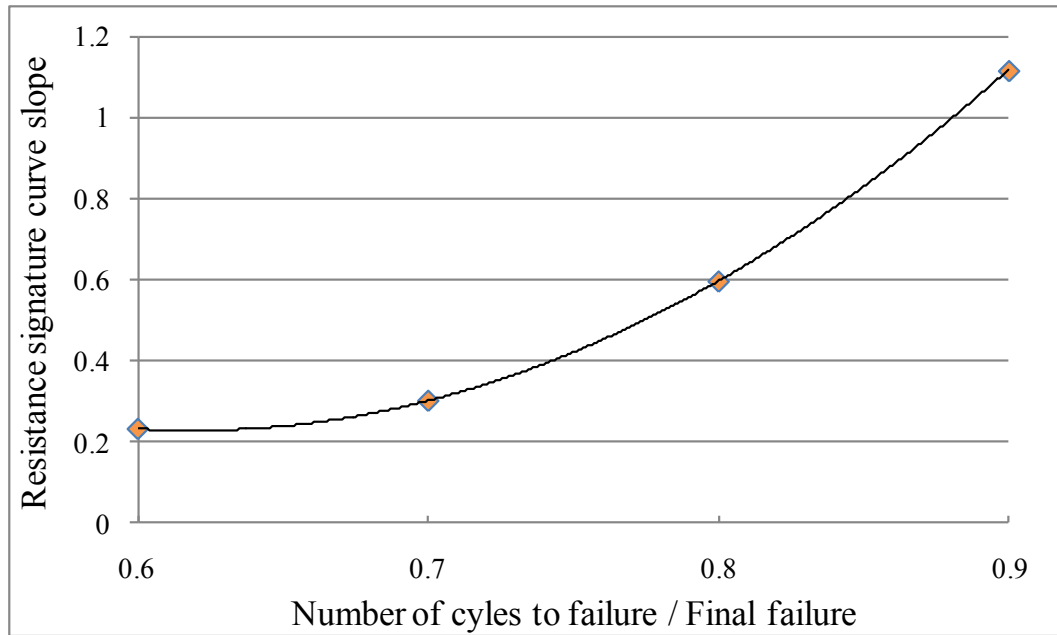


Figure 4-39 Slope of the average resistance signature curve from 60% of the life to 90% of the life

Phase 2, the transition zone, covers from 60% to 90% of the joints fatigue life. In this phase the resistance change from the initial value becomes more pronounced and picks up to more than 10% increase and on average reaches 20% increase of the initial resistance. The first derivative of the fit curve equation was used to plot the slope of the resistance curve between 60 to 90% fatigue life intervals. The results indicates when the resistance signature shifts from phase 1 to phase 2, the signature curve slope changes dramatically and reaches to 1 ($\Omega/100$ Cycle) between 80 to 90% of the fatigue life (Figure 4-39). The pronounced increase in resistance in this phase can be explained by multiple cracks which in turn break more of the nanotube network and reduces the

number of electrical paths dramatically. Figure 4-40 shows SEM images of multiple cracks in the form of striation on the fracture surface of the adhesive joints which contributed to the dramatic increase in the resistance. This zone is considered as the caution zone or warning zone. Two warning points are associated with this zone, the first is the resistance change of more than $10\%+2\%$ of the initial value which for 93% of the samples occurred between 60 to 90% of the fatigue life, and the second warning point is the change in the signature curve slope of more than 1 ($\Omega/100$ Cycle) which in 93% of the samples corresponded to $80\%-3\%$ to $90\%+3\%$ of their fatigue life. Therefore, if the resistance signature indicates that the joint is in this phase, more caution should be applied and depending upon the joint application proper measures, such as repair, strengthening or complete replacement should be executed to ensure the safe performance of the joint. Phase 3, the final or failure phase, contains the last 10% of the fatigue life of the joint. In this phase the electrical resistance changes dramatically up to 100% of the initial resistance or even more. The slope of the curve is changing rapidly and on average reaches more than 4 ($\Omega/100$ Cycle) to almost 80 ($\Omega/100$ Cycle) which indicates a nonlinear curve with sharp increase in its slope. In this phase, multiple crack and delamination between the adhesive layer and substrates are responsible for the nonlinear dramatic increase in resistance. The delamination between the adhesive layer and the substrate can be recorded using long-distance microscope; delamination may also occur around the end of phase 2. Figure 4-41 shows the long distance microscopic image of sample 0.5-7. The images show the edge of the sample at a) the beginning of the test, at b) before 60% of the fatigue life while resistance change was less than 10% of the initial value at c) 91% of the life while the first sign of delamination was seen and the

resistance change was more than 10% of the initial value and at d) when the final failure occurred at 30811 cycles. Likewise Figure 4-42 shows long distance microscopic image of the edge of the sample 0.5-10. At few last cycles the delamination was also visible to naked eyes.

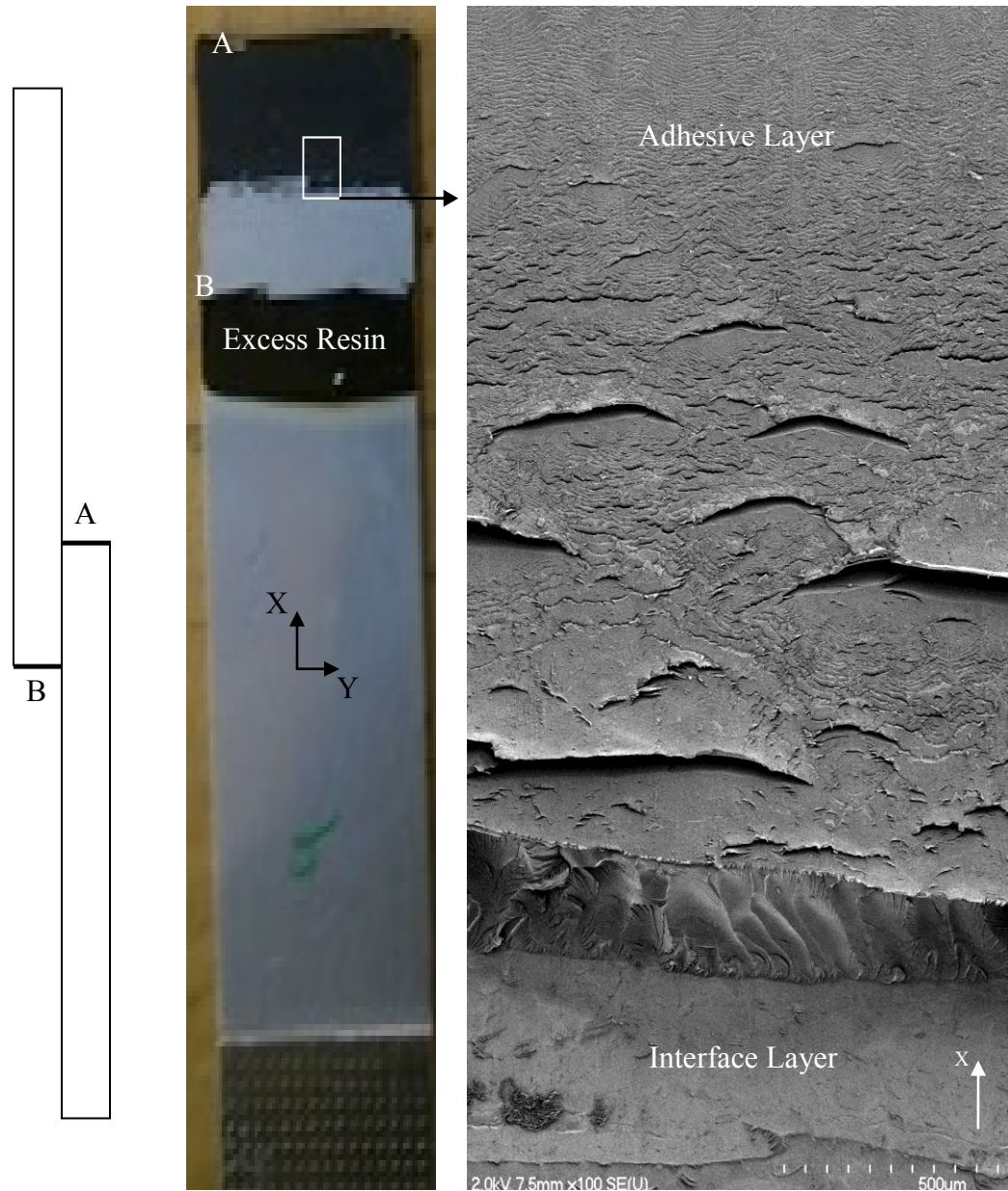


Figure 4-40 SEM images of the fracture surface of a single lap joint containing 0.5 wt% MWCNTs and evidence of multiple cracks (The image was taken after the sample was broken)

4.5.1.1 Summary

Electrical resistance change of 93% of the 30 single lap joints containing 0.5 wt% MWCNTs reached 10%±2% of the initial resistance between 60 to 90% of the fatigue life. Moreover, the resistance signature slope reached 1 ($\Omega/100$ Cycle) and more between 80 to 90% of the fatigue life. These two specific changes should be considered as the warning points to prevent the catastrophic failure.

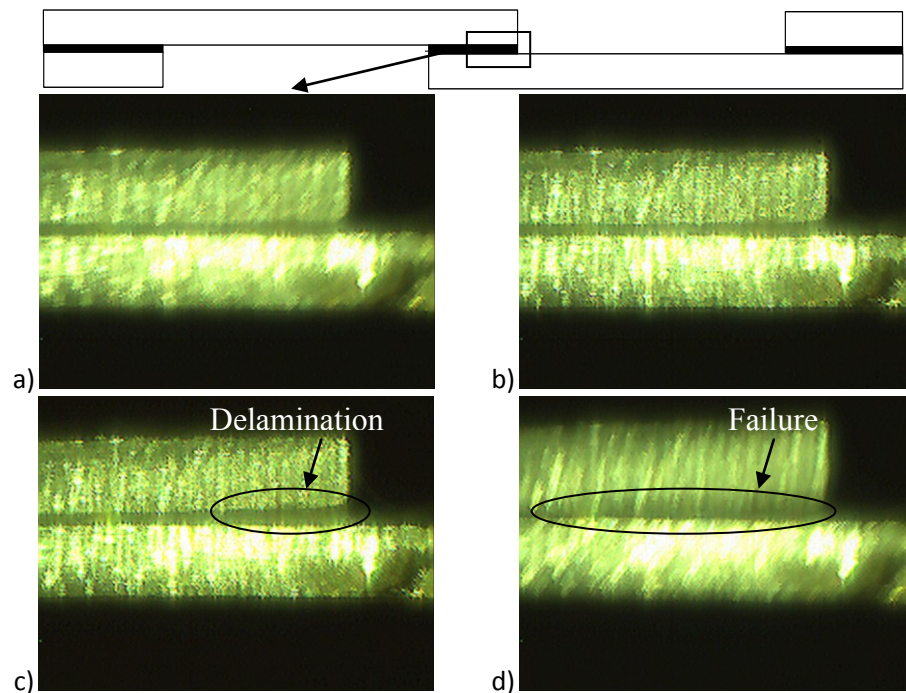


Figure 4-41 Long-distance microscopic view of the edge of sample 0.5- 7, a) beginning of the test b) below 60% of the fatigue life, c) first sign of delamination around 90% of the life, c) final failure at 30811 cycles

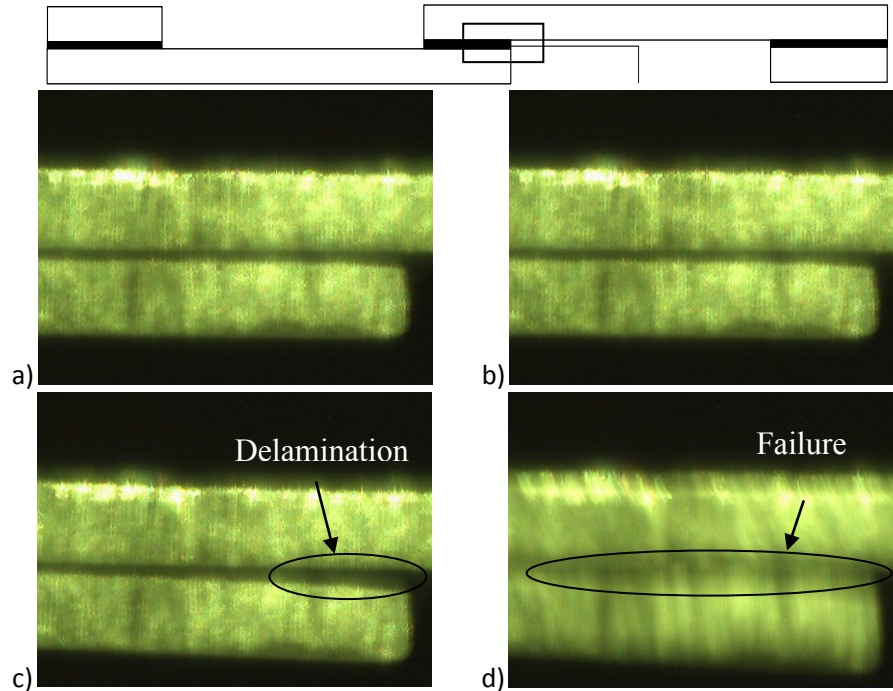


Figure 4-42 Long-distance microscopic view of the edge of sample 0.5- 10, a) beginning of the test b) bellow 60% of the fatigue life, c) first sign of delamination around 85% of the life, c) final failure at 14350 cycles

4.5.2 Single lap joints containing 1wt% MWCNT

Figure 4-43 and Figure 4-52 show 5 electrical resistance signatures and ratios as example. Graphs for all 30 specimens are shown in Appendix1. The electrical resistance graph of each sample provides the initial resistance, the final resistance and the fatigue failure cycle of that sample. Figure 4-53 shows the superposition of normalized resistance ratios of the 5 specimens. Samples numbering is based on the concentration of the nanotubes, for instance, sample 1-4 represents the joint number 4 which contains 1wt% MWCNTs. The numbering of the joints from 1 to 30 is completely arbitrary and is only a means to refer to the specimens. Figure 4-53 shows the superposition of electrical resistance ratios of the 5 examples specimens.

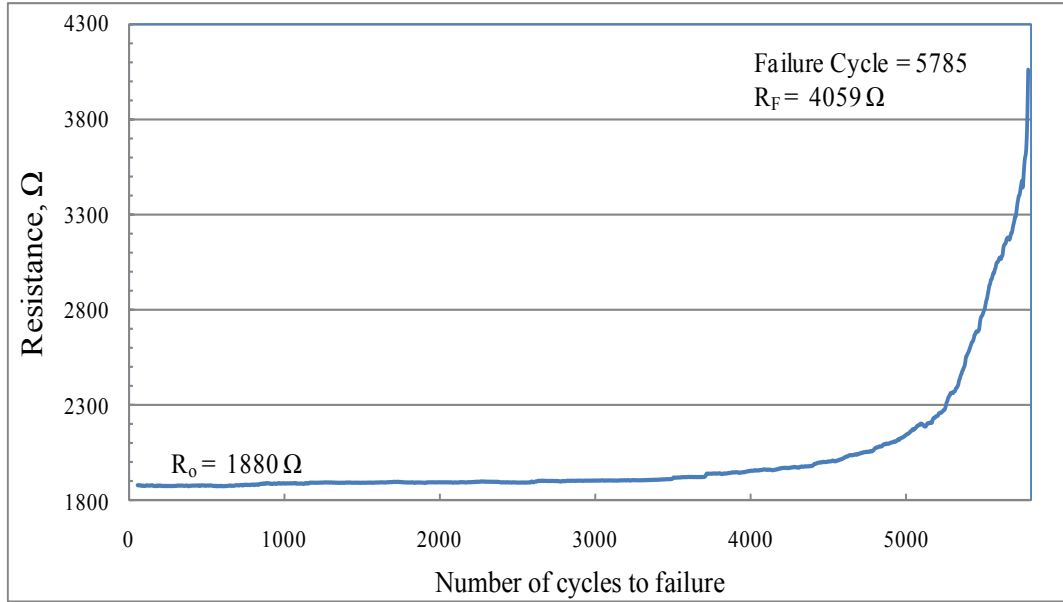


Figure 4-43 Electrical resistance signature vs. fatigue life of sample number 4 containing 1 wt% MWCNTs (sample 1-4)

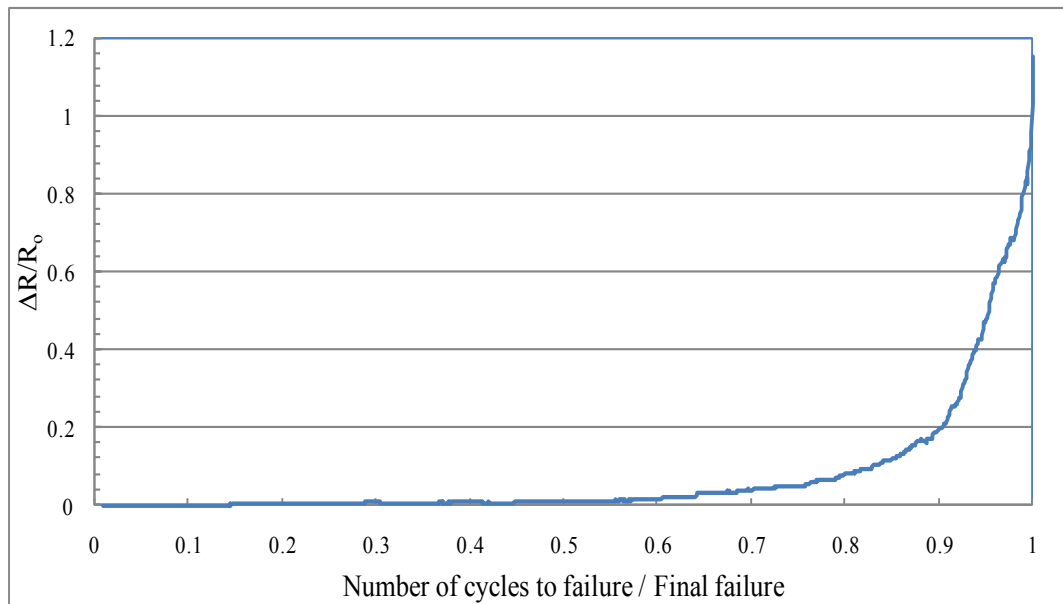


Figure 4-44 Electrical resistance ratio vs. fatigue life for sample 1-4

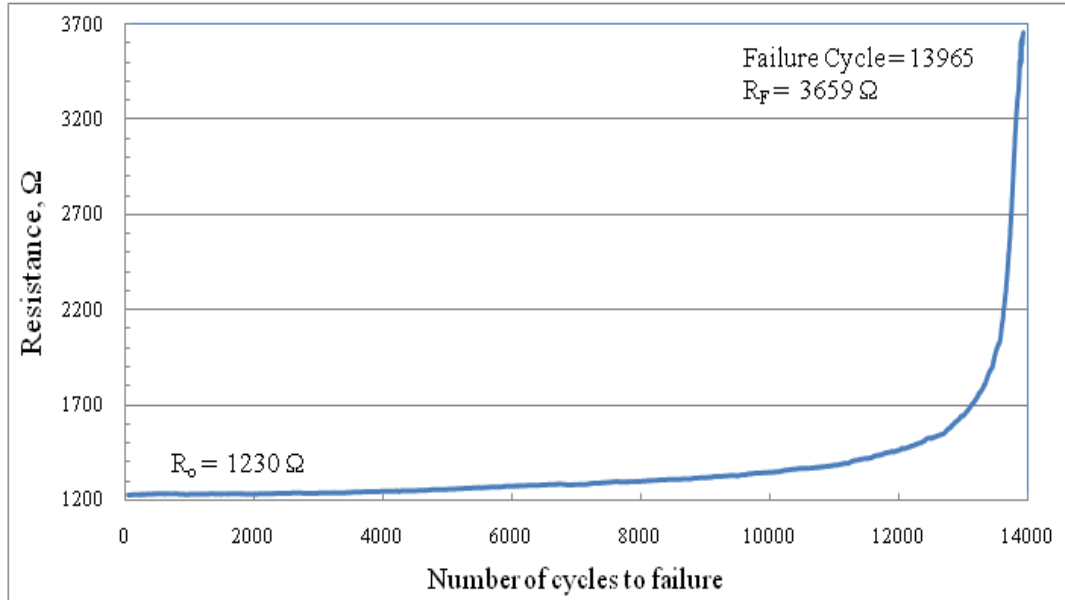


Figure 4-45 Electrical resistance signature vs. fatigue life of sample number 9 containing 1 wt% MWCNTs (sample 1-9)

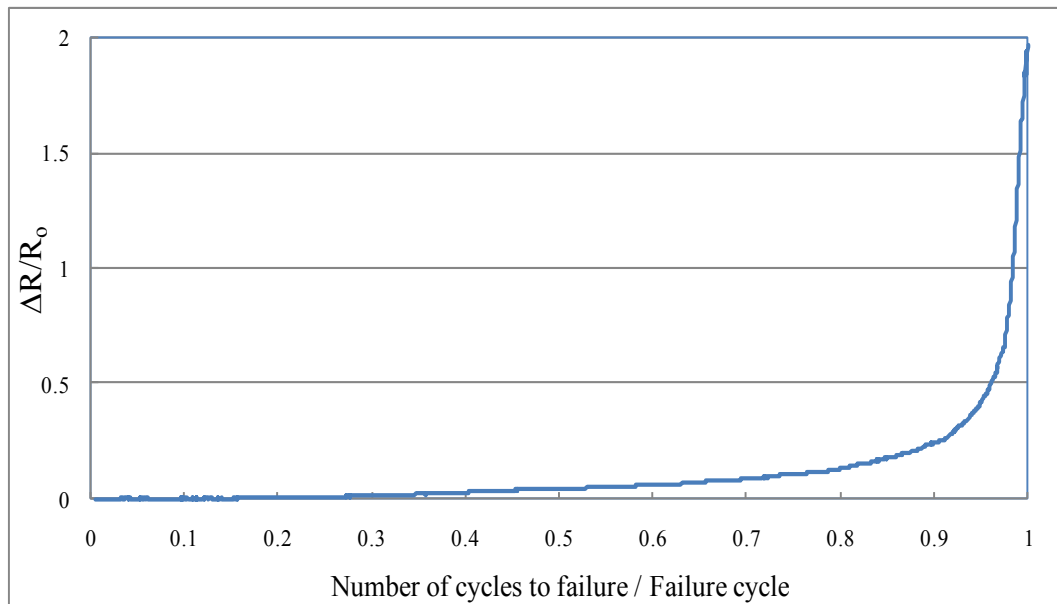


Figure 4-46 Electrical resistance ratio vs. fatigue life for sample 1-9

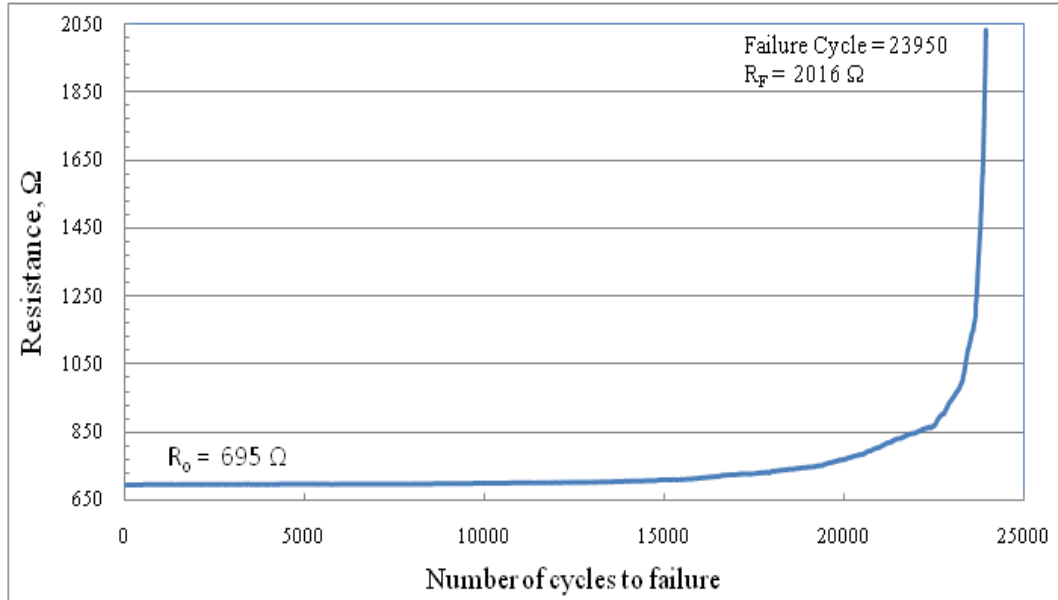


Figure 4-47 Electrical resistance signature vs. fatigue life of sample number 10 containing 1 wt% MWCNTs (sample 1-10)

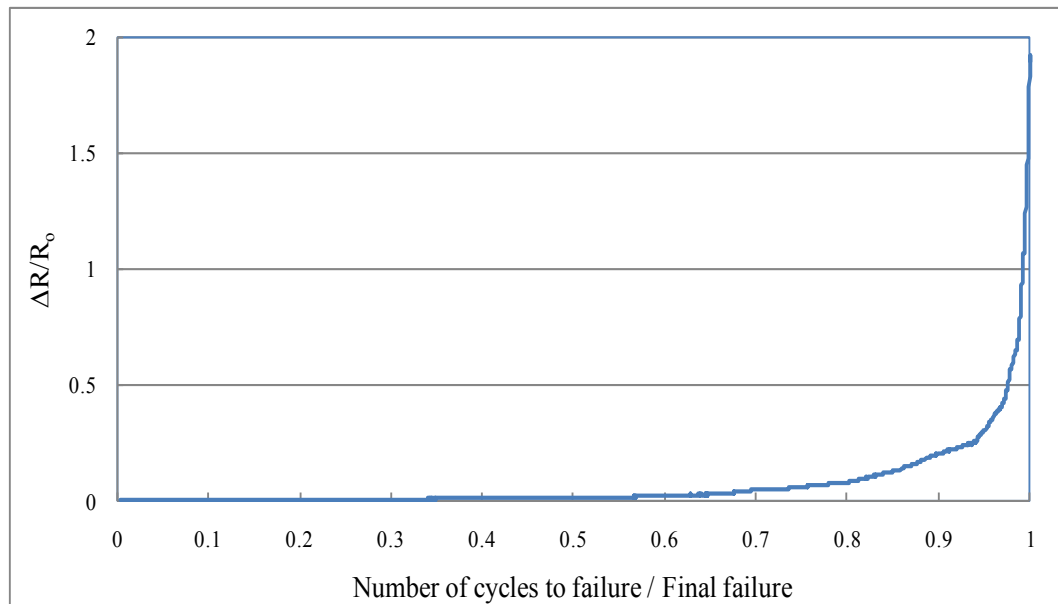


Figure 4-48 Electrical resistance ratio vs. fatigue life for sample 1-10

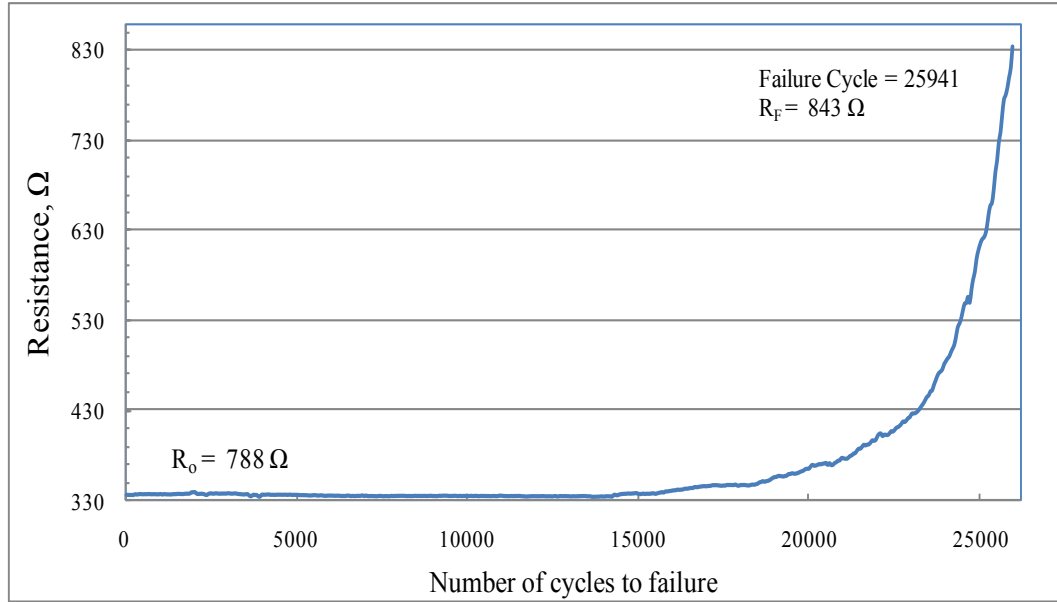


Figure 4-49 Electrical resistance signature vs. fatigue life of sample number 18 containing 1 wt% MWCNTs (sample 1-18)

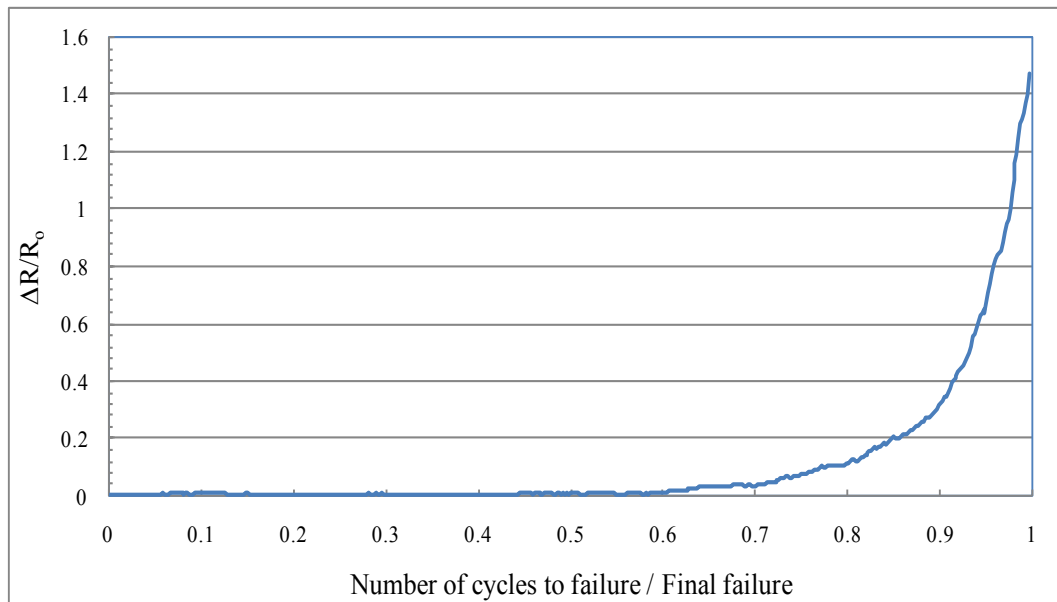


Figure 4-50 Electrical resistance ratio vs. fatigue life for sample 1-18

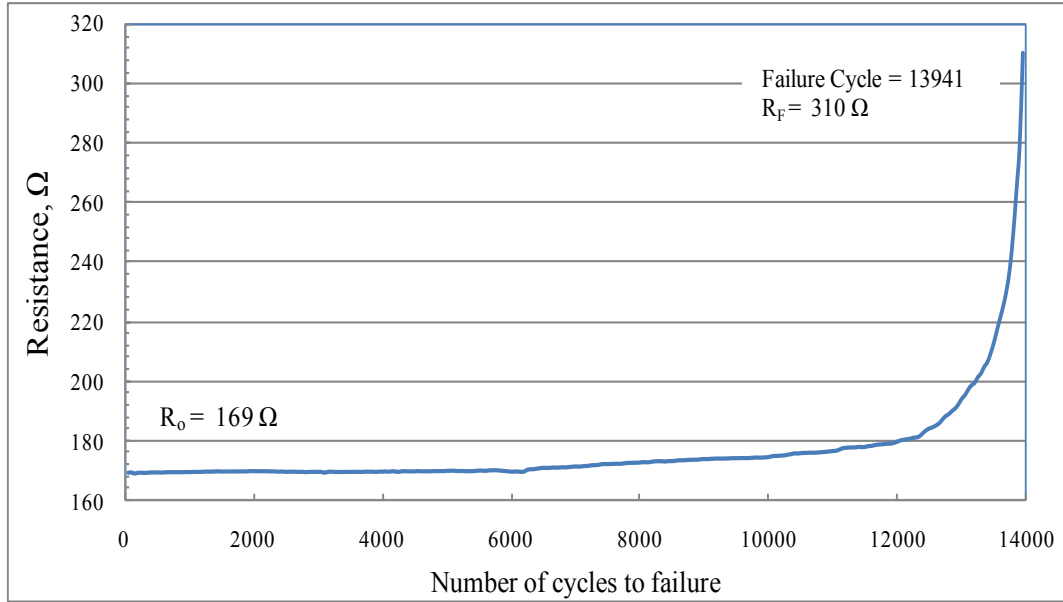


Figure 4-51 Electrical resistance signature vs. fatigue life of sample number 19 containing 1 wt% MWCNTs (sample 1-19)

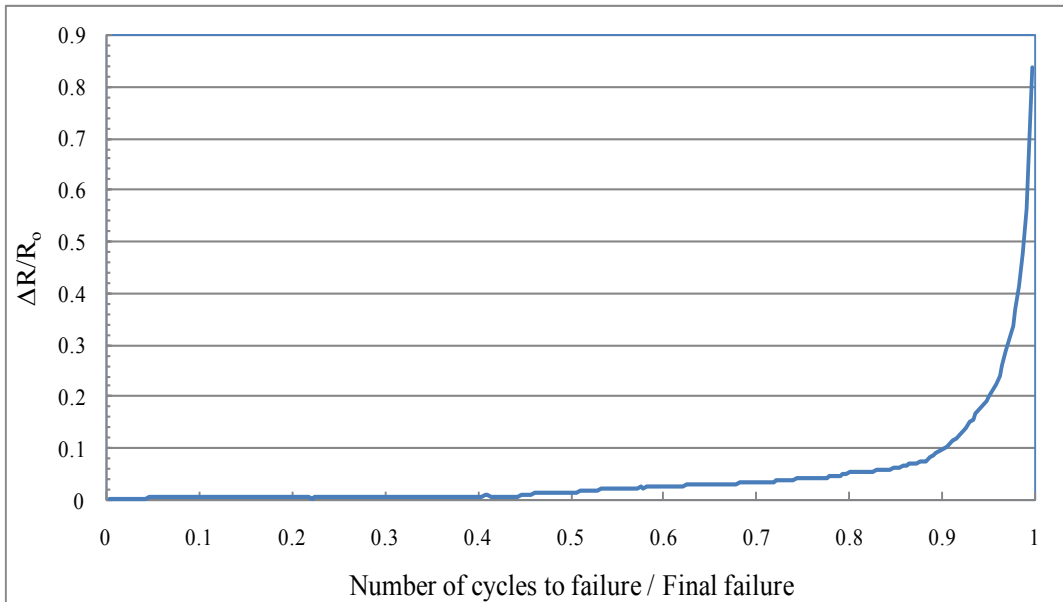


Figure 4-52 Electrical resistance ratio vs. fatigue life for sample 1-19

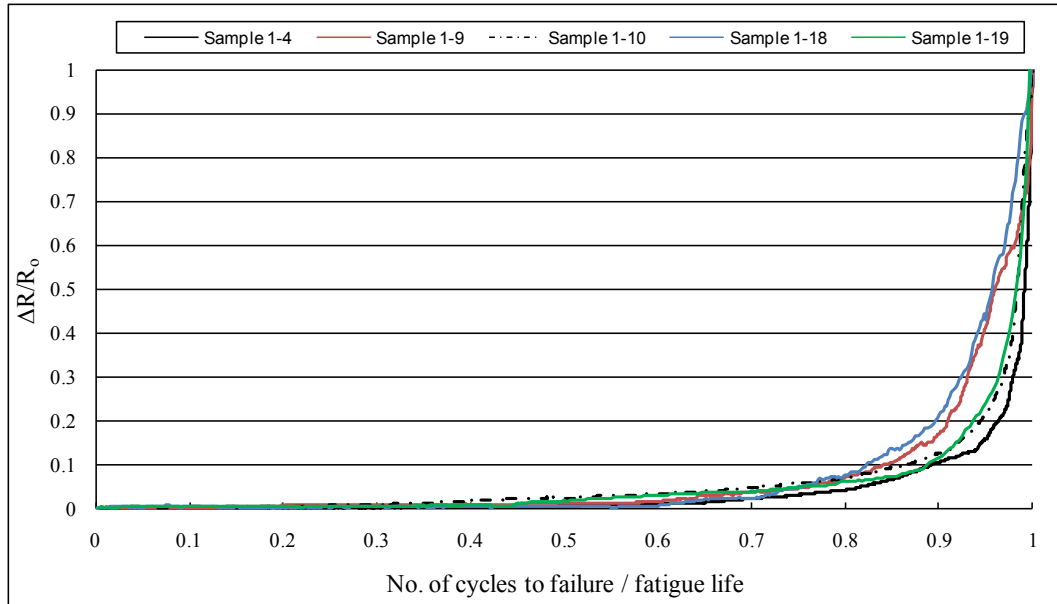


Figure 4-53 Superposition of normalized electrical resistance ratios of the 5 example specimens containing 1wt% MWCNT

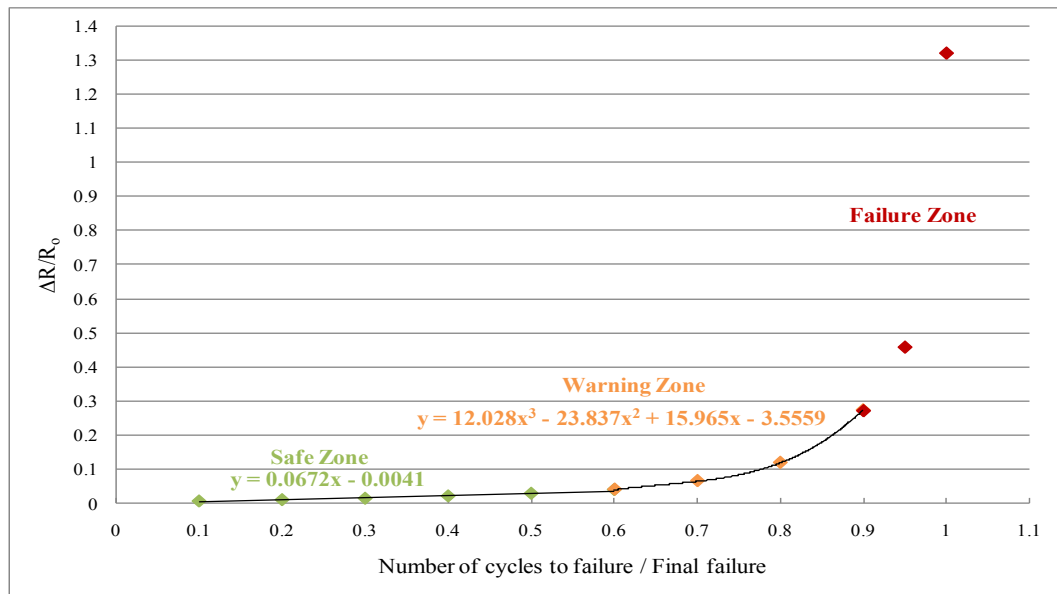


Figure 4-54 The average electrical resistance signatures of all 30 specimens containing 1wt% MWCNTs

The average electrical resistance change at each 10% fatigue life interval was calculated and the measured values were plotted. Then the Trendline function was used to draw and calculate the best curve to fit the data. The average electrical resistance signatures of the

samples containing 1 wt% MWCNT (Figure 4-54), follow the same pattern as the samples containing 0.5 wt% MWCNT. Therefore, their electrical resistance signature can be divided into the same three phases as the safe phase, transition phase (warning phase) and failure phase. Phase 1, which is considered as the safe zone, covers up to approximately 60% of the fatigue life and is recognized by the resistance change of less than 10% of the initial resistance and/or the slope of the resistance signature curve as less than 0.1 ($\Omega/100$ Cycle); A Matlab code was generated to calculate the resistance curve slope at each point. The small change in resistance in this phase is due to initiation of small cracks which breaks the nanotube networks. Therefore, if the resistance signature indicates that the joint is in this zone the joint is safe for its application since no evidence of catastrophic failure is observed in this phase.

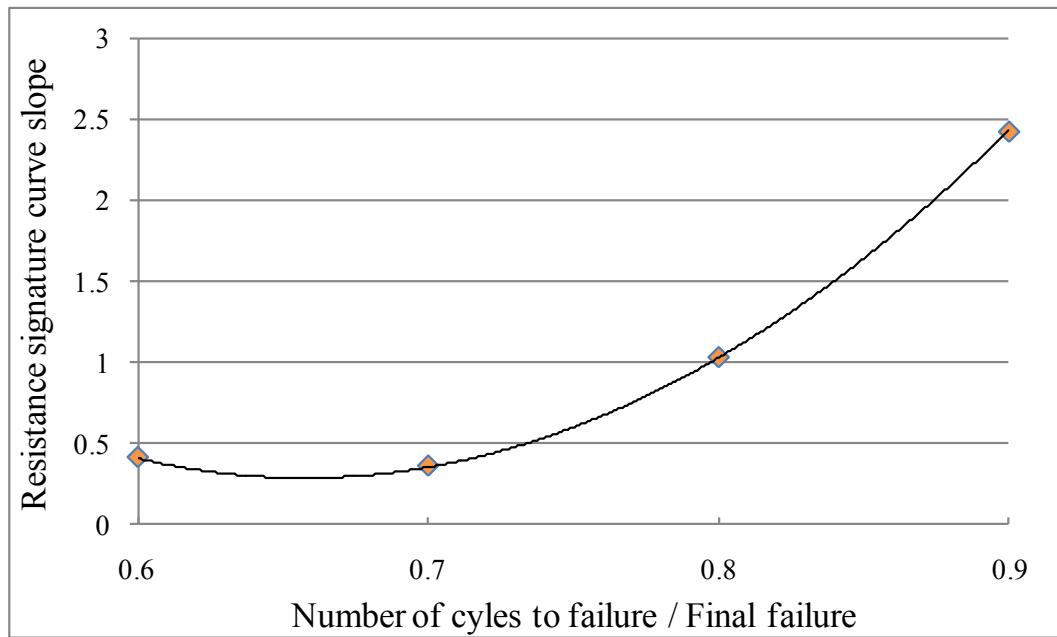


Figure 4-55 Slope of the average resistance signature curve from 60% of the life to 90% of the life

Phase 2, which is considered as the alert or caution zone, envelopes from 60% to 90% of the fatigue life. Electrical resistance signature exhibited sharp increase in resistance of

more than 10% of the initial value in this region and the slope of the curve increased to more than 1 ($\Omega/100$ Cycle) between 80 to 90% of the life (Figure 4-55). The sharp increase in resistance is due to formation and propagation of multiple cracks which breaks more of the nanotube electrical network and contributes to the reduction of electrical paths. Figure 4-56 shows an SEM image of a fracture surface of a sample containing 1 wt% MWCNTs after it was broken due to fatigue test, and multiple cracks in the form of striations are clearly visible.

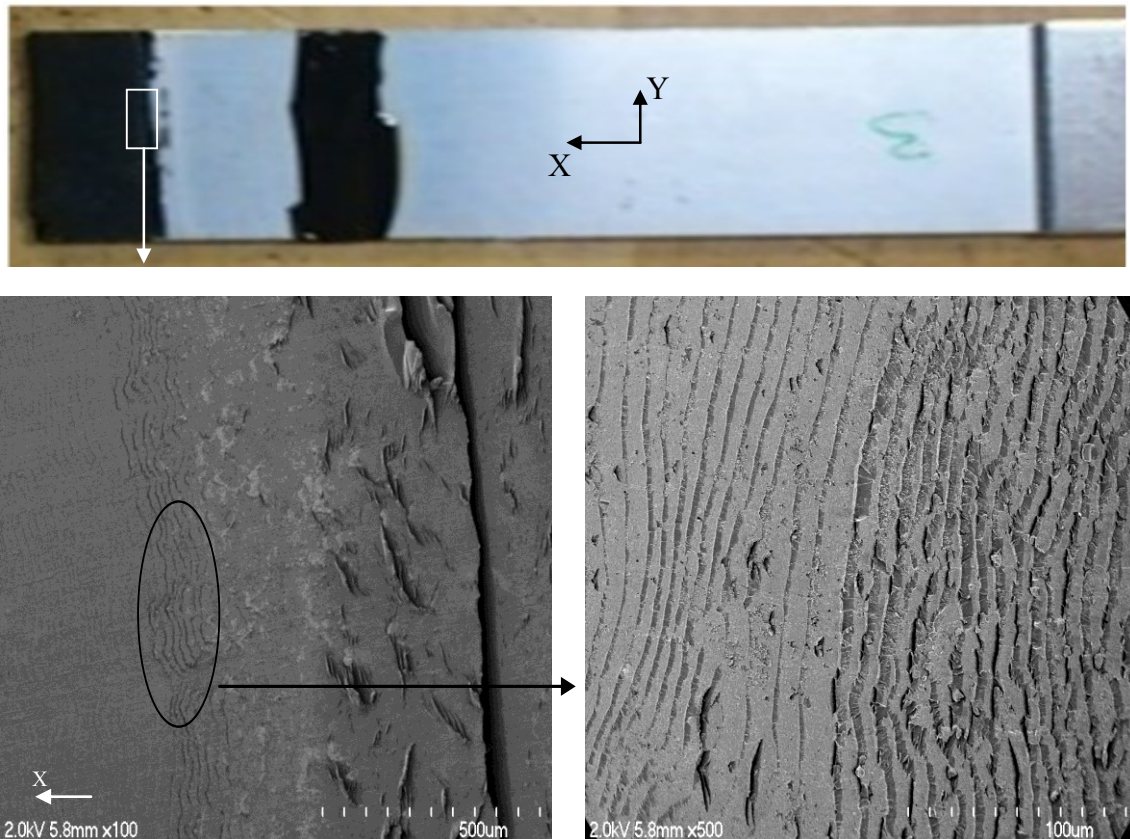


Figure 4-56 SEM images of the fracture surface of a single lap joint containing 1 wt% MWCNTs and evidence of multiple cracks (The image was taken after the sample was broken)

This phase is the warning phase and if the resistance signature indicates that the sample is in this region more caution should be applied on the use of the joint and proper measures should be taken to strengthen the structure and prevent catastrophic failure. Finally, phase

3, which represents the failure zone, covers the final 10% of the fatigue life. In this phase the resistance change showed exponential increase, over 10% of the total fatigue life, to more than 50% of the initial resistance. Delamination and multiple cracks are responsible for the dramatically sharp increase in resistance in this phase; delamination may also occur around the end of phase two. Figure 4-57 shows the long distance microscopic image of sample 1-6. The images show the edge of the sample at a) the beginning of the test, at b) before 60% of the fatigue life while resistance change was less than 10% of the initial value c) at 83% of the life while the first sign of delamination was seen and the resistance change was more than 10% of the initial value and at d) when the final failure occurred at 10580 cycles. Likewise Figure 4-58 shows long distance microscopic image of the edge of the sample 1-21. At few last cycles the delamination is also visible to naked eyes. The slope of the resistance curve in this region followed an increasing pattern at each point and showed raise from 4 ($\Omega/100$ Cycle) to almost 80 ($\Omega/ 100$ Cycle). This phase is the failure phase and if the resistance signature indicates that the specimen is in this phase rapid measures should be taken to prevent catastrophic failure.

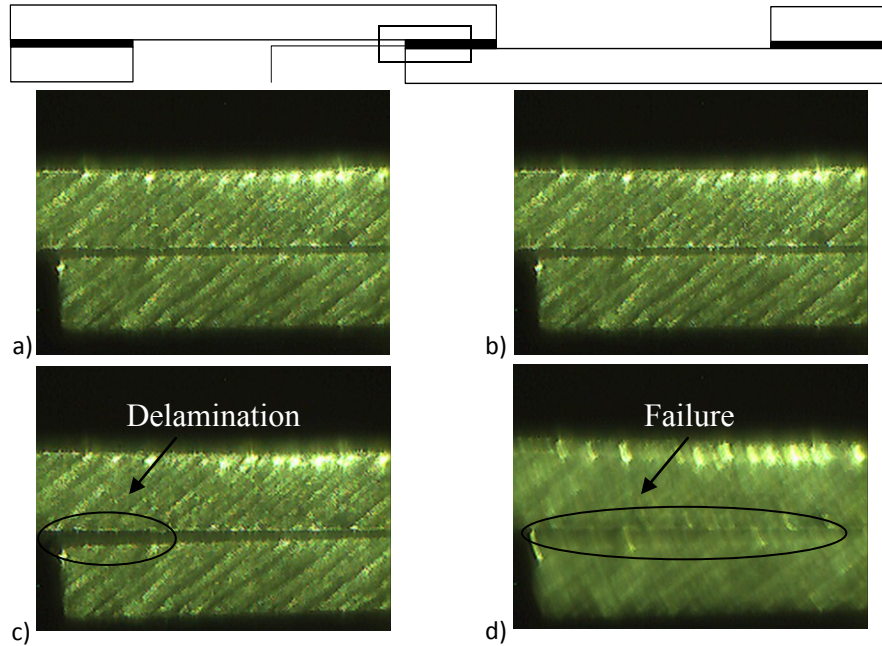


Figure 4-57 Long-distance microscopic view of the edge of sample 1- 6, a) beginning of the test b) below 60% of the fatigue life, c) first sign of delamination around 83% of the life, d) final failure at 10580 cycles

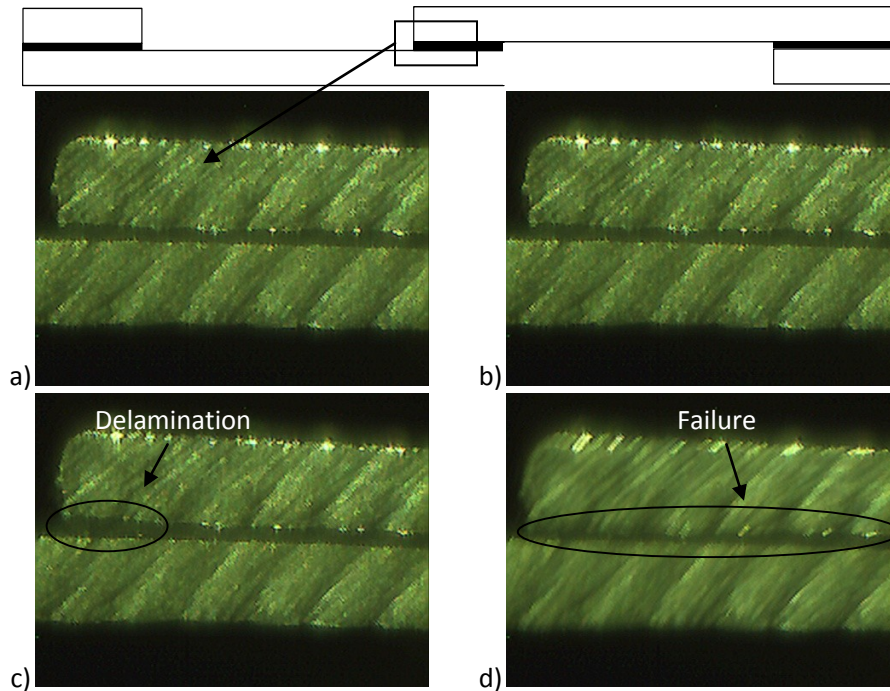


Figure 4-58 Long-distance microscopic view of the edge of sample 1- 21, a) beginning of the test b) below 60% of the fatigue life, c) first sign of delamination around 88% of the life, d) final failure at 7041 cycles

4.5.2.1 Summary

The results of 90% of the 30 specimens containing 1 wt% MWCNTs showed increase of more than 10%+2% of the initial resistance between 60% to 90% of their fatigue life. The specific increase of 10% in resistance should be taken as the first warning point and more caution should be taken in the application of the joints. Moreover, in 97% of the specimens the change in the resistance curve slope to more than 1 ($\Omega/100$ Cycle) occurred between 80%-4% to 90%+4% of their fatigue lives. The slope change of more than 1 ($\Omega/100$ Cycle) should be considered as the second warning and necessary measures should be taken to strengthen, repair and/or replacing the joint according to the end user requirements.

4.5.3 Single lap joints containing 2 wt% MWCNT

Figure 4-59 and Figure 4-68 show the electrical resistance signatures and ratios of all 5 specimens containing 2 wt% MWCNT. The electrical resistance graph of each sample provides the initial resistance, the final resistance and the fatigue failure cycle of that sample. Samples numbering is based on the concentration of the nanotubes, for instance, sample 2-1 represents the joint number 1 which contains 2 wt% MWCNTs. The numbering of the joints from 1 to 5 is completely arbitrary and is only a mean to refer to the specimens. Figure 4-69 shows the superposition of the electrical resistance ratios.

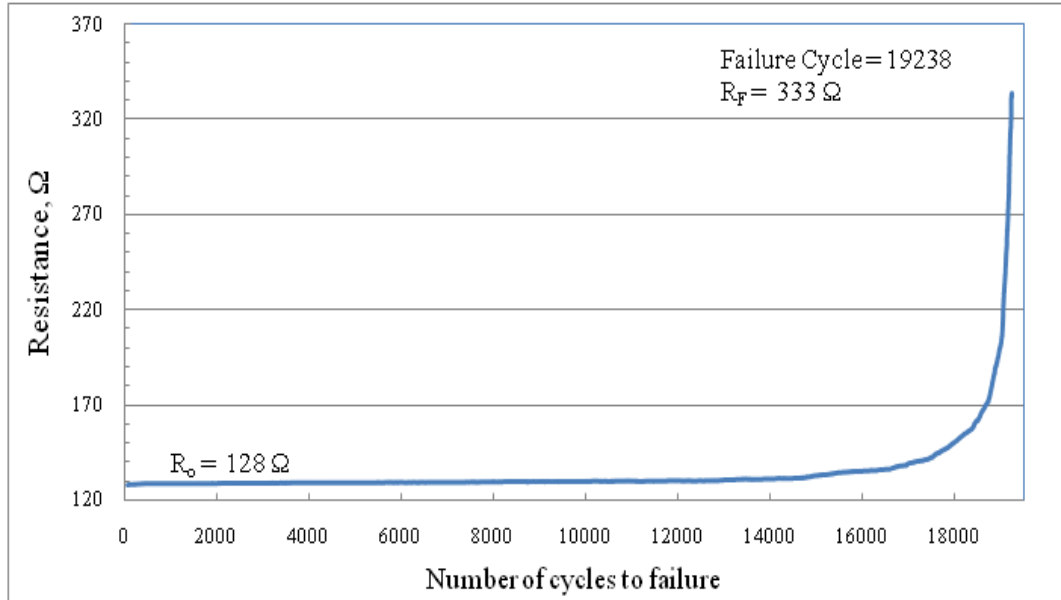


Figure 4-59 Electrical resistance signature vs. fatigue life of sample number 1 containing 2 wt% MWCNTs (sample 2-1)

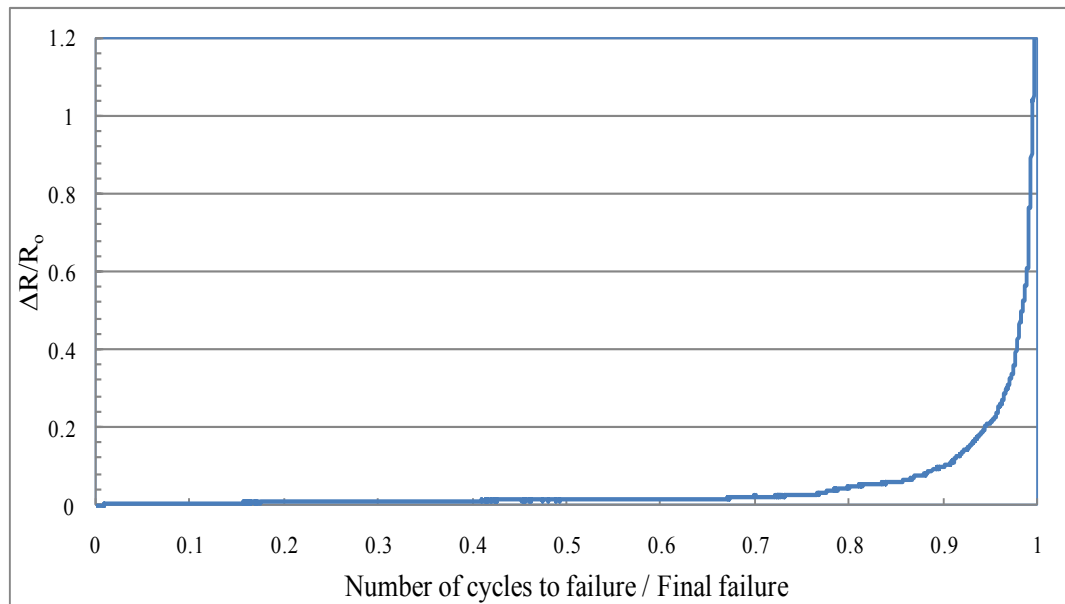


Figure 4-60 Electrical resistance ratio vs. fatigue life for sample 2-1

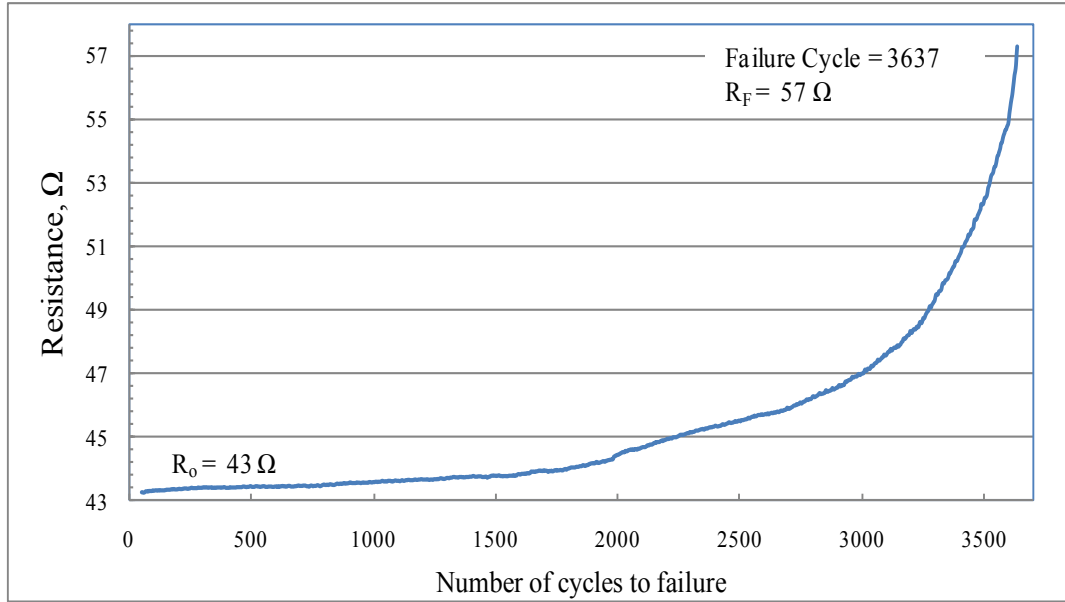


Figure 4-61 Electrical resistance signature vs. fatigue life of sample number 2 containing 2 wt% MWCNTs (sample 2-2)

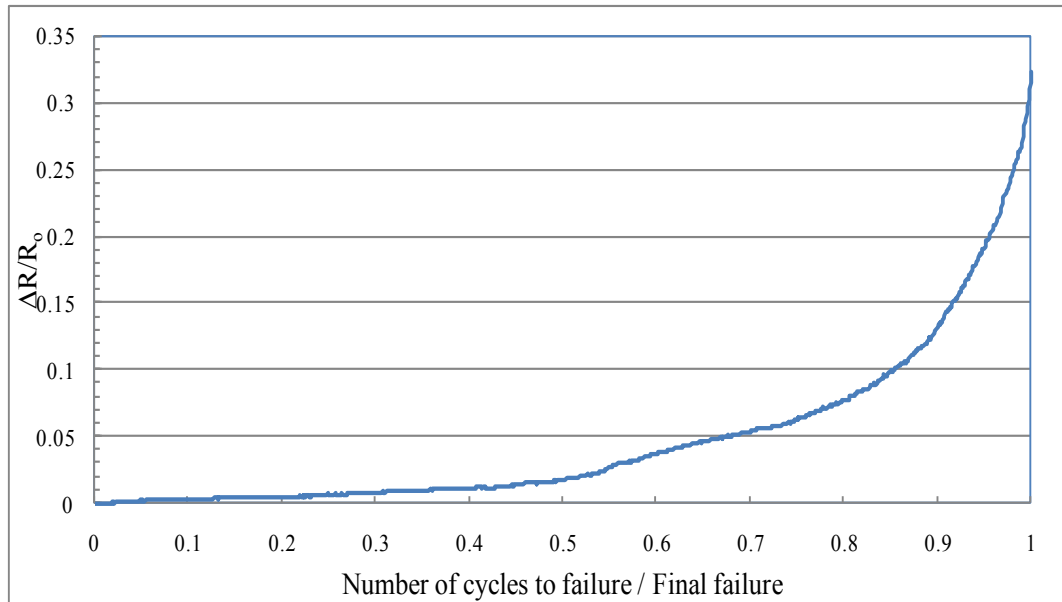


Figure 4-62 Electrical resistance ratio vs. fatigue life for sample 2-2

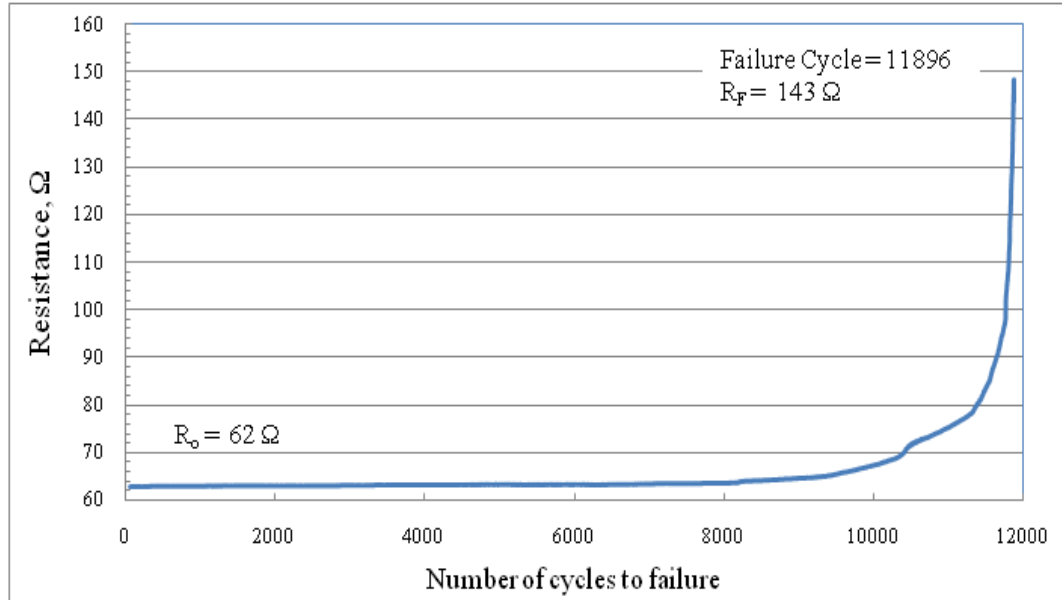


Figure 4-63 Electrical resistance signature vs. fatigue life of sample number 3 containing 2 wt% MWCNTs (sample 2-3)

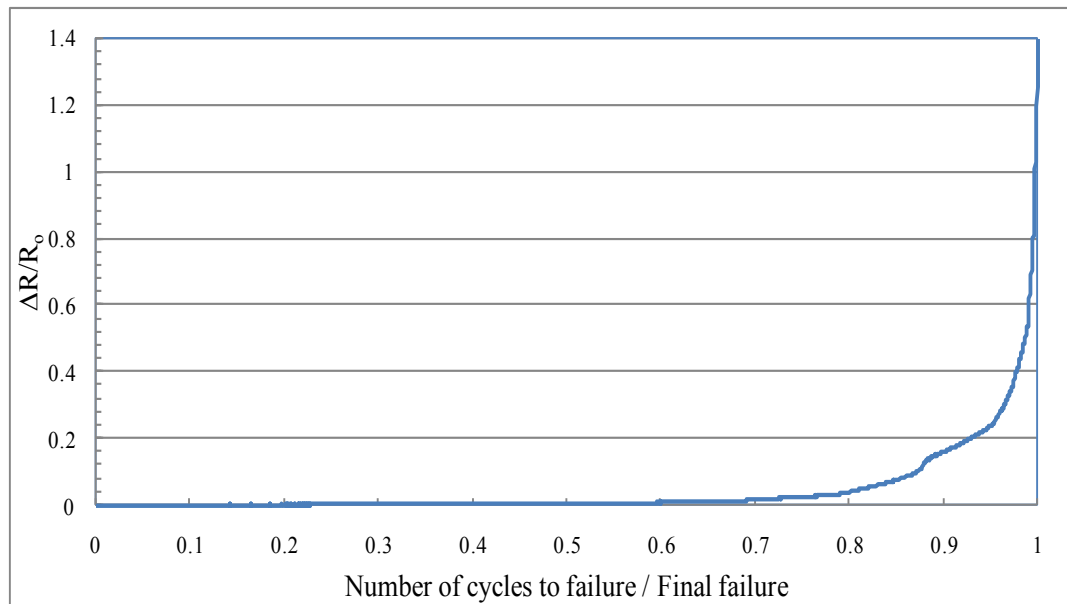


Figure 4-64 Electrical resistance ratio vs. fatigue life for sample 2-3

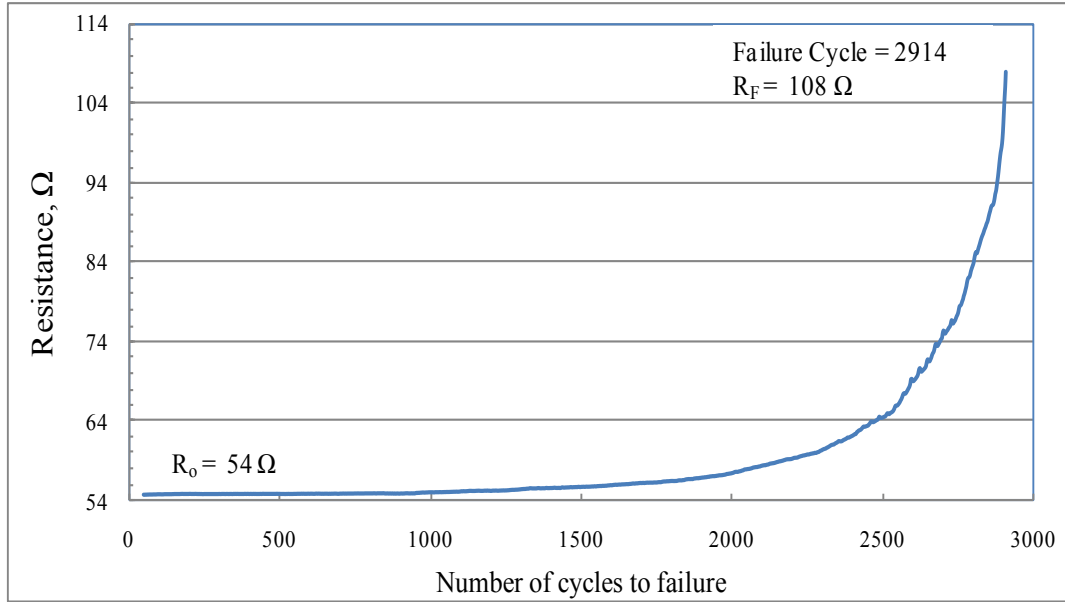


Figure 4-65 Electrical resistance signature vs. fatigue life of sample number 4 containing 2 wt% MWCNTs (sample 2-4)

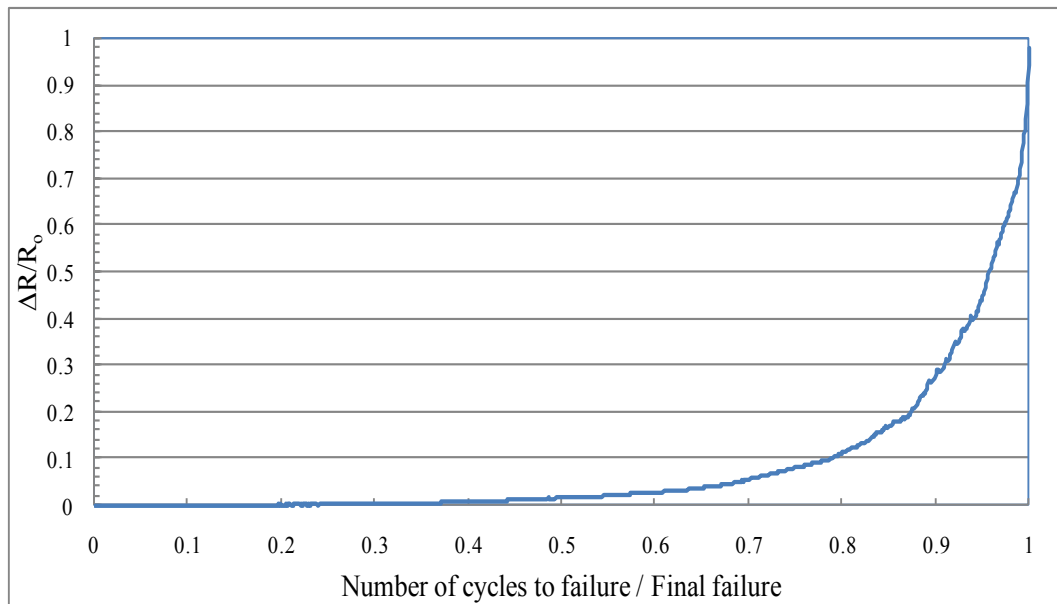


Figure 4-66 Electrical resistance ratio vs. fatigue life for sample 2-4

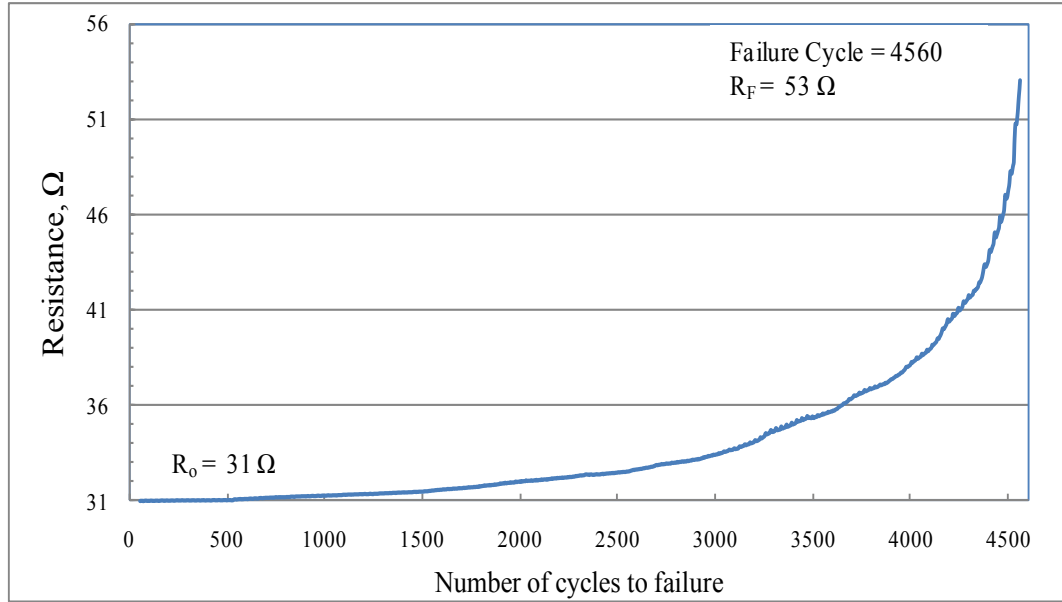


Figure 4-67 Electrical resistance signature vs. fatigue life of sample number 5 containing 2 wt% MWCNTs (sample 2-5)

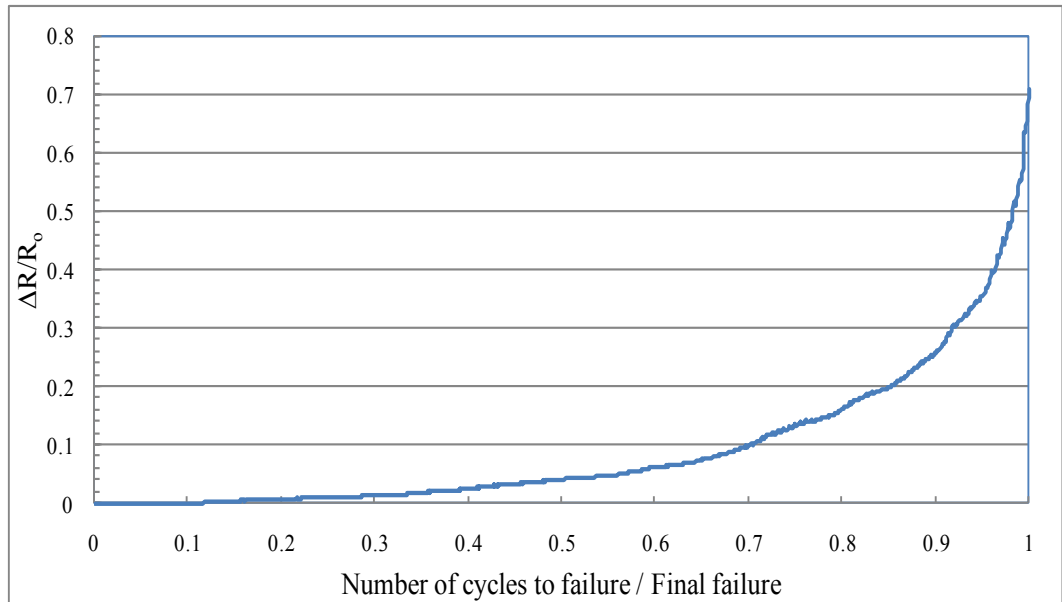


Figure 4-68 Electrical resistance ratio vs. fatigue life for sample 2-5

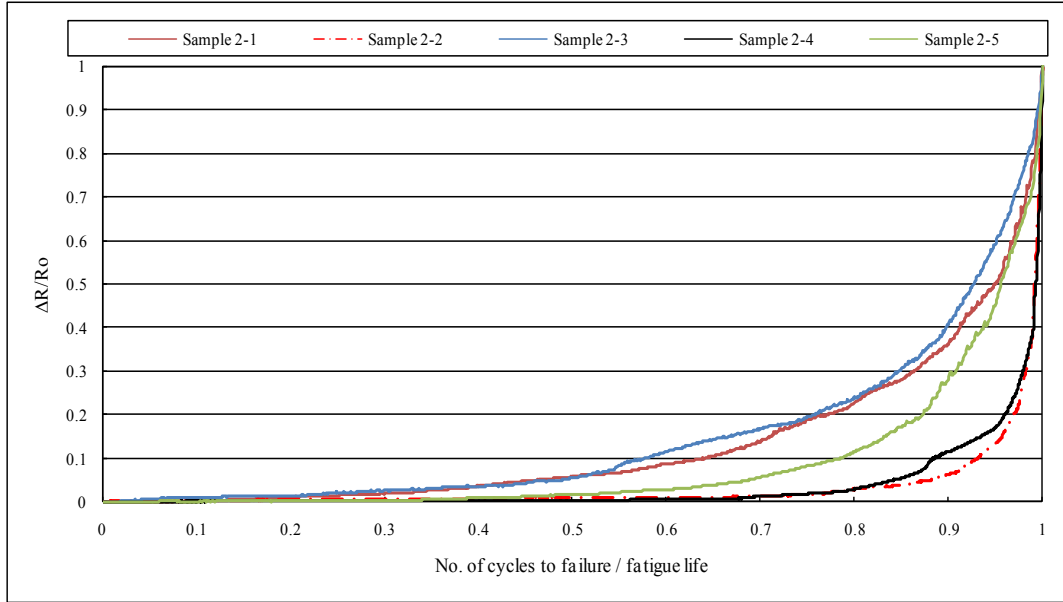


Figure 4-69 Superposition of normalized electrical resistance ratios of all 5 specimens containing 2 wt% MWCNT

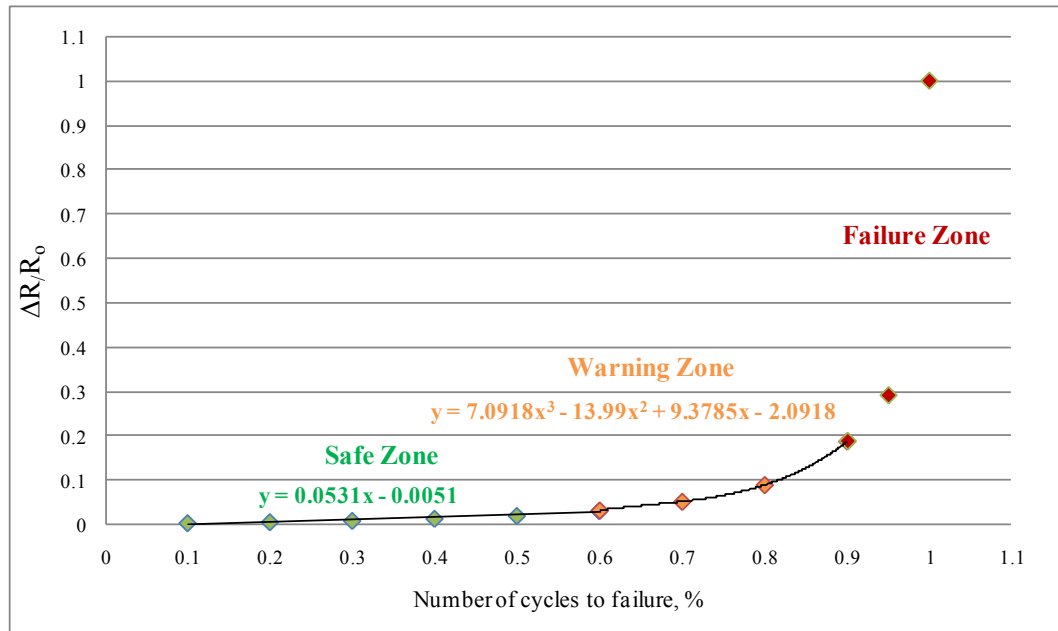


Figure 4-70 The average electrical resistance signatures of all 5 specimens containing 2 wt% MWCNTs

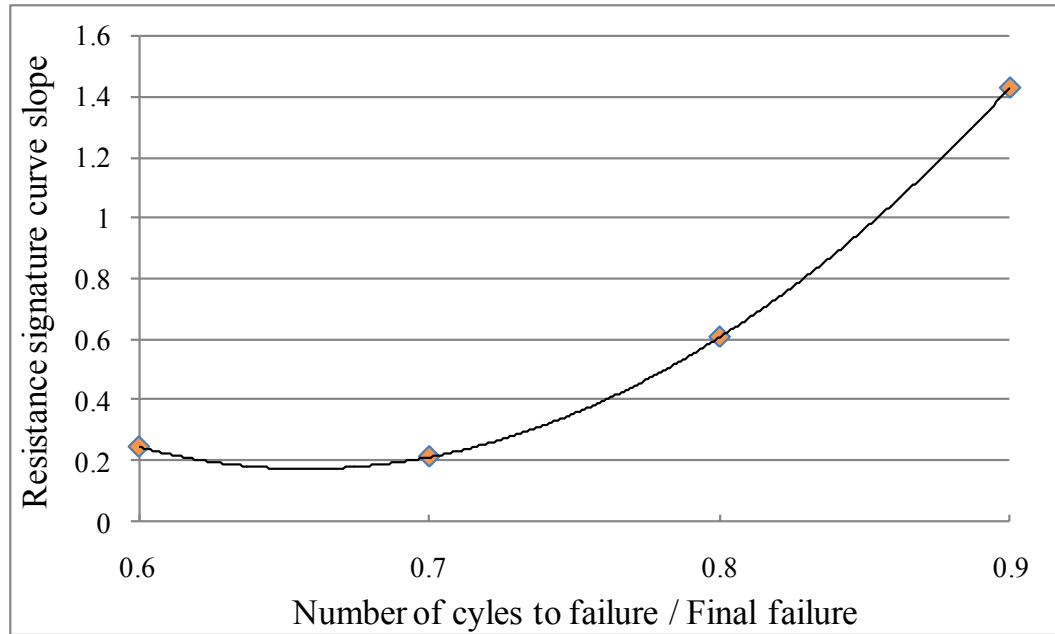


Figure 4-71 Slope of the average resistance signature curve from 60% of the life to 90% of the life

The average electrical resistance change at each 10% fatigue life interval was calculated and the measured values were plotted. Then the Trendline function was used to draw and calculate the best curve to fit the data. Figure 4-70 indicates that specimens containing 2 wt% MWCNT, acted the same manner as the ones with 0.5 and 1 wt%. The resistance signatures followed the same phases as safe zone, warning zone, and failure zone. The safe zone corresponded to the zone that the resistance change was less than 10% of the initial resistance and the slope of the curve was below 0.1 ($\Omega/100$ Cycle); this zone covered 60% of the fatigue life of the samples. The warning zone showed resistance change more than 10% of the initial resistance and covered from 60% to 90% of the fatigue life of the samples. The slope of the resistance signature curve in this zone was not constant and reached to 1 ($\Omega/100$ Cycle) between 80 to 90% of the fatigue life (Figure 4-71). The failure zone covered the last 10% of the life of the samples and the resistance change showed an exponentially sharp increase to more than 50% of the initial

resistance. The slope of the curve in this stage changed from 4 ($\Omega/100$ Cycle) to almost 80 ($\Omega/100$ Cycle).

4.5.3.1 Summary

The results of the 100% of the specimens containing 2 wt% MWCNTs showed the resistance change of more than 10% between 70 to 90% of the fatigue life. Moreover, in 100% of the specimens the resistance signature curve slope reached more than 1 between 80 to 90% of the fatigue life. Therefore, 2 warning points namely as 10% increase in resistance and the slope of more than 1 ($\Omega/100$ Cycle) should be considered for the joints, and necessary measures according to the end user requirements should be taken for safe performance of the joints.

4.5.4 Comparison

Figure 4-72 shows the comparison between the electrical resistance signatures of the single lap joints containing 0.5, 1, and 2 wt% MWCNTs. No difference between the electrical resistance signatures of samples with different CNT loading is observed up to 80% of the fatigue life. However, after 80% of the life samples containing 1 wt% MWCNTs shows slightly faster increase in resistance than the samples containing 0.5 or 2 wt% MWCNTs. Moreover, the final increase in resistance at the time of failure in samples with 1wt% and 2 wt% MWCNTs on average reaches up to 100% of the initial resistance while for samples containing 0.5 wt% MWCNTs the final increase in resistance reaches on average to 60% of the initial resistance. However, all three different CNT loadings proved to be equally capable of in situ monitoring of the bonded joints and to give failure warning well in advance to prevent catastrophic failure.

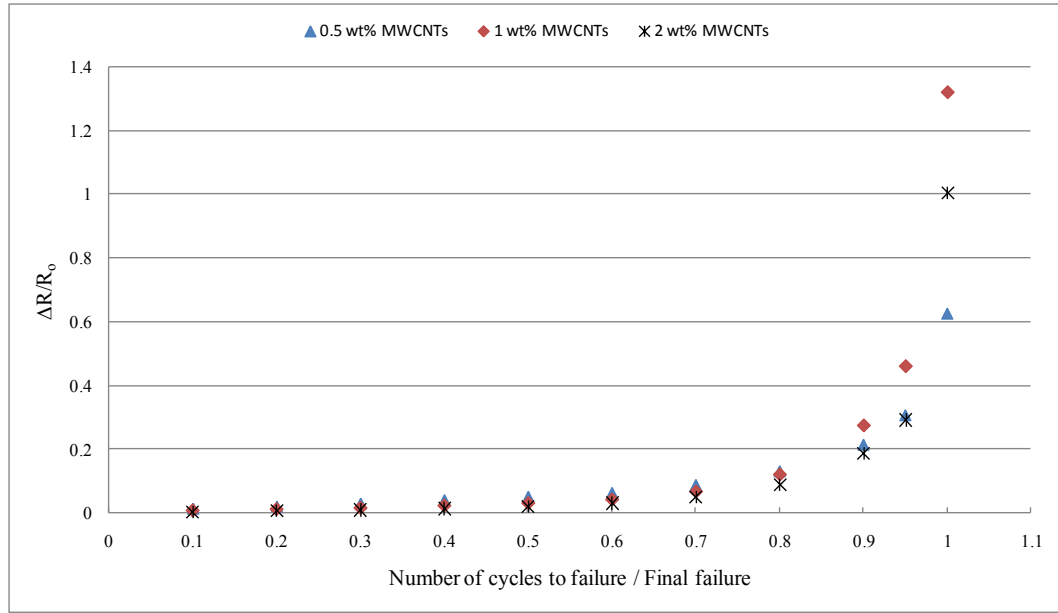


Figure 4-72 Comparison between the electrical resistance signatures of samples containing 0.5, 1 and 2 wt% MWCNTs

4.5.5 Summary

Our electrical resistance measurement technique proved not only to be capable of in situ health monitoring of adhesively bonded aluminum joints, but more importantly could provide valuable information about the residual life of the joints. The electrical network of MWCNTs inside the adhesive grants the opportunity to measure the electrical resistance change during the fatigue testing. The author believes that crack initiation and propagation, which are inherent characteristics of fatigue, cause the breakage of the CNT network inside the adhesive during the fatigue test and thus contributes to the increase of electrical resistance. The experimental results on samples containing different MWCNT loadings namely as, 0.5, 1, and 2 wt% demonstrated that the resistance change of more than 10% of the initial resistance value occurred between 60 to 90% of the fatigue life and the change in the resistance curve slope of more than 1 ($\Omega/100$ Cycle) occurred between 80 to 90% of the fatigue life. Therefore, these specific changes should be

considered as the warning points during the service life of the joints to predict and prevent the catastrophic failure well in advance.

4.5.6 SEM Images of the Fracture Surface of Single Lap Joints after Fatigue

4.5.6.1 Single Lap Joints with No MWCNTs

Fracture surface of a single lap joints containing 0 wt% MWCNTs is shown in Figure 4-73. The specimen was broken after 19898 cycles. The image shows long continuous cracks which travel through the width of the joint. Figure 4-74 shows magnified image of the square area marked on Figure 4-73 and shallow cracks in the form of striations are also visible in the picture.

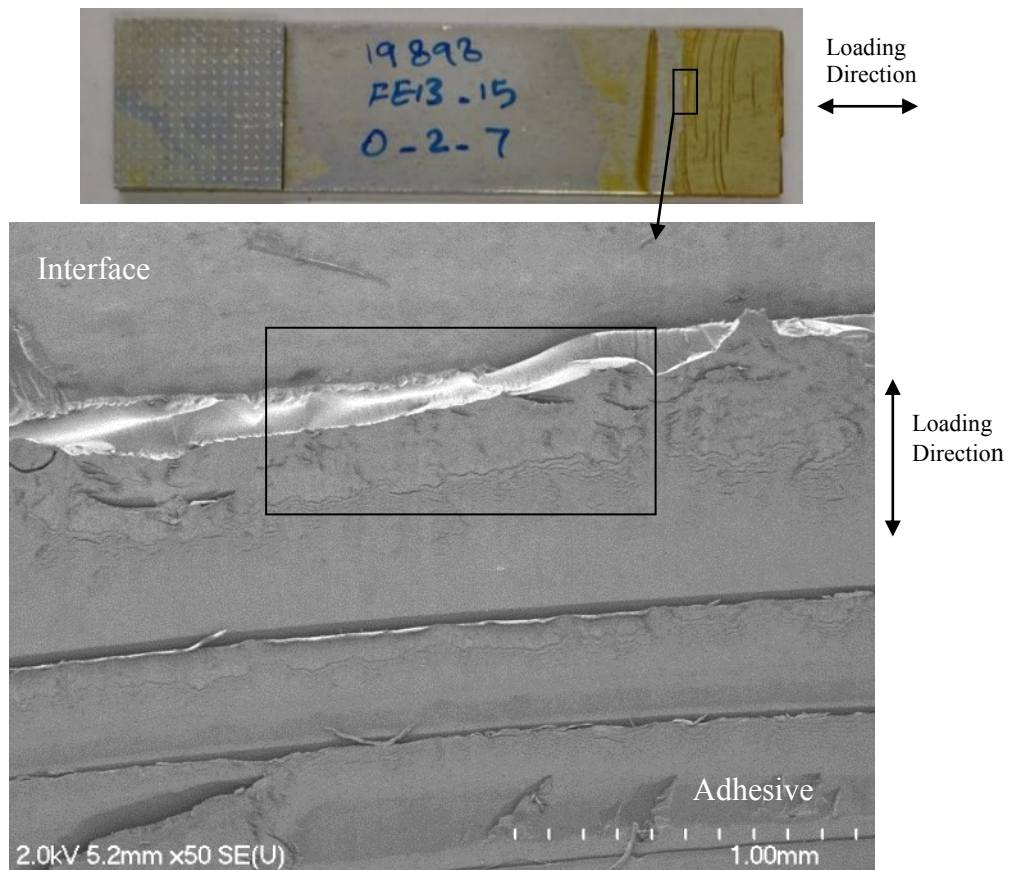
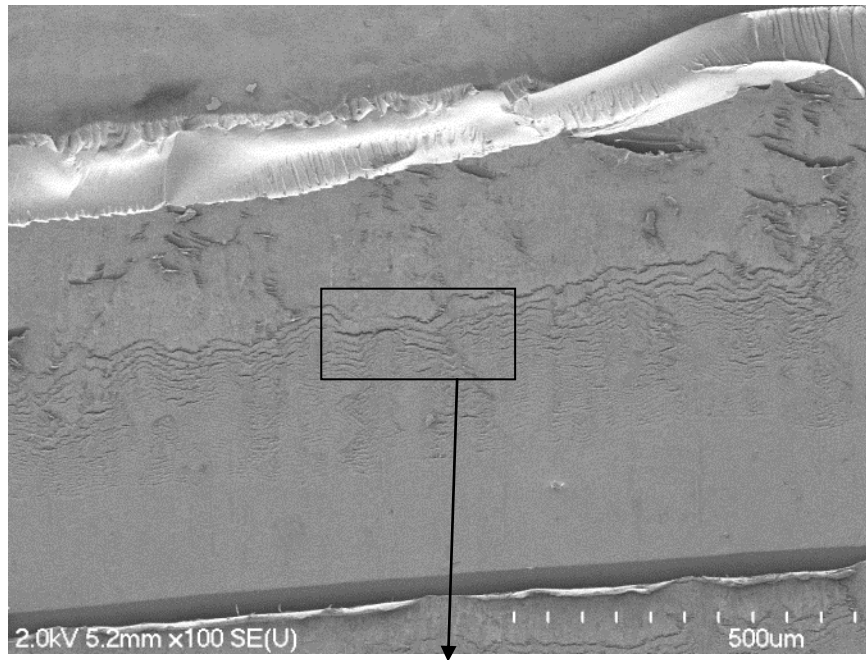


Figure 4-73 Fracture surface of a sample containing 0wt% MWCNTs which was broken after 19898 cycles.(Sample 0-19)

a)



b)

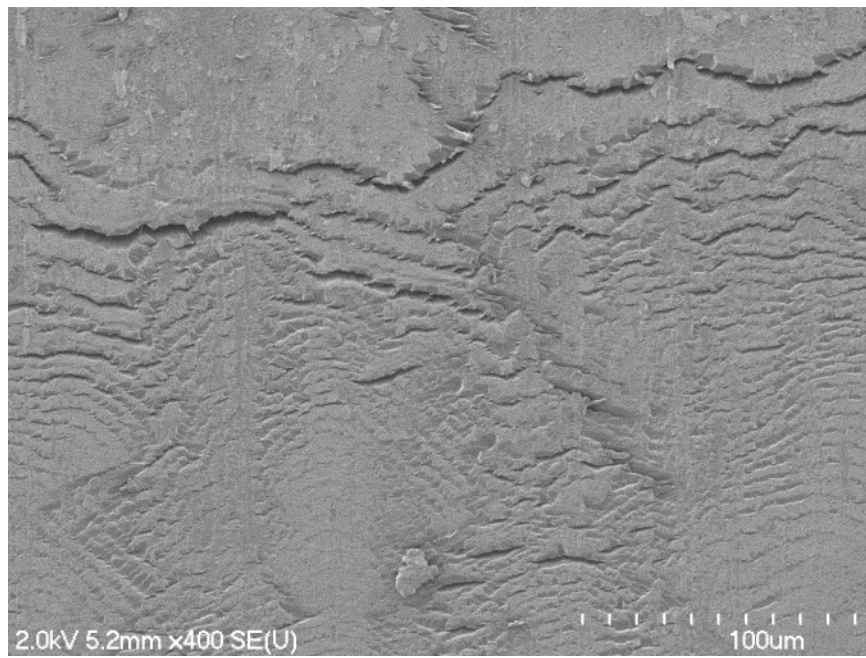


Figure 4-74 Magnified image of the square area marked on Figure 4-73, a) 500µm, b) 100 µm

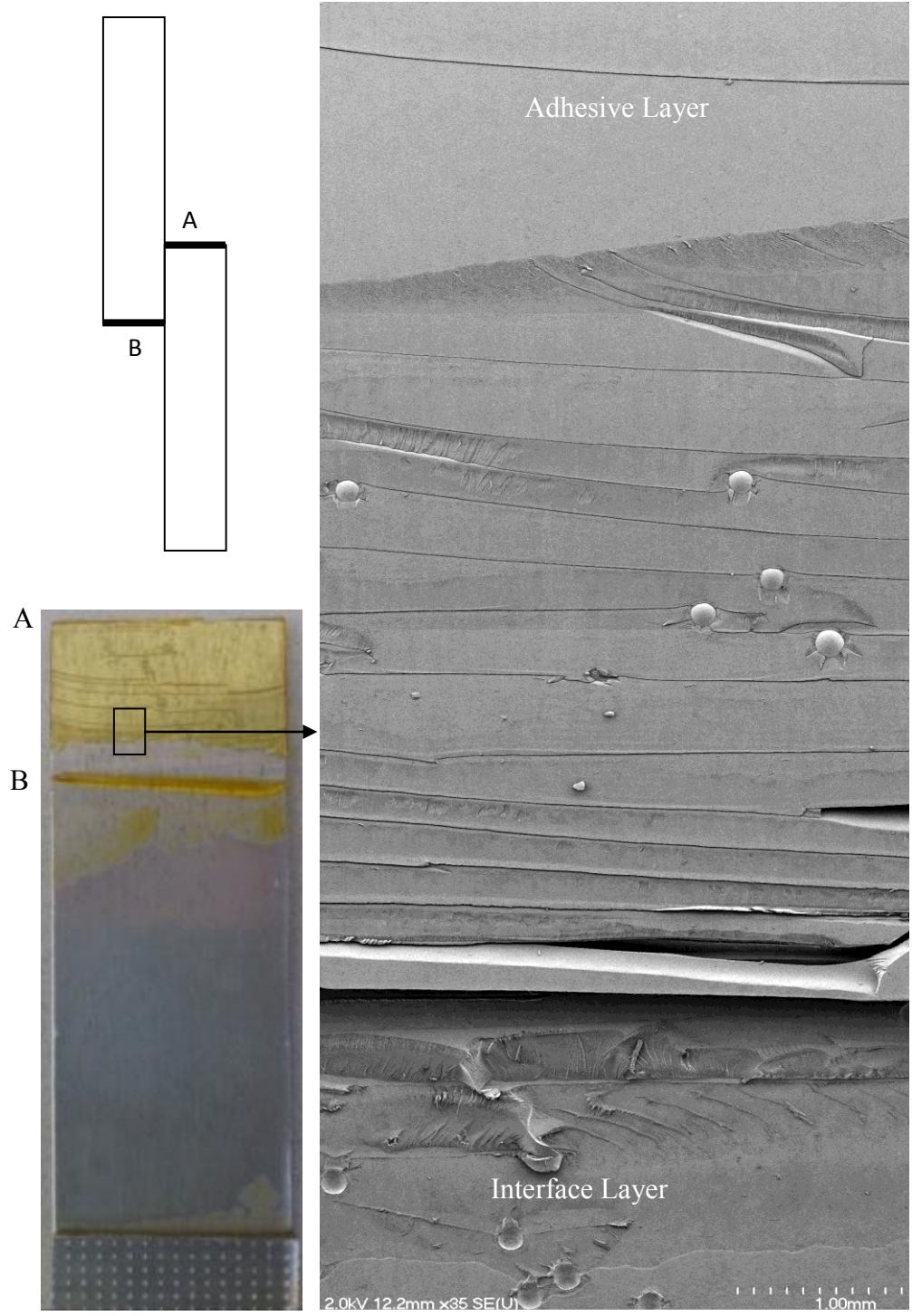


Figure 4-75 Fracture surface of a sample containing 0wt% MWCNTs which was broken after 18193 cycles.
 (Sample 0-17)

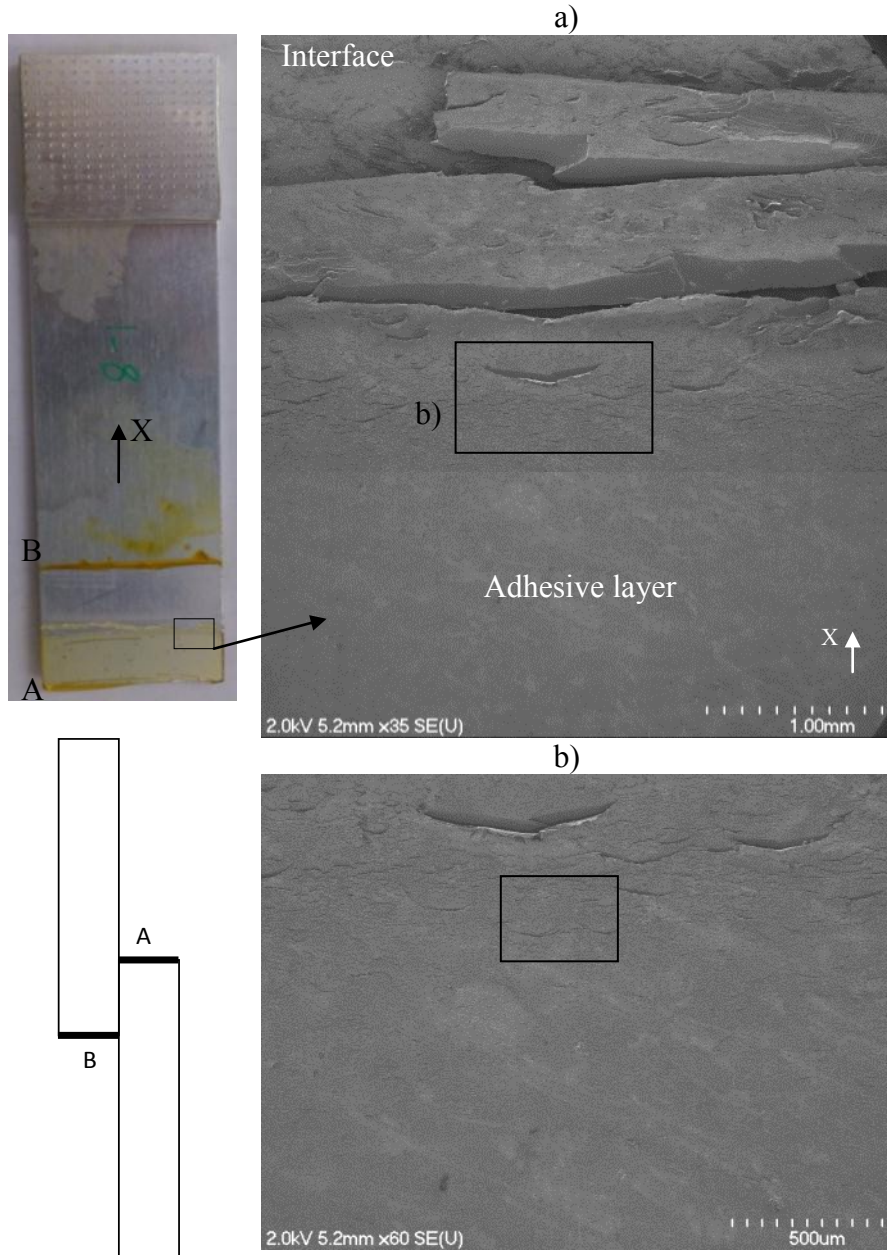


Figure 4-76 Fracture surface of a sample containing 0wt% MWCNTs which was broken after 12726 cycles. (Sample 0-11)

Figure 4-75 shows SEM image of another sample containing no MWCNTs. This sample was broken after 18200 fatigue cycles. As the picture illustrates, there are plenty of deep continuous cracks which travel through the width of fracture surface. However, unlike previous sample, there is no evidence of crack striations on the fracture surface of this specimen. Figure 4-76 shows SEM image of a sample containing 0 wt% MWCNTs

which was broken after 12730 fatigue cycles. The image shows no continuous long crack. Figure 4-77 shows magnified image of the mark area on Figure 4-76 (b) and it clearly illustrates cracks in the form of striations.

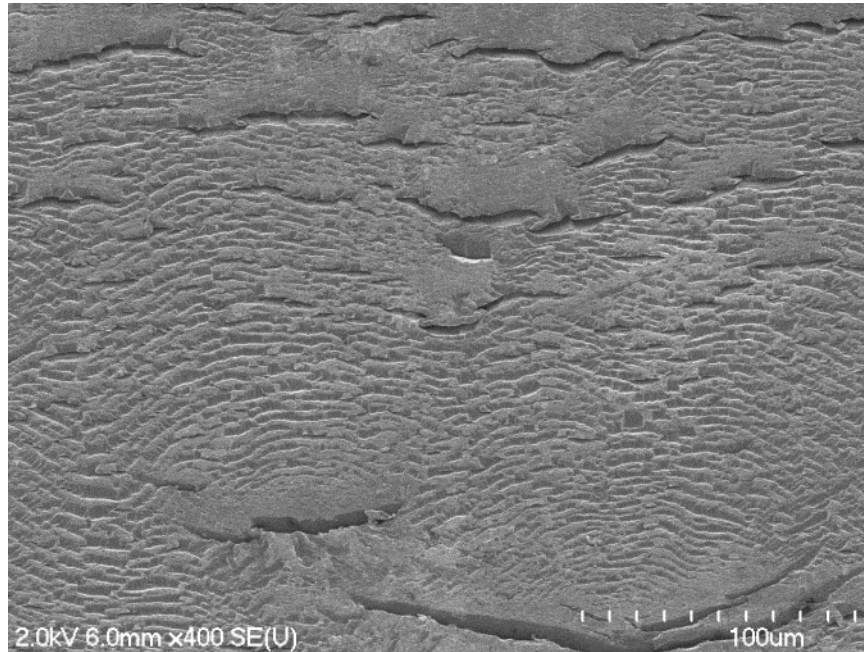


Figure 4-77 Magnified image of the marked area on Figure 4-73 (b)

4.5.6.2 Single Lap Joints containing 0.5 wt% MWCNTs

Figure 4-78 shows the fracture surface of a sample containing 0.5 wt% MWCNTs which was broken after 9200 fatigue cycles. The image illustrates that there are three types of cracks; long continuous cracks which travels the width of the surface; localized short and deep cracks; and also cracks in the form of striations that travels through the width of the surface. Figure 4-79 (a) and (b) magnifies the marked area (a) and (b) on Figure 4-78, respectively. Figure 4-79 (a) shows localized short and deep cracks while Figure 4-79 (b) illustrates cracks in the form of striations.

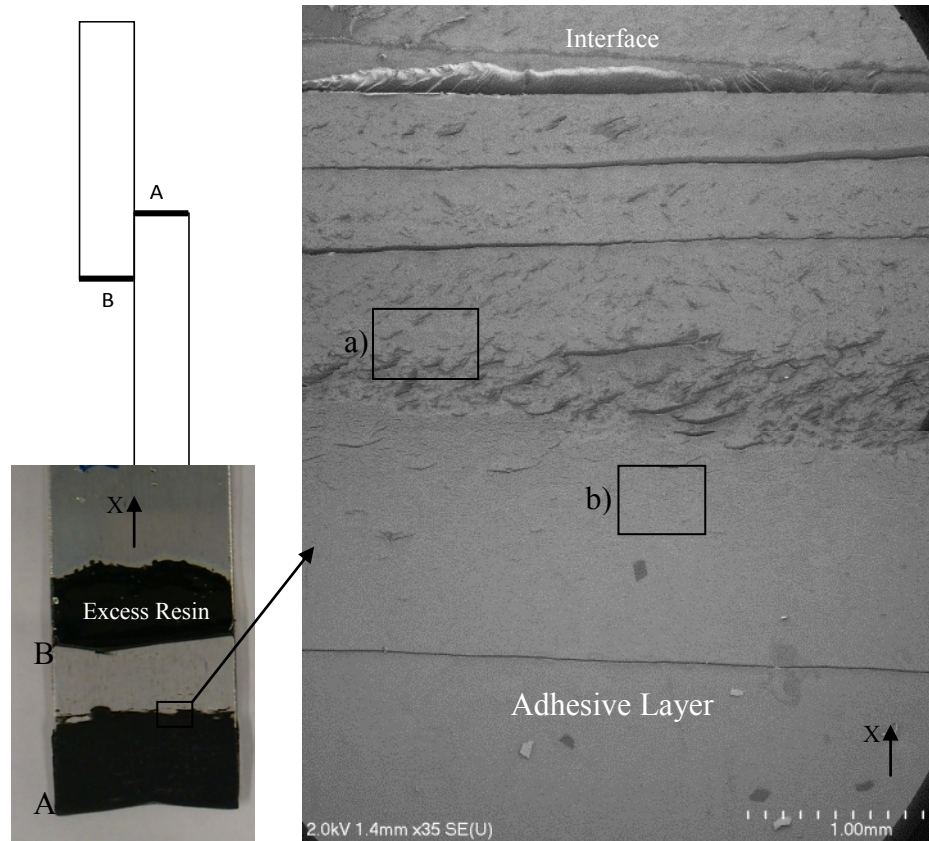


Figure 4-78 Fracture surface of a sample containing 0.5 wt% MWCNTs which was broken after 9200 cycles. (Sample 0.5-9)

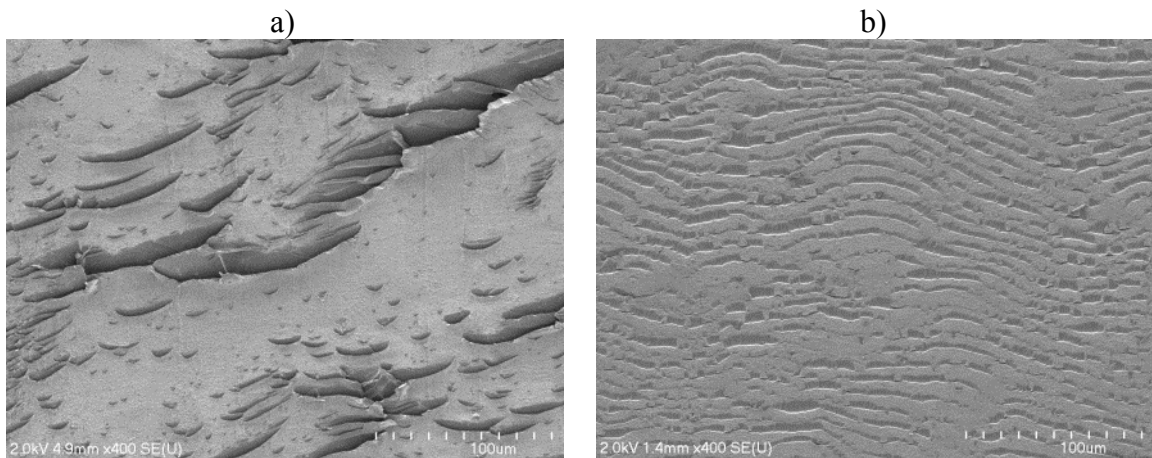


Figure 4-79 Magnified image of marked section a) and b) on Figure 4-78

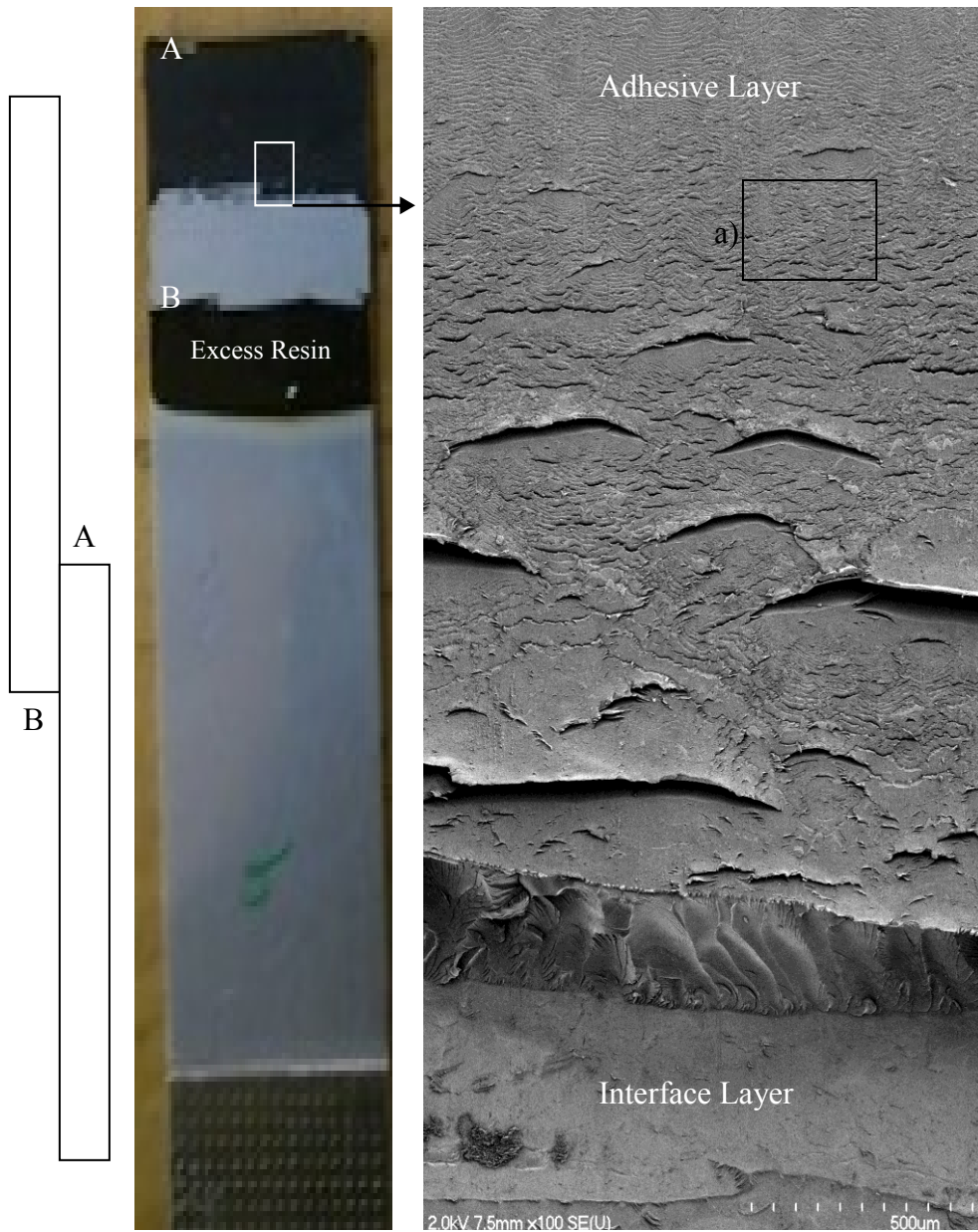


Figure 4-80 Fracture surface of a sample containing 0.5 wt% MWCNTs which was broken after 18193 cycles. (Sample 0.5-4)

Figure 4-80 shows the fracture surface of a single lap joint containing 0.5 wt% MWCNTs which was broken after 18190 fatigue cycles. There is no evidence of long continuous cracks, however, short deep cracks and cracks in the form of striations are visible on the fracture surface. Figure 4-81 magnifies the marked area (a) on Figure 4-80 which clearly shows crack striations.

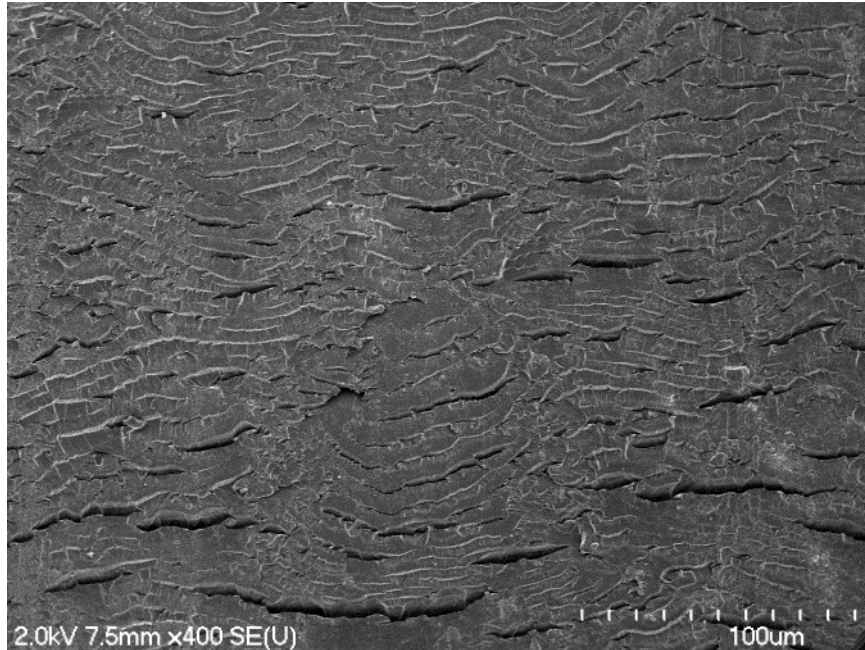


Figure 4-81 Magnified image of the marked area (a) on Figure 4-80

Figure 4-82 shows the fracture surface of a single lap joint containing 0.5 wt% MWCNTs which was broken after 36000 fatigue cycles. Image (a) shows evidence of few long continuous cracks along with short and deep cracks. Image (b) magnifies the marked area (b) on image (a) which illustrates evidence of cracks in the form of striations.

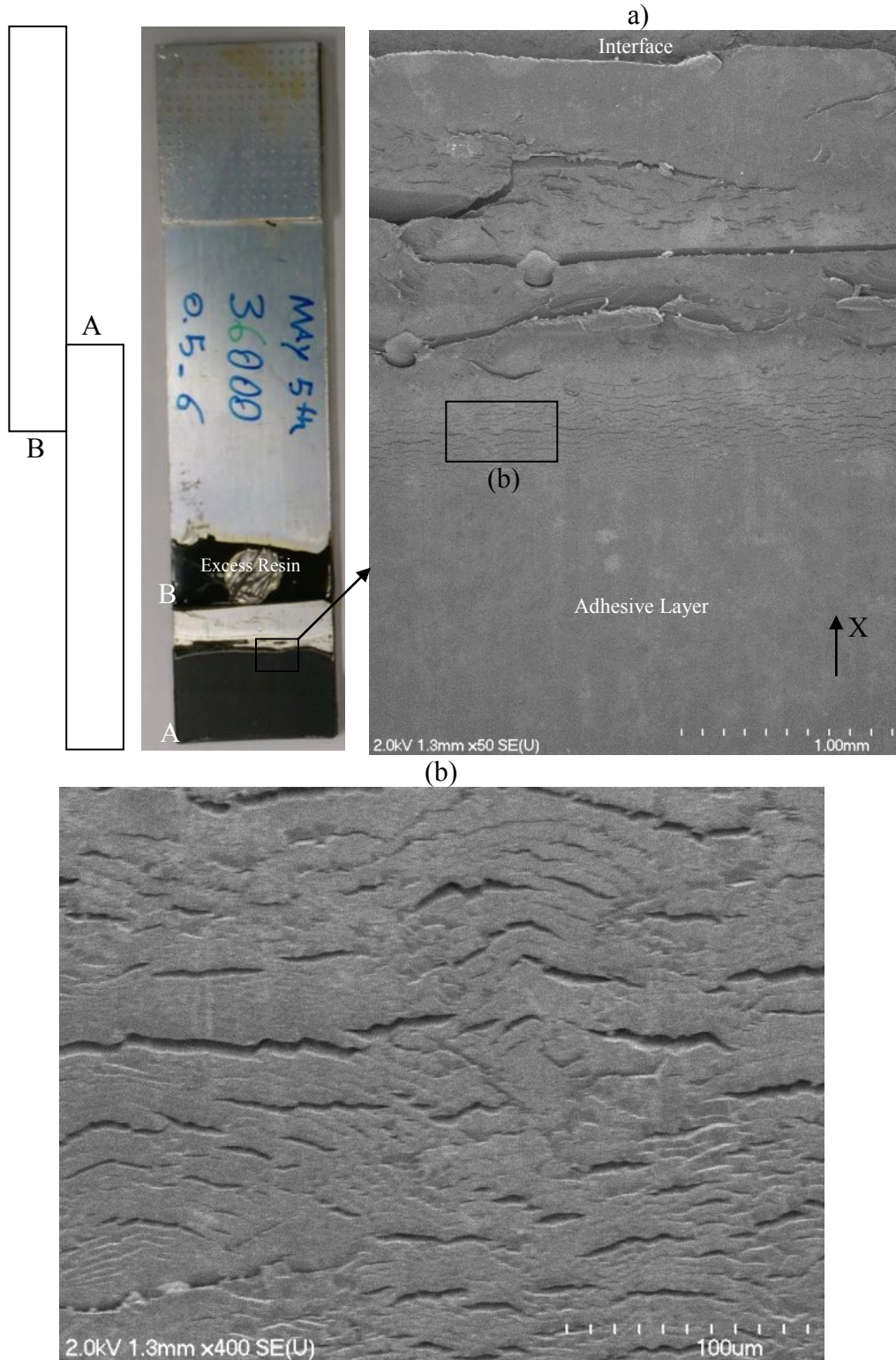


Figure 4-82 a) Fracture surface of a sample containing 0.5 wt% MWCNTs which was broken after 36000 cycles. (Sample 0.5-14) and b) magnified image of the square marked area (b)

4.5.6.3 Single Lap Joints containing 1 wt% MWCNTs

Figure 4-83 shows the fracture surface of a single lap joint containing 1 wt% MWCNTs which was broken after 5255 cycles. Figure 4-84 magnifies the marked areas (a) and (b) on Figure 4-83 and crack striations are visible on the fracture surface.

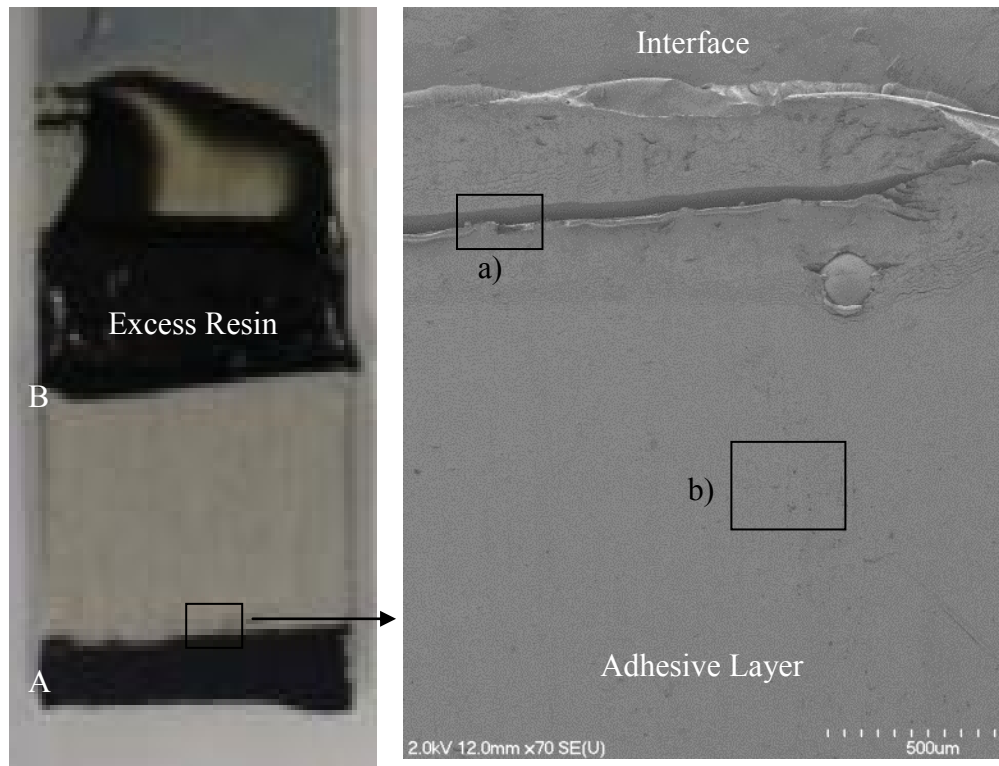


Figure 4-83 Fracture surface of a sample containing 1 wt% MWCNTs which was broken after 5255 cycles. (Sample 1-29)

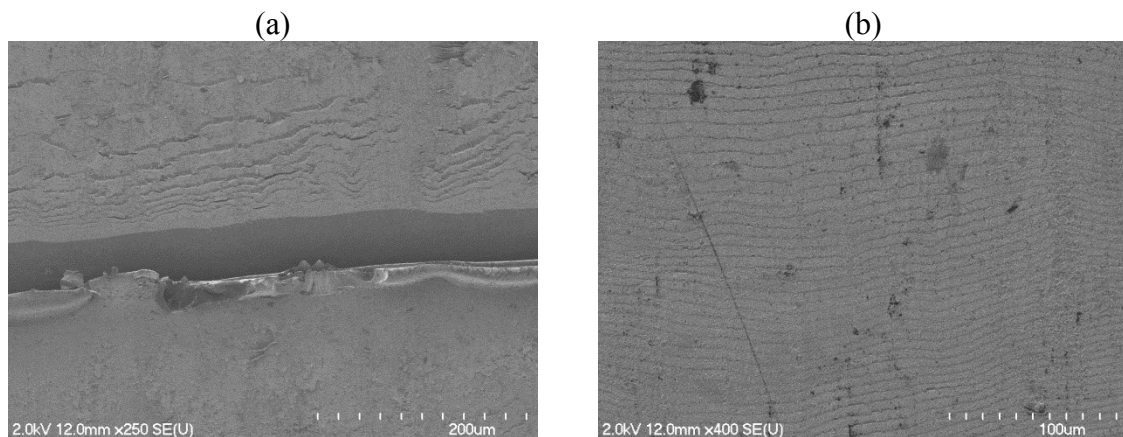


Figure 4-84 Magnified image from the marked area a) and b) on Figure 4-83

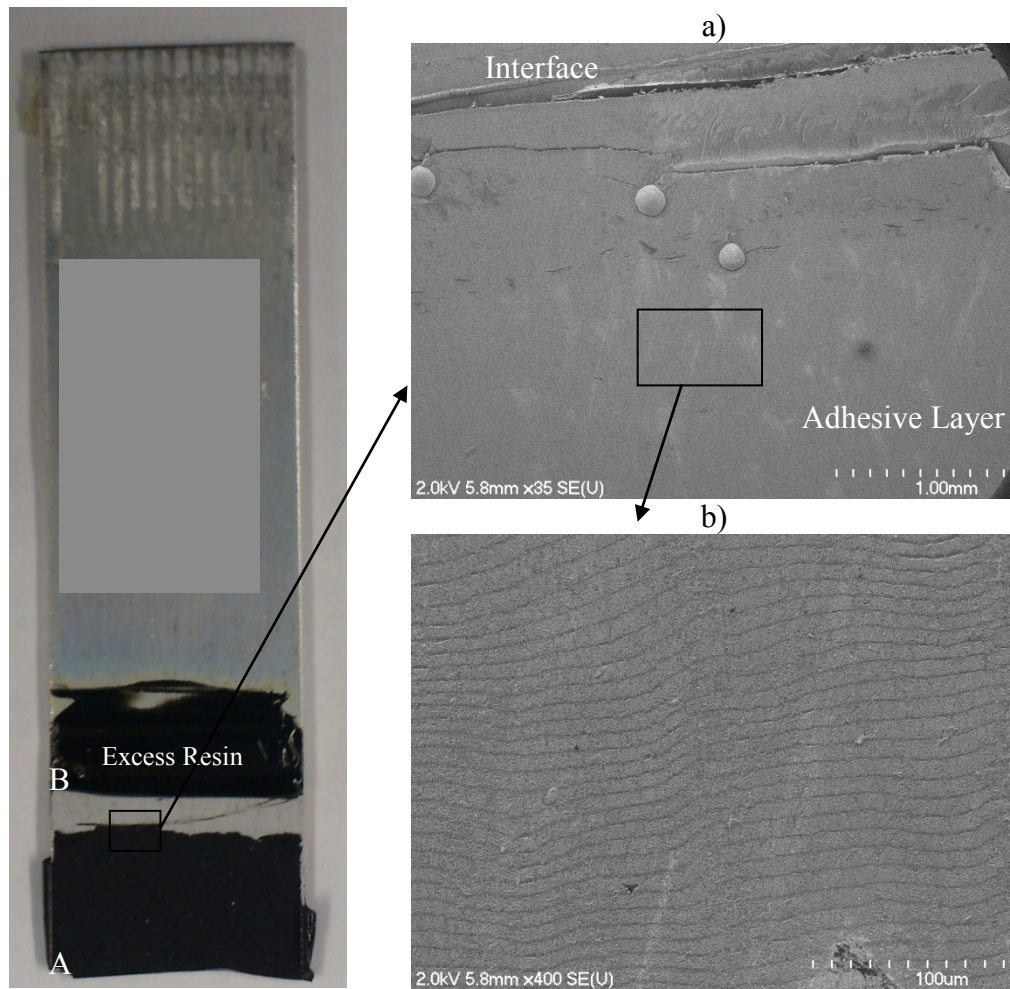


Figure 4-85 a) Fracture surface of a sample containing 1 wt% MWCNTs which was broken after 14000 cycles. (Sample 1-28) and b) magnified image of the marked area on a)

Figure 4-85 a) shows the fracture surface of a single lap joint containing 1 wt% MWCNTs which was broken after 14000 fatigue cycles. Figure 4-85 b) shows magnified image of the mark area on image a) and cracks in the form of striations are clearly visible.

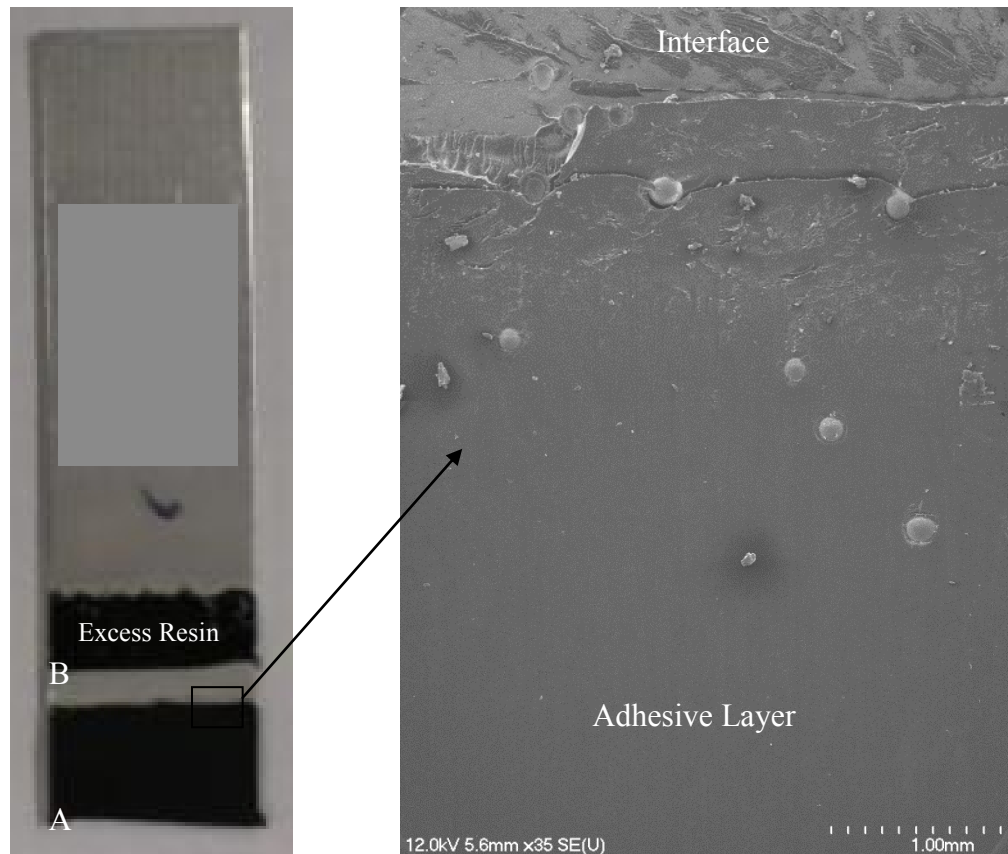


Figure 4-86 Fracture surface of a sample containing 1 wt% MWCNTs which was broken after 135750 cycles. (Sample 1-13)

Figure 4-86 shows the fracture surface of a single lap joint containing 1 wt% MWCNTs which was broken after 135750 fatigue cycles. As the image indicates there is no evidence of either crack striations or long continuous crack on the fracture surface.

4.5.6.4 SEM Image of Glass Beads

Figure 4-87 to Figure 4-89 are SEM images of glass beads on the fracture surface of joints containing 0, 0.5, and 1 wt% MWCNTs. As the images illustrate, there are multiple cracks and wrinkles in the vicinity of the glass bead in the joint with no CNT loading, however, the images for the joints with 0.5 wt% and 1 wt% MWCNTs show almost no or few cracks in the vicinity of the glass bead. This phenomenon can also be explained that

the addition of MWCNTs toughened the adhesive and reduced the number of cracks that would have occurred due to existence of glass beads.

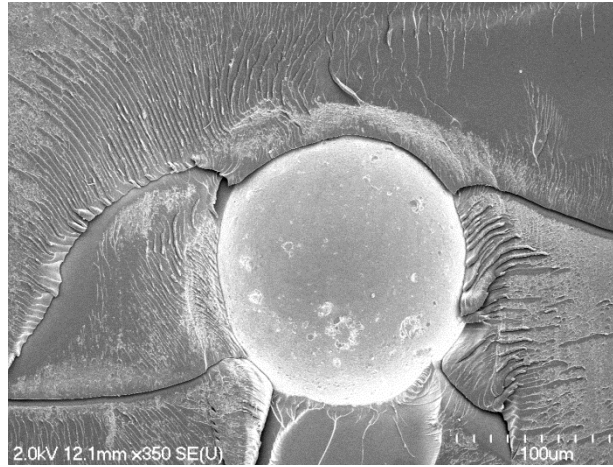


Figure 4-87 SEM image of glass bead on the fracture surface of a joint with 0 wt% MWCNTs

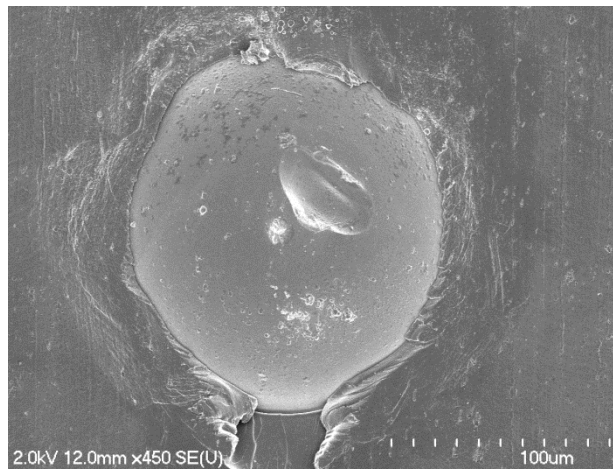


Figure 4-88 SEM image of glass bead on the fracture surface of a joint with 0.5 wt% MWCNTs

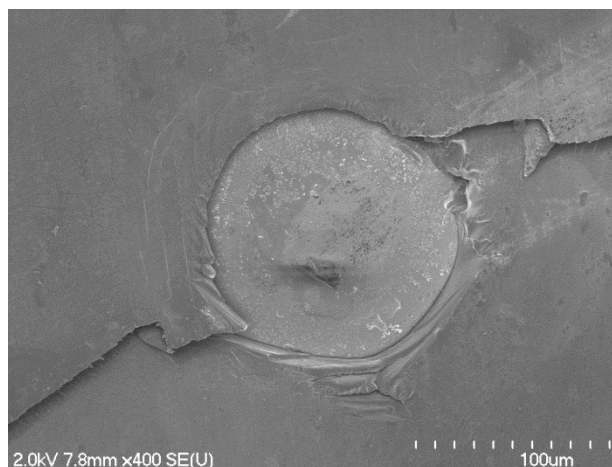


Figure 4-89 SEM image of glass bead on the fracture surface of a joint with 1 wt% MWCNTs

4.5.6.5 Comparison

Based on the images provided in previous sections, three types of cracks occur inside adhesive after fatigue loading. These cracks are, long cracks which travels through the width of the fracture surface, small cracks which are deep and short in length, and cracks that forms striations. It appears that these cracks occur randomly through the fracture surface and are independent of the fatigue loading and CNT concentration. However, long cracks seem to be more prevalent in joints with no CNTs. Introducing MWCNTs inside the adhesive reduces the number of long cracks in other word it toughened the adhesive by preventing the cracks to grow longer. Short cracks and striations are common between joints with and without CNTs. Nevertheless, as Figure 4-25 and Figure 4-26 illustrates, existence of carbon nanotube between these types of cracks strengthens the adhesive due to CNT bridging and pull outs. Moreover, as explained in section 4.5.6.4 addition of MWCNTs improved the adhesive in the vicinity of the glass beads.

4.5.6.6 Conclusion

Author believes that a comprehensive study should be carried out in order to fully understand the phenomenon described above. Further study on the fracture surface of different joints with different CNT loading is recommended since, multiple factor can affect the formation of cracks inside the adhesive. Some of these factors are, maximum and minimum fatigue loading, frequency of the fatigue loading, different CNT concentrations, different CNT types, and the fatigue cycle at which a specific joint is broken.

Chapter 5

Conclusions and

Future Works

5 Conclusions and Future Works

5.1 Conclusions

Although adhesive joints have found application in aerospace and automotive industries, lack of confidence in performing well under dynamic loadings may lead to reduction in their usage on critical applications. Manager added confidence requires manufacturers to add bolts or rivets to adhesive joints to bring confidence on their performance. In effect, this manager added confidence leads to the structure to become heavy again. This research projects introduced an in-situ monitoring technique which is capable of evaluating the integrity of adhesively bonded joints and also provide valuable indicators which predicts catastrophic failure well in advance. Application of this technique in real structures can bring back the confidence in using adhesive joints in aerospace and automotive industries.

On-line health monitoring and residual life prognosis using carbon nanotube networks inside the adhesive proved to be capable of assessing the integrity of the joints throughout dynamic loading. Three regions were observed on the electrical resistance signature curve.

1. The safe zone which covered approximately 60% of the fatigue life. The resistance increased linearly to less than 10% of the initial resistance.
2. The waning zone in which the resistance changes accelerated and reached to more than 10% of the initial resistance.

3. The failure zone which indicates the final 10% of the fatigue life. The resistance change was dramatic in this zone.

Moreover, two warning indicators were observed on the electrical resistance signatures of adhesively bonded joints.

1. The resistance change of more than 10% of the joint initial resistance which corresponded to the 60% to 90% of the fatigue life.
2. The slope of the resistance signature curve reached 1 ($\Omega/100$ cycles) between 80 to 90% of the fatigue life.

This technique opened up a window in using adhesive joints with more confidence regarding their fatigue behavior.

Comparison of adhesive joints with different MWCNTs loadings illustrates that addition of 0.5 wt% CNTs increased the shear strength 10% compared to that of neat adhesive. However, addition of more CNTs than 0.5 wt% did not have any significant effect on the shear strength of the joints. Introducing 1 wt% MWCNTs improved the fatigue life of the joints by more than 20% compared to neat adhesive. Electrical resistance dropped more than 7 orders of magnitude by only dispersing 0.5 wt% MWCNTs inside adhesive resin.

5.2 Contribution

The main contribution of this project was introducing a structural health monitoring technique to be used for adhesively bonded joints to increase their reliability throughout their service life. Although adhesive joints have good fatigue behavior, catastrophic failure without any warning is common between them. Therefore, it is necessary to

provide an in-situ technique to improve their reliability throughout dynamic loading. In this research project the sensitivity of the carbon nanotube networks inside the adhesive towards damages and cracks was used to evaluate the integrity of the joints and to predict the failure well in advance. The probability to predict the catastrophic failure before it occurs offers more confidence and reliability in the application of adhesive joints which is of prime importance in aerospace and automotive industries. Therefore, improving the reliability of adhesive joints to perform under dynamic loading is the most outstanding outcome of this thesis project.

5.3 Future Works

The proposed technique is just a beginning of a journey to improve the reliability of adhesive joints under dynamic loading. More has to be done to create a complete technique to monitor the integrity of adhesive bonds and predict their failure under all real life circumstances. Long term effects of moisture, temperature, relaxation, and corrosion should be investigated on adhesive bonds and in effect the capability of the technique to perform well under these effects should be evaluated. A theoretical model based on this technique should be generated to complement the experimental results and to present insight into the fatigue behavior of adhesively bonded joints. Therefore, more experiments on different joint geometry in different loading conditions should be performed to produce a complete data archive on the fatigue life of adhesively bonded joints. Hence the data archive should be used to generate a comprehensive theoretical model along with a complete in-situ technique to provide accurate residual life prognosis under complex real life conditions.

6 References

1. Zhang W., Sakalkar V., and Koratkar N., "*In Situ Health Monitoring and Repair in Composites using Carbon Nanotube Additives*," Applied Physics Letters, 2007, 91(13) pp. 133102.
2. KahramanRamazan, Sunar Mehmet, and YilbasBekir, "*Influence of Adhesive Thickness and Filler Content on the Mechanical Performance of Aluminum Single-Lap Joints Bonded with Aluminum Powder Filled Epoxy Adhesive*," Journal of Materials Processing Technology, 2008, 205(1-3) pp. 183-189.
3. Borsellino C., Di Bella G., and Ruisi V. F., "*Adhesive Joining of Aluminium AA6082: The Effects of Resin and Surface Treatment*," International Journal of Adhesion and Adhesives, 2009, 29(1) pp. 36-44.
4. Pereira, A. M., Ferreira, J. M., Antunes, F. V., and Bártolo, P. J., "*Study on the Fatigue Strength of AA 6082-T6 Adhesive Lap Joints*," International Journal of Adhesion and Adhesives, 2009, 29(6) pp. 633-638.
5. M PEREIRA A. M FERREIRA J. V ANTUNES F., and J BARTOLO P., "*Analysis of Manufacturing Parameters on the Shear Strength of Aluminium Adhesive Single-Lap Joints*," 2010, 210(4) pp. 610; 8-617.
6. Jen Yi-Ming, and KoChih-Wei, "*Evaluation of Fatigue Life of Adhesively Bonded Aluminum Single-Lap Joints using Interfacial Parameters*," International Journal of Fatigue, 2010, 32(2) pp. 330-340.
7. Barnes T. A., and Pashby I. R., "*Joining Techniques for AluminiumSpaceframes used in Automobiles: Part II — Adhesive Bonding and Mechanical Fasteners*," Journal of Materials Processing Technology, 2000, 99(1-3) pp. 72-79.
8. Mollie A. Bily, Young W. Kwon, Randall D. Pollak, "*Technical Report Naval Postgraduate School: Damage Detection in Composite Interfaces Through Carbon Nanotube Reinforcement*." 2010.
9. Daniel Balageas, Claus-Peter Fritzen, Alfredo Guemes, "*Structural Health Monitoring*," ISTE Ltd,2006.
10. Baldev Raj, T. Jayakumar, M. Thavasimuthu, "*Practical non-destructive testing*," 2007, Oxford, U.K. : Alpha Science Internationa, U.K., .
11. Gros X. E. (Xavier Emanuel), "*NDT data fusion / X.E. Gros*." Elsevier Science Ltd,1997, .
12. Prolongo S. G., Gude M. R., Sanchez J., and Ureña A., "*Nanoreinforced Epoxy Adhesives for Aerospace Industry*," The Journal of Adhesion, 2009, 85(4-5) pp. 180-199.
13. Thostenson Erik T., and ChouTsu-Wei, "*Carbon Nanotube-Based Health Monitoring of Mechanically Fastened Composite Joints*," Composites Science and Technology, 2008, 68(12) pp. 2557-2561.
14. BiernackiJacek M., and Beall Frank C., "*Acoustic Monitoring of Cold-Setting Adhesive Curing in Wood Laminates*," International Journal of Adhesion and Adhesives, 1996, 16(3) pp. 165-172.

15. Yang Shuo, GuLan, and Gibson Ronald F., *"Nondestructive Detection of Weak Joints in Adhesively Bonded Composite Structures,"* Composite Structures, 2001, 51(1) pp. 63-71.
16. MICKENS T., SCHULZ M., SUNDARESAN M., GHOSHAL A., NASER A. S., and REICHMEIDER R., *"STRUCTURAL HEALTH MONITORING OF AN AIRCRAFT JOINT,"* Mechanical Systems and Signal Processing, 2003, 17(2) pp. 285-303.
17. Jones R., and Galea S., *"Health Monitoring of Composite Repairs and Joints using Optical Fibres,"* Composite Structures, 2002, 58(3) pp. 397-403.
18. Brotherhood C. J., Drinkwater B. W., and Dixon S., *"The Detectability of Kissing Bonds in Adhesive Joints using Ultrasonic Techniques,"* Ultrasonics, 2003, 41(7) pp. 521-529.
19. Herszberg I., Li H. C. H., Dharmawan F., Mouritz A. P., Nguyen M., and Bayandor J., *"Damage Assessment and Monitoring of Composite Ship Joints,"* Composite Structures, 2005, 67(2) pp. 205-216.
20. Kesavan A., Deivasigamani M., John S., and Herszberg I., *"Damage Detection in T-Joint Composite Structures,"* Composite Structures, 2006, 75(1-4) pp. 313-320.
21. Palaniappan J., Wang H., Ogin S. L., Thorne A. M., Reed G. T., Crocombe A. D., Rech Y., and Tjin S. C., *"Changes in the Reflected Spectra of Embedded Chirped Fibre Bragg Gratings used to Monitor Disbonding in Bonded Composite Joints,"* Composites Science and Technology, 2007, 67(13) pp. 2847-2853.
22. Palaniappan J., Ogin S. L., Thorne A. M., Reed G. T., Crocombe A. D., Capell T. F., Tjin S. C., and Mohanty L., *"Disbond Growth Detection in composite-composite Single-Lap Joints using Chirped FBG Sensors,"* Composites Science and Technology, 2008, 68(12) pp. 2410-2417.
23. Karp Baruch, Rittel Daniel, and Durban David, *"Health Monitoring of Joints using Dynamic End Effects,"* Journal of Sound and Vibration, 2008, 312(1-2) pp. 257-272.
24. Zhang Ye, Vassilopoulos, Anastasios P., and Keller Thomas, *"Stiffness Degradation and Fatigue Life Prediction of Adhesively-Bonded Joints for Fiber-Reinforced Polymer Composites,"* International Journal of Fatigue, 2008, 30(10-11) pp. 1813-1820.
25. VotsisRenosA., and ChryssanthopoulosMarios K., *"Assessment of Debonding in GFRP Joints using Damage Identification Techniques,"* Construction and Building Materials, 2009, 23(4) pp. 1690-1697.
26. Fasel Timothy R., and Todd Michael D., *"An Adhesive Bond State Classification Method for a Composite Skin-to-Spar Joint using Chaotic Insonification,"* Journal of Sound and Vibration, 2010, 329(15) pp. 3218-3232.
27. Fasel T. R., and Todd M. D., *"Chaotic Insonification for Health Monitoring of an Adhesively Bonded Composite Stiffened Panel,"* Mechanical Systems and Signal Processing, 2010, 24(5) pp. 1420-1430.

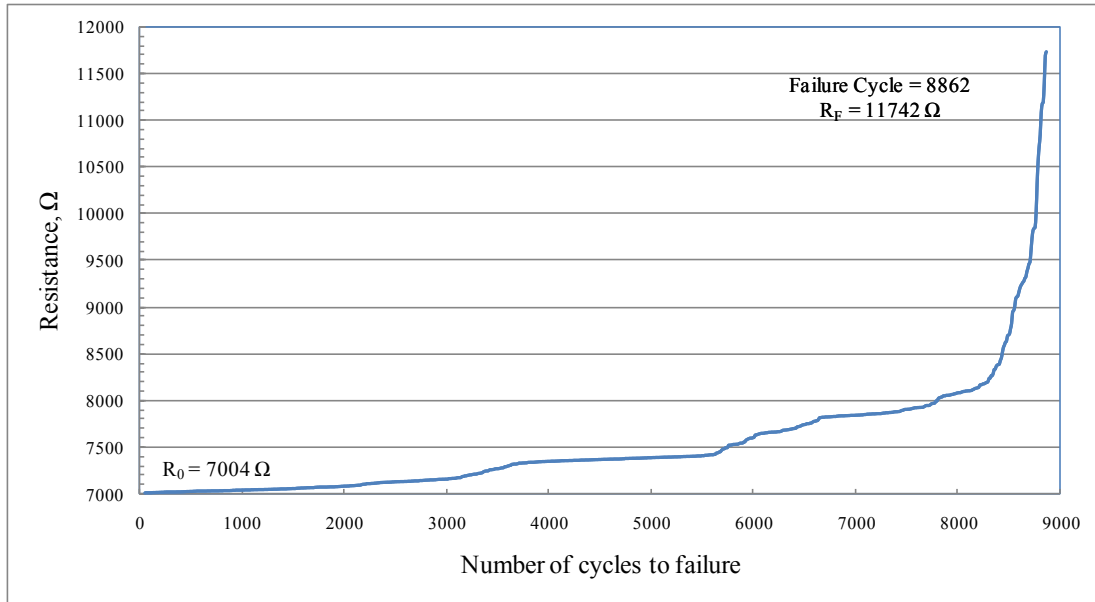
28. Argatov Ivan, and Sevostianov Igor, *"Health Monitoring of Bolted Joints Via Electrical Conductivity Measurements,"* International Journal of Engineering Science, 2010, 48(10) pp. 874-887.
29. Balle Frank, Huxhold Stefan, Wagner Guntram, and EiflerDietmar, *"Damage Monitoring of Ultrasonically Welded Aluminum/ CFRP-Joints by Electrical Resistance Measurements,"* Procedia Engineering, 2011, 10pp. 433-438.
30. Bernasconi Andrea, Carboni Michele, and Comolli Lorenzo, *"Monitoring of Fatigue Crack Growth in Composite Adhesively Bonded Joints using Fiber Bragg Gratings,"* Procedia Engineering, 2011, 10pp. 207-212.
31. BrankoGlisicI., *"Fiber Optic Methods For Structural Health Monitoring,"* John Wiley & Sons Ltd.2007, .
32. Kroto H. W., Heath J. R., O'Brien S. C., Curl R. F., and Smalley R. E., *"C60: Buckminsterfullerene,"* Nature, 1985, 318(6042) pp. 162-163.
33. IijimaSumio, *"Helical Microtubules of Graphitic Carbon,"* Nature, 1991, 354(6348) pp. 56-58.
34. Thostenson Erik T., Li Chunyu, and ChouTsu-Wei, *"Nanocomposites in Context,"* Composites Science and Technology, 2005, 65(3-4) pp. 491-516.
35. T THOSTENSON E., REN ZHIFENG, and Tsu-Wei CHOU, *"Advances in the Science and Technology of Carbon Nanotubes and their Composites : A Review,"* 2001, 61(13) pp. 1899-1912.
36. EsawiAmal M. K., and Farag Mahmoud M., *"Carbon Nanotube Reinforced Composites: Potential and Current Challenges,"* Materials & Design, 2007, 28(9) pp. 2394-2401.
37. Breuer O., and SundararajUttandaraman, *"Big Returns from Small Fibers: A Review of polymer/carbon Nanotube Composites,"* Polymer Composites, 2004, 25(6) pp. 630-645.
38. Jing Li, and Lump J. K., 2007, *"Carbon Nanotube Filled Conductive Adhesives for Aerospace Applications,"* Aerospace Conference, 2007 IEEE, Anonymous pp. 1-6.
39. SihSangwook, GanguliSabyasachi, Roy Ajit K., QuLiangti, and Dai Liming, *"Enhancement of through-Thickness Thermal Conductivity in Adhesively Bonded Joints using Aligned Carbon Nanotubes,"* Composites Science and Technology, 2008, 68(3-4) pp. 658-665.
40. Yu Suzhu, Tong Min N., and Critchlow Gary, *"Use of Carbon Nanotubes Reinforced Epoxy as Adhesives to Join Aluminum Plates,"* Materials & Design, 2010, 31(Supplement 1) pp. S126-S129.
41. Gojny Florian H., WichmannMalte H. G., Fiedler Bodo, and Schulte Karl, *"Influence of Different Carbon Nanotubes on the Mechanical Properties of Epoxy Matrix Composites – A Comparative Study,"* Composites Science and Technology, 2005, 65(15-16) pp. 2300-2313.

42. Yu Suzhu, Tong Min N., and Critchlow Gary, "*Wedge Test of Carbon-Nanotube-Reinforced Epoxy Adhesive Joints*," *Journal of Applied Polymer Science*, 2009, 111(6) pp. 2957-2962.
43. Xu L. R., Li Lang, Lukehart Charles M., and KuaiHuacheng, "*Mechanical Characterization of Nanofiber-Reinforced Composite Adhesives*," *Journal of Nanoscience and Nanotechnology*, 2007, 7(7) pp. 2546-2548.
44. Wu H. P., Wu X. J., Ge M. Y., Zhang G. Q., Wang Y. W., and JiangJianzhong, "*Properties Investigation on Isotropical Conductive Adhesives Filled with Silver Coated Carbon Nanotubes*," *Composites Science and Technology*, 2007, 67(6) pp. 1182-1186.
45. Kuang-Ting Hsiao, Justin Alms, and Suresh G Advani, "*Use of epoxy/multiwalled Carbon Nanotubes as Adhesives to Join Graphite Fibre Reinforced Polymer Composites*," *Nanotechnology*, 2003, 14(7) pp. 791.
46. Baughman Ray H., Cui Changxing, ZakhidovAnvar A., IqbalZafar, Barisci Joseph N., Spinks Geoff M., Wallace Gordon G., Mazzoldi Alberto, De Rossi Danilo, Rinzler Andrew G., Jaschinski Oliver, Roth Siegmar, and KerteszMiklos, "*Carbon Nanotube Actuators*," *Science*, 1999, 284(5418) pp. 1340-1344.
47. Li Chunyu, and ChouTsu-Wei, "*Atomistic Modeling of Carbon Nanotube-Based Mechanical Sensors*," *Journal of Intelligent Material Systems and Structures*, 2006, 17(3) pp. 247-254.
48. Thostenson E. T., and Chou Tsu-Wei, "*Carbon Nanotube Networks: Sensing of Distributed Strain and Damage for Life Prediction and Self Healing*," *Advanced Materials*, 2006, 18(21) pp. 2837-2841.
49. Nofar M., Hoa S. V., and Pugh M. D., "*Failure Detection and Monitoring in Polymer Matrix Composites Subjected to Static and Dynamic Loads using Carbon Nanotube Networks*," *Composites Science and Technology*, 2009, 69(10) pp. 1599-1606.
50. GaoLimin, Thostenson Erik T., Zhang Zuoguang, and ChouTsu-Wei, "*Sensing of Damage Mechanisms in Fiber-Reinforced Composites Under Cyclic Loading using Carbon Nanotubes*," *Advanced Functional Materials*, 2009, 19(1) pp. 123-130.
51. Lim Amanda S., Melrose Zachary R., Thostenson Erik T., and ChouTsu-Wei, "*Damage Sensing of Adhesively-Bonded Hybrid composite/steel Joints using Carbon Nanotubes*," *Composites Science and Technology*, 2011, 71(9) pp. 1183-1189.
52. Roscalosif D., and HoaSuong V., "*Highly Conductive Multiwall Carbon Nanotube and Epoxy Composites Produced by Three-Roll Milling*," *Carbon*, 2009, 47(8) pp. 1958-1968.
53. Pereira A. M., Ferreira J. M., Antunes F. V., and Bártolo P. J., "*Study on the Fatigue Strength of AA 6082-T6 Adhesive Lap Joints*," *International Journal of Adhesion and Adhesives*, 2009, 29(6) pp. 633-638.

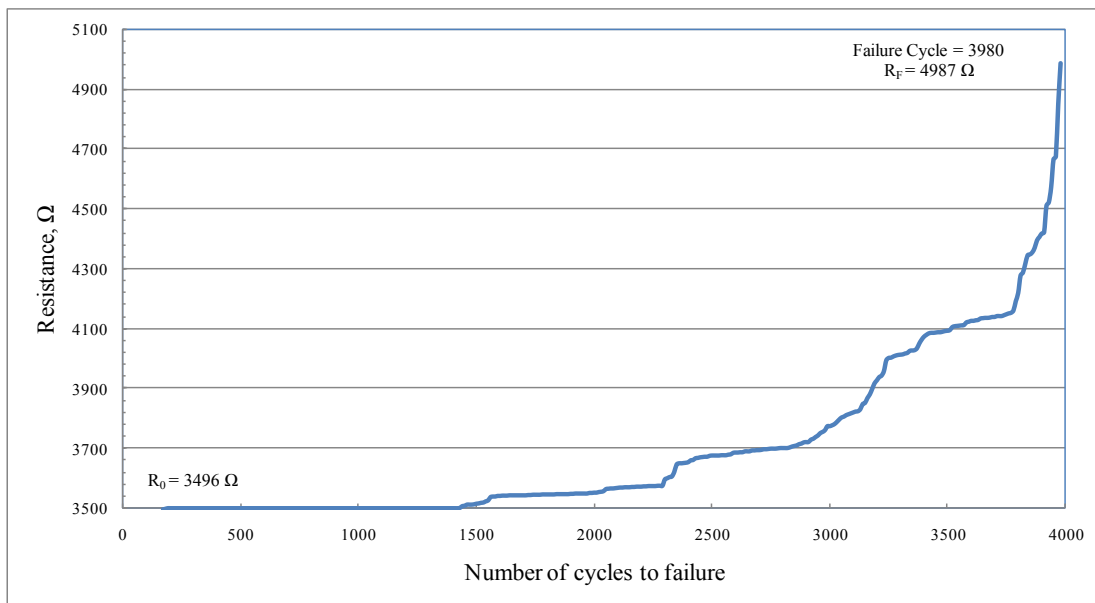
54. Liang Zhiyong, GouJihua, Zhang Chuck, Wang Ben, and Kramer Leslie, "Investigation of Molecular Interactions between (10, 10) Single-Walled Nanotube and Epon 862 resin/DETDA Curing Agent Molecules," *Materials Science and Engineering A*, 2004, 365(1-2) pp. 228-234.
55. Nagy Peter B., "Ultrasonic Classification of Imperfect Interfaces," *Journal of Nondestructive Evaluation*, 1992, 11(3) pp. 127-139.
56. <http://asm.matweb.com>
57. <http://www.hexion.com>
58. <http://www.cheaptubesinc.com/MWNTs.htm>

Appendix I) Electrical resistance signatures of all specimens tested under fatigue

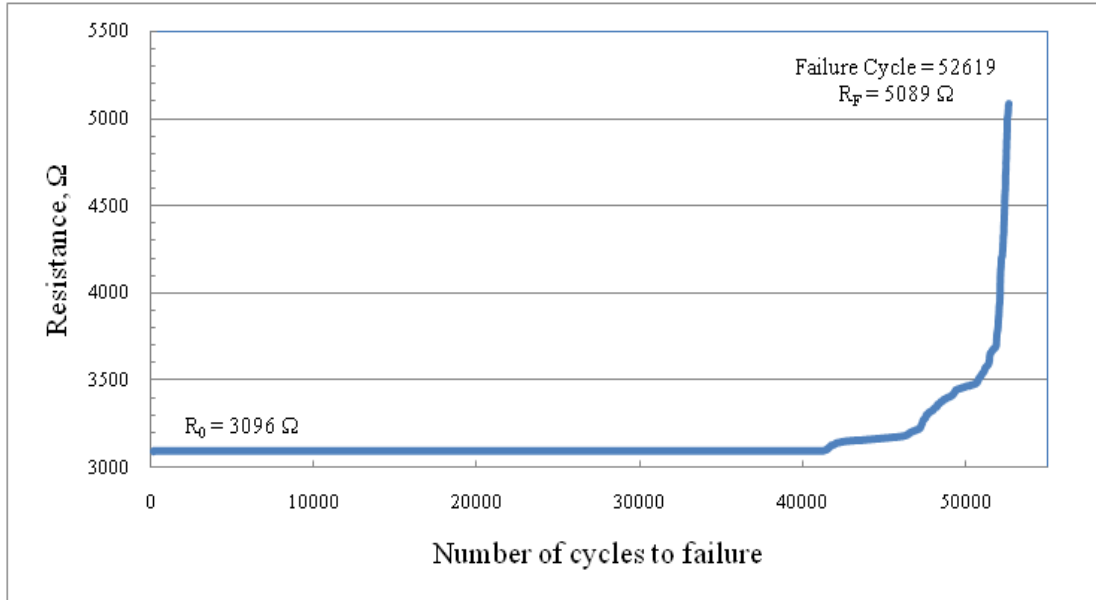
Joints with 0.5 wt% MWCNT



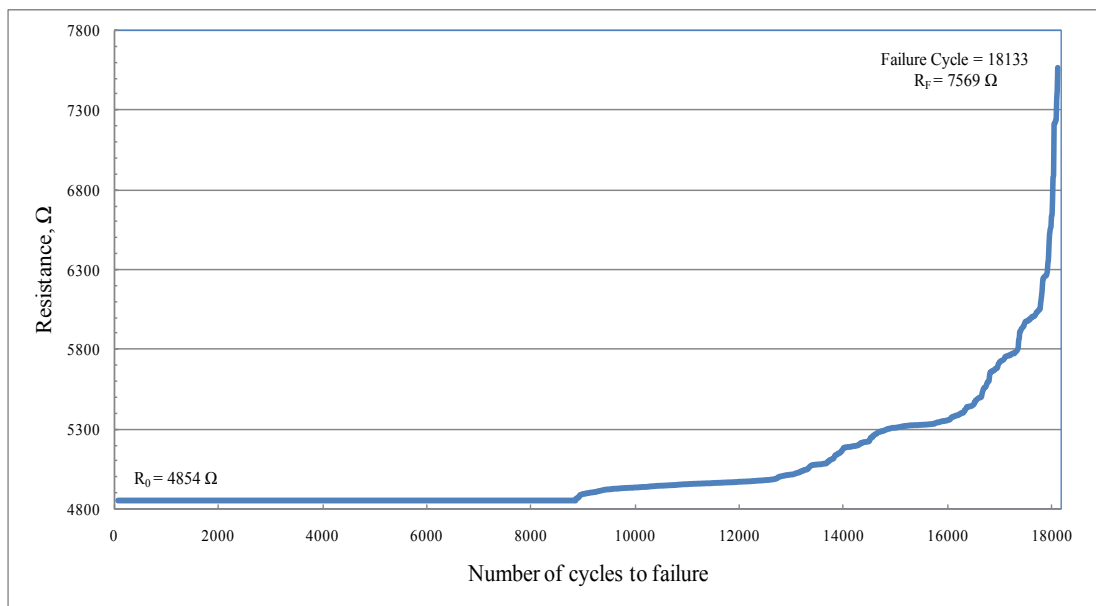
I-1 Electrical resistance signature for sample 0.5-1



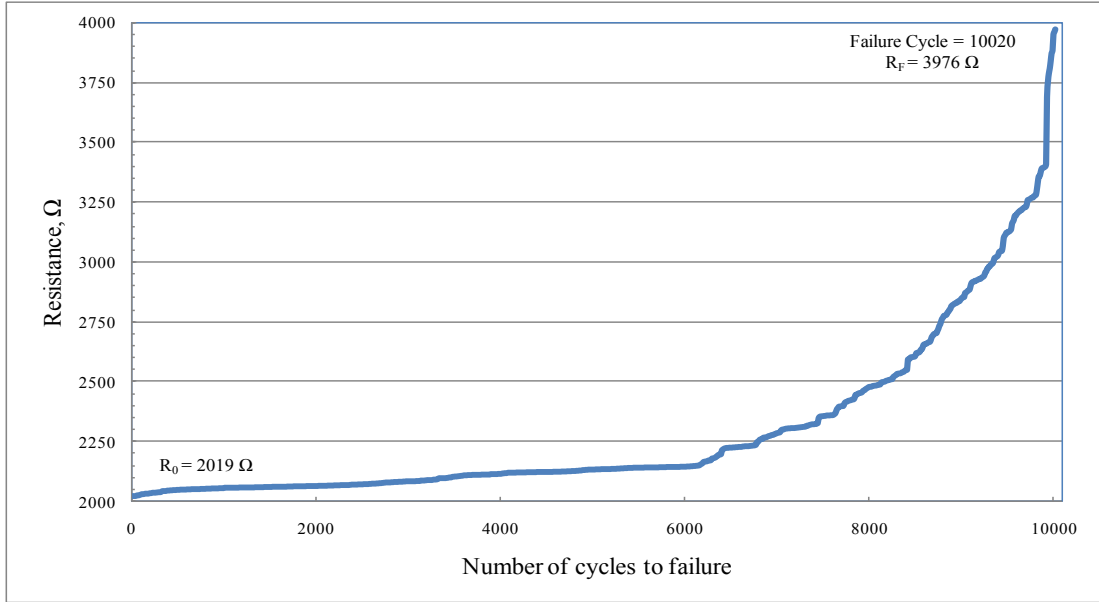
I-2 Electrical resistance signature for sample 0.5-2



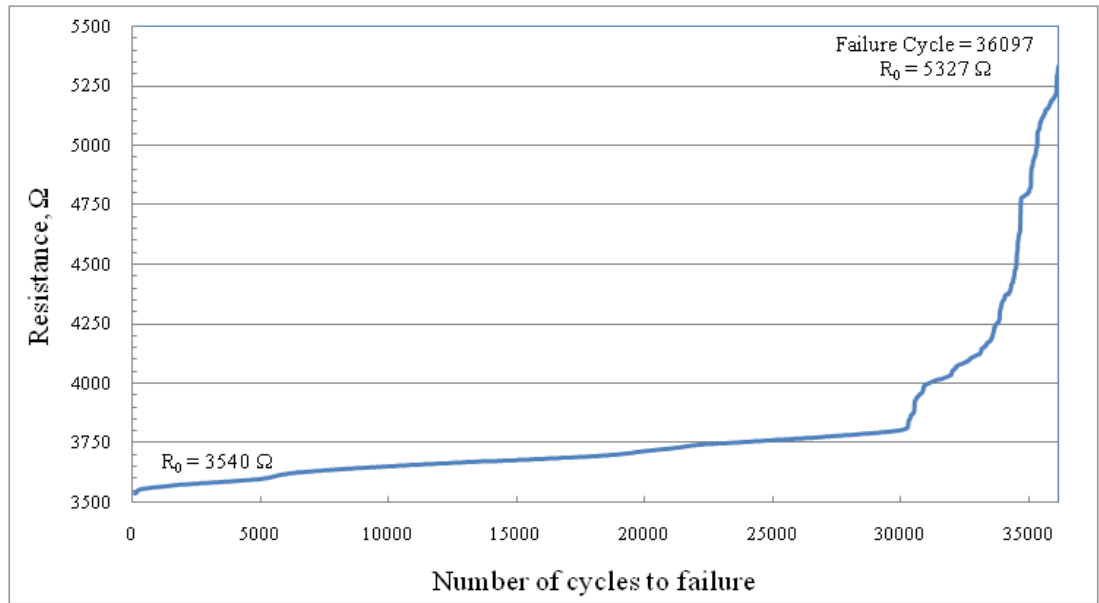
I-3Electrical resistance signature for sample 0.5-3



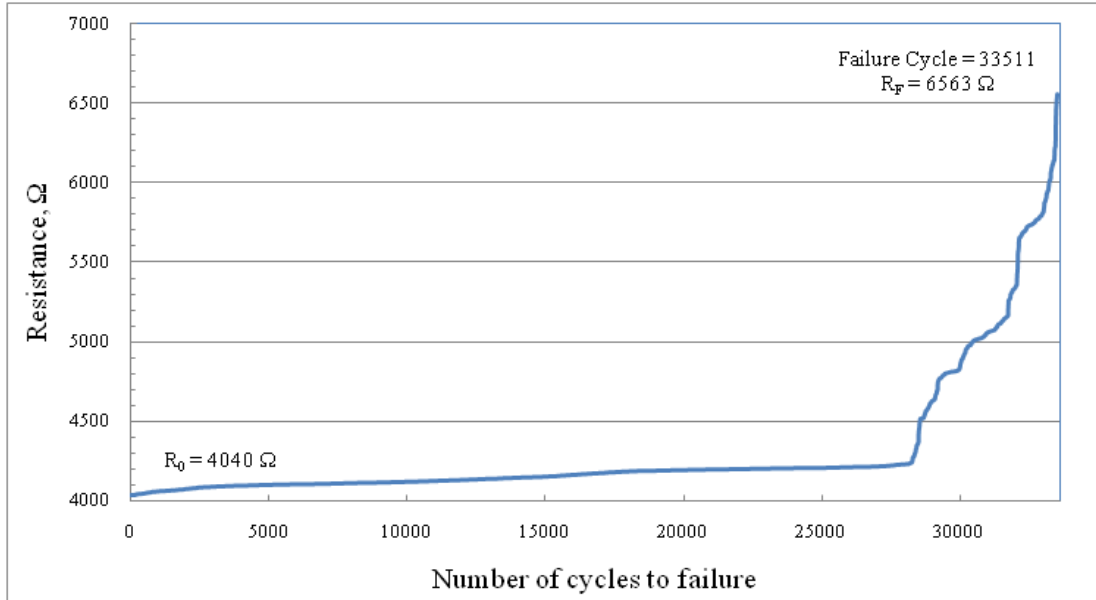
I-4Electrical resistance signature for sample 0.5-4



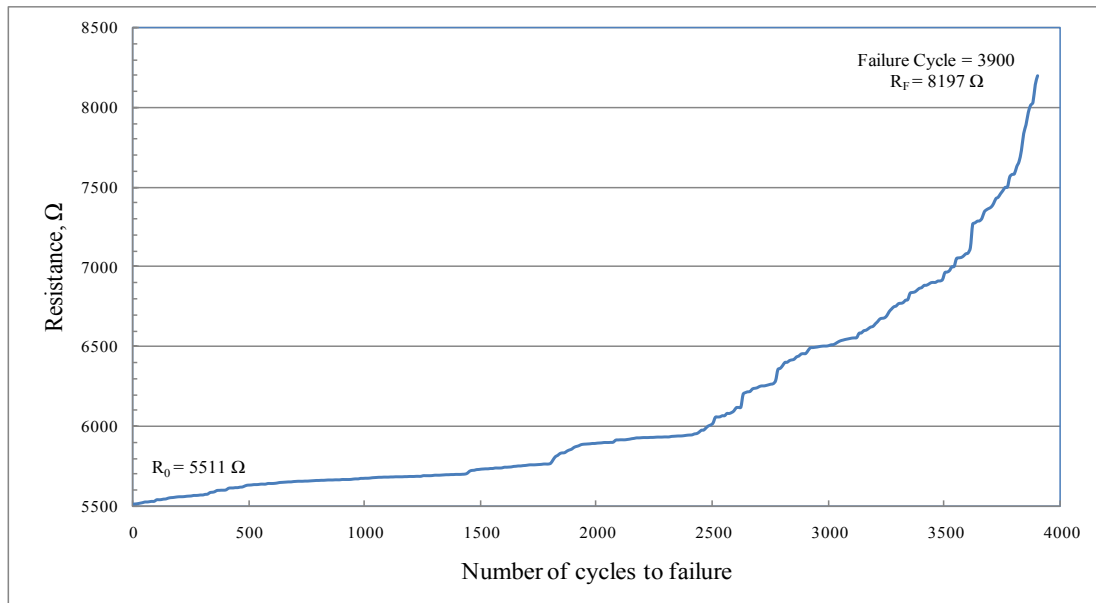
I-5Electrical resistance signature for sample 0.5-5



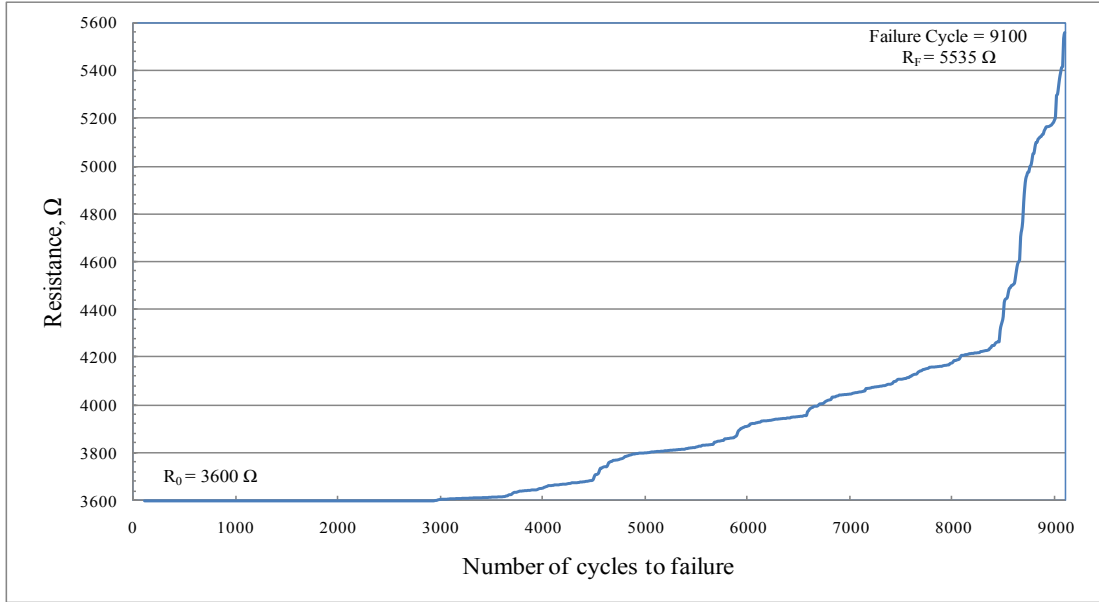
I-6Electrical resistance signature for sample 0.5-6



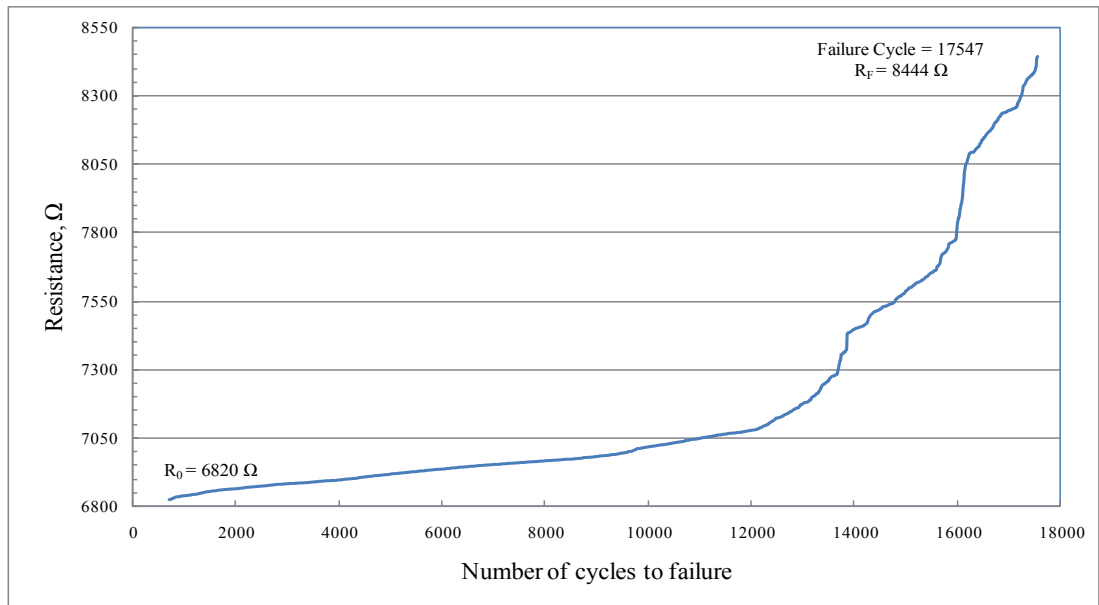
I-7Electrical resistance signature for sample 0.5-7



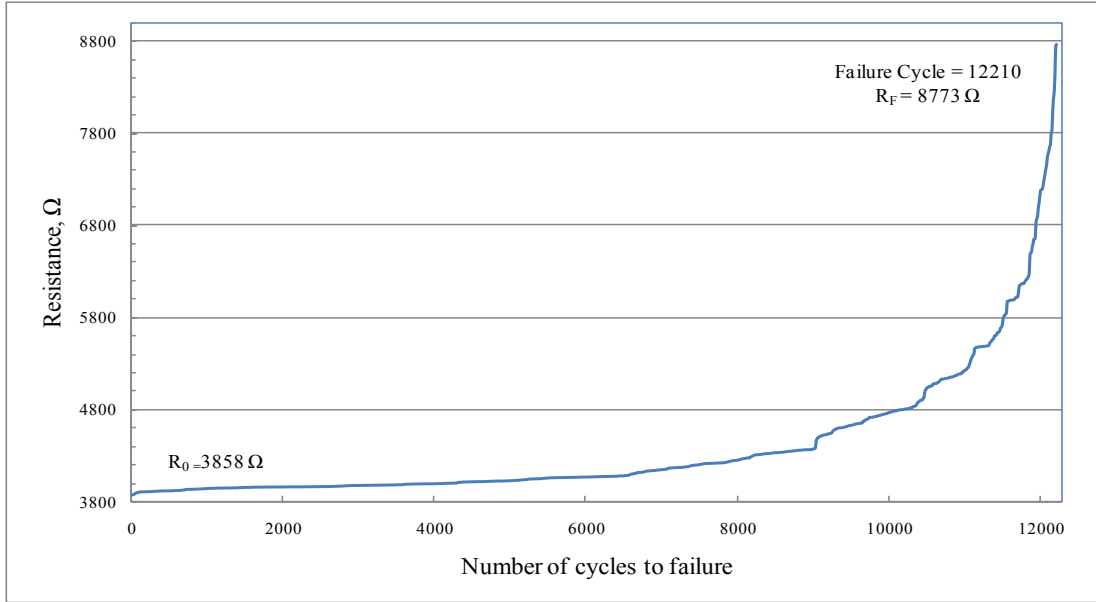
I-8Electrical resistance signature for sample 0.5-8



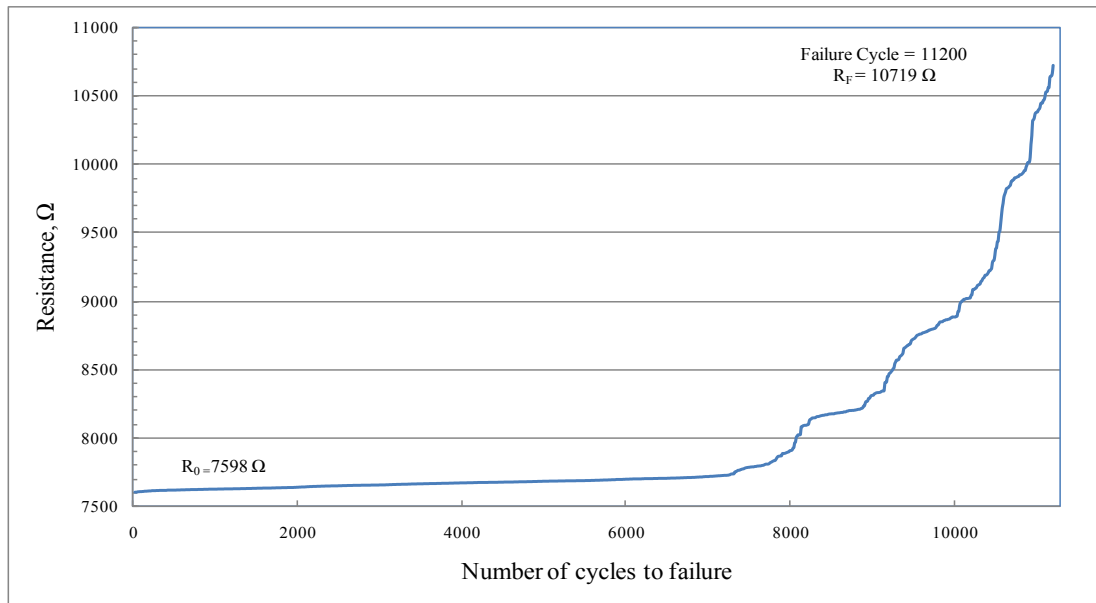
I-9Electrical resistance signature for sample 0.5-9



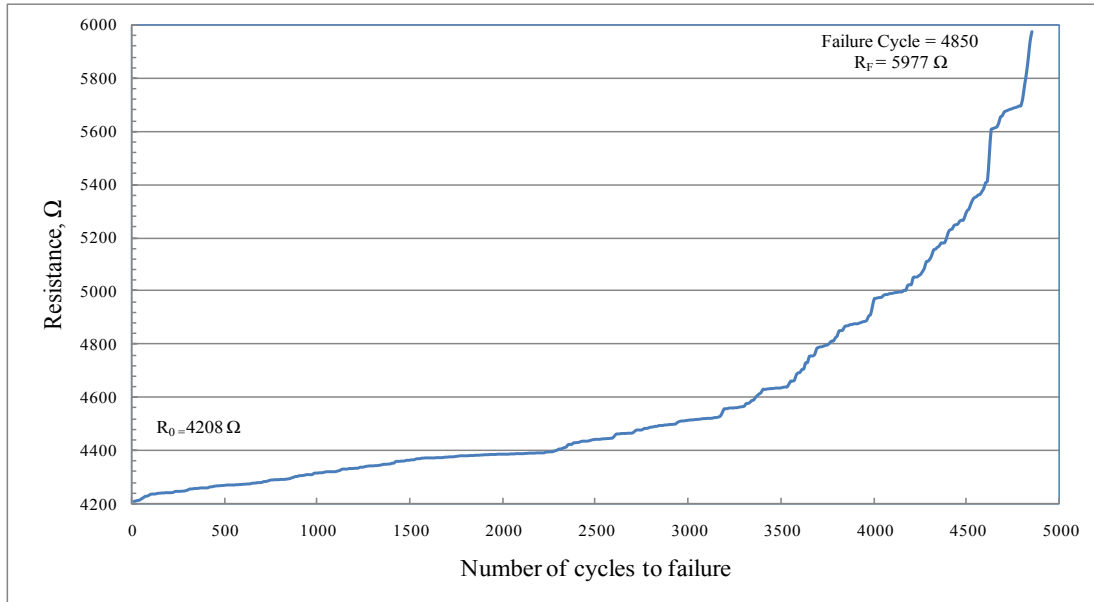
I-10Electrical resistance signature for sample 0.5-10



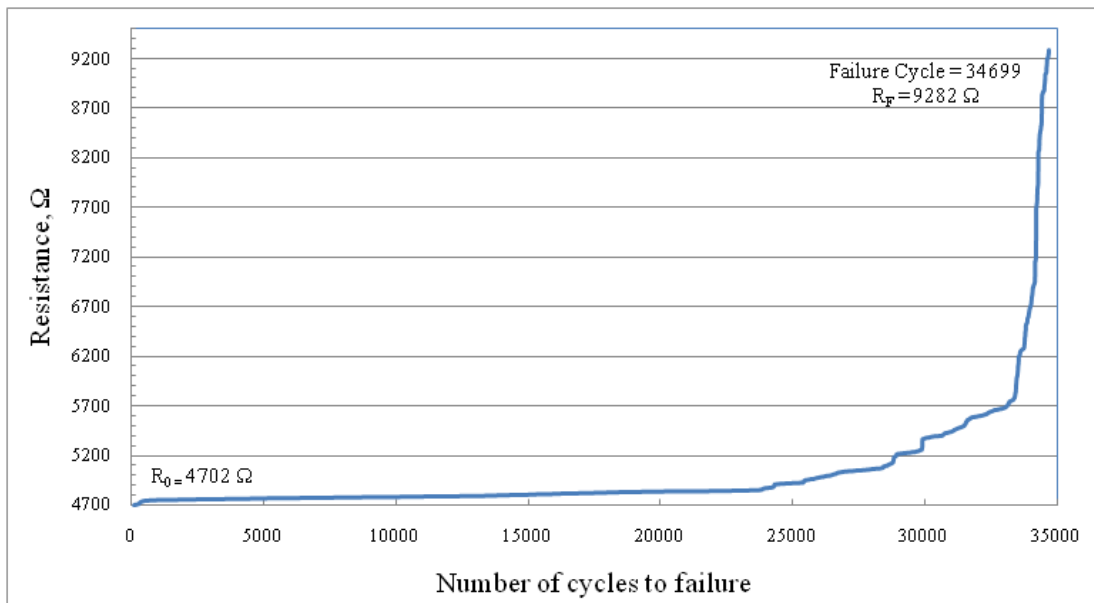
I-11Electrical resistance signature for sample 0.5-11



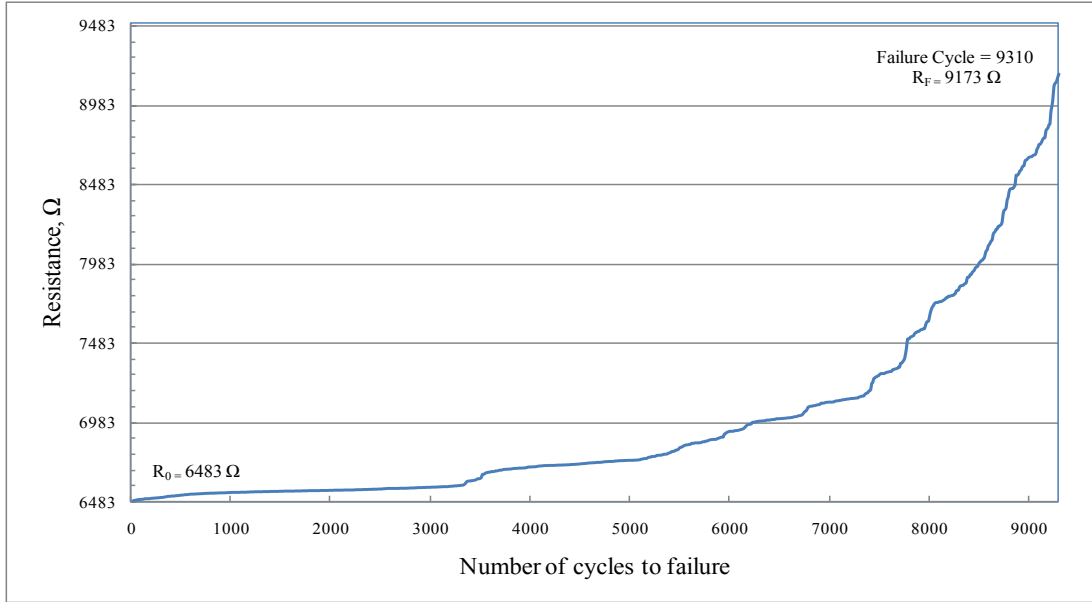
I-12Electrical resistance signature for sample 0.5-12



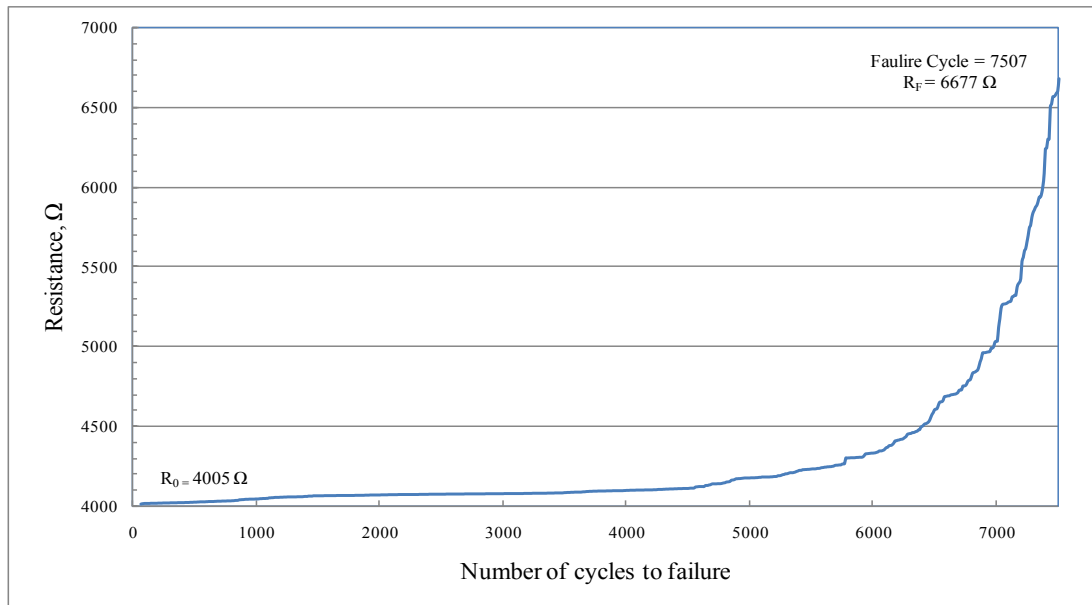
I-13Electrical resistance signature for sample 0.5-13



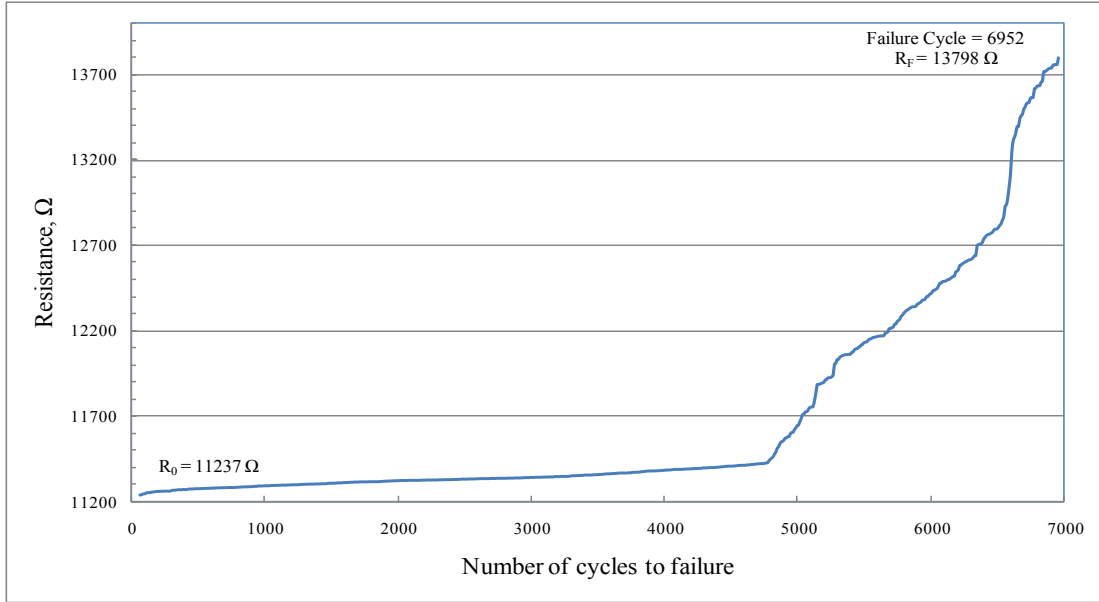
I-14Electrical resistance signature for sample 0.5-14



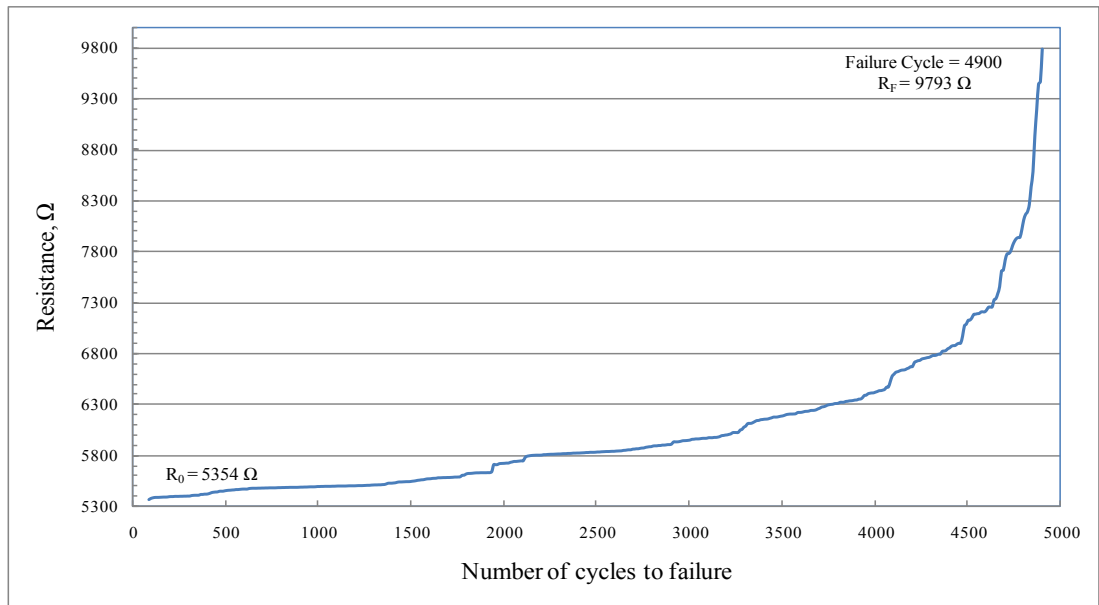
I-15Electrical resistance signature for sample 0.5-15



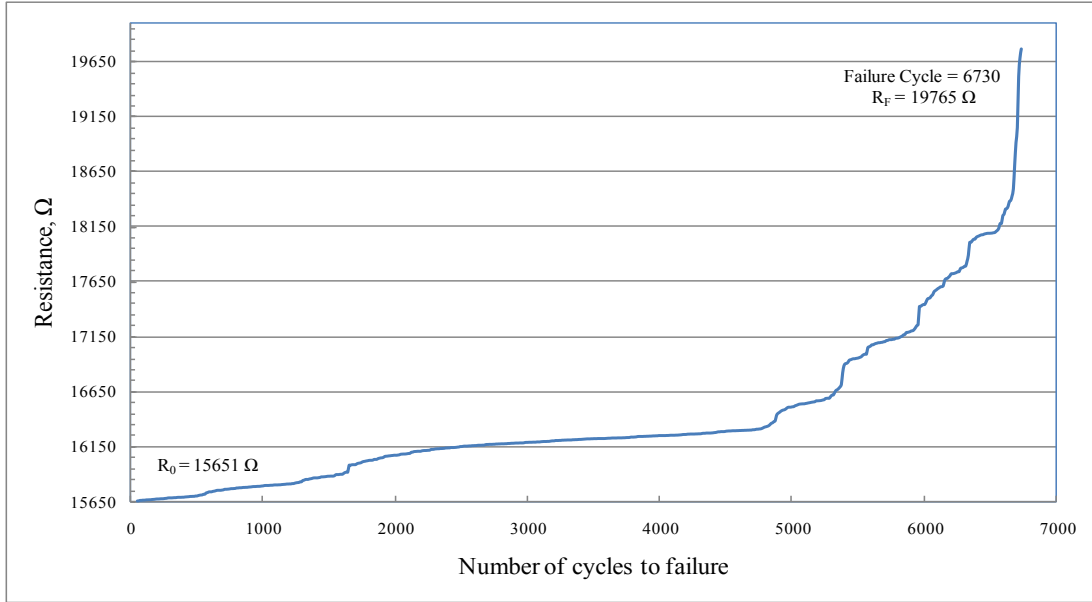
I-16Electrical resistance signature for sample 0.5-16



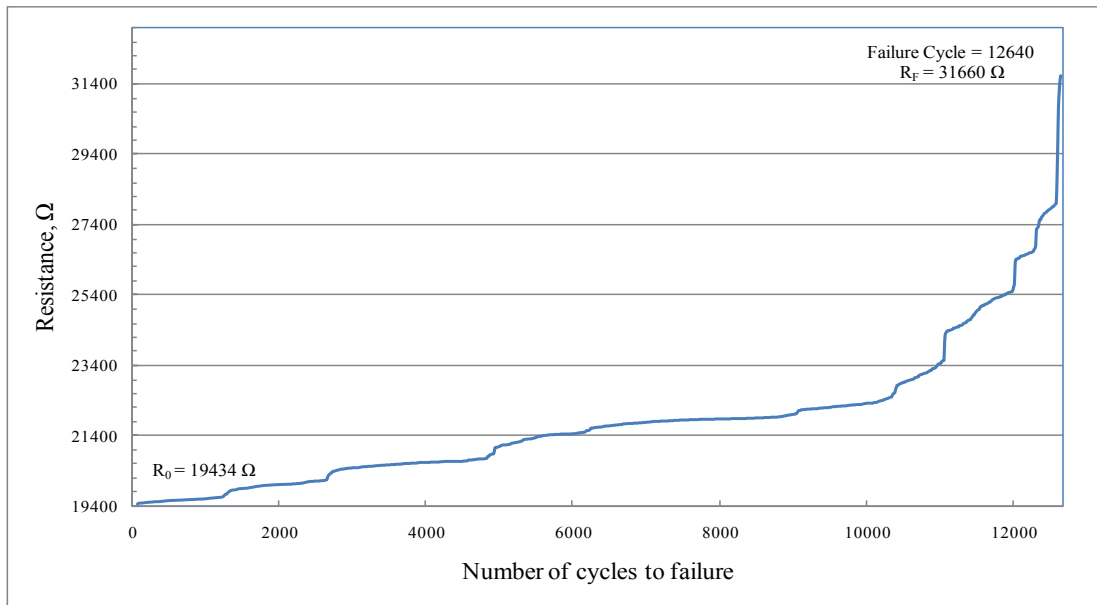
I-17Electrical resistance signature for sample 0.5-17



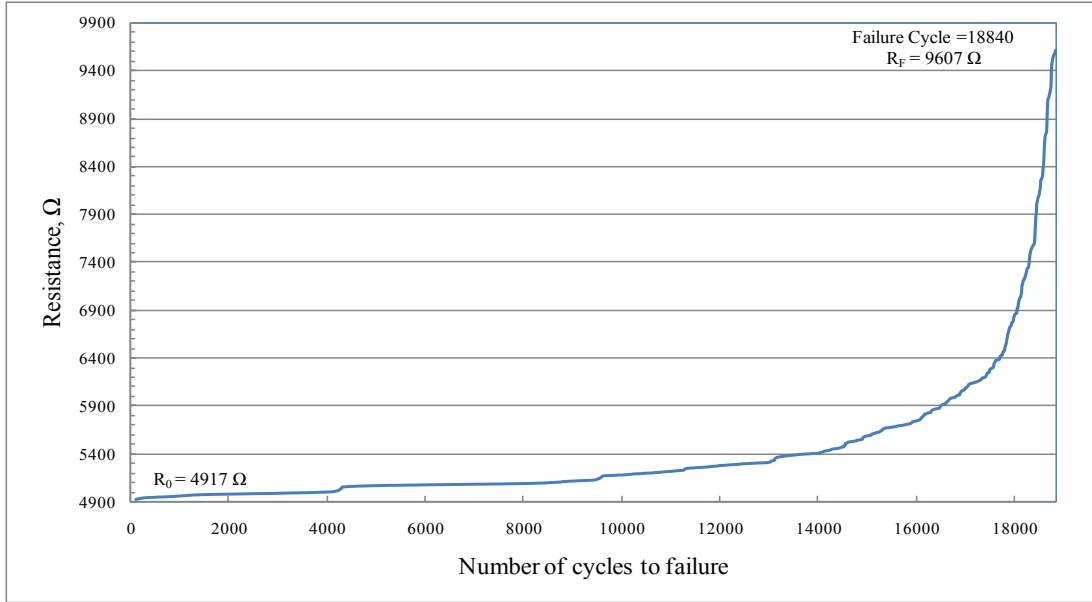
I-18Electrical resistance signature for sample 0.5-18



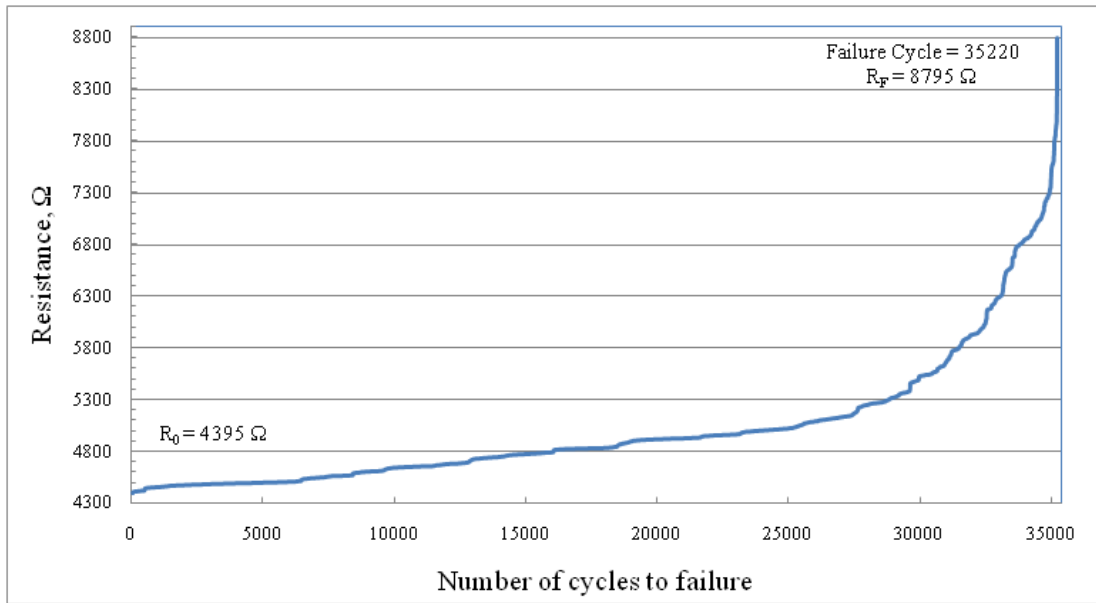
I-19Electrical resistance signature for sample 0.5-19



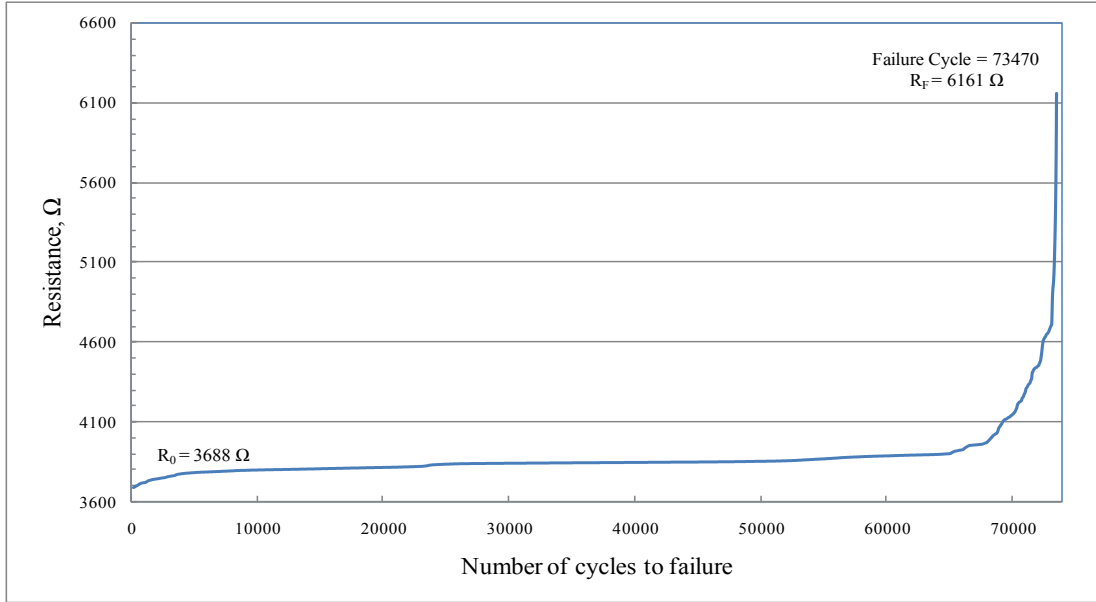
I-20Electrical resistance signature for sample 0.5-20



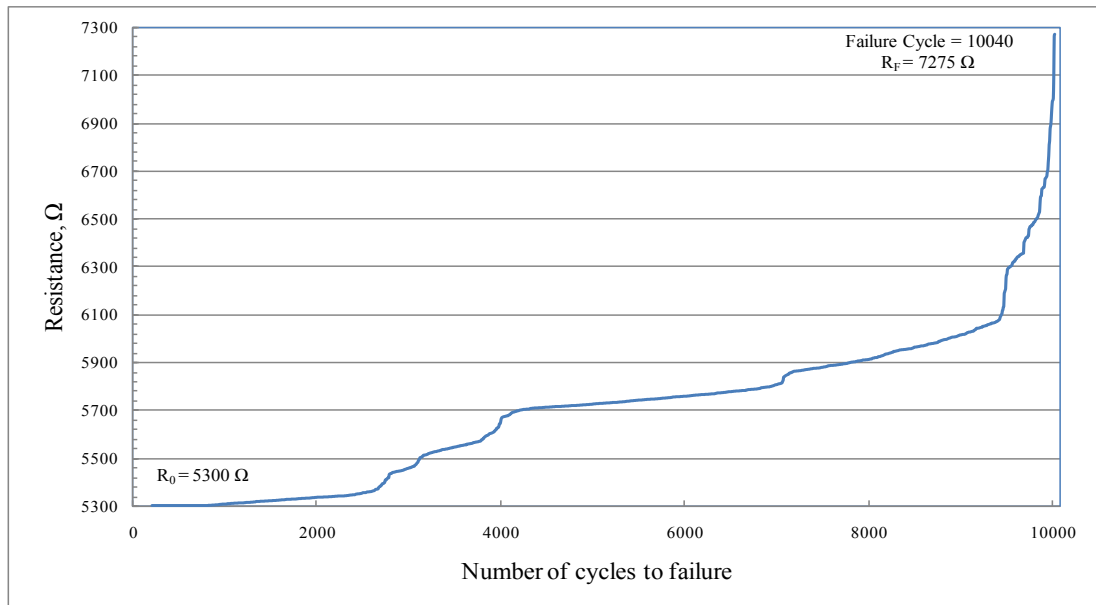
I-21Electrical resistance signature for sample 0.5-21



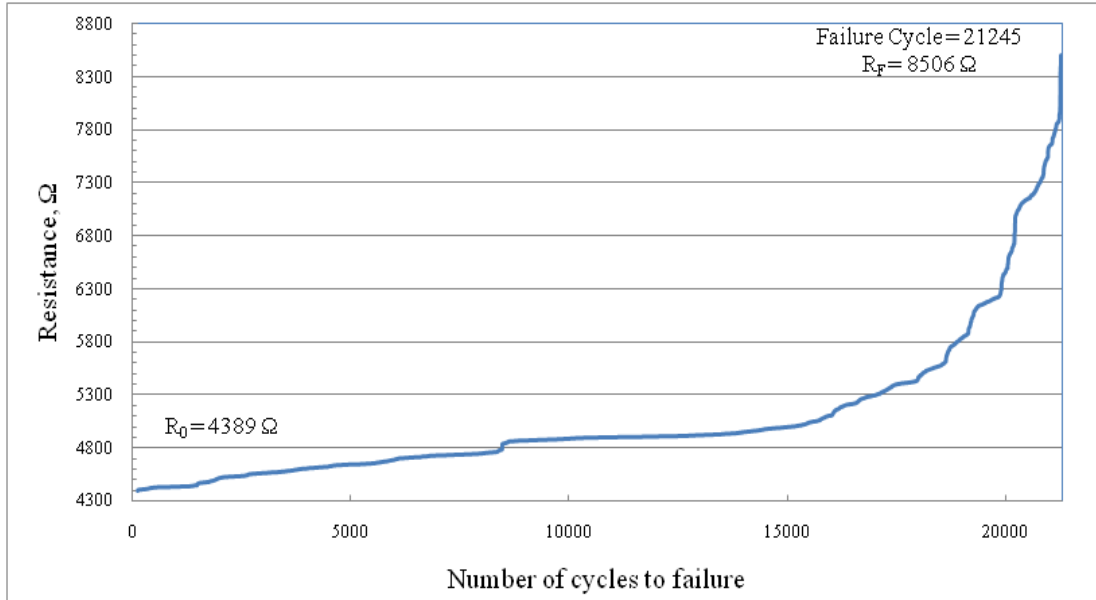
I-22Electrical resistance signature for sample 0.5-22



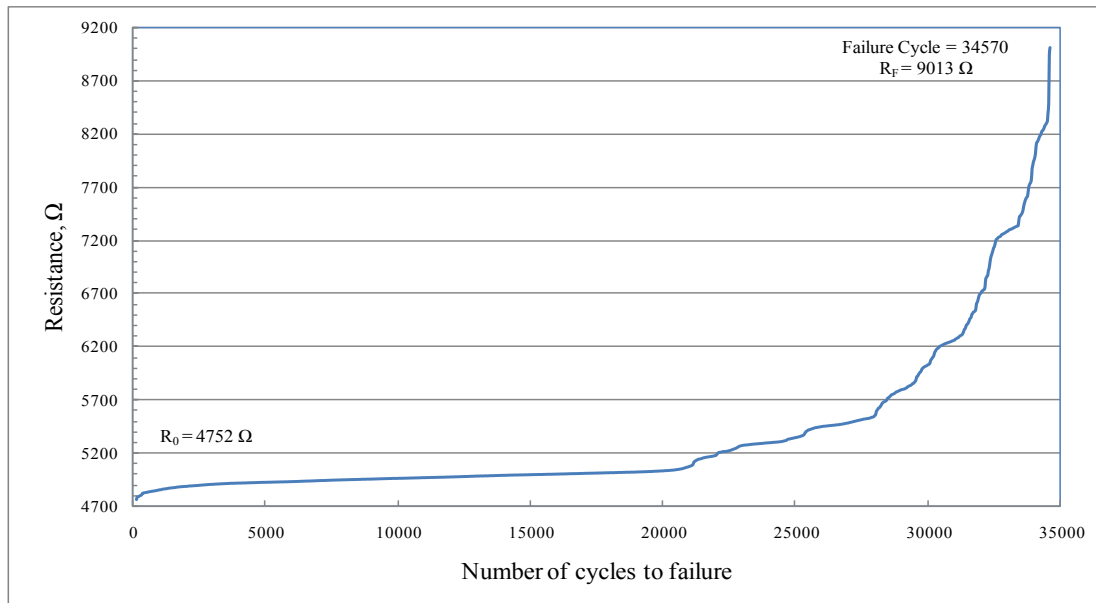
I-23Electrical resistance signature for sample 0.5-23



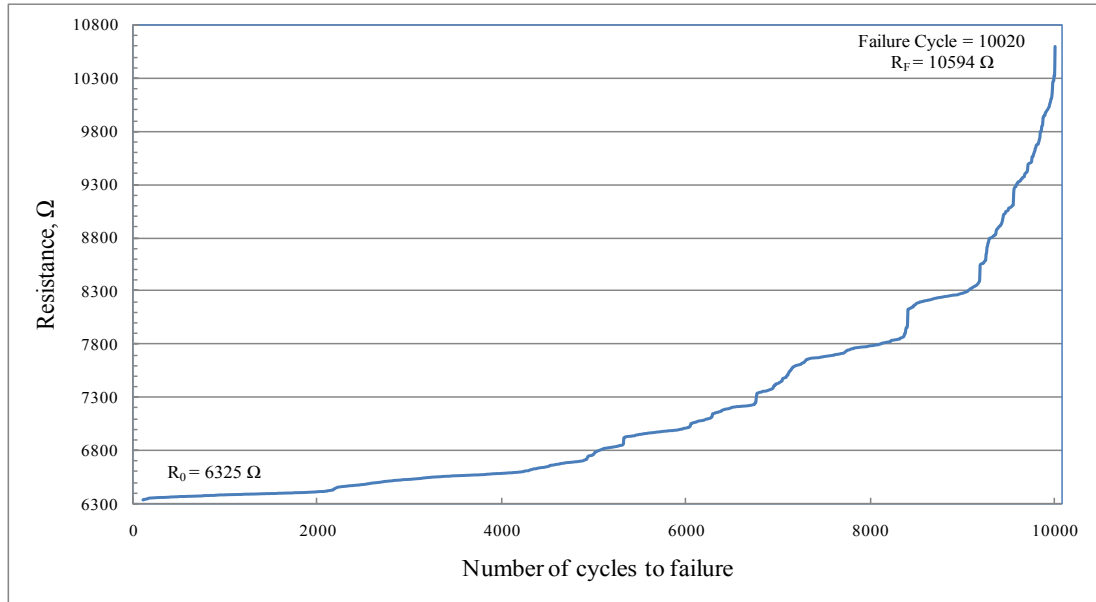
I-24Electrical resistance signature for sample 0.5-24



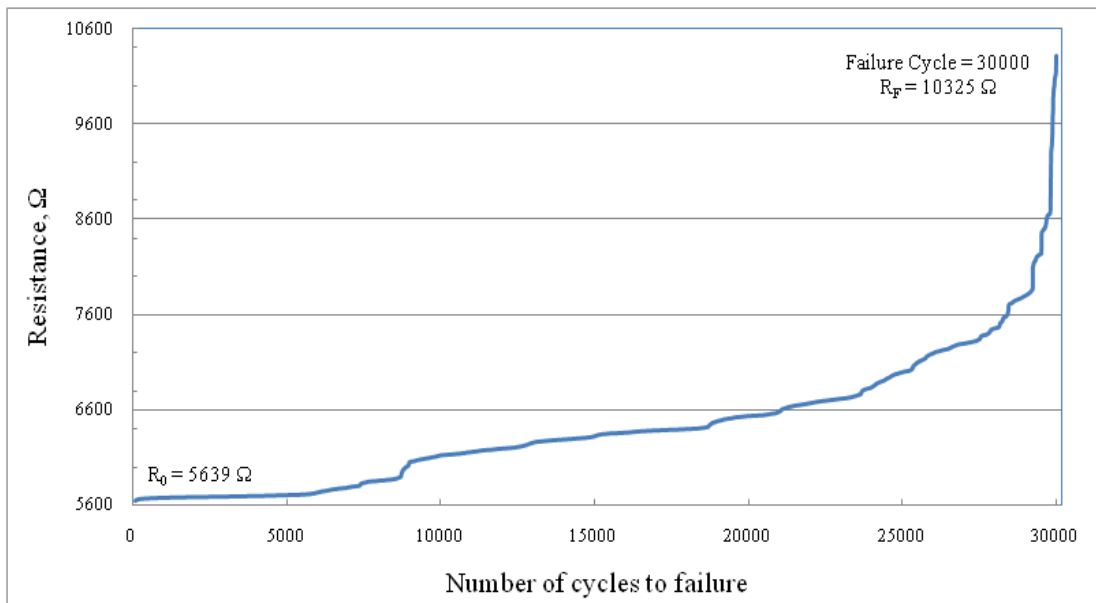
I-25Electrical resistance signature for sample 0.5-25



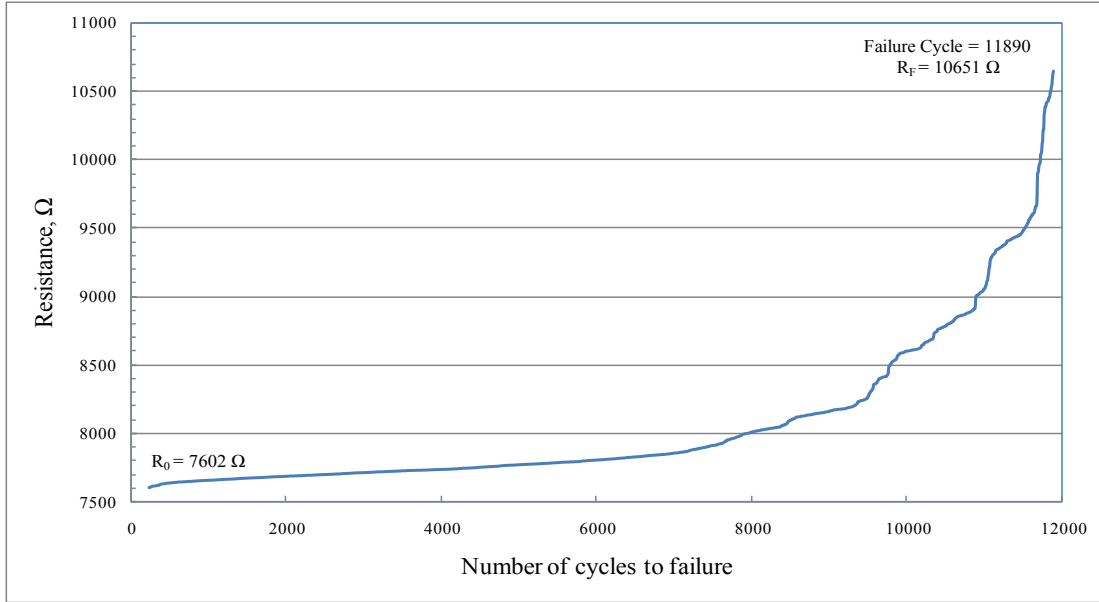
I-26Electrical resistance signature for sample 0.5-26



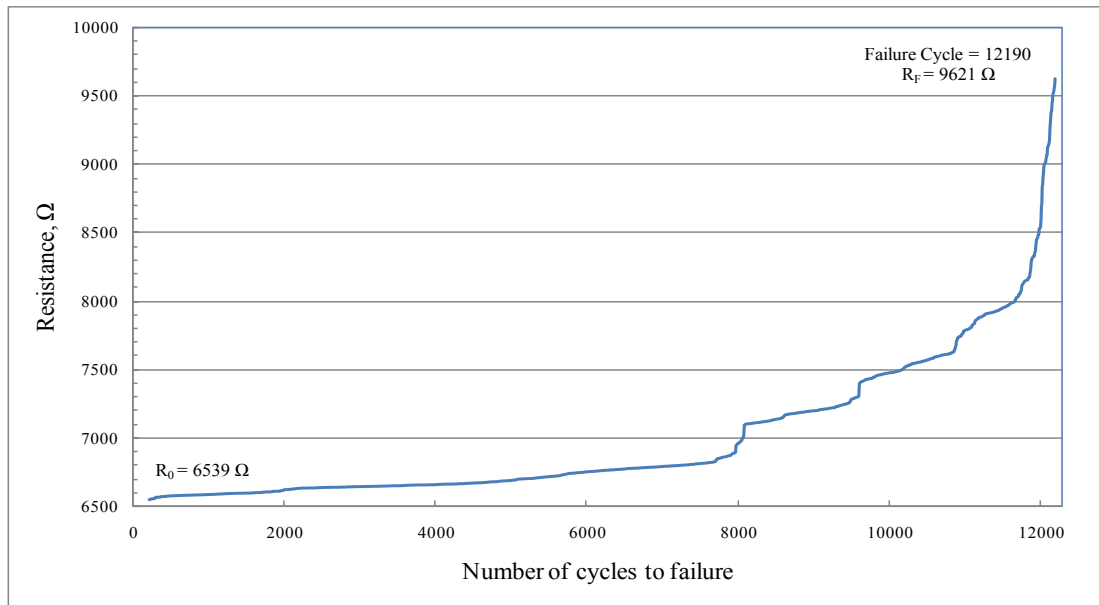
I-27Electrical resistance signature for sample 0.5-27



I-28Electrical resistance signature for sample 0.5-28

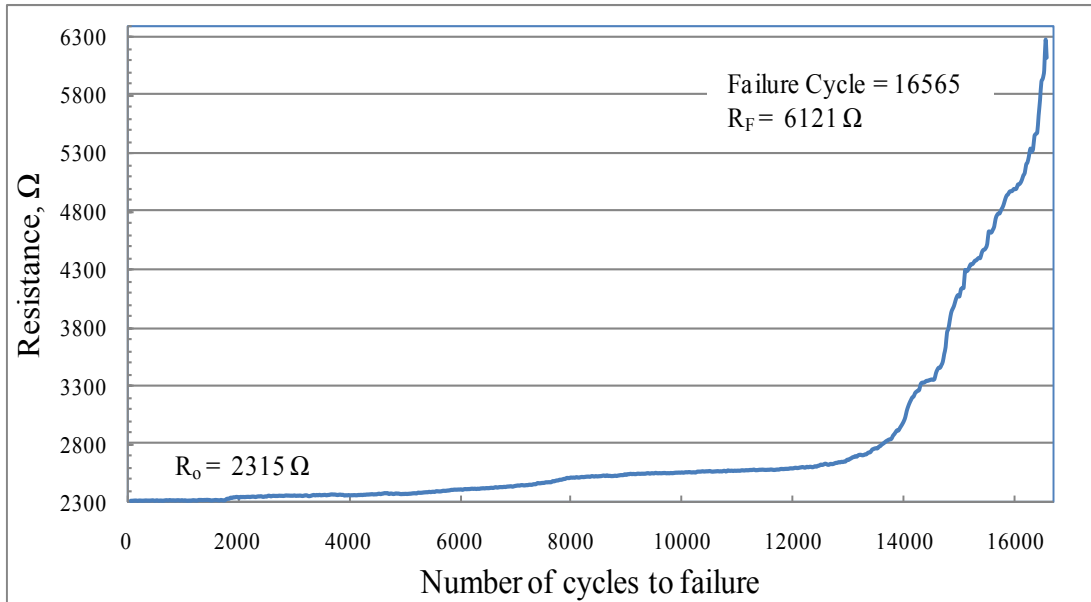


I-29Electrical resistance signature for sample 0.5-29

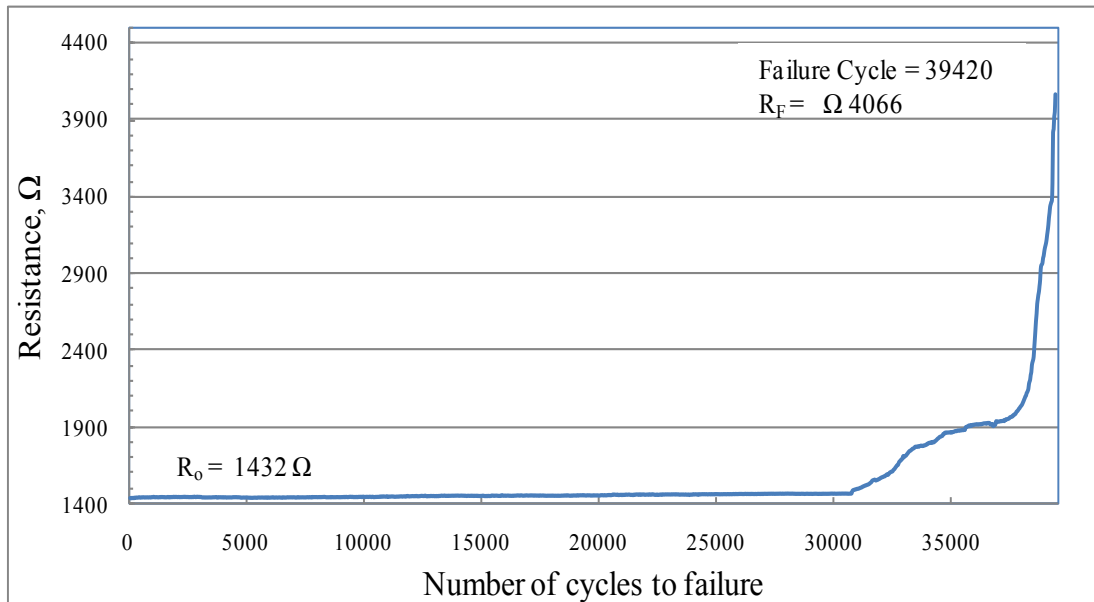


I-30Electrical resistance signature for sample 0.5-30

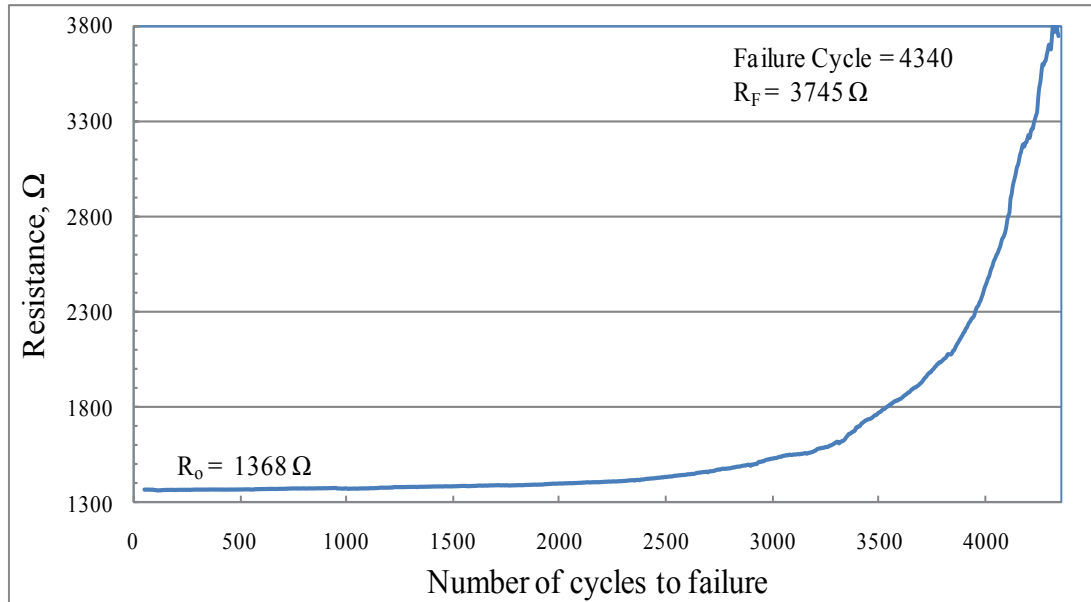
Joints with 1 wt% MWCNT



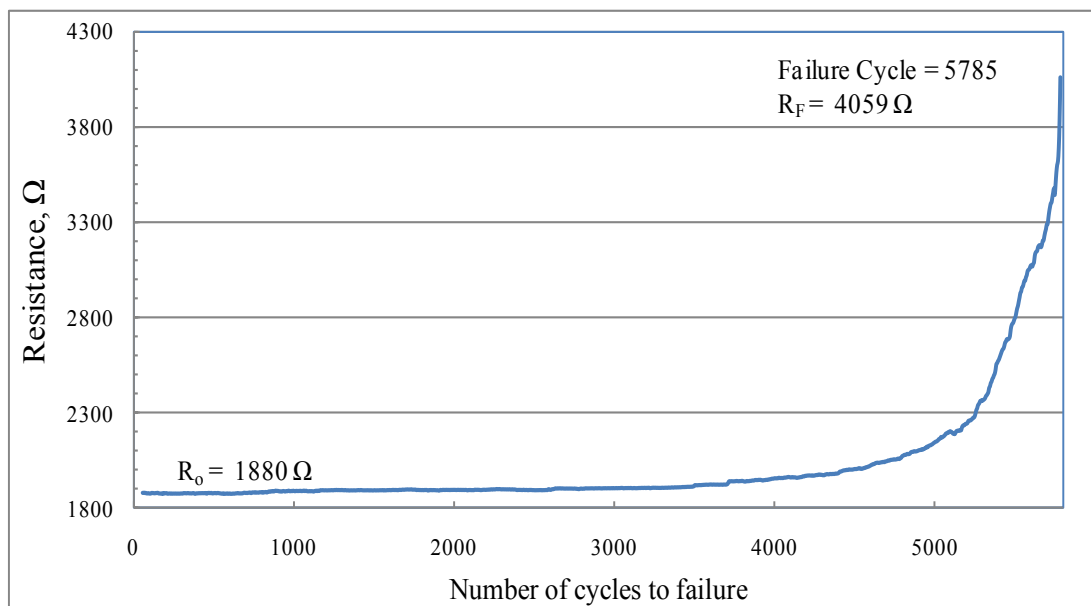
I-31Electrical resistance signature for sample 1-1



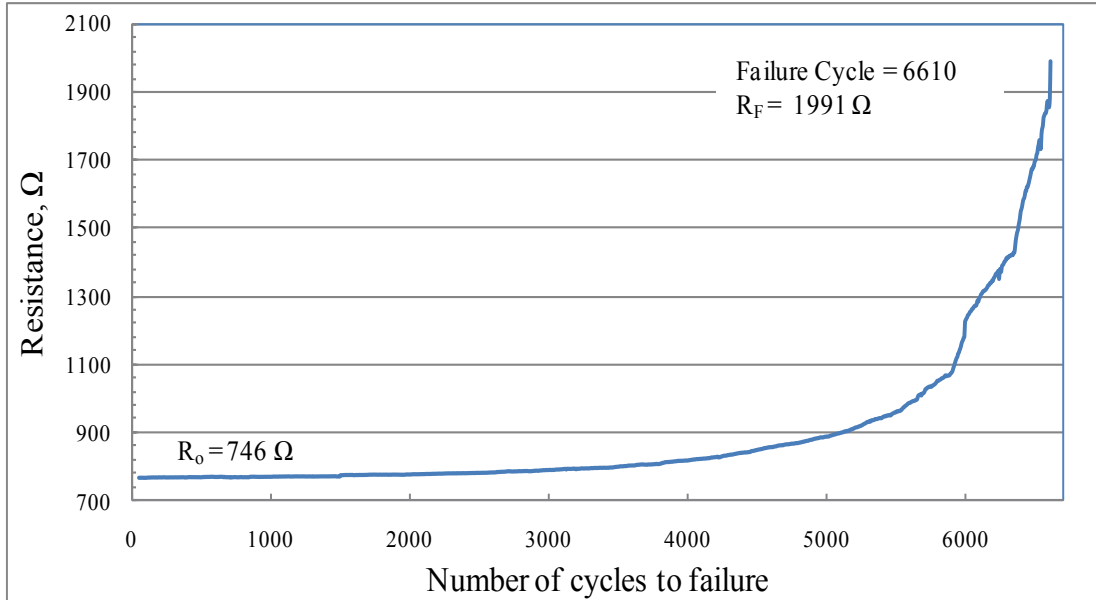
I-32Electrical resistance signature for sample 1-2



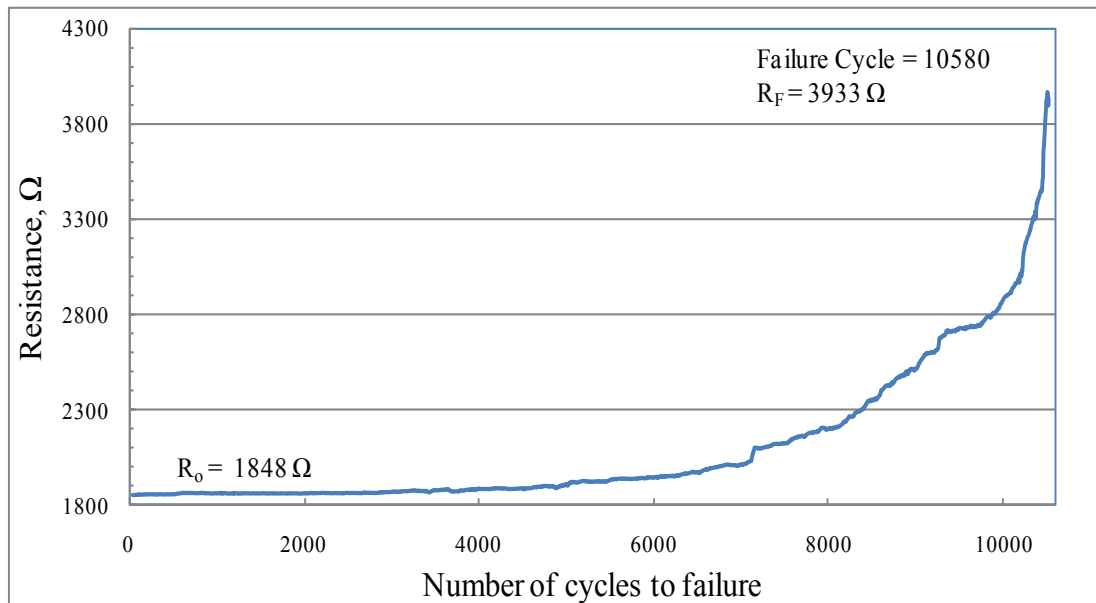
I-33Electrical resistance signature for sample 1-3



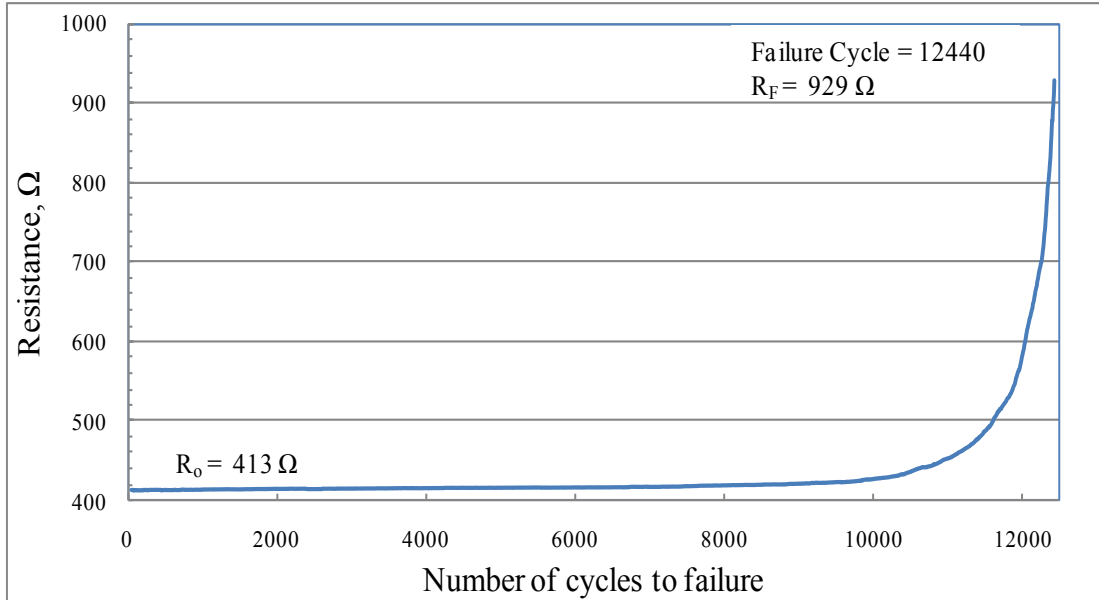
I-34Electrical resistance signature for sample 1-4



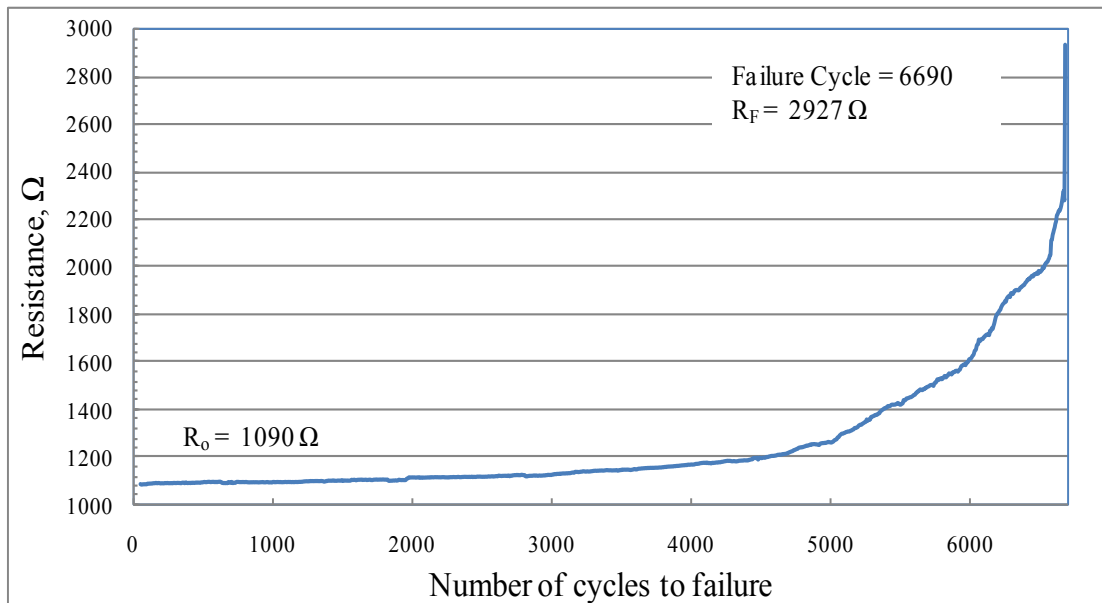
I-35Electrical resistance signature for sample 1-5



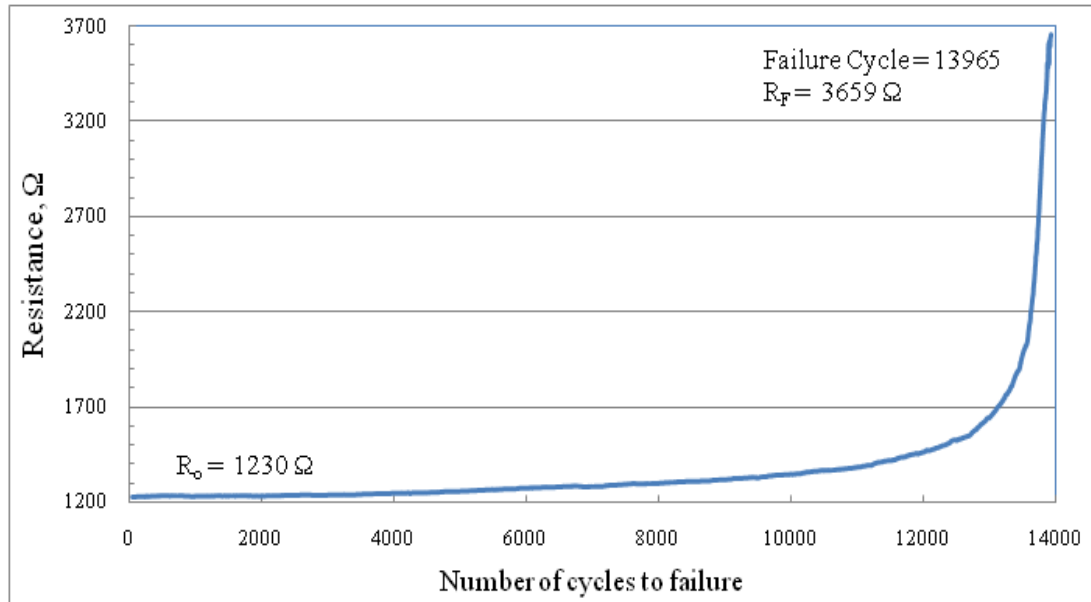
I-36Electrical resistance signature for sample 1-6



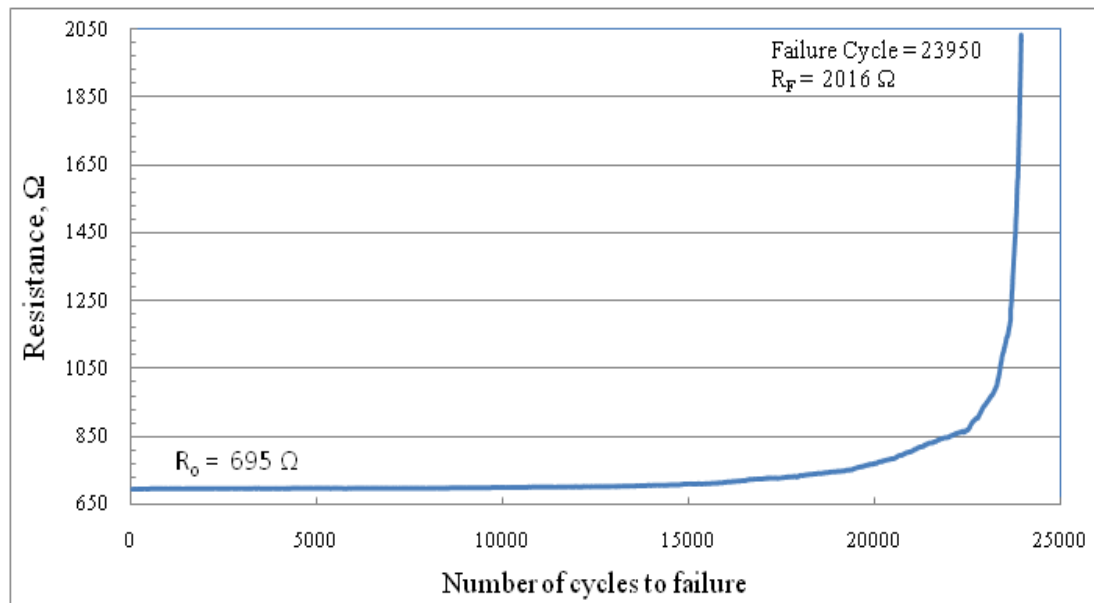
I-37Electrical resistance signature for sample 1-7



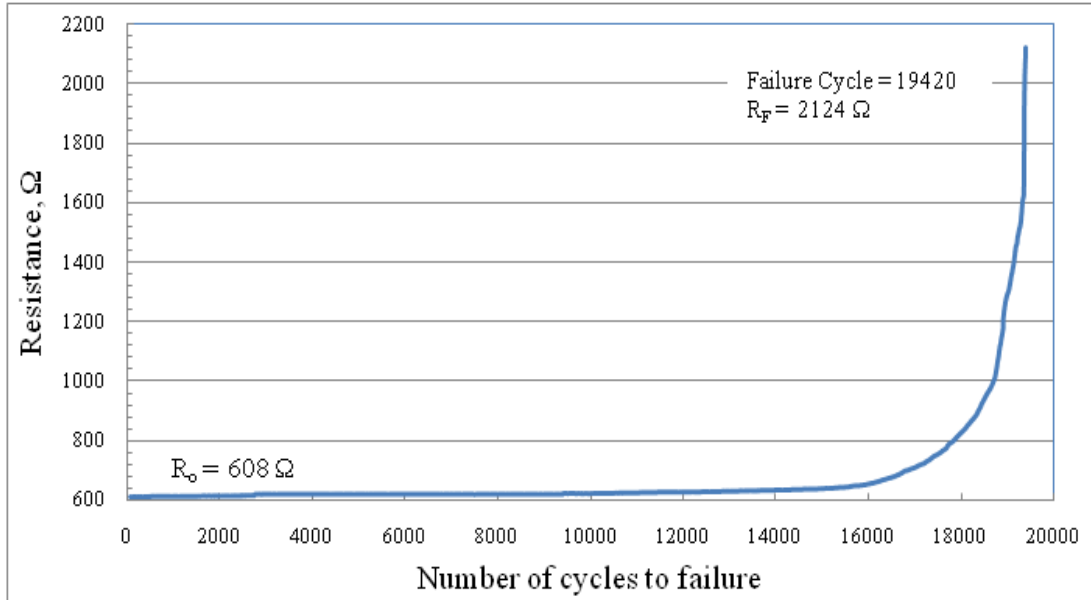
I-38Electrical resistance signature for sample 1-8



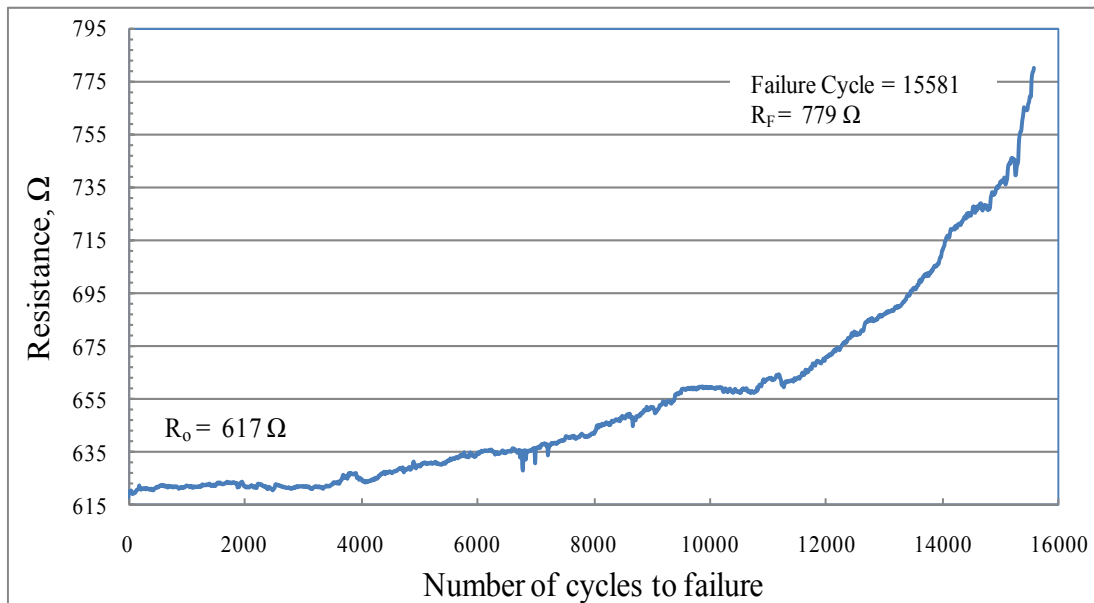
I-39Electrical resistance signature for sample 1-9



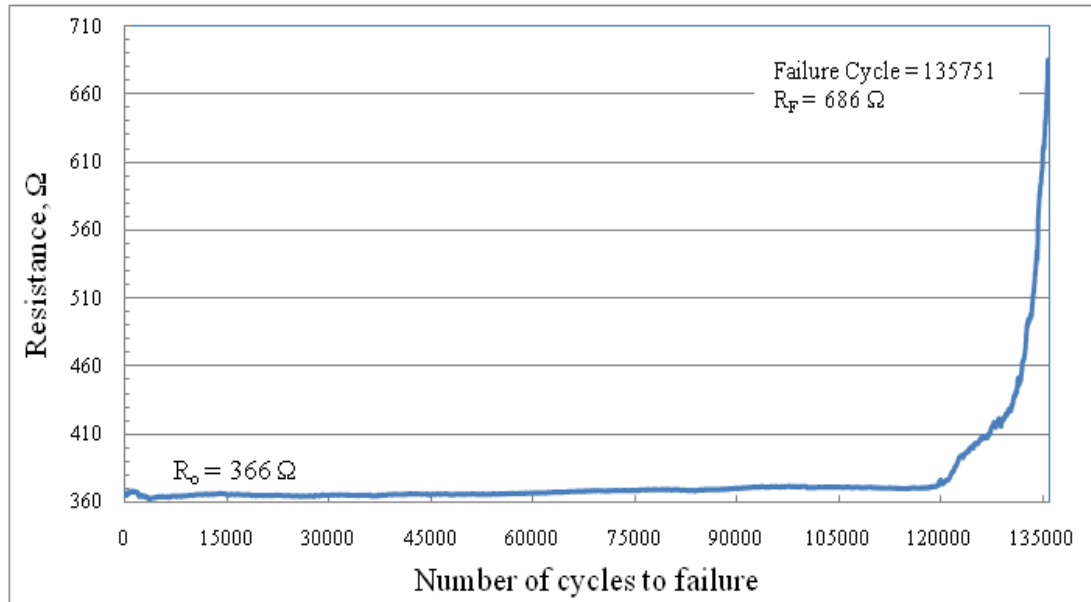
I-40Electrical resistance signature for sample 1-10



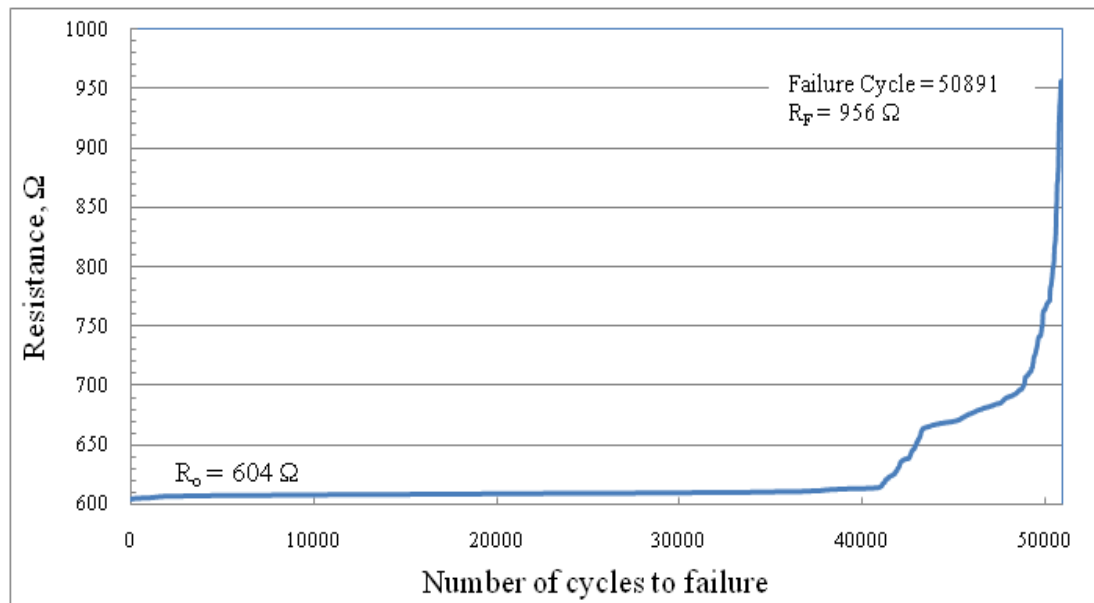
I-41Electrical resistance signature for sample 1-11



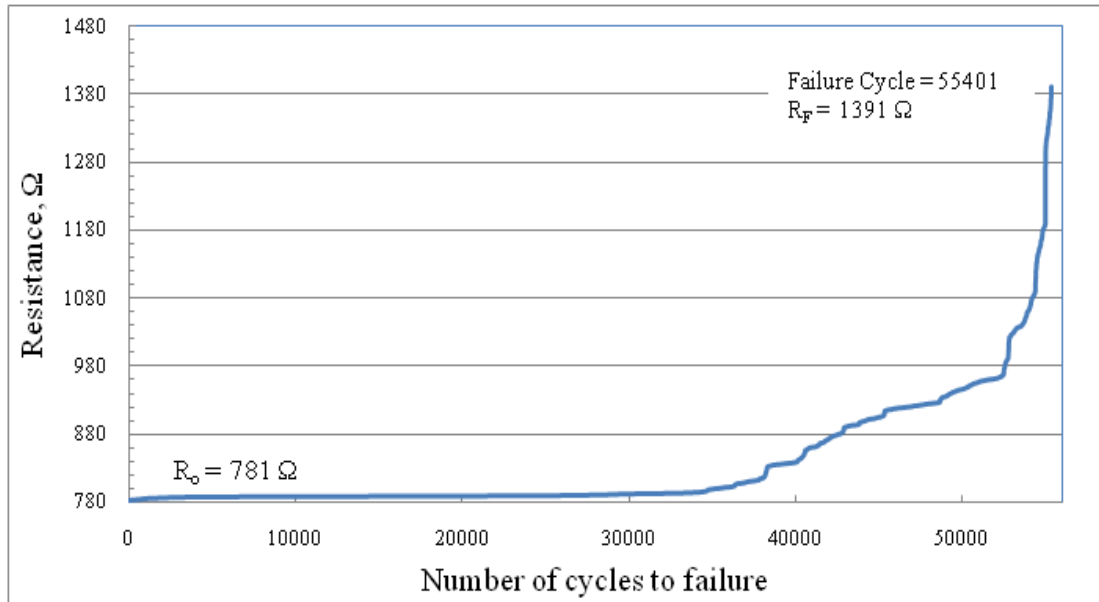
I-42Electrical resistance signature for sample 1-12



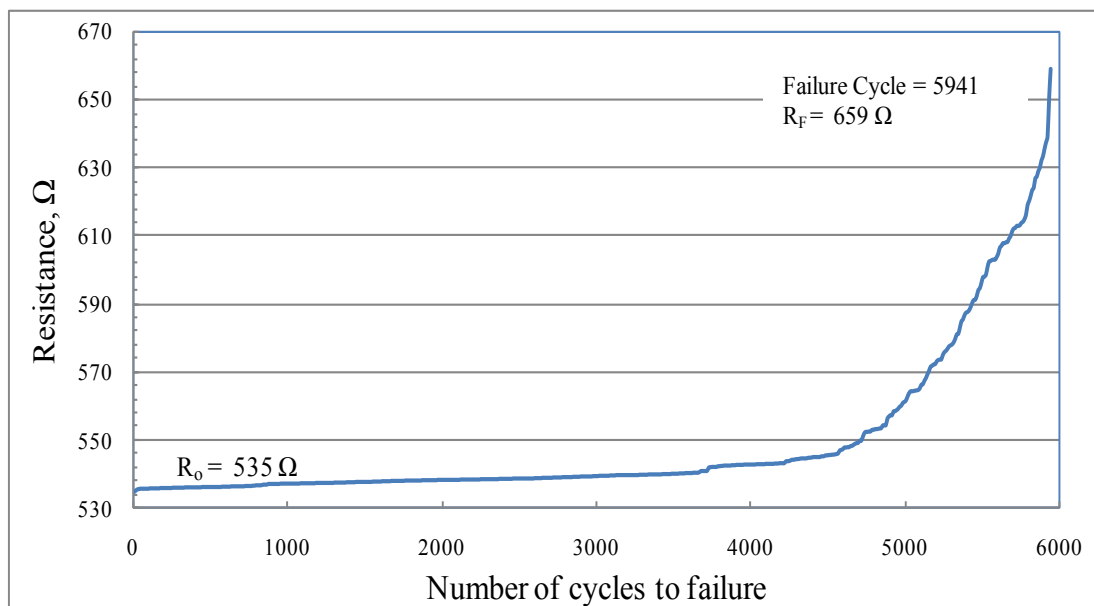
I-43Electrical resistance signature for sample 1-13



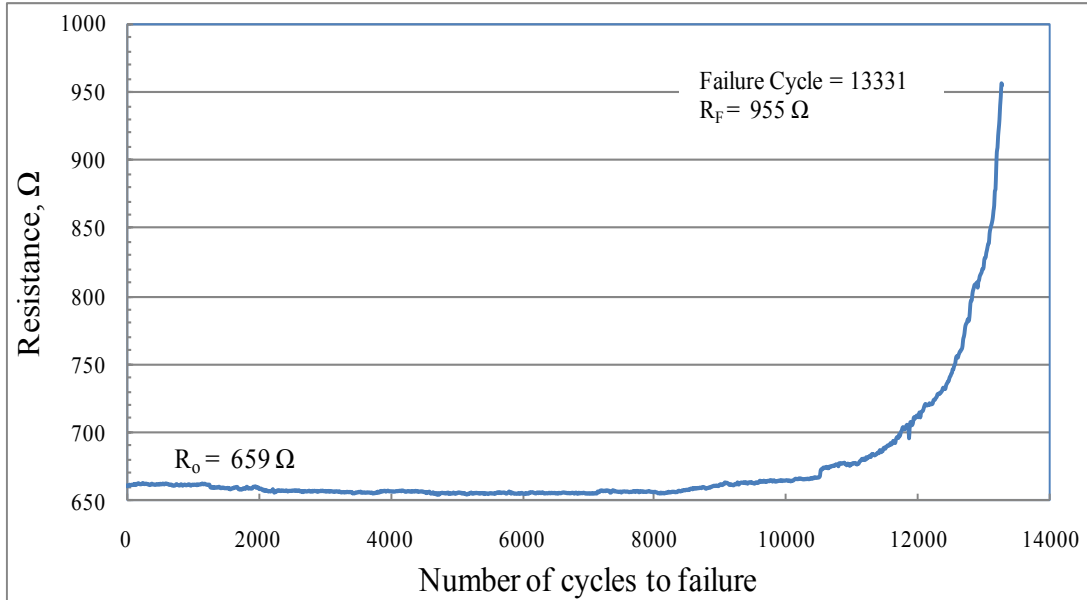
I-44Electrical resistance signature for sample 1-14



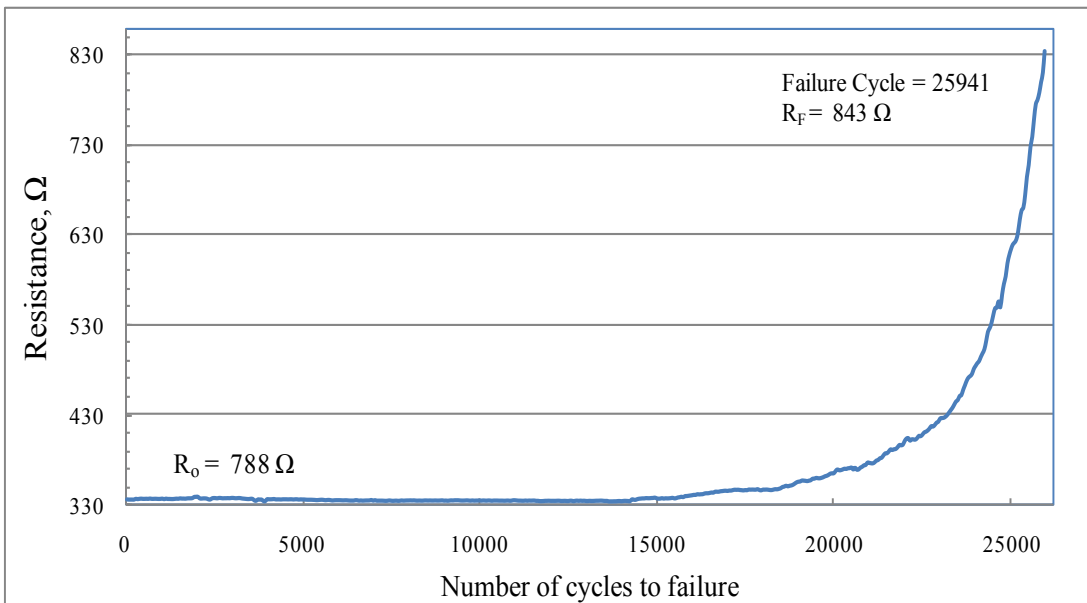
I-45Electrical resistance signature for sample 1-15



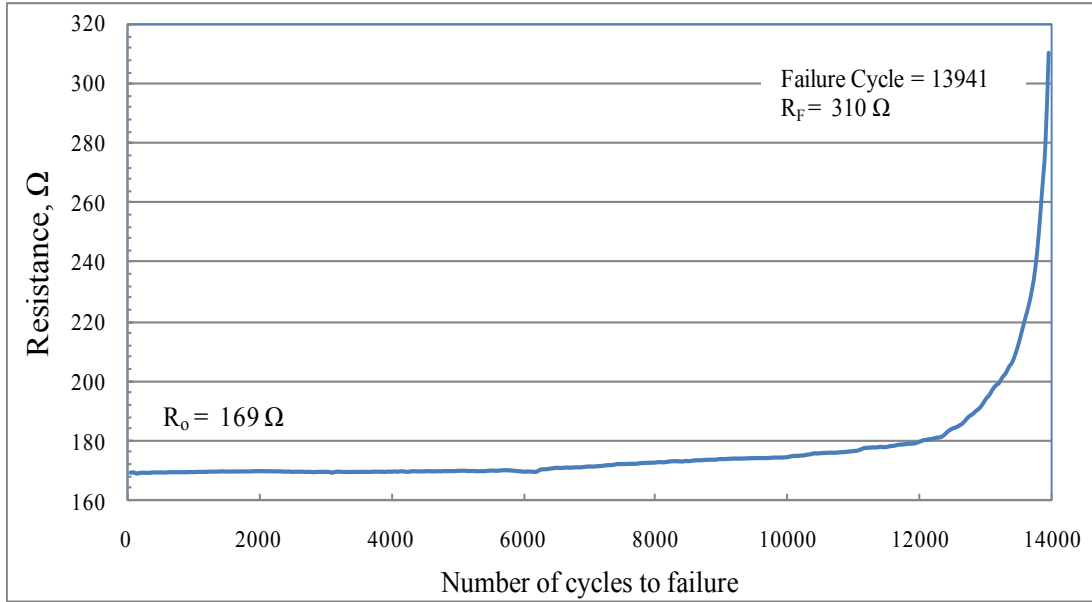
I-46Electrical resistance signature for sample 1-16



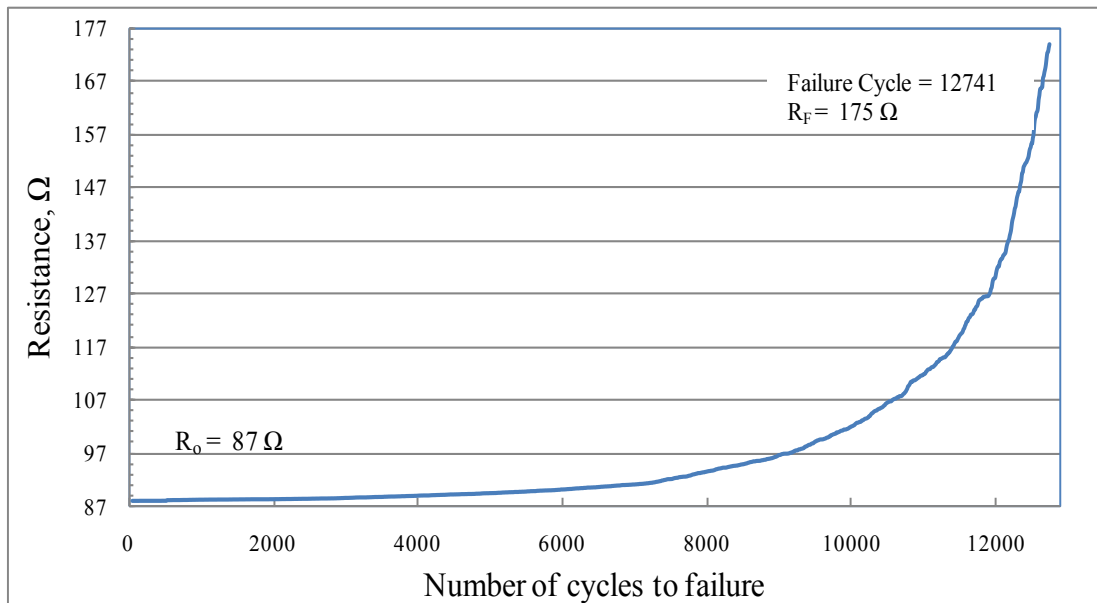
I-47Electrical resistance signature for sample 1-17



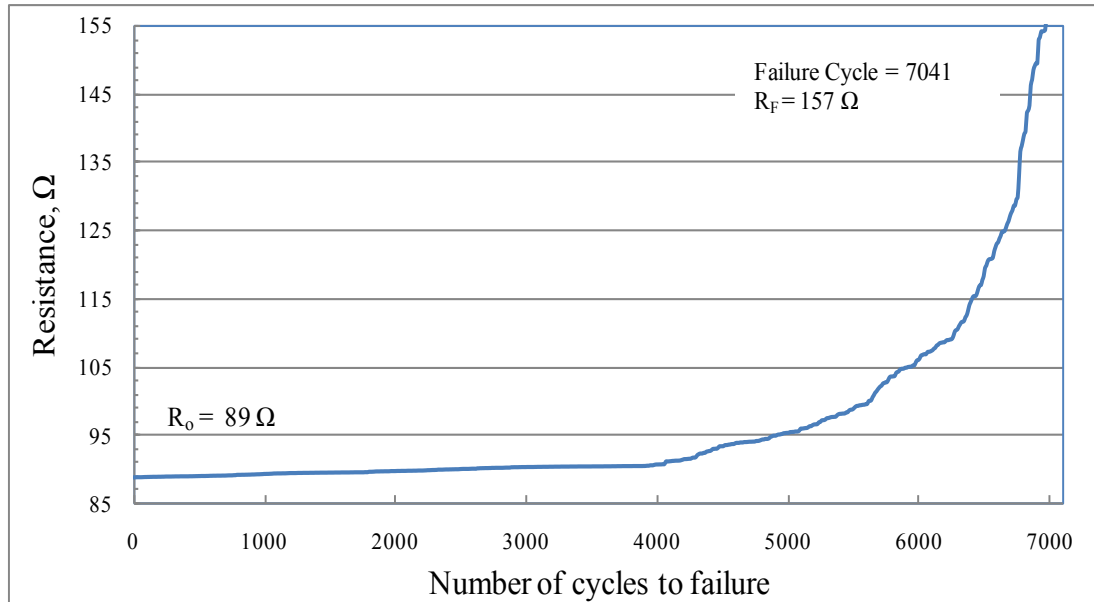
I-48Electrical resistance signature for sample 1-18



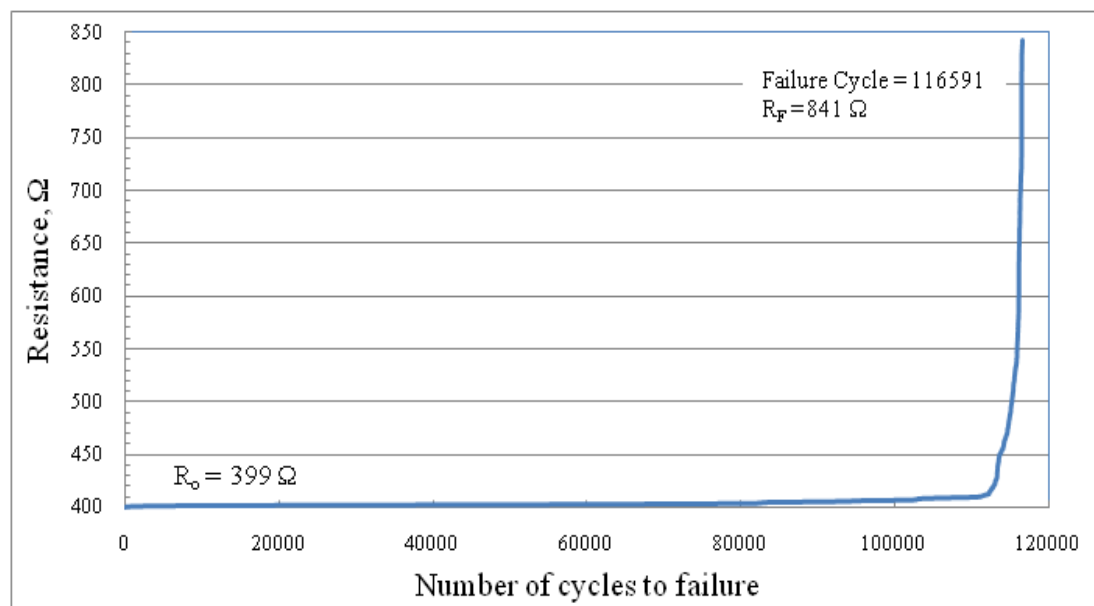
I-49Electrical resistance signature for sample 1-19



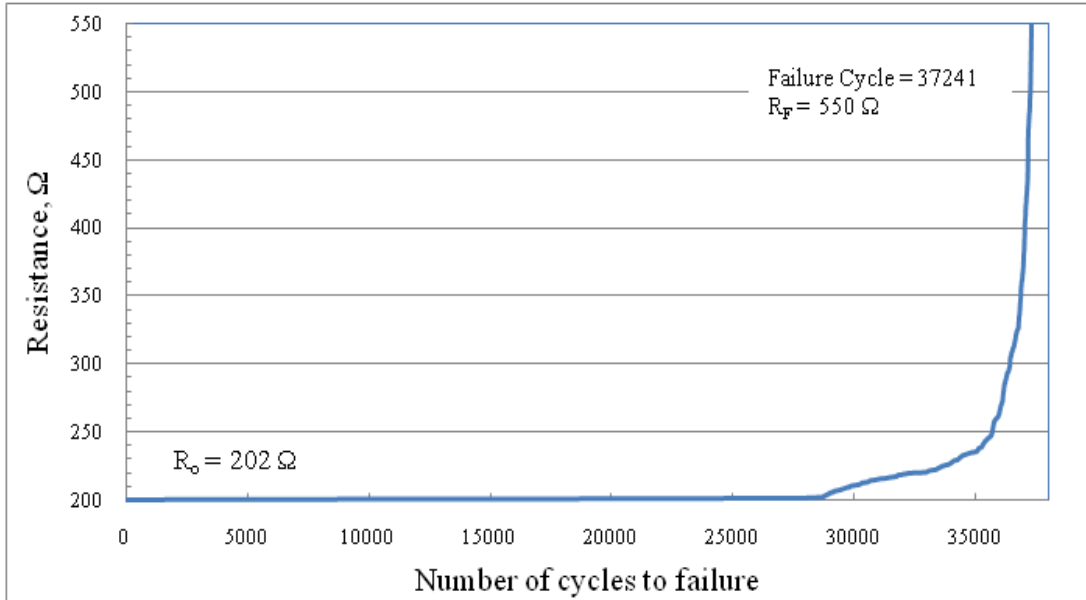
I-50Electrical resistance signature for sample 1-20



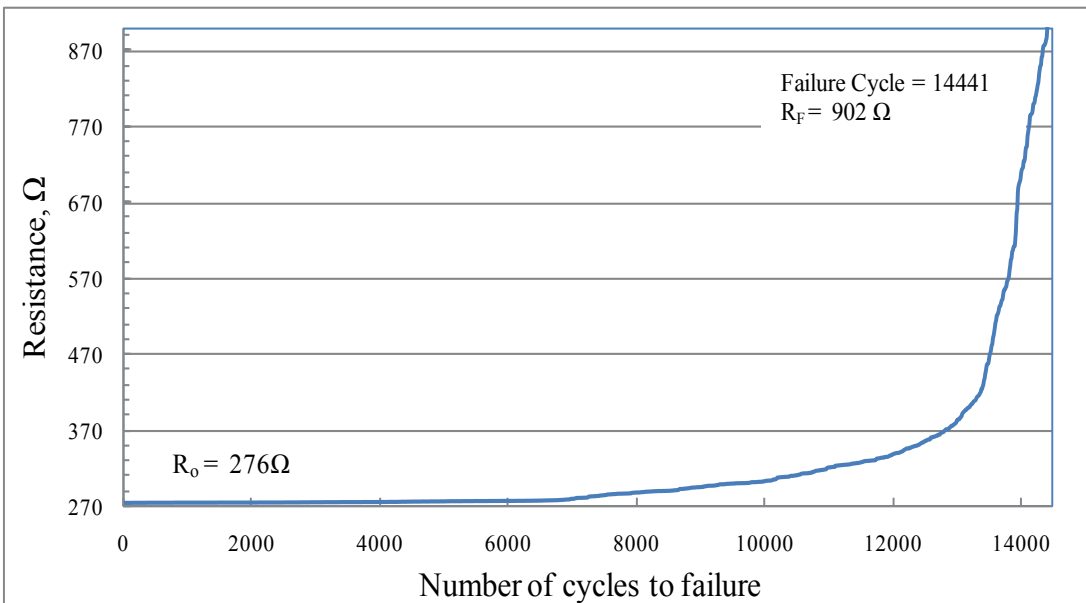
I-51Electrical resistance signature for sample 1-21



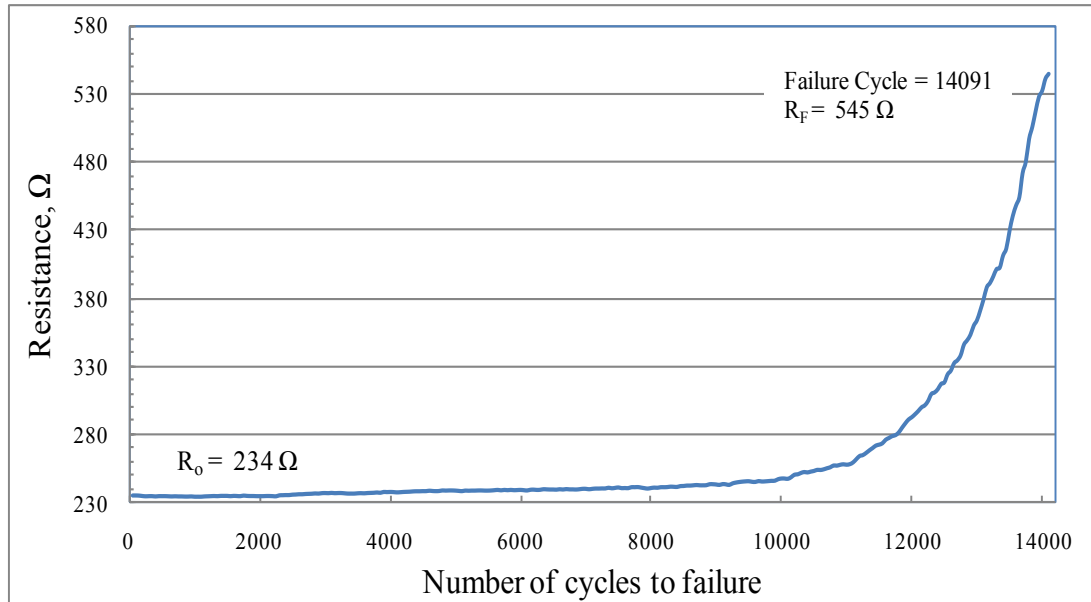
I-52Electrical resistance signature for sample 1-22



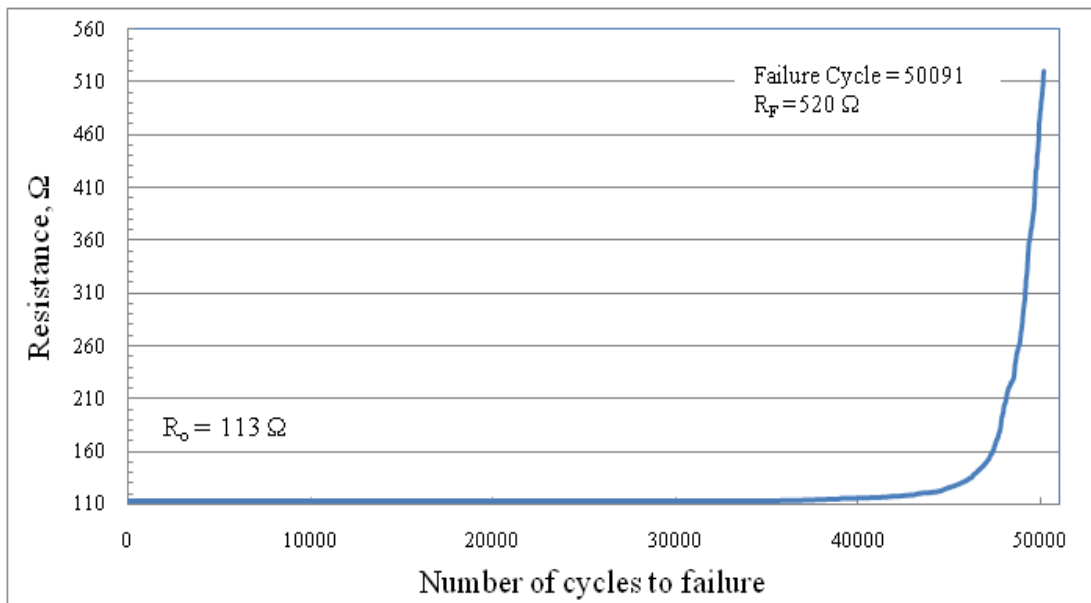
I-53Electrical resistance signature for sample 1-23



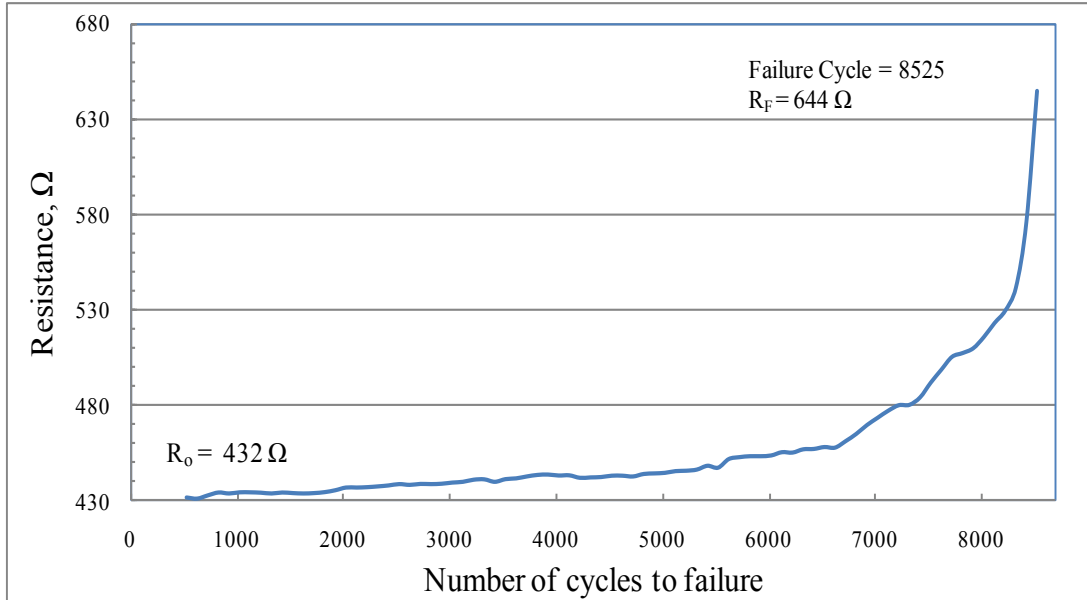
I-54Electrical resistance signature for sample 1-24



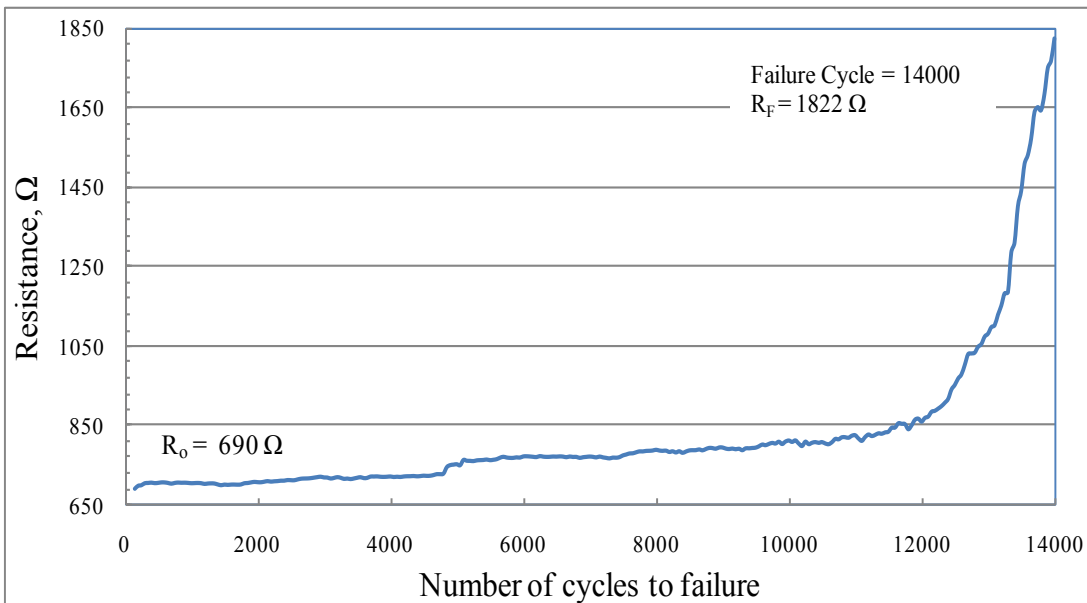
I-55Electrical resistance signature for sample 1-25



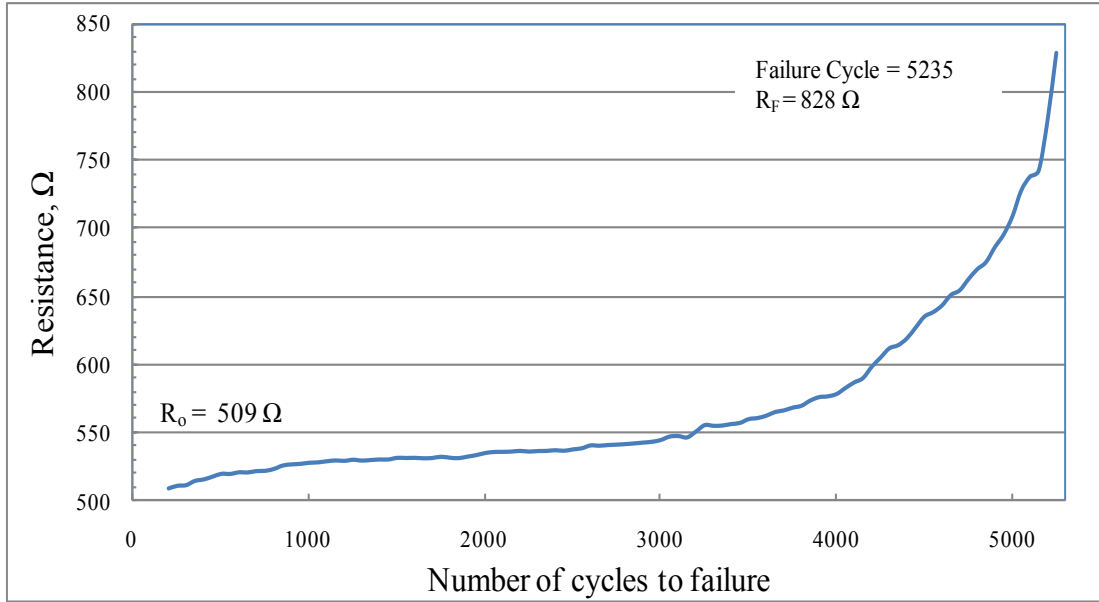
I-56Electrical resistance signature for sample 1-26



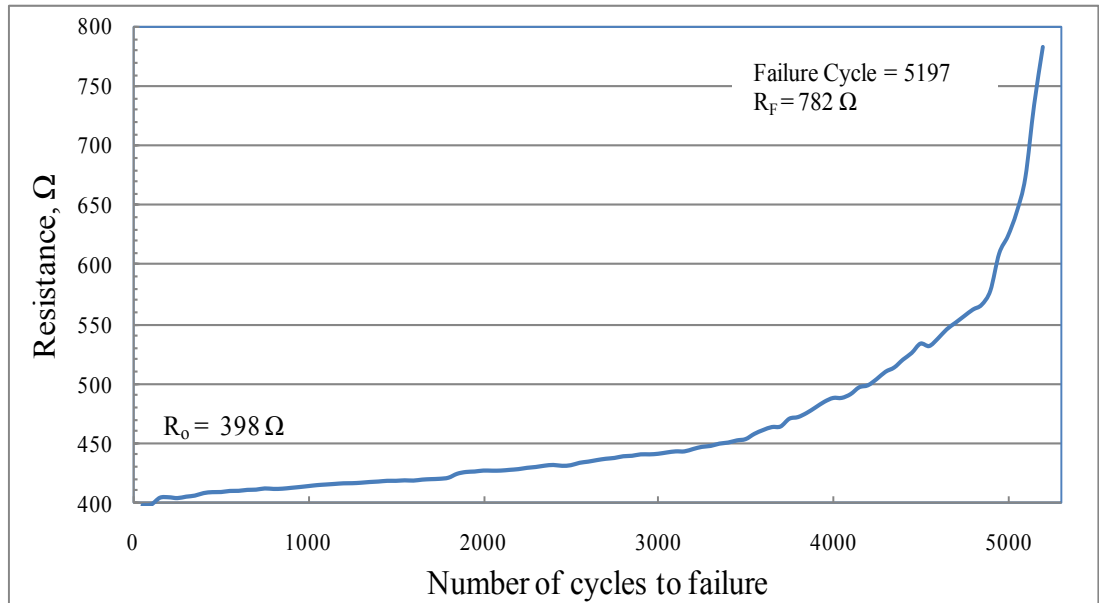
I-57Electrical resistance signature for sample 1-27



I-58Electrical resistance signature for sample 1-28



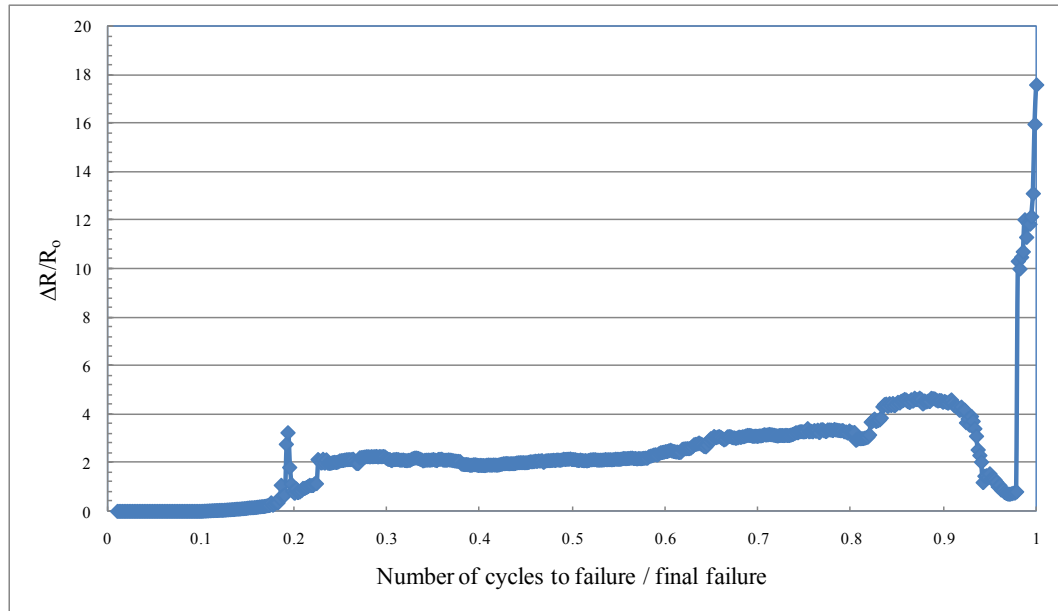
I-59Electrical resistance signature for sample 1-29



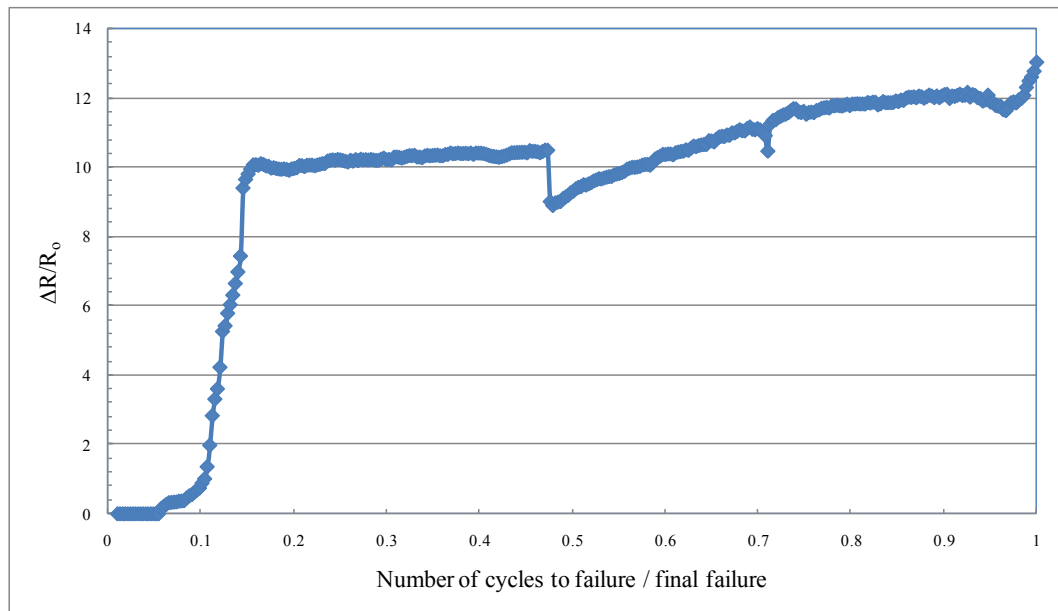
I-60Electrical resistance signature for sample 1-30

Appendix II) Electrical resistance signatures of adhesively bonded graphite composites

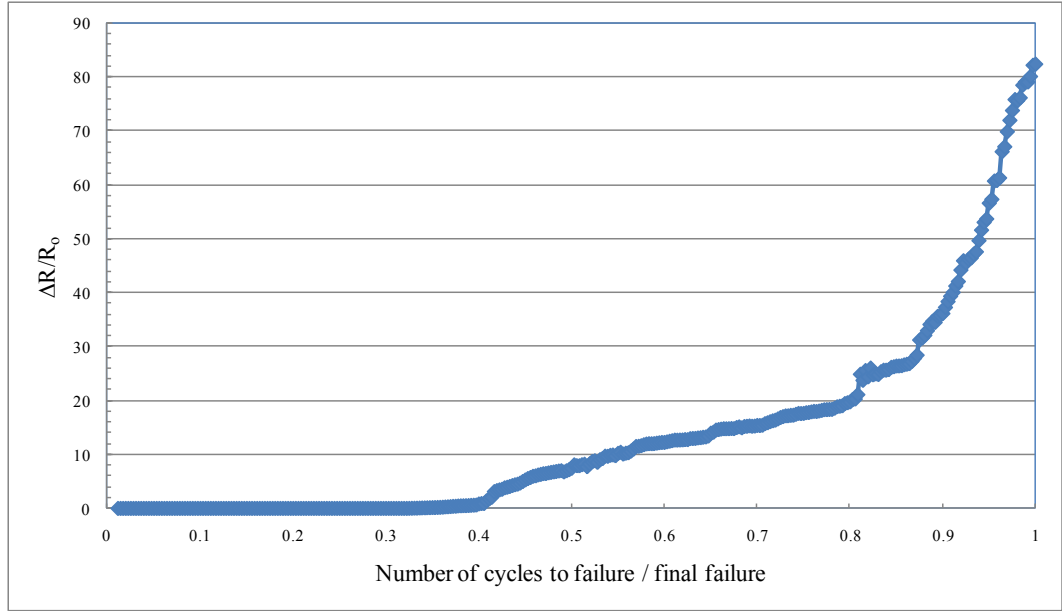
1 wt% MWCNT-reinforced-adhesively bonded graphite fiber laminates



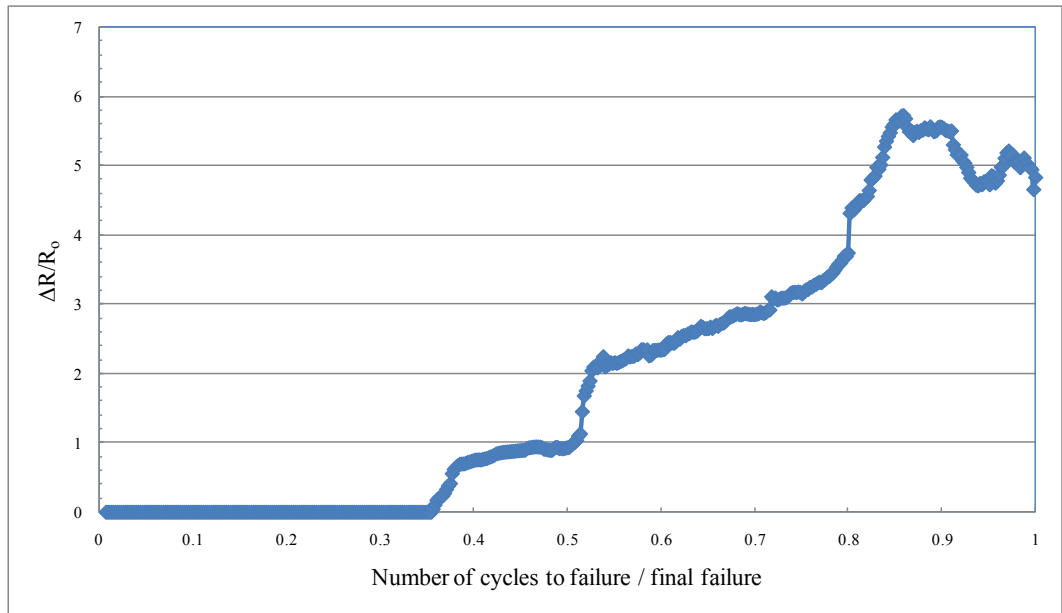
II-1 Electrical resistance signature for sample 1



II-2 Electrical resistance signature for sample 2



II-3Electrical resistance signature for sample 3



II-4Electrical resistance signature for sample 4